1-1-2011

Biopharmaceutical approaches for improved drug delivery across ocular barriers

Ketan Hippalgaonkar
University of Mississippi

BIOPHARMACEUTICAL APPROACHES FOR IMPROVED DRUG DELIVERY ACROSS OCULAR BARRIERS

A Dissertation
presented in partial fulfillment of requirements
for the degree of Doctor of Philosophy
in the Department of Pharmaceutics
The University of Mississippi

by

KETAN HIPPALGAONKAR

July 2011

ABSTRACT

The eye is protected from the external environment by various physiological and anatomical barriers. These barriers through there protective actions drastically diminish the ocular bioavailability of drugs. The corneal epithelium acts as a major barrier towards the permeation of hydrophilic agents, whereas poor aqueous solubility presents a formulation challenge for lipophilic compounds. Additionally, P-glycoprotein (P-gp) expressed on the retinal pigmented epithelium (RPE P-gp) limits the penetration of substrates, in therapeutically relevant concentrations, into the back-of-the-eye.

In the present research, use of penetration enhancers (chitosan, benzalkonium chloride (BAK) and ethylenediaminetetraacetic acid (EDTA)) and formulation approaches (cyclodextrins and solid lipid nanoparticles (SLNs)) were evaluated in terms of their ability to improve the ocular bioavailability of hydrophilic and lipophilic compounds, respectively. A novel approach, localized modulation of RPE P-gp using topically co-administered P-gp inhibitors, was investigated to improve the back-of-the eye delivery of P-gp substrates.

In vitro transcorneal permeation results demonstrated that chitosan brought about a dose dependent increase in the permeability of acyclovir, a model hydrophilic compound. Combination of chitosan, BAK and EDTA resulted in a synergistic effect on the permeation of acyclovir. Dramatic increase in aqueous solubility, stability and *in vitro* transcorneal permeability of delta-8-tetrahydrocannabinol, a model lipophilic agent, was observed in the presence of 2-Hydroxypropyl-β-cyclodextrin (HPβCD), randomly methylated-β-cyclodextrin and

sulfobutylether-β-cyclodextrin. The indomethacin loaded SLN (IN-SLNs) formulation was physically stable following sterilization and on storage. The IN-SLNs formulation increase stability and *in vitro* corneal permeability of indomethacin in comparison to the solution formulations (cosolvent and HPβCD based) tested.

Furthermore, for the first time, studies in anesthetized male New Zealand rabbits demonstrate that topically applied P-gp inhibitors can diffuse to the RPE and alter the elimination kinetics of a systemically or intravtireally administered P-gp substrate, probably through inhibition of the basolateral RPE P-gp. The degree of inhibition was found to be dependent on the physicochemical characteristics of the inhibitor and its affinity for P-gp and the concentration of the therapeutic agent in the plasma or in the vitreous humor. Formulation factors such as inclusion of permeation enhancers may play a major role in yielding effective levels of the inhibitor at the RPE.

DEDICATION

This dissertation is dedicated to my parents Uday Kumar Hippalgaonkar and Sanjivani Hippalgaonkar. I would not have reached this milestone without their unending encouragement, patience, support, understanding and love. This dissertation is also dedicated to my lovely wife Swetha Mahalaxmi for being my oxygen and strength.

ACKNOWLEDGMENTS

Obtaining a Ph.D. degree could not be realized without my advisor Dr. Soumyajit Majumdar. His expertise, intellectual support and professional guidance were imperative for this work. I thank him dearly for his encouragement, patience, understanding and support throughout my graduate studies. I am truly grateful and indebted to him for his help and attention towards my academic and personal requests. Thank you for being my advisor!

I express my heartfelt gratitude to my dissertation committee members Dr. Michael A. Repka, Dr. John S. Williamson and Dr. Walter G. Chambliss for their valuable time, guidance, suggestions and help during the evaluation of this dissertation. I extend my thanks to Dr. S. Narasimha Murthy, Dr. Bonnie A. Avery, Dr. Seongbong Jo and Dr. Christy M. Wyandt for making the experience at Ole Miss worthwhile, Ms. Deborah King for her help, patience and affection. I also thank the support and technical help extended by Dr. Harry Fyke and Ms. Penni Bolton during animal experiments.

I thank all graduate students at Department of Pharmaceutics for their support and for making my stay at Ole Miss memorable. I profusely thank my colleagues and friends, especially Ramesh Srirangam and Tushar Hingorani for being such a great support and fun to work with. I also thank them for their help during experimental work and during my stay at Ole Miss. Special thanks to my lovely little sister and colleague Kanchan Hippalgaonkar for her love, moral

support, and encouragement. Working with her during this dissertation was special, fun and memorable.

My warmest thanks to my wife Swetha Mahalaxmi, the support, encouragement, inspiration, love and strength that she has provided me is priceless. The years I spent pursuing my Ph.D. degree would have been more strenuous, less delightful and unsatisfactory without her. Thank you so much!

I specially fall short of words to thank my brother Bipin Hippalgaonkar. He has been my inspiration, strength and moral support. Without his support, encouragement and sacrifices I would not have attended Ole Miss. Thank you for everything!

Most importantly I thank my parents Uday Kumar Hippalgaonkar and Sanjivani Hippalgaonkar for their unyielding encouragement, patience, moral support and guidance. Thank you Aai and Baba!

TABLE OF CONTENTS

LIST OF TABLES

LIST OF FIGURES

CHAPTER 1

REVIEW OF LITERATURE

This chapter provides an overview of the anatomy of the eye and the barriers in ocular drug delivery. Additionally, it also discusses limitations and challenges in ocular delivery of hydrophilic/lipophilic drugs, and strategies that may be employed to enhance the ocular permeation and therapeutic efficacy of these drugs. This section would help in understanding the goals and findings presented in the subsequent chapters.

1.1. Anatomy of the eye

Figure 1-1 is a schematic representation of the anatomy of the eye. The eye, organ of sight, is a secluded organ and can be anatomically divided into the anterior and posterior segments. The anterior segment comprises of the cornea, conjunctiva, aqueous humor, iris-ciliary bodies and the lens. The posterior segment consists of the retina, choroid, vitreous humor, choroid, sclera and the optic nerve.

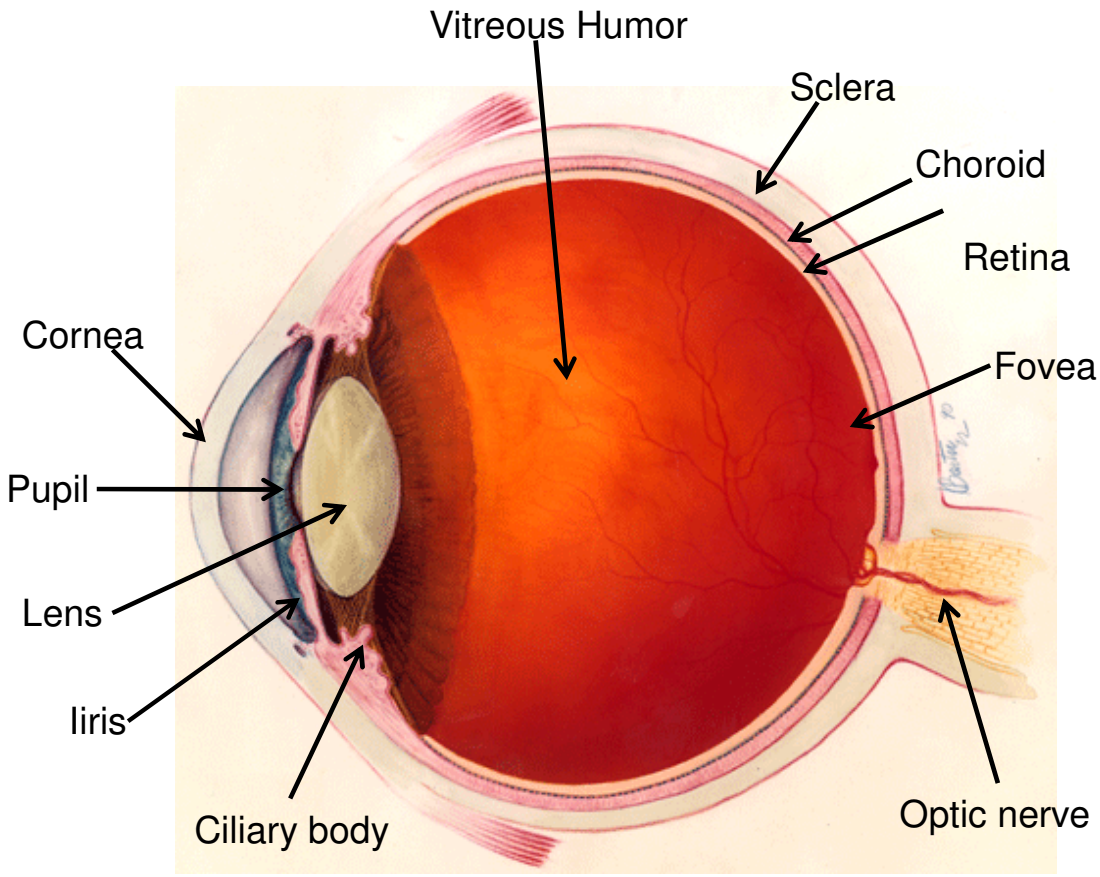

Figure 1-1: Cross-sectional view of the eye showing different anatomical regions.

Adapted from National Eye Institute, National Institutes of Health

1.1.1. Cornea

The cornea is the anterior most, clear, transparent membrane of the eye and acts as the principal refractive element of the eye. It has a refractive power of more than 40 diopters and accounts for 70% of the refractive power of the eye (1). The border between the sclera and the

cornea is called the limbus. Normal cornea is devoid of blood vessels. The peripheral parts of the cornea receive nutrition and oxygen from the capillaries of the limbal area. The rest of the cornea gets its nourishment and oxygen from the aqueous humor and tear film, respectively (1). The structure of cornea is complex (Figure 1-2) and is composed of five to six layers: the epithelium, Bowman's membrane, the stroma, Descemet's membrane, and the endothelium. The Bowman's membrane is absent in the rabbit cornea and is found only in the eyes of humans and other primates (1-3).

The epithelium, constituting about 10% of total corneal thickness, is the outermost layer of the cornea and plays a critical role in maintaining balanced stromal hydration and acts as a major barrier against xenobiotics, microorganisms, dust etc. It consists of five to six layers of cells which exhibit tight junctions. These layers can be further subdivided into one or two layers of flattened superficial cells with microvilli on their anterior surface, which helps to anchor the tear film and prevent the cells from drying, two to three layers of polygonal wing cells and a single layer of columnar basal cells. The Bowman's membrane is acellular in nature and is composed of a layer of collagen fibers and glycosaminoglycans which forms a relatively tight and impermeable barrier and protects the stroma (2-5).

The stroma contributes towards 90% of the corneal thickness and is composed of water, collagen fibrils, glycosaminoglycans and non-collagenous proteins. It is highly hydrophilic and porous in nature, and can be considered to be an open structure. On the interior surface of the stroma is the collagen rich Descemet's membrane which forms the basement membrane for the corneal endothelium (2-5). The endothelium, consisting of a single layer of hexagonal cells,

forms the innermost layer of the cornea facing the anterior chamber. It plays a major role in the maintenance of corneal hydration. Disruption of the endothelium may result in corneal edema (3, 4).

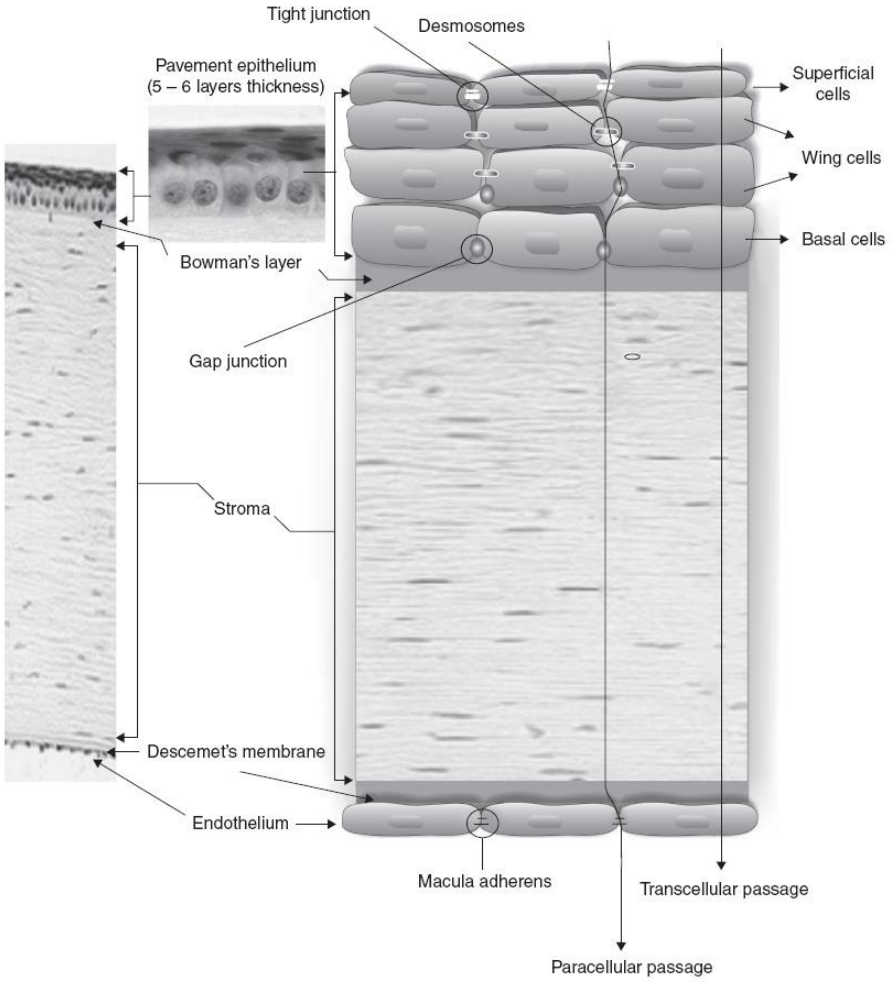

Figure 1-2: Cross-section of the cornea.

Reproduced with permission from Informa Plc., ref (6)

1.1.2. Conjunctiva

Conjunctiva is a thin, mucus membrane covering the inner surface of the eyelid and the visible part of the sclera. While primarily serving as a protective barrier for the eye, the conjunctiva secretes mucus which is believed to be essential for tear film stability and corneal nourishment. In rabbits and in humans, the conjunctiva surface area is nine and seventeen times larger, respectively, than that of the cornea (7). The conjunctiva differs from the cornea in that it is highly vascularized, and is capable of mucus secretion and transdifferentiation (7). The conjunctiva is composed of three sections: palpebral conjunctiva, bulbar conjunctiva and fornix conjunctiva (Figure 1-3). Palpebral conjunctiva lines the posterior surface of the eyelid and is covered with thick, opaque, red muscles. The bulbar conjunctiva, a thin semitransparent and colorless tissue, covers the eye ball over the sclera. The palpebral conjunctiva is firmly attached to the eyelids, while the bulbar conjunctiva is loosely attached to the underlying sclera and moves with the movements of eye ball (7). Fornix forms the junction between the eye lid and the eyeball, where the palpebral conjunctiva reflects to become the bulbar conjunctiva. The conjunctiva consists of goblet cells, which secrete mucin, and melanocytes.

The conjunctiva can be divided into three layers: the outer epithelium, a permeability barrier; the substantiapropria, which consist of nerves, lymphatics and blood vessels; and the submucosa, which provides a loose attachment to the underlying sclera (2). The outer epithelium is similar to the corneal epithelium in that it consists of superficial, wing and basal cells. However, the thickness of the conjunctiva varies from region to region; it is ten to fifteen layers thick towards the cornea and five to six layer thick at the lids. A greater number of wing cells are

present in the conjunctival epithelium when compared to corneal epithelium (7). The cells of the superficial layer, similar to that of the cornea, consists of dense microvilli covered with a glycocalyx and a mucin layer. The presence of tight junctions in the superficial conjunctival epithelium renders it a relatively impermeable barrier (2, 7). The basal cells layer consists of melanocytes and Langerhans' cells (1).

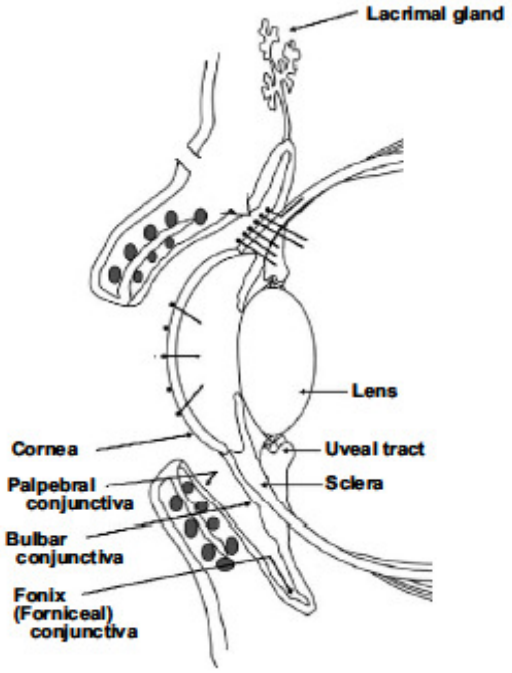

Figure 1-3: Schematic representation of Conjunctiva.

Reproduced with permission from Elsevier., ref (8)

1.1.3. Iris-ciliary Body

The iris is a thin, round, contractile membrane of the eye, suspended in the aqueous humor between the cornea and lens and is perforated by the pupil. The iris is continuous with the ciliary body at its periphery and the ciliary body and the iris together comprise the anterior uvea. The iris consists of the pigmented epithelial cell layer, the iridial sphincter and dilator muscles,

and the stroma (1, 4). It receives its blood supply from the major arterial circle, which lies in the stroma of the ciliary body near the iris root (2). Contraction and dilation of the sphincter and dilator muscles causes a decrease (mitosis) and increase (mydriasis), respectively, in the size of the pupil. The extent of melanin present in the stroma determines the color of the iris. The epithelial cell layer is absent on the anterior surface of the iris (1, 4).

The ciliary body comprises of the ciliary muscle and the ciliary processes (Figure 1-4). The ciliary muscle is smooth in nature and consists of longitudinal, circular and oblique muscles. The ciliary muscle helps in accommodation by altering the shape of the lens. When the muscles contract; the lens zonules relax, and the lens becomes more convex, increasing the eye's ability to focus on nearby objects. The ciliary processes are highly vascular and are formed by inward folding of the various layers of the choroid. The processes are covered by inner non-pigmented epithelium (facing the posterior chamber) and outer pigmented epithelium (facing the stroma of the processes). The non-pigmented epithelial cells are attached to each other by tight junctions and are primarily responsible for the production of aqueous humor (1). The ciliary body is the main target of anti-glaucoma drugs acting through the mechanism of decreasing aqeous humor production and thus reducing the intraocular pressure.

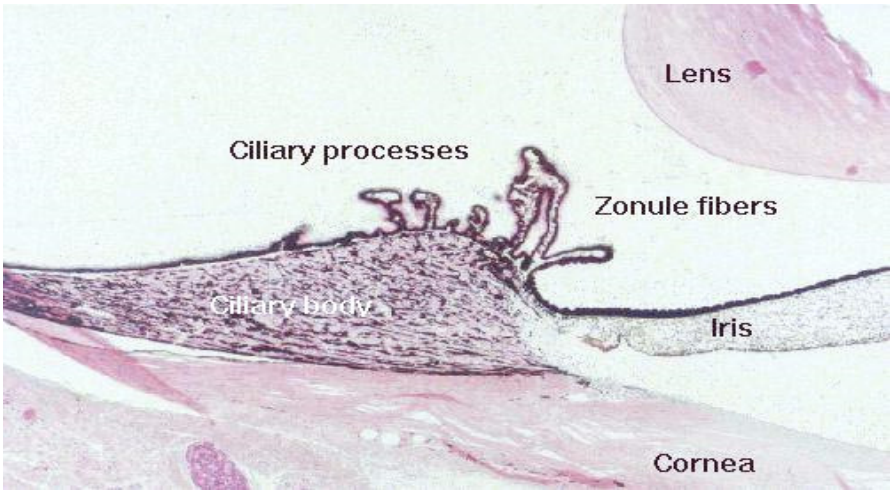

Figure 1-4: Ciliary body structure.

Reprinted with permission from http://education.vetmed.vt.edu/Curriculum/VM8054/EYE/UVEA.HTM (August 11 2010)

1.1.4. Aqueous Humor

The void between the lens, ciliary body process and the iris is called the posterior chamber, while that between the iris, the chamber angle and the cornea is called the anterior chamber (Figure 1-5). Both chambers, which together have a volume of 200-300µL, are filled with a clear, watery fluid known as aqueous humor (3). The aqueous humor is devoid of cells and is rich in ascorbic acid, chloride and lactates. It consists of very little proteins to avoid light scattering (1, 4, 9). The main functions of the aqueous humor includes nourishment (glucose and amino acids) of the avascular tissues of the eye such as the cornea, the trabecular meshwork, the lens and the anterior vitreous, elimination of metabolic products (lactate) from surrounding structures, and maintenance of intraocular pressure (1, 3, 4).

The aqueous humor is produced, at a rate of 2-3 µL/min, by the non-pigment epithelium of the ciliary processes by ultrafiltration and is secreted into the posterior chamber. It enters the

anterior chamber through the pupil and exits the eye via the trabecular meshwork into the Schlemm's canal, which empties the aqueous humor into the veins under the conjunctiva (Figure 1-5). Most of the aqueous humor leaves the eye through the trabecular meshwork known as the conventional pathway. However, some of the aqueous humor leaves the eye through the ciliary body into the supraciliary and suprachoroidal space and finally exits through the sclera pores. This route is referred to as uveo-scleral or non-conventional outflow pathway (1).

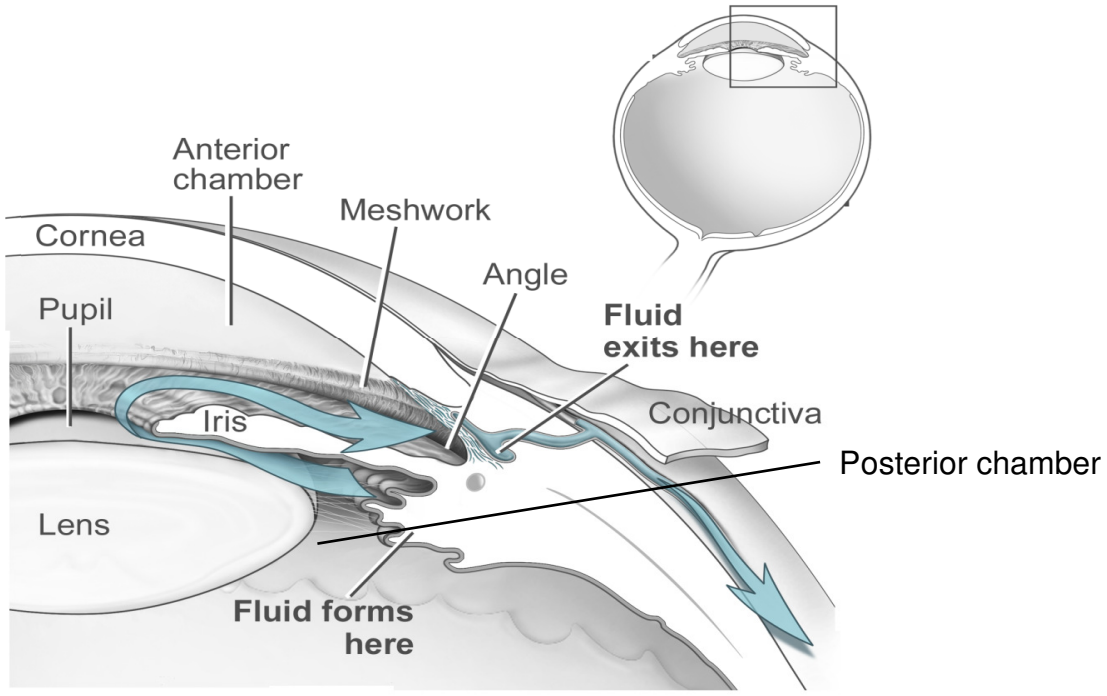

Figure 1-5: Cross-sectional view of the eye showing production and elimination of aqueous humor fluid.

Adapted from National Eye Institute, National Institutes of Health

1.1.5. Lens

The lens is a transparent, biconvex structure of the eye that is situated behind the iris and in front of the vitreous. It contains 65% water and the remainder is comprised of proteins. The anterior surface of the lens which is directly in contact with the aqueous humor is less curved than the posterior surface. The lens is flexible and its curvature is controlled by the ciliary muscle through the zonules. Lens, by changing its curvature, refracts light to help focus the image on the retina for proper visual sensation (1, 2).

The lens has three major components: the lens capsule, the lens epithelium and the lens fiber (Figure 1-6). The lens capsule forms the outermost layer of the lens and encloses the epithelium and lens fiber cells. It is cellular, transparent and elastic in nature and is mainly composed of type IV collagen and glycosaminoglycans. The lens epithelium consists of monolayers of cuboidal cells located in the anterior portion of the lens, between the lens capsule and lens fibers (1, 2). The epithelium regulates most of the homeostatic functions of the lens (10). The lens fiber forms the bulk of the lens. These fibers are formed from the differentiation of epithelial cells. Since the lens does not shed any cellular components, the older layers of the fiber cells are displaced towards the center or nucleus of the lens. The fiber cells peripheral to the nucleus form the lens cortex (1, 2, 4).

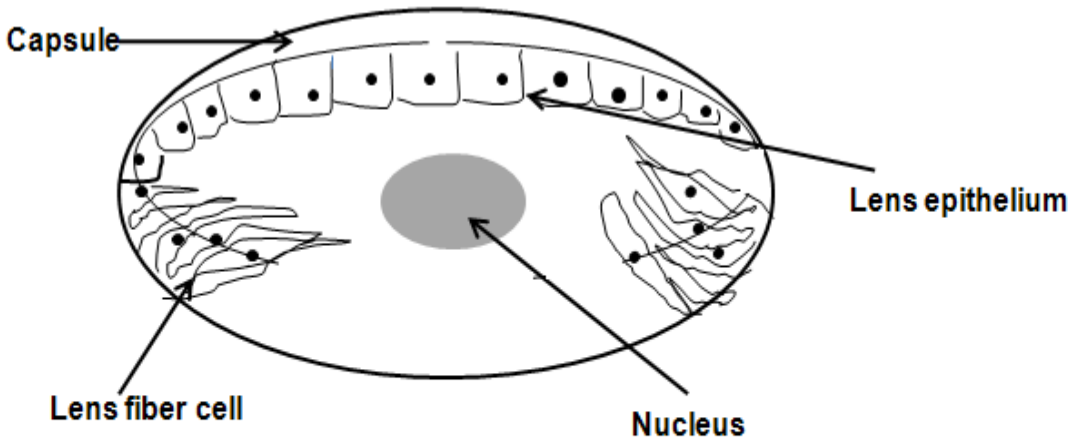

Figure 1-6: The Lens.

1.1.6. Sclera

Sclera or the white of the eye is the outermost tunic of the eye and protects the sensitive intraocular tissues as well as the cornea. It has a 17-fold larger surface area compared to that of the cornea (11). The sclera thickness varies with age, species, and as a function of distance from the limbus. The mean thickness of the human sclera is reported to be 0.53 mm at the limbus, 0.39 mm at the equator and 0.9-1.0mm near the optic nerve. These thicknesses are subject to great variation, with equatorial thickness frequently below 0.1 mm (12, 13).

The composition of the sclera is similar to that of the corneal stroma. However, the fibers in the sclera are arranged in an irregular network making it opaque (5). The sclera is composed of collagen bundles and some elastic fibers which form a fine network with fibroblast and melanocytes. The sclera does not present much of a diffusional barrier to drug molecules (1, 4, 12-15).

1.1.7. Choroid

The choroid is a thin, soft, spongy and highly vascularized membrane located between the retinal pigmented epithelium and the sclera. It provides nourishment and oxygen to the outer layers of retina (16). Anteriorly, the choroid continues into the ciliary body and iris, and ends posteriorly at the optic nerve. Along with the iris and the ciliary body the choroid forms the uveal tract. The choroid can be divided into four or five layers. The epichoroid or suprachoroid is the outermost layer of choroid facing the sclera. It consists of a thin elastic collagen fiber network, fibroblasts and melanocytes. The space within the suprachoriod layer and fibers is known as the suprachoroidal space. This space plays an important role in aqueous humor dynamics. The aqueous humor that leaves the eye via the non-conventional route ends up in the supracholroidal space from where it drains out through the scleral pores. The vascular layer is the thickest layer of the choroid and consists of veins and arteries of medium and large size embedded in loose connective tissues. The choriocapillary layer is a single layer of very thin and densely packed fenestrated capillaries. The capillaries are leaky and permeable to plasma proteins and colloids. The innermost layer of the choroid is the five layered Bruch's membrane. The Bruch's membrane consists of the basal lamella of the retinal pigmented epithelium, endothelial cells of choriocapillaries, and collagen and elastic fibers(1, 17).

1.1.8. Retina

The retina is the light-sensitive tissue lining the inner posterior surface of the eye. The retina consists of two major sections: the neural retina and the retinal pigmented epithelium (1). The neural retina is a multilayered structure and is involved in light transduction. It consists of

the photoreceptor layer, outer limiting membrane, outer nuclear layer, outer plexiformlayer, inner nuclear layer, inner plexiform layer, ganglion cell layer, nerve fiber layer and inner limiting membrane. Large retinal vessels are present in the optic nerve fiber layer and retinal capillaries are present in between the inner nuclear layer and the outer plexiform layer (2) (Figure 1-7).

The photoreceptor layer faces the retinal pigmented epithelium and is composed of the rods and the cones. The macula is situated laterally to the optic nerve head and the center of the macula is the avascular fovea which contains only cones. The photoreceptors are connected to the bipolar neurons, through complex horizontal neurons, that are coupled to the ganglion cells of the retina. The axon of the ganglion cells extend into the optic nerve. The amacrine neurons connect to the vertical neural pathway at the level of bipolar and ganglion cells (1). Light enters the retina through the ganglion cell layer and reaches the photoreceptor layer. The transduced signals from the photoreceptor layer are then conducted out to the optic nerve, through various neurons described above, and into the brain where it is registered in the form of images (4).

The retinal pigmented epithelium (RPE) is a monolayer of cuboidal epithelial cells, connected by tight junctions, between the photoreceptor layer and the choroid. The human RPE consists of 3.5 million epithelial cells arranged in a continuous hexagonal pattern extending through the entire retina. The RPE cells can be differentiated into an apical portion, facing the photoreceptors, and a basolateral portion, facing the choroid. The apical portion consists of long microvilli that integrate with the outer segment of the rods (4, 18). The RPE plays a vital role in the removal of the tips of the outer segment of the photoreceptors, storage and metabolism of Vitamin A, production of cytokines necessary for retinal development and survival, and acts as barrier to the transport of xenobiotics(18).

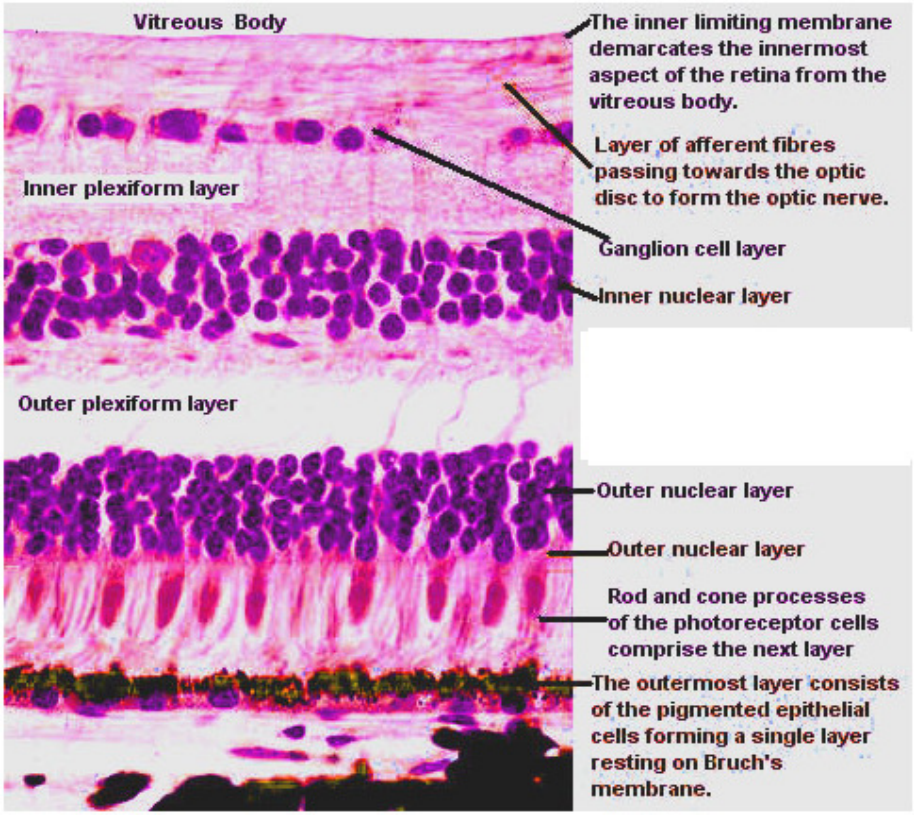

Figure 1-7: Cellular organization of retina.

Reprinted with permission from http://www.surgical-pathology.com/retina_image.htm. (August 11 2010)

1.1.9. Vitreous Humor

The vitreous humor is a clear gel which fills the space between the lens and the neural retina lining the back of the eye. It is also known as the vitreous body and occupies about 80% of the volume of the eye. It is attached to the retina by ligaments and is separated from the lens capsule and the posterior chamber by the anterior hyaloids membrane (1). The vitreous humor mainly consists of water (99%). The remainder consists of small amount of glycosaminoglycans, chondroitin sulfates, collagen, hyaluronic acid, inorganic salts, sugar and ascorbic acid. The pH

of vitreous humor is approximately 7.5. In contrast to the aqueous humor, which is continuously produced in adults, no new vitreous humor is produced. It is static in nature and small drug molecules or solutes transport in vitreous body occurs via diffusion (1, 4, 19).

1.2. Barriers in Ocular Drug Delivery

The external surface of the eye is readily accessible for drug administration. However, the eye is very well protected from the external environment and the systemic circulation by various physiological and anatomical barriers. The major role of these barriers is to protect the ocular cells from harmful toxic substances. However these barriers through their protective action, also drastically diminish the amount of drug permeating across the epithelial cell layers which results in low ocular bioavailability. Additionally, these barriers are unique and specific to the route of administration viz. topical, systemic, intravitreal and transscleral. Figure 1-8 is a schematic representation of different routes of drug administration to eye.

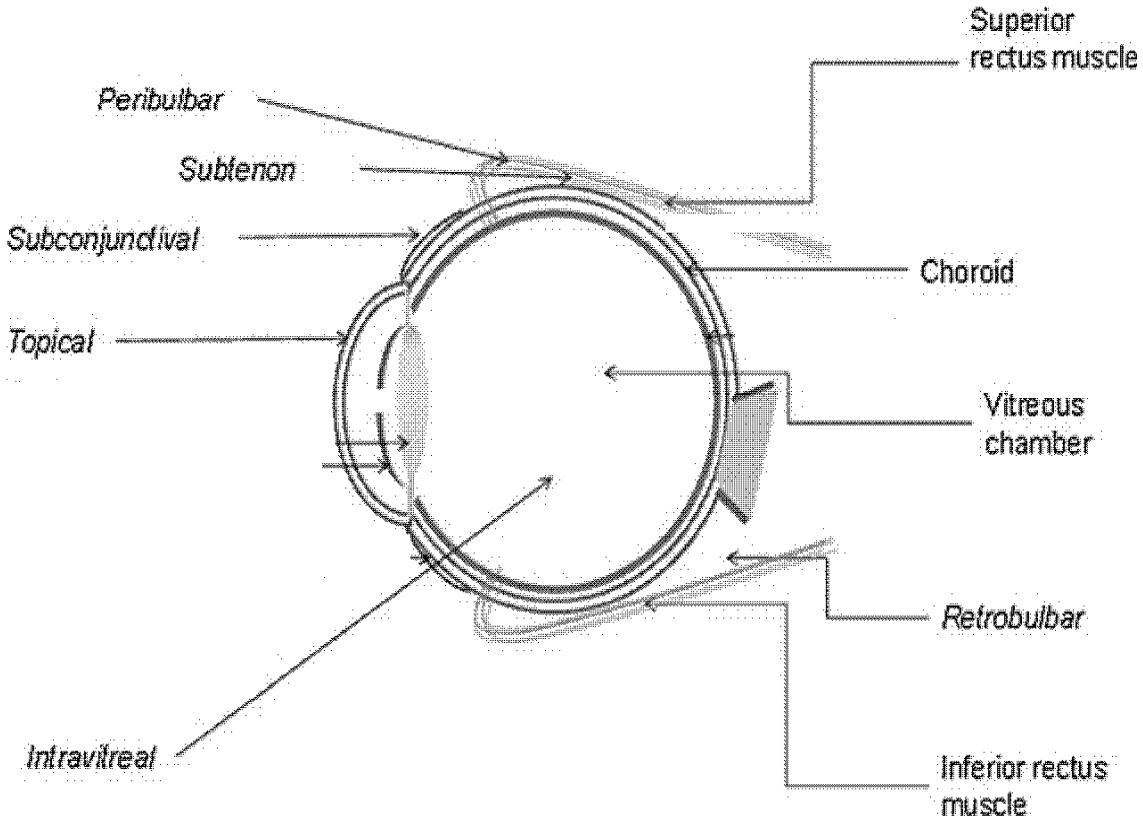

Figure 1-8: Route of drug administration to eye.

Reproduced with permission from Springer., ref (20)

1.2.1. Topical administration

Topical administration of eye drops into the lower cul-de-sac is the most patient preferred method to treat ocular disorders. This route of administration presents a number of potential advantages: (i) a convenient, self-administrable, inexpensive and noninvasive method of administration; (ii) drug effects are localized and decreases systemic exposure; and (iii) it avoids hepatic first-pass metabolism in the liver. However, despite proven advantages, a major problem in topical ocular therapeutics is attainment of optimal drug concentration at the site of action. It

is estimated that the intra-ocular bioavailability of topically applied drug is only 1-10%. This poor ocular bioavailability of drugs is mainly attributed to precorneal barriers, non-productive conjunctival absorption, permeability barrier imposed by the cornea, and inherent physiochemical insufficiencies of the drug molecule. To achieve therapeutic drug concentrations in the ocular tissues these challenges need to be overcome.

1.2.1.1. Pre-corneal barriers

Following topical administration, the ophthalmic drug solution will mix with the tear fluid and get dispersed over the ocular surface. However, various pre-corneal barriers such as drainage of the instilled solution, lacrimation and tear dilution and tear turnover, limit the ocular bioavailability of the drugs (Figure 1-9).

The volume dispensed by most commercial ophthalmic eye drop dispensers is approximately 50 µL. However, the maximum quantity of fluid that the lower conjunctival cul-de-sac can hold without overflow or spillage onto cheeks is about 30 µL. Thus, approximately 20 µL of drug solution is lost due to instillation of excess volume. Following removal of the excess solution the natural tendency of the cul-de-sac is to reduce the volume to 7-10µL, which is the normal resident volume of tears in the cul-de-sac (21). A major part of the remaining instilled drug is quickly removed from the cul-de-sac into the systemic circulation, which can cause some systemic side effects, through the nasolarcimal duct into the highly vascularised inferior nasal passage. This nasolacrimal drainage is facilitated by the pumping action of the canaliculi associated with the blink movements. The second mechanism that efficiently clears the remaining drug solution from the cul-de-sac is continual turnover of the tear film. The pre-

corneal tear film is the first structure encountered by topically applied agents. The tear film is continuously produced and secreted, by lachrymal and conjunctival glands, at a rate of approximately 1-2 µL/min, which equates to a 16% turnover of the tear film per min. Secretion of tear and its spreading across the surface of the eye by blinking ensures constant bathing of the corneal and conjunctival membrane and protects these tissues from drying. Additionally, the tear film helps in the elimination of cellular debris and foreign substances and in maintaining a smooth refractive surface over the cornea. However, the continual turnover of the tear film also washes away the instilled drug, through the nasolacrimal drainage, minimizing the duration of drug exposure.

In addition to dilution of the instilled drug solution, which reduces the transcorneal flux of the drug remaining in the cul-de-sac, the tear film also acts as a barrier to the penetration of the molecules into the ocular tissues. Tear film has a trilammelar structure. The outer layer, secreted by the meibomian glands, is an oily layer and consists of various waxes, esters, free fatty acids and sterols. The middle layer is an aqueous layer and contains inorganic salts, glucose, urea, proteins and biopolymers. It is secreted by the lachrymal gland and the accessory glands of Krauss and Wolfring. The inner layer is called the mucus layer, consisting of glycoproteins, and is produced by the conjunctival goblet cells and the lachrymal glands (3). Therefore, drug molecules need to demonstrate an optimum hydrophilic and lipophilic balance to traverse the tear film efficiently. Other physiological factors that affect ocular delivery of topical drugs are protein binding and drug metabolism. Normal tear film consists of 0.6-2 % of proteins, which may increase in diseased states. Major components include albumin, globulin and lysozyme. Binding of drug to the proteins renders it unavailable for ocular absorption and will be

removed from the eye through nasolacrimal drainage (22, 23). Additionally, tears consist of enzymes such as esterases, monoamine oxidase and aminopeptidases which can significantly metabolize the therapeutic agents and thus decrease ocular bioavailability (22).

1.2.1.2. Conjunctival barrier

The fraction of the instilled drug that does not get immediately expelled from the ocular surface reaches the deeper ocular tissues either by the corneal route or the non-corneal route (Figure 1-9). The non-corneal route of absorption involves penetration across the conjunctiva and underlying sclera into the cornea and aqueous humor, uveal tract and vitreous humor. Conjunctiva is a highly vascularized, thin, mucous membrane lining the inside of the eyelids and anterior sclera. It is an important competitive route covering five-sixth of the total surface area of the eye ball. The conjunctival surface area is about 9 to 17 times greater than the surface of the cornea in rabbits and in humans, respectively (24). The tight junctions of the superficial conjunctival epithelium are the main barriers to the penetration of drug molecules across the cornea. However, the paracellular spaces are wider and leakier than those of the corneal epithelium (25). Therefore, the permeation of hydrophilic and large molecules such as inulin (MW 5000) and FITC dextran (MW 20000) across the conjunctiva is significantly greater than that across the cornea (24-27). Additionally, many studies have shown that conjunctival permeation is significant for compounds with poor corneal permeability, such as gentamycin, bimatoprost and prostaglandin PGF2-ALPHA, peptides and oilgonucleotides (6, 28, 29). However, transconjunctival penetration is generally undesirable because the conjunctival membrane is richly perfused with blood vessels and lymphatics and a major portion of the

topically applied agent is rapidly removed into the systemic circulation (3, 6, 20, 28, 29). Additionally, several carrier proteins such as nuclesoside, glucose and amino acid transporters expressed by the conjunctival cells removes drug molecules from the ocular surface into the systemic circulation and aids in precorneal clearance (4, 30-33). Therefore, this non-corneal route is considered to be non-productive for most ophthalmic drugs, reducing the fraction available for corneal absorption (34).

1.2.1.3. Corneal Barrier

In addition to the precorneal and conjunctival constraints, the major limiting step in the penetration of topically administered therapeutic agents into the inner layers of the eye is the diffusion across the cornea. The cornea is the main route of penetration of ophthalmic agents into the intra-ocular tissues (Figure 1-9) (3, 26, 34, 35). However, the small surface of the cornea, its relative impermeability and complex structure render the cornea a formidable barrier to topical drug delivery (34). The cornea is composed of the outermost epithelium, Bowman's membrane, stroma, Descemet's membrane, and inner endothelium. Descemet's and Bowman's membrane do not present a significant barrier to drug permeation (36). The epithelium and the stroma are the most significant barriers. The outer epithelium makes up 90% of the total cells of the cornea and is lipophilic in nature. On the other hand, the underlying stroma consist of 90% of water and is hydrophilic in nature (37). The epithelium is the primary barrier to corneal permeation of hydrophilic drugs while for lipophilic drugs partitioning form the epithelium into the hydrophilic stroma is the rate limiting step (38). Additionally, the epithelial cells are tightly bound just below the apical surface by cell adhesion proteins forming tight junctions. These tight junctions,

composed of occludins, Z0-1 and Z0-2 proteins, in a regulated manner acts as the principal barrier to passive movement of fluid, electrolytes, macromolecules and drugs through the paracellular pathway (39). The monolayer of endothelium with large intercellular junctions does not restrict the passage of hydrophilic compounds; however, it may play a small role in determining the permeability of lipophilic compounds (36).

1.2.1.3.1. Barriers and factors determining corneal permeation:

High corneal permeability is important in the development of new therapeutic compounds and delivery strategies. Physiochemical characteristics such as lipophilicity, aqueous solubility, molecular size and shape, and charge and degree of ionization, act as the major determininants of the rate and the route of permeation across the cornea (5, 37).

Passive diffusion along a concentration gradient, either transcelllulary or paracellularly, is the main mechanism of permeation across the cornea for most of the topically applied drugs (Figure 1-2). Occasionally, carrier-mediated active transport mechanisms, utilizing transporters expressed on the corneal epithelium, is involved (40). Lipophilic drugs prefer the transcellular pathway. Hydrophilic drugs penetrate primarily through the paracellular pathway through the intercellular spaces (41). For a compound to be effective topically, it must possess sufficient aqueous solubility and at the same time exhibit sufficient lipophilicity for efficient permeability across the cornea. The corneal membrane contains both hydrophilic and lipophilic layers. A highly lipophilic drug will be entrapped in the epithelial layer while a hydrophilic compound will not be able to diffuse across the lipoidal epithelial layer. Parabolic (24, 42, 43) and sigmoidal curves (24, 44) have been reported to describe the influence of lipophilicity on corneal drug

permeability. The optimum range for the octanol/buffer pH 7.4 partition coefficient (log P) for corneal permeation is in the range of 2-3, which is consistent with the lipophilic nature of the corneal epithelium (24). Aqueous solubility of the therapeutic agents must also be sufficient to enable the formulation of aqueous eye drops. In addition, the surface of the eye is constantly bathed with lachrymal fluid. If the drug molecule is not soluble in the tear film it is unavailable for ocular absorption, except in nano drug delivery systems where endocytosis is considered as a major mechanism by which the drug accesses the intraocular tissue. Therefore, ideal potential ophthalmic agents should maintain a balance between water solubility and lipid solubility (38, 45, 46).

Weakly acidic and weakly basic drugs are capable of existing in both unionized and ionized forms and the ionization state of these drug molecules can affect its permeability across the corneal epithelium. The unionized drug usually permeates the lipophilic corneal membrane more easily than the ionized form. The ratio of ionized to unionized drug will depend on the pKa of the molecule and the pH of the formulation and the lachrymal fluid. Therefore, drugs formulated at a pH which provides a higher concentration of unionized drug usually shows higher corneal permeation. The nature of the charge as well as the degree of ionization will affect the corneal permeability of ionizable drugs. The cornea is negatively charged above its isoelectric point (pI 3.2). Thus, cationic drug molecules permeate the cornea more easily than the anionic species. Below the isoelectric point, the cornea is selective to negatively charged drugs, however, this pH would be too acidic and irritating to use in a clinical setting (22, 24, 47).

The molecular size of the drug molecules also affects corneal permeation. The cornea is an effective barrier to compounds larger than 10A because these molecules cannot cross the

corneal membrane at any significant rate (37, 48). Apparently, there is no dependence of permeation on the molecular radius of the drug molecules; however, for macromolecular peptides a trend is observed with increasing molecular size (37, 49).

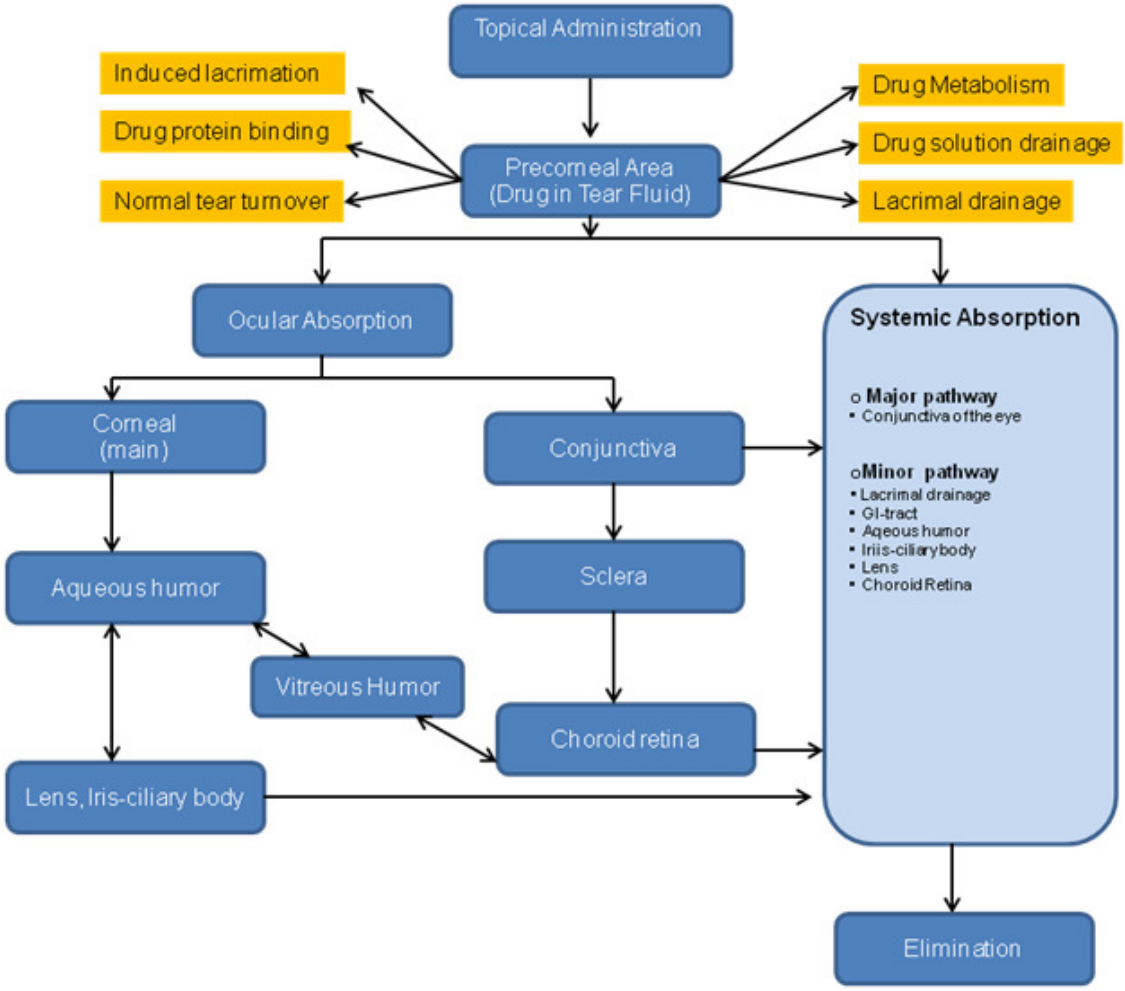

Figure 1-9: Absorption, distribution and elimination pathways for topically administered drugs.

1.2.2. Systemic administration

Systemic administration is the preferred route of administration when topical drug administration fails to establish and maintain therapeutic concentrations for treatment of some of the ocular disorders. Drugs such as steroids and nonsteroids are generally administered systemically for the treatment of uveitis and scleritis, acetazolamide for macula edema, and antivirals and antibiotics for prophylaxis or therapy of chorioretinitis and endophthalmitis. Additionally, application of systemic therapy includes thalidomide for the treatment of proliferative disease, antioxidants for the protection against macular degeneration, and the use of neuroprotective agents in patients with glaucoma (50). However, only a very small fraction of the systemically administered drug reaches the ocular tissue due to the presence of blood-ocular barriers (51). Blood-ocular barrier consists of two components: (i) blood-aqueous barrier (BAB), and (ii) blood-retinal barrier (BRB) (52).

1.2.2.1. Blood-aqueous barrier (BAB)

The BAB is located in the anterior part of the eye. It is formed by two discrete layers of cells, the endothelium of the iris/ciliary blood vessels and the non-pigmented ciliary epithelium. Both cell layers express tight junctions which prevents unrestricted diffusion of drug molecules into the aqueous humor from the systemic circulation (53). Additionally, the outward movement of drug molecules from the aqueous humor into the iris blood vessels, and then into the systemic circulation, is less restricted. The iris is porous in nature and agents dissolved in the aqueous humor, especially small molecules, can freely diffuse across its anterior surface and enter into the

uveal blood circulation via the blood-aqueous barrier from where they are rapidly removed into the blood circulation. Large hydrophilic molecules are removed by the continuous outflow of aqueous humor through the canal of Schlem (51).

1.2.2.2. Blood-retinal barrier (BRB)

The BRB is located in the posterior part of the eye and comprises of the outer and inner BRB's. The inner BRB is formed by the endothelial cells lining the lumen of the retinal blood vessels (blood vessels penetrating into the retina) and the outer BRB is formed by the retinal pigmented epithelial (RPE) cells (52, 54).

The inner BRB covers the lumen of the retinal capillaries and selectively protects the retina from circulating molecules in the blood. Unlike capillary endothelium in most tissues, retinal endothelial cells do not exhibit fenestrations and express intercellular tight junctions in a regulated manner which restricts passive paracellular diffusion. Additionally, similar to blood-brain barrier, the inner BRB has been reported to consist of astrocytes and pericytes in close apposition to the basal lamella of the retinal blood vessels. A combination of these cellular structure and functions enable retinal endotheial cells to form the inner BRB (4, 54). RPE is a monolayer of highly specialized cells which separates the outer surface of the neural retina from the Bruch's membrane (55). In contrast to the retinal blood vessels, the choroidal vasculature possesses large fenestrations and pinocytic vesicles that allow unrestricted movement of endogenous/exogenous substances into/out of the choroidal stroma (52, 56, 57). Bruch's membrane (basement membrane seprating choroid from the RPE) acts as a diffusional barrier only to macromolecules like proteins, oligonucleotides and genes. The RPE, however, due to the

presence of tight junctions presents a formidable barrier to the permeation of small hydrophilic drug molecules into the retina from the choroid (53). Additionally, P-glycoprotein, an efflux pump, acts as a barrier to the diffusion of hydrophobic molecules across the RPE. Thus, the outer BRB and inner BRB collectively form the BRB and acts in conjunction to restrict the exchange of molecules between the blood and vitreous chamber. These physiological mechanisms, while protecting the ocular structures from xenobiotics, make drug delivery to the back-of-the-eye an extremely challenging task.

1.2.2.3. P-glycoprotein (P-gp)

P-gp, a 170-kDa membrane bound efflux protein, is able to decrease uptake or increase efflux of a variety of structurally, mechanistically, and functionally unrelated hydrophobic xenobiotics. Various mammalian tissues, e.g. lungs, brain endothelial cells, liver, epithelial lining of the proximal kidey tubules, and intestinal enterocytes express this efflux proteins. P-gp belongs to the ATP-binding cassette super-family. ATP binding and subsequent hydrolysis is essential for the functioning of P-gp (58-60). It is encoded by the MDR1 gene in humans whereas in mice two genes mdr1a and mdr1b encode these proteins (61). P-gp is expressed as a single polypeptide consisting of 1280 amino acid residues that are arranged in two structurally similar domains Tansmembrane domains (TMD) of 610 amino acids, joined by a 60 amino acid segment referred to as the linker region (62). Each domain consists of an NH2-terminal with six transmembrane α-helices, separated by three hydrophilic loops. The two halves of P-gp interact to form a single transporter. These TMD are believed to form the transmembrane pathway through which solutes cross the membrane and plays a major role in determining substrate

specificity. Each hydrophobic transmembrane domain is followed by the hydrophilic nucleotide-binding domain (NBD) which is located at the cytosolic surface or the plasma membrane. The NBD contains the ATP binding site and couples ATP hydrolysis to the transport process (63) (Figure 1-10).

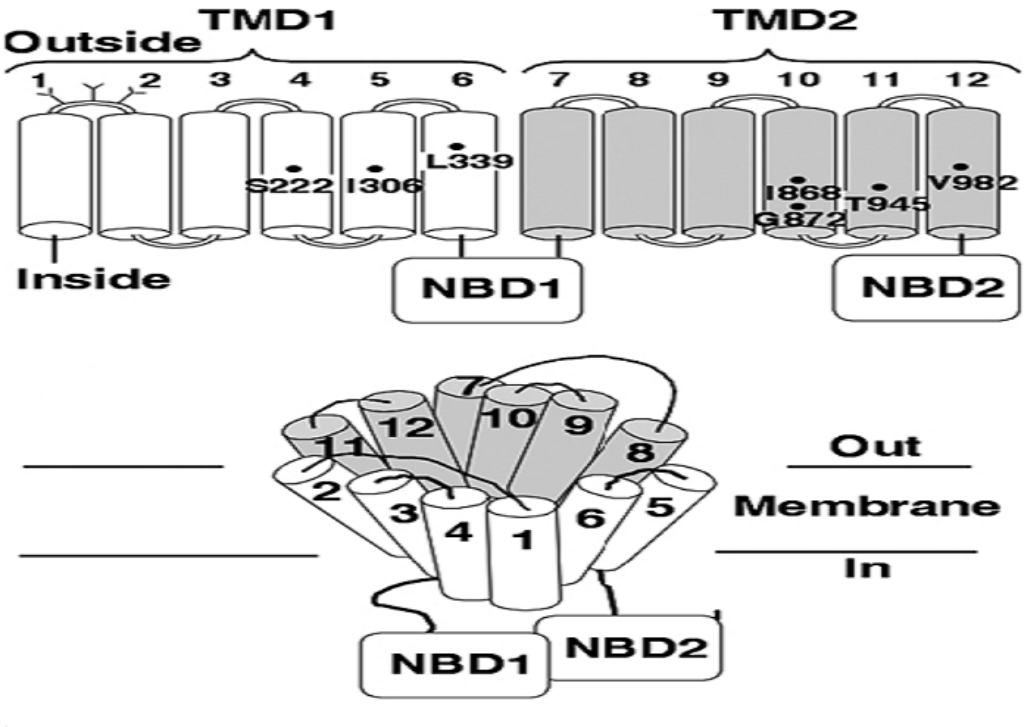

Figure 1-10: Structure of P-gp.

Reproduced with permission from Springer., ref (64)

Mechanism of action of these proteins is still controversial. Several models such as the "aqueous pore model", the "vacuum cleaner model" and "flippase model" have been proposed to explain their involvement in multidrug resistance (60). According to the aqueous pore model, following passive diffusion of molecules across the cell membrane, they may be recognized by P-gp and exported back across into the extracellular space, in association with ATP hydrolysis,

through the formation of a hydrophobic channel (pore) between the intracellular and extracellular space (60, 65). The vacuum cleaner model suggests that the lipid soluble drug interacts with P-gp with in the lipid bilayer and is subsequently expelled into the extracellular space without entering the cytoplasm (65, 66). On the other hand, fillpase model proposes that the drug after entering the cytoplasm is flipped from the inner leaflet to the outer leaflet of the cell membrane (60, 67).

1.2.2.3.1. Contribution of P-gp to the barrier properties of the RPE for systemic administration

P-gp expressed on the RPE is a vital component of RPE's barrier properties (68-71). This protein is expressed on the apical and basal membranes of the RPE and is responsible for the efflux of substrates back into the extracellular space. The physiological role of this efflux protein is to protect cells from harmful toxic substances by maintaining sub-therapeutic intracellular drug concentrations at the target site. However, P-gp, through its protective action, also drastically diminishes the amount of drug permeating across the epithelial cell layers, which results in low bioavailability of substrates. P-gp displays broad substrate specificity, accepting many structurally dissimilar compounds including HIV protease inhibitors, steroids, calcium channel blockers and anticancer, cardiac and anti-fungal agents, as substrates (72). The RPE is perhaps unique in that P-gp is expressed on both apical (facing the neural retina) as well as basal (facing the choroid) membranes of the RPE cells (69). Generally, P-gp is expressed on the apical membrane of epithelial cells preventing drug transport from the lumen into the systemic circulation (e.g. intestinal epithelium) or from the systemic circulation into the brain (endothelial cells of BBB). Considering the unique distribution of P-gp in the RPE cells, P-gp mediated efflux may restrict systemic to vitreous as well as vitreous to systemic permeation of substrates.

Since most of the chemotherapeutic agents are substrates of P-gp, diffusion of these agents from the systemic circulation into the neural retina is severely restricted. Thus, a possible reason for the inability of the systemic route to generate therapeutic drug concentrations in the retina is the interaction of these efflux proteins with its substrates.

1.2.3. Intravitreal administration

Intravitreal injection involves direct application of therapeutic agents into the vitreous body through the pars plana. This mode of administration avoids all the barriers encountered with topical and systemic administration and is the most effective route of delivery for the posterior chamber of the eye. This mode of administration is, thus, currently the most acceptable and effective method to treat vitreoretinal diseases. Anti-VEGF drugs such as pegaptanib, ranibizumab and becavizumab are new intravitreal treatments for age related macular degeneration (AMD) and macular edema (73). Additionally, intravitreal antibiotics such as vancomycin and ceftazidime are a main-stay for the treatment of bacterial endophthalmitis (74).

Although, effective, rapid elimination of the drug form the vitreous humor, in most cases, necessitates frequent administration of intravitreal injections (2-3 times a week) to maintain therapeutic efficacy of the drugs (75). Frequent injections are associated with risks such as retinal detachment, retinal hemorrhage, endophthalmitis and other retinal toxicities and patient incompliance (75). Following intravitreal administration the drug is eliminated from the vitreous by a first order process through either anterior or posterior routes. Anterior route involves diffusion of drug across the vitreous to the posterior chamber followed by elimination through aqueous turnover and uveal blood flow. On the other hand, posterior route involves drug

permeation across the blood-retinal barrier into the systemic circulation (76, 77). P-gp, an efflux pump, expressed on the RPE plays an important role in the elimination of substrates from the vitreous humor. Therefore, strategies that can increase the half-life of such P-gp substrates, which includes a wide range of therapeutic agents, in the vitreous humor could significantly enhance the therapeutic efficacy and thus lead to decreased frequency of administration and hence lower associated risk.

1.2.4. Transscleral administration

Transscleral route of administration includes subconjunctival, subtenon, retrobulbar and peribulbar injections (Figure 1-8). Table 1 represents the site of application of these injections (73, 75).

Table 1-1: Site of Application of Transscleral Injections.

Injections	Site of Application
Subconjuctival	• Drug is injected beneath the conjunctiva
Sub-tenon	• Injection of drug into a fascial sheet of connective tissue between the conjunctiva and episcleral plexus.
Retrobulbar	• Deposition of drug solution in between the inferior and lateral rectus muscles (retrobular space), and the needle is directed in the retrobulbar space within the muscle cone
Peribulbar	• Injection in the inferiorlateral quadrant of the orbit. • Further classified intocircum-ocular (sub-tenon's, episcleral); peri-ocular (anterior, superficial); peri-conal (posterior, deep) and apical (ultra deep); depending on the depth of needle.

Transscleral administration is less invasive and eliminates some of the adverse effects associated with intravitreal administration (73). However, this route of administration has its own risks and complications. Reterobulbar injections are associated with the highest number of complications such as blood vessel laceration, globe perforation, orbial hemorrhage, diplopia, artery occlusion and brainstem anesthesia. The limitations associated with peribulbar delivery are similar to retrobulbar but the risk of injury to intraorbital structures is lower (73). Swelling of the conjunctiva or chemosis and subconjunctival hemorrhage are complications associated with sub-tenon injections (78).

Furthermore, following transscleral administration static and dynamic barriers limit the entry of the drug into the vitreous/neutral retina. Static barriers include the choroid and the RPE. Dynamic barriers include choroidal blood and lymphatic flow, and efflux proteins expressed on the RPE (73, 79). The sclera does not present a major diffusional barrier and is more permeable than the cornea However, in contrast to the conjunctiva and the cornea, the permeation across the sclera is independent of lipophilicity, but rather depends on the molecular radius (20). Blood vessels and lymphatics in the choroid, however, lead to rapid drug elimination. Retinal access of the remaining fraction, which escapes the choroidal circulation, into the neutral retina is further restricted by the RPE. Additionally, P-gp, an efflux pump, expressed by the RPE cells restricts permeation of substrates into the neutral retina (20, 79). Therefore, strategies that can modulate the activity of P-gp expressed on the RPE could significantly enhance the therapeutic efficacy of transclerally administered drugs.

1.3. Strategies to Overcome Ocular Barriers

1.3.1. Topical administration

1.3.1.1. Hydrophilic drugs

Topical instillation of an active compound is the first choice for ocular diseases and more that 90% of the currently marketed ophthalmic formulations are developed in the form of eye drops (80). Topically applied hydrophilic drugs, which can be formulated in the form of eye drops, have to reach the inner parts of the eye through the paracellular route of the corneal epithelium to elicit response. However, the tight junctions expressed across the intercellular spaces of the corneal epithelium serves as the selective and primary diffusional barrier for hydrophilic agents. The underlying stroma and endothelial layer do not present any significant challenge to the corneal penetration of hydrophilic moieties.

In the past a number of strategies have been investigated attempting to increase corneal penetration of topically instilled hydrophilic compounds. Approaches such as the use of viscosity enhancers (e.g. cellulose derivatives), mucoadhesive polymers (e.g. hyaluronic acid, hydroxypropyl cellulose, carboxymethyl cellulose, poly acrylic acid derivatives) and in situ gel-forming agents have been used to minimize precorneal drug loss (81, 82). However, factors such as lachrymal duct blockage, increased tear turnover and corneal irritation have constrained the effectiveness of these approaches. Additionally, these approaches do not address the basic problem of poor corneal permeation of hydrophilic molecules. To maximize corneal permeation, strategies such as use of absorption promoting agents and lipophilic chemical modification

through prodrug derivatization have been investigated. However, side effects of the absorption enhancers limit the effectiveness of this strategy. Repeated application of 0.5 % ethylenediaminetetraacetic acid was observed to significantly alter the corneal epithelial architecture (83). Azone (0.1%) and saponin (0.5%) has been reported to be irritating, discomforting and toxic to the eye. Bile salts and surfactants were also shown to cause irritation to the ocular tissues and nasal mucosa (84-87). Chetoni et al. demonstrated that polysteryl ether, polyethaoxylated castor oil and cetylpyridinium chloride and deoxycholic acid sodium salt significantly altered the electrophysiological parameters and corneal hydration indicative of ocular toxicity of these enhancers (88). Using confocal laser scanning ophthalmoscopy Furrer et al. demonstrated that cationic surfactants such as sodium lauryl sulfate and sodium cholate caused corneal lesions and irritation (89). Rojananasakul et al. reported that use of digitonin and sodium deoxycholate caused severe membrane damage (90).

Lipophilic modification and transporter targeted amino acid / peptide prodrugs have, perhaps, been the most successful approach so far (56). Chemical modification by prodrug design has been demonstrated to improve the partition coefficient of hydrophilic drugs, and thus to increase the intrinsic corneal permeability, or through transporter meditated translocation. However, the major drawback of these approaches is that not all compounds are amenable to prodrug derivatization or transporter targeting. Additionally, achieving the desired lipophilicity often requires compromising on the aqueous solubility of the molecule.

In recent years, polymers that can safely and reversibly disrupt the tight junctions expressed on epithelial cells have been identified (91). Among these, chitosan appears to be the most promising candidate due to its inherent biological activity and favorable properties**.**

1.3.1.1.1. Chitosan

Chitosan is a liner aminopolysaccharide composed of randomly distributed N-acetyl-D-glucosamine (2-*N*-acetyl-2-deoxyglucose) and glucosamine (2-amino-acetyl-2-deoxyglucose) with β-(1-4)-linkage. It is derived from alkaline N-deacetylation of chitin, which is an abundant natural polysaccharides, mostly derived from the exoskeleton of crustaceans (92).

Chitosan has been extensively studied as a potential absorption enhancer. Both *in vitro* and *in vivo* studies demonstrate chitosan's ability to increase passive diffusion of compounds across intestinal (93), nasal (94, 95), buccal (96, 97) and vaginal mucosa (97-100), urinary bladder wall (101, 102) and Caco-2 cells (98-100, 103). Chitosan's effect on transepithelial permeability, mostly determined using Caco-2 cells has been suggested to be through F-acitn depolymerisation and disbandment of tight junction proteins (ZO-1, Occludin). In contrast to most absorption enhancers which are cytotoxic in nature, a number of studies suggest that chitosan is well tolerated by the corneal cells and is non irritating (104). Additionally, the effect of chitosan on tight junctions and membrane permeabilization has been demonstrated to be reversible (56, 98-100). In addition to permeation enhancing property, chitosan exhibits other attractive features, mentioned below, which makes it a promising transcorneal absorption promoter.

Chitosan through its mucoadhesive properties can lead to increased retention of topically instilled ophthalmic formulations, and thus facilitate greater corneal drug penetration and prolonged exposure. The mucoadhesive characteristics of chitosan is related to the interaction between the positively charged amino groups of the chitosan and the negatively charged residue

of sialic acid in the mucos of the tear film, along with other forces such as hydrogen bonding (105, 106). Felt et al in a rabbit model demonstrated a increase in corneal residence time in the presence of chitosan, when compared to commercial solution, Tobrex® (107). Additionally, chitosan is biodegradable, which enables the safe administration and degradation of topically applied ocular chitosan vehicle. Chitosan biodegradation, which is an exclusive characteristic of chistosan with respect to other polysaccharides, is mediated by hydrolytic actions of lysosymes, chitinase and N-acetyl-β-glucosaminidases (108-112). Moreover, chitosan solution has favourable pseudoplastic and viscoelastic properties. These properties are very important characteristics, since the pre-corneal tear film has a pseudoplastic character that should not be disturbed by the applications of liquid formulations. Visoelastic fluids exhibit high viscosity under low shear rate and low viscosity under high shear rate conditions this behavior is particularly important in ophthalmic formulations since it facilities retention while permiting the easy spreading of the formulation due to the blinking of eye lids (35, 113, 114). Furthermore, chitosan possesses wound healing and antimicrobial properties (115) which could be beneficial in the treatment of a number of corneal diseases and infections, making chitosan a promising transcorneal absorption promoter.

1.3.1.2. Lipophilic drugs

Better understanding of the disease processes and molecular targets and use of computational and high throughput screening techniques in drug discovery is yielding highly potent lipophilic drug candidates with limited aqueous solubility. It is estimated that > 40% of these compounds are highly lipophilic. Delivering these lipophilic agents into the deeper layers of the corneal tissue and anterior chamber of the eye is a challenging task.

Contrary to the hydrophilic compounds, for which the corneal epithelial tight junctions act as the limiting barrier to transcorneal diffusion, lipophilic molecules can easily cross the corneal epithelium transcellularly. Additionally, the storma may act as reservoir for lipohilic drugs from which the drugs will be slowly deliverd to the intraocular tissues. The underlying endothelial layer does not present any significant resistance to corneal penetration of lipophilic molecules (24, 26). However, limited aqeous solubility presents a formulation challenge in the development of topical ophthalmic formulations of these lipophilic compounds. The classical approach to deal with these compounds has been to generate their water soluble derivatives (eg hydrochloride salt of verapmail and qunidine) or formulate them in the form of suspensions. However, not all compounds are amenable to salt formation. Additionally, as mentioned earlier, due to the effective barrier properties of the corneal epithelium, the corneal permeability of an ionized form is much lower than the unionized species. Formulation of a lipophlic agent in the form of a topical ophthalmic suspension suffers from a number of limitations such as physical instability, difficulty in sterilization and non-uniformity of dosing. Additionally, the discomfort caused by these formulation (due to submicron sized particles) may lead to blinking and thus to the loss of a significant amount of the drug. Many other vehicles and techniques have also been employed to formulate and improve ocular absorption of these poorly water soluble drugs, including oils, liposomes, emulsions and polymeric micro- and nano-particles (116). Investigations employing sesame oil and mineral oil to deliver lipophilic compounds have been made in the past. Unfortunately, oil solutions are irritating, difficult to sterilize and influence the IOP by themselves (117, 118). Emulsions have also been investigated as topical vehicles to delivery water-insoluble drugs to the eye. However, a major disadvantage with this carrier

includes physical instability which can lead to agglomeration, drug expulsion and eventual cracking of the emulsions, which make emulsion vehicles secondary candidates for delivery of lipophilic therapeutic agents (119). The potential of liposomes as a topical delivery system for lipophilic drugs remains limited because of their short half-life on the corneal surface, drug leakage, low drug loading and relatively poor stability. Furthermore, large scale manufacturing of sterile liposomes is expensive and technically challenging (120). In ophthalmology, topical polymeric nanoparticles, primarily developed for intravenous administration, have demonstrated promising results over the last 10 years. These systems are able to protect the drug against chemical and enzymatic degradation, improve tolerance, reduce systemic side effects and increase corneal uptake and intraocular half-lives. However, issues such as cytotoxicity of polymers before or after internalization into the cells, lack of suitable large scale production methods and formation of toxic degradation products hindered progress in the development of polymeric nanoparticles (120). In contrast to all these systems, the use of cyclodextrins, and solid lipid nanopartilces (SLNs) offer new perspectives to the development of topical ophthalmic formulations of poorly water soluble drugs (121).

1.3.1.2.1. Cyclodextrins (CD)

CDs are a group of homologous cyclic oligosaccharides consisting of D-(+) glucopyranose units linked by α-(1, 4) glycosidic bonds. The chair conformation of the glycopyranose units imparts a truncated conical shape to the CD molecules. The surface of the CD molecule is hydrophilic in nature due to the presence of secondary hydroxyl groups (extending from the wider edge of the cone) and primary hydroxyl groups (residing at the narrow

edge of the cone) (122). On the other hand, the central cavity of the CD molecule is lined with skeletal carbons and ethereal oxygen's of the glucose residue, which gives it a relatively lipophilic polarity similar to that of a 40% aqueous ethanolic solution (122-124). The natural α- , β- and γ-CDs consists of six, seven, and eight glucopyranose units, respectively (Figure 1-11). Although hydrophilic in nature these natural CD molecules exhibit limited aqueous solubility due to the relatively strong intramolecular hydrogen bonding in the crystal lattice (124, 125). Substitution of any of the hydrogen-bonding hydroxyl groups with lipophilic functions, leads to dramatic improvement in their aqueous solubility. Modified CD derivatives, with increased solubility, of interest in ophthalmology include the hydroxypropylderivatives of βCD (HPBCD) and γ-CD, the randomly methylated-β-CD (RMBCD) and sulfobutyl ether-β-CD (SBCD) (Figure1-12) (45, 46, 122, 124, 125).

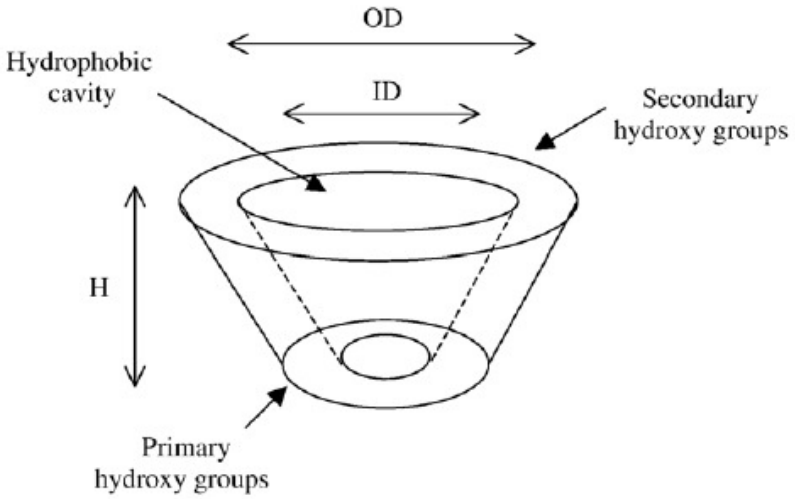

Cyclodextrin	Number of glucose units	Dimensions (nm)			$t_{1/2}$ of ring opening (h)	Mean $K_{1:1}$ [a] (M^{-1})
		H	OD	ID		
α-Cyclodextrin (αCD)	6	0.78	1.37	0.57	33	130±8
β-Cyclodextrin (βCD)	7	0.78	1.53	0.78	29	490±8
γ-Cyclodextrin (γCD)	8	0.78	1.69	0.95	15	350±9

[a] Stability constants (binding constants) of 1:1 guest/CD complexes in aqueous solutions at 25±5 °C Population mean±standard deviation.

Figure 1-11: Characteristic of natural α- , β- and γ-cyclodextrins.

Reproduced with permission from Elsevier., ref (124)

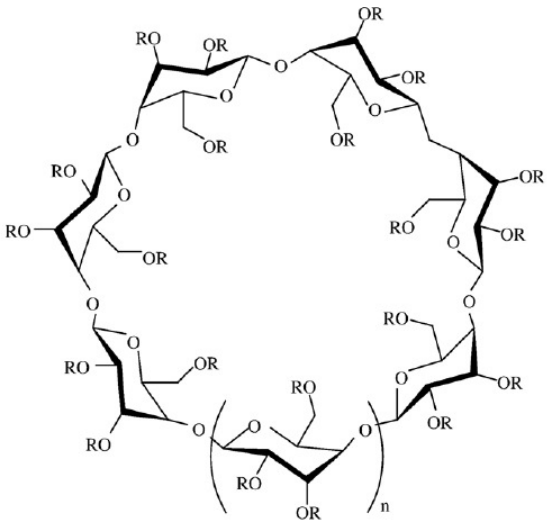

Cyclodextrin	*n*	*R*=H or	Substance [a]	MW [b] (Da)	Solubility in water [c] (mg/ml)	Indicative bulk price ($US/kg) [d]
2-Hydroxypropyl-β-cyclodextrin (HPβCD; Kleptose® HPB)	1	$^{-}CH_2CHOHCH_3$	0.65	1400	>600	300
Sulfobutylether β-cyclodextrin sodium salt (SBEβCD; Captisol®)	1	$^{-}(CH_2)_4SO_3^{-}$ Na^{+}	0.9	2163	>500	–
Randomly methylated β-cyclodextrin (RMβCD)	1	$^{-}CH_3$	1.8	1312	>500	350

[a] Average number of substituents per glucose repeat unit.
[b] MW: Molecular weight.
[c] Solubility in pure water at approx. 25 °C.
[d] Approximate bulk price given as the price of 1 kg in US dollars. The price will depend on purity and technological grade of the CD.

Figure 1-12: Structural and physiochemical properties of selected cyclodextrins of interest for ophthalmic formulations.

Reproduced with permission from Elsevier., ref (124)

CDs act as a host for the guest molecules. The lipophilic central cavity provides a microenvironment into which the whole molecule or some part of it enters forming an inclusion complex. The formation of the inclusion complexes is thought to be an enthalpy-driven process. The water molecules inside the central cavity exist at a higher energy state (enthalpy-rich), due to an inability to satisfy the hydrogen bonding potential, and are readily expelled by less polar drug molecules, thus lowering the energy of the system (124, 126). Additionally, the release of the CD ring strain, hydrophobic interactions, van der waals interaction and London dispersion forces

have been suggested to participate in complex formation (126, 127). In aqueous solution, the guest molecules continuously associate with and dissociate from the host CD generating a dynamic equilibrium between the free drug, drug/CD complex and free CD. No covalent bonds are formed or broken during complex formation and the rate of formation and dissociation of complexes is thought to be similar to diffusion controlled mechanisms (124, 126, 128). Therefore, complexation with CD neither affects the fundamental ability of the free drug to permeate across biological membranes nor does it alter its ability to interact with membrane receptors. They act as true carriers by keeping the guest molecules in solution and making them available for permeation across the biological membrane (126). Complex formation depends on a number of factors such as size, shape and polarity of the guest molecule and on the properties of the cyclodextrins used. Too small a molecule will not be enclosed in the cyclodextrin cavity and highly hydrophilic molecules will not expel the enthalpy-rich water molecules, located in the central cavity of the cyclodextrins, to form a complex (38, 126).

CDs, through formation of inclusion complexes in the solution state, have been successfully used in ocular therapeutics to increase aqueous solubility, bioavailability, stability of drugs and to reduce the ocular irritation.

Dramatic increase in aqueous solubility of a number of poorly water soluble drugs such as steroids, cyclosporine A, carbonic anhydrase inhibitors, prostaglandins and tropicamide have been reported in the presence of cyclodextrins (126). Additionally, hydrocortisone, available in the form of suspension, has now been successfully reformulated as a CD based solution (129). The fold increase in solubility of a therapeutic compound in aqueous solution is dependent on the concentration of the CD used. Effect of increasing concentrations of CD on aqueous solubility of

a poorly water soluble drugs is usually determined using phase-solubility studies according to the method of Higuchi and Connors (130). Based on the shape of the phase-solubility plot generated, several types of behaviors can be recognized (A type and B type) (Figure1-13). In A-type phase-solubility profile apparent solubility of the therapeutic agent increases with increasing concentration of CD. The A-type curve is further classified into A_P, A_L and A_N types. An A_L type curve (linear increase in solubility of the compound as a function of CD concentration) indicates formation of a first order complex with CD. If the complex is first order with respect to substrate, but second or higher order with respect to the CD then an A_P type curve is obtained (positive deviation from linearity with increasing concentrations of CD). In an A_N type curve, there is a negative deviation from linearity with increasing concentrations of CD due to induced changes in the dielectric constant of the aqueous complexation medium. A B-type phase solubility curve suggests the formation of complexes with limited solubility in the aqueous complexation medium. The B-type curve is further classified into two subclasses B_S and B_i. In the B_S type curve the aqueous solubility of the compound increases with increasing concentrations of CD, however, after a point in this type of solubilization process a plateau is reached. Further addition of CD results in the formation of additional insoluble inclusion complex which precipitates and lowers the drug concentration in solution. The B_i systems are similar to the B_S types; however, the initial increase in solubility of the drug with increasing CD concentrations is not observed (122, 124).

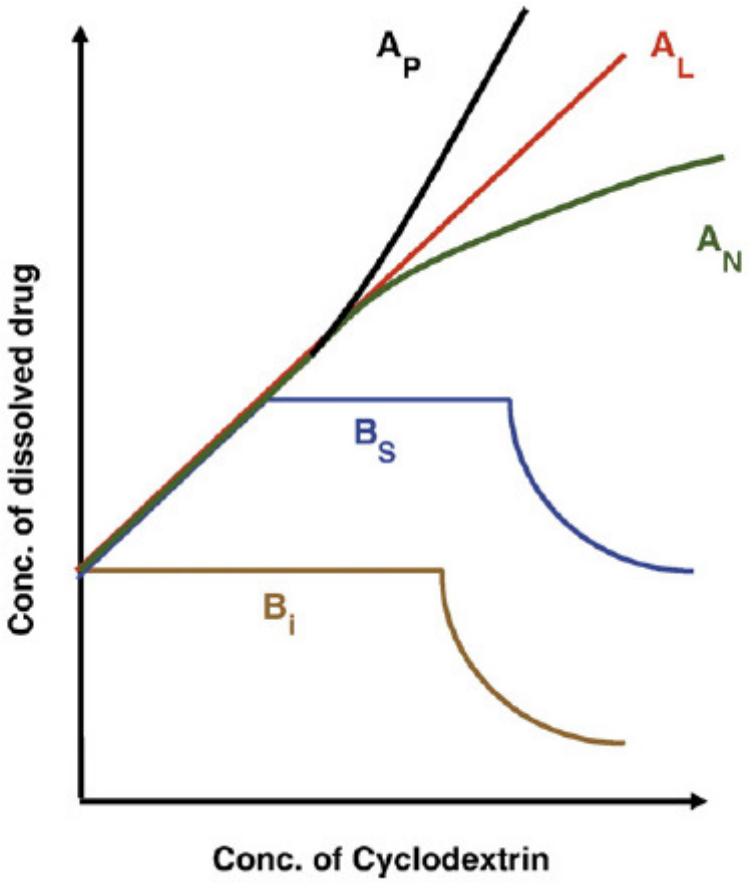

Figure 1-13: Schematic representation of A- and B-type phase solubility diagram with applicable sub-types.

Reproduced with permission from Elsevier., ref (124)

Additionally, a number of *in vitro* and *in vivo* reports indicate that complexation of poorly water soluble drugs, such as acetazolamide, dexamethasone, hydrocortisone, rufloxacin and tropicamide, with cyclodextrins increase their ocular bioavailability when compared with suspension formulations or a control solution of the compound (38, 126, 131, 132). The increase in ocular bioavailability has been attributed to increased solubility, interaction of CDs with the cell membrane, and fast dissociation of the drug/CD complex (38, 126, 133). CDs are relatively

large molecules and literature reports indicate that they will permeate the biological membrane with great difficulty. Additionally, unlike conventional drug penetration enhancers such as EDTA and BAK which disrupt the biological barrier, CDs act as penetration enhancers by increasing the availability of drug at the surface of the cornea (45, 126). However, some reports indicate that addition of CD resulted in a decrease in drug bioavailability (126, 134). This can be attributed to non-optimized usage of CD in the formulations. Maximum bioavailability is achieved when just enough CD is added to the vehicle to solubilize the available drug. Excess CD will decrease the ocular bioavailability of the drug through enhanced retention of the drug molecules in the central CD cavity (125, 134).

Vehicles used in ocular formulations should be non-irritating to the eye to prevent rapid washout of the instilled drug by reflex tearing and blinking. SβCD and HPβCD has been reported to be safe, nontoxic and well tolerated by the eye, even at concentrations as high as 10% and 45% w/v, respectively (126, 135, 136). Additionally, CDs have also been used to reduce ocular irritation and to increase the stability of drugs in ophthalmic formulations (45, 137). Encapsulation of drug within the CD cavity protects the drug from attack by various reactive species and thus reduces the rate of hydrolysis, oxidation, steric rearrangement, racemization and enzymatic decomposition (123). Additionally, CDs have also been reported to decrease the photo degradation of various light sensitive compounds (138).

1.3.1.2.2. Solid Lipid Nanoparticles (SLNs)

SLNs were introduced in 1991 as an alternative nanoparticulate carrier system to existing traditional colloidal carriers such as emulsions, liposomes and polymeric micro- and nano-particles. They were developed especially to deliver lipophilic drugs, and combine the advantages of the traditional systems (emulsions, liposomes and nanoparticles) while avoiding some of their major disadvantages (described above) (119). These particulates are in the submicron size range (50-1000 nm) and are made up of biocompatible and biodegradable materials. Aqueous SLN dispersions are composed of solid lipids, i.e., the lipids are solid at both body and room temperatures, and are stabilized with suitable surfactant/s (Figure 1-14).

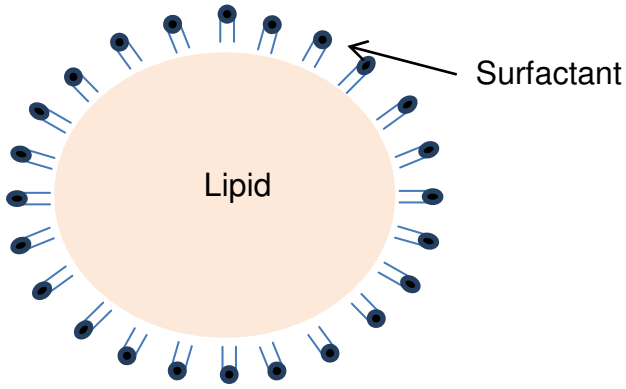

Figure 1-14**: Schematic representation of solid lipid nanoparticles**

Table 1-2 represents trade name, manufacturer and physiochemical characteristics of some of the solid lipids. All the excipients used in their manufacture have approved 'Generally Regarded as Safe' (GRAS) status and are free from the risk of acute or chronic toxicity (139-141). Prolonged and/or controlled release of drug can be achieved depending on the localization of the drug in the SLN. Three models, namely homogenous matrix model (drug molecularly dispersed in the lipid matrix), drug-enriched shell model (drug in the shell) and drug-enriched

core model (drug in solid core of the particles), have been described (142). Factors that affect the incorporation of the drug in the SLN include the chemical nature of the drug and the lipid, drug/lipid ratio, the solubility of drug in the melted lipid, nature and concentration of surfactants, and production method and process temperature (143). A striking advantage of these particles is that large scale production can be carried out in a cost-effective and relatively simple manner using high pressure homogenizers (139-141). The use of a solid lipid matrix also provides greater flexibility in controlling drug release and achieving greater stability, by protecting the encapsulated ingredients from chemical degradation.

Table 1-2: Trade name, manufacturer and physiochemical description of some of the solid lipids used in the present study

Product Name	Manufacturer	Physiochemical description
Compritol 888®ATO	Gattefosse GmbH (Weil am Rhein, Germany)	• Glycerol esters of behenic acid and composed of glycerol tribehenate (28-32%), glycerol dibehenate (52-54%) and glycerol monobehenate (12-18%) • Main fatty acid present behenic acid (≥85%) and amphiphilic in nature • MP: 69°C -74°C; HLB: 2; Peroxide value ≤ 6 mEq O_2/kg • Soluble in chloroform, methylen chloride and Xylene, Insoluble in ethanol and water
Precirol®ATO 5	Gattefosse GmbH (Weil am Rhein, Germany)	• Sray dried cetyl palminate • MP: 61.9°C-55.9°C • Insoluble in water and ethanol
Dynasan® 116	Salsol Germany GmbH (Witten, Germany)	• Triglyceride of palmitic acid. • Glycerol esters of selected, even-numbered and unbranced fatty acids • MP: 61°C -65°C; AV: 3mg KOH/g; SV:

		205-215 mg KOH/g; IV: 1g I_2/100. • Hardly soluble in n-hexane, ether and ethanol, and insoluble in water
Dynasan® 114	Salsol Germany GmbH (Witten, Germany)	• Triglyceride of myristic acid • MP: 55°C -58°C; AV: 3mg KOH/g; SV: 229-238 mg KOH/g; IV: 1g I_2/100. • Dynasan 114 is slightly soluble in n-hexane and diethylether and has a very low solubility in ethanol.
Dynasan® 118	Salsol Germany GmbH (Witten, Germany)	• Triglyceride of stearic acid • MP: 70°C -73°C; AV: 3mg KOH/g; SV: 186-192 mg KOH/g; IV: 1g I_2/100. • Dynasan 116 and 118 is slightly soluble in n-hexane, as well as in diethylether and ethanol. • All types are virtually insoluble in water.

Additionally, due to the high degree of stability of aqueous dispersions (more than 3 years) and high drug payload, SLNs can be formulated as nanodispersions in liquid dosage forms. These dispersions can be administered as topical eye drops. Such formulations will avoid blurred vision and will be comfortable due to the small size of the particles (144). Moreover, the small size and muco-adhesive properties (141) of SLNs would lead to enhanced ocular bioavailability by increasing the residence time in the cul-de-sac and uptake into corneal or conjunctival tissues by endocytotic mechanisms. Furthermore, lipid nanoparticles with excellent long term stability can be produced in large scale, be lyophilized and also heat sterilized (143).

Over the past few years a plethora of studies have been published depticing the importance of solid lipid nanoparticles in various administration routes such as parental (intravenous, intramuscular or subcutaneous), oral, pulmonary, rectal and topical (in cosmetic and dermatological preparations). Controlled drug delivery, enhanced bioavailability, increased dissolution rates and improvement of tissue distribution and targeting of drugs using these SLNs and routes of administration have been achieved (139, 140, 145). It is, however, surprising that the number of reports on the potential of SLNs as ocular drug delivery systems is still limited. Cavalli et al incorporated tobramycin in SLNs (146) and reported that, compared to an equal dose of tobramycin administered by standard commercial eye drops, SLN formulations produced improved passage of drug into the aqueous humor. Gokce et al evaluated SLNs as a carrier for ocular delivery of cyclosporine. The authors reported improved corneal penetration and increased aqueous humor concentrations of cyclosporine, reduced irritation *in vivo*, and negligible cyctotoxicty to corneal cell lines with SLN formulations (144, 147). In a recent study, Attama et al. reported sustained release and high permeation of timolol maleate loaded SLNs through a bioengineered cornea compared to a timolol maleate solution in distilled water (148). Results from these studies demonstrate that formulation of water in-soluble drugs as solid lipid nanoparticles may present advantages such as higher solubility, higher dissolution rates, higher bioadhesion, corneal penetration and lower tearing and drainage of instilled dose. Additionally, formulation as SLN would likely lower the dose needed to achieve clinical effects.

1.3.2. Systemic and other routes of administration

1.3.2.1. Modulation of P-gp expressed by the retinal pigmented epithelium

For posterior segment ocular disorders topical administration is usually ineffective. Therfore, alternative routes such as systemic administration, intravitreal administration and transscleral administration are considered for increasing ocular bioavailability of drugs into the back-of-the-eye. However, as discussed earlier, P-gp an efflux pump expressed by the RPE is the principle contributor to the barrier properties of the RPE, with respect to its substrates. These proteins are expressed on the apical and basal membranes of the RPE and are responsible for the efflux of substrates back into the extracellular space.

Following systemic or transscleral administration P-gp substrates would diffuse across the choroid to the RPE. Transcellular diffusion of P-gp susbtrates across the RPE would however be limited as P-gp expressed on the basolateral membrane of the RPE would efflux the compound out of the RPE cytoplasm and/or inner membrane leaflet, back into the choroid. Thus permeation of P-gp substrates across the RPE basolateral membrane will be restricted (Figure 1-15 A). If basolateral efflux is inhibited increased vitreal penetration and decreased elimination will take place following systemic and/or transscleral administration (Figure 1-15 B). Similarly, intravitreally administered P-gp substrates would be effluxed by the basolateral P-gp facilitating elimination of the drug from the vitreous humor (Figure 1-16 A). If the basolateral P-gp is inhibited decreased elimination from the vitreous would take place (Figure 1-16 B).

1-15 A

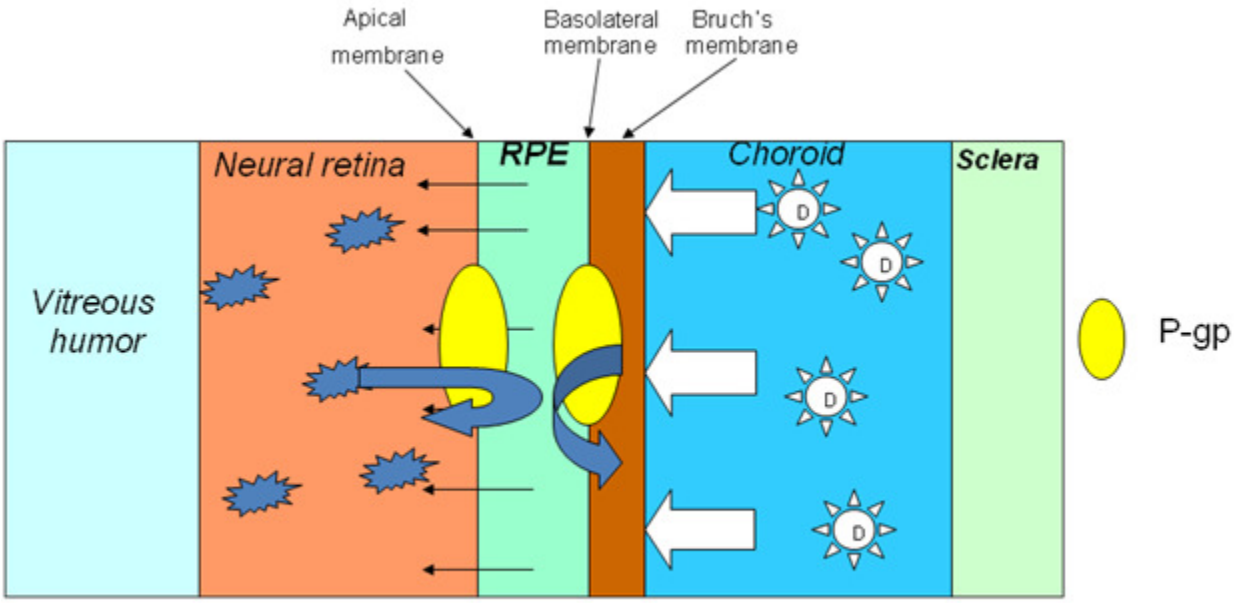
Apical membrane
Basolateral membrane
Bruch's membrane
Vitreous humor
Neural retina
RPE
Choroid
Sclera
D
D
D
D
P-gp

1-15 B

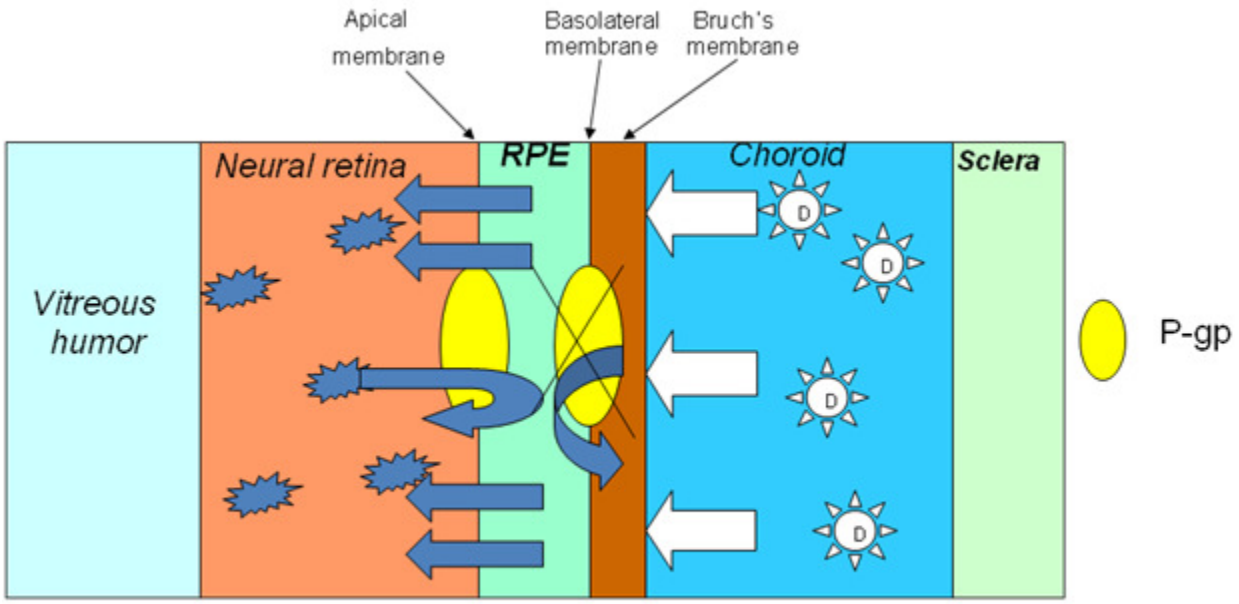

Figure 1-15: Schematic representation of (A) impact and (B) inhibition of P-gp on ocular bioavailability of systemically/transsclerally administered P-gp substrates. (A) A significant amount of the systemically / transsclerally administered dose that reaches the RPE cytoplasm through the choroidal stroma is translocated back into the choroidal circulation by the basolateral P-gp on the RPE ; (B) Inhibition of the basolateral P-gp would allow greater concentrations of drug to permeate into the neural retina and vitreous humor. Arrow thickness depicts diffusion rate and drug amount.

1-16 A

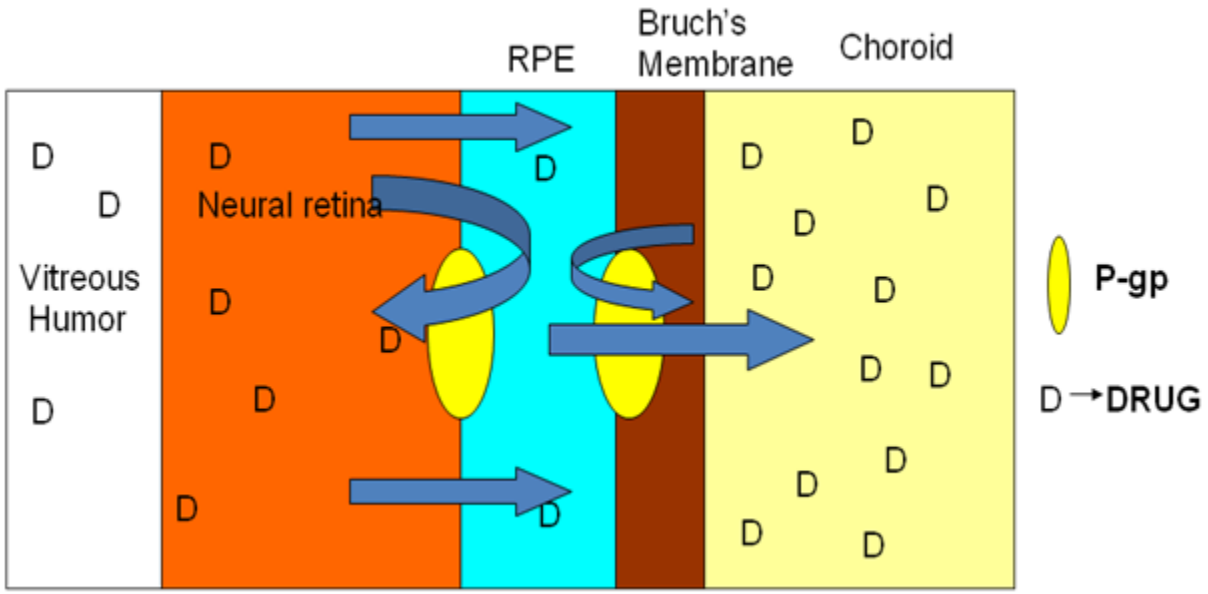

1-16 B

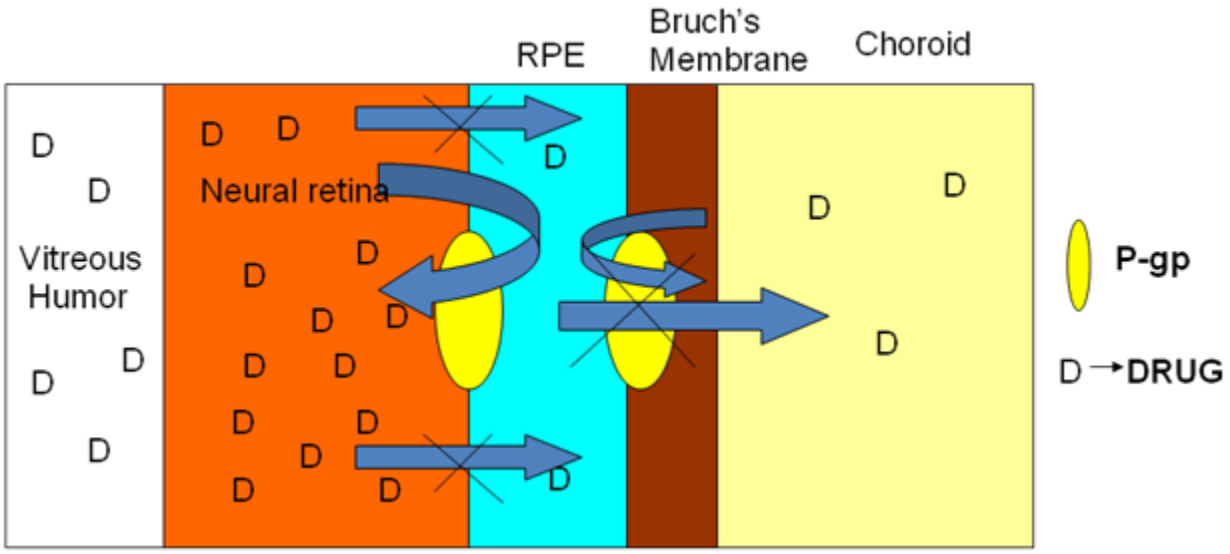

Figure 1-16: Schematic representation of (A) impact and (B) inhibition of P-gp on ocular bioavailability of intravitreally administered P-gp substrates. (A) A significant amount of the intravitreally administered dose that reaches the neural retina from the vitreous is translocated into the choroidal circulation by the P-gp on the basolateral membrane of the RPE; (B) Inhibition of the basolateral P-gp would allow greater concentrations of the drug to remain in the vitreous.

With back-of–the eye diseases such as retinoblastoma, diabetic retinopathy, macular degeneration, proliferative vitreoretinopathy, retinitis and endophthalmitis growing rapidly in significance, and a spurt in the discovery and development of lead candidates, many which are potential substrates of P-gp and other efflux pumps, a need for non-invasive approaches to inhibit the RPE P-gp and improve the back-of-the eye delivery is the need of the day. Thus, factors/agents that can modulate the efflux activity of RPE P-gp could probably alter ocular pharmacokinetics of P-gp substrates.

In the past, a number of strategies attempting to modulate the activity or expression of efflux proteins on various mammalian tissues have been investigated. These include the use of chemosensitisers, prodrugs, polymers, nanoparticles, transcriptional regulators and monoclonal antibodies (149-151). Surprisingly, there are only three studies, to our knowledge, investigating the effect of drug-drug interaction at the level of the RPE P-gp and its effect on ocular drug pharmacokinetics *in vivo*. These recent reports evaluated the effect of systemic/systemic, systemic/intravitreal or intravitreal/intravitreal co-administration of substrates or inhibitors on ocular pharmacokinetics (71, 152, 153). From a therapeutic point of view, with respect to delivery of P-gp substrates to the posterior chamber ocular tissues, the use of an intravitreal inhibitor is not feasible considering that high intravitreal levels of the inhibitor can only be maintained through multiple intravitreal injections. On the other hand, the use of systemic inhibitors is not attractive because of nonspecific systemic exposure to the inhibitor and the limited, clinically relevant, inhibitor dose that can be administered. A hitherto uninvestigated and

novel alternative approach that could be therapeutically effective as well as minimize systemic exposure would be modulation of efflux mediated by P-gp expressed on the RPE through topical substrate/inhibitor application.

Topical eye drops containing antimicrobial, anti-inflammatory, steroids and other agents are routinely administered to treat various anterior chamber and / or conjunctival infections or diseases. Many of these topically applied xenobiotics are established substrates / inhibitors of P-gp. Topically applied P-gp substrates / inhibitors can diffuse into the sclera and choroid and could thus potentially modulate this efflux activity of RPE P-gp and disturb its barrier function. Consequently, ocular pharmacokinetics of co-administered (e.g. intravitreally, periocularly, systemically, orally administered) agents, that are substrates of this efflux protein, may be significantly altered. This could result in changes in ocular tissue drug distribution. Similarly, topically applied P-gp substrates may alter elimination of intravitreally administered substrates.

CHAPTER 2

AIMS OF THE STUDY

The overall goal of this dissertation is to improve drug delivery across ocular barriers using various biopharmaceutical approaches.

The specific aims are:

- To determine the effect of chitosan, benzalkoniumchoride and ethylene diaminetetraacetic acid on transcorneal permeation of acyclovir, a model hydrophilic compound (Chapter 3).
- To investigate the effect of modified cyclodextrins on solubility, stability and transconreal permeability of delta-8-tetrahydrocannabinol, a model lipophilic compound. (Chapter 4).
- To develop, optimize and evaluate solid lipid nanoparticles as ocular drug delivery systems for another model lipophilic compound, indomethacin. (Chapter 5).
- To delineate the effect of topically co-administered P-gp substrates/modulators on vitreal kinetics of intravitreally administered quinidine, a model P-gp substrate, in rabbits (Chapter 6).

- To determine the interaction between topically and systemically co-administered P-glycoprotein substrates/inhibitors and evaluate its effect on vitreal kinetics of quinidine, a model P-gp substrate (Chapter 7)

The rational for choosing the drugs in these specific aims are provided in the introduction of their respective chapters.

CHAPTER 3

EFFECT OF CHITOSAN, BENZALKONIUM CHLORIDE AND ETHYLENEDIAMINETETRAACETIC ACID ON TRANSCORNEAL PERMEATION OF ACYCLOVIR

3.1. Abstract

The objective of this research was to evaluate the effect of chitosan, benzalkonium chloride (BAK) and disodium ethylendiaminetetraacetic acid (EDTA), alone and in combination, on the permeation of acyclovir (ACV) across excised rabbit cornea. Corneas of male New Zealand White rabbits weighing 2-2.5 kg were used for these studies. Transcorneal permeation studies were conducted at 34°C using a side-bi-side diffusion apparatus. In the presence of 0.01% w/v BAK transcorneal permeability of ACV was observed to increase by almost 10.5-fold, from 3.5 x 10^{-6} to 37.4 x 10^{-6} cm/s. When the concentration of BAK was decreased from 0.01% to 0.005% w/v transcorneal permeability of ACV was almost 3-fold higher (10.4 x 10^{-6} cm/s) compared to that of ACV alone. Combination of BAK 0.005% w/v and EDTA 0.01% w/v increased the transcorneal penetration of ACV by 2.5-fold (from 3.5 x 10^{-6} to 8.6 x 10^{-6} cm/s). Chitosan 0.2% and 0.1% w/v increased corneal permeability of ACV by 5.8-fold (7.61 x 10^{-6} cm/s) and 3.1-fold (4.1 x 10^{-6} cm/s), respectively, compared to transcorneal permeability of ACV alone. Chitosan at 0.02% w/v did not exhibit any statistically significant effect on ACV's corneal

permeability. BAK at 0.005% w/v, in combination with 0.01% w/v EDTA and 0.1% w/v chitosan, increased transcorneal permeation of ACV by 5.5-fold (from 1.32 x 10^{-6} to 7.3 x 10^{-6} cms^{-1}). This study demonstrates that judicious combination of chitosan, BAK and EDTA in ophthalmic solutions containing ACV can lead to several folds increase in ACV's transcorneal permeability. The results thus indicate that chitosan can enhance paracellular diffusion of hydrophilic agents across the corneal membrane.

3.2. Introduction

In recent years, several polymers have been identified that can safely and reversibly disrupt cellular tight junctions (91). Among these, chitosan appears to be a very promising candidate. In vitro and in vivo studies demonstrate chitosan's ability to increase passive diffusion of compounds across biological membranes, probably through its effect on the tight junction proteins (93-103). In the past, utility of absorption enhancers in ophthalmic formulations has been limited by their potential adverse effects (116, 154). In contrast, chitosan appears to be well tolerated by the corneal cells (115, 155, 156), and also possesses wound healing and antimicrobial properties(115), making it a promising transcorneal absorption promoter. Additionally, chitosan may increase retention of topically instilled ophthalmic formulations. Another significant advantage of chitosan is that its action appears to be reversible (98-100)

Although the utility of chitosan as an absorption enhancer across multiple epithelial barriers has been well established [1-11], its effect on transcorneal permeation of hydrophilic molecules and corneal epithelial tight junctions has just recently started attracting attention. Reports indicate that N-trimethyl chitosan (TMC), a chitosan derivative that is more soluble than

chitosan at neutral pH, can enhance transcorneal penetration of ofloxacin (154). However, since multiple mechanisms may be involved in the translocation of this agent across the corneal epithelium, the study was inconclusive as to whether chitosan was enhancing transcellular or paracellular diffusion of the compound. A recent report by Zambito et al. (157) suggests that TMC fails to disrupt the tight junctions of the corneal epithelium and increase paracellular transport of tobramycin (used as a paracellular marker). On the other hand, transcellular transport of dexamethasone was observed to increase in this study. The results are intriguing as in all other epithelial tissues chitosan has been observed to disrupt cellular tight junctions and enhance paracellular transport.

Considering its multi-faceted therapeutic utility, chitosan appears to be an extremely promising tool for ocular drug delivery strategies. Thus, further investigation into its effect on transcorneal permeation of hydrophilic agents is desired. In view of this, the purpose of this study was to evaluate the effect of chitosan on the paracellular diffusion of acyclovir (ACV), in an *in vitro* set up using isolated rabbit cornea. ACV is a hydrophilic antiviral nucleoside analog that is highly effective against herpes simplex virus (HSV) induced corneal keratitis. However, ACV is known to traverse the corneal epithelium through the paracellular route (158). Consequently, permeation of ACV into the deeper layers of the cornea is severely restricted by the tight junctions expressed by the corneal epithelial cells. Thus, even though ACV is more potent and several folds less toxic than triflurothymidine (TFT), the current drug of choice for corneal herpetic keratitis in the United States (159), ACV's therapeutic utility is limited to superficial corneal keratitis. Strategies that can increase ACV's corneal permeability could improve its utility in the treatment of stromal infections. The goal of this study was to investigate

whether chitosan could enhance paracellular transport of ACV and thus increase transcorneal diffusion. Since *in vitro* studies using the isolated rabbit cornea have been conducted at pH values as low as 5.0, without any damage to the corneal epithelium (160), the parent compound, chitosan, rather than TMC was used for this study.

Another objective of this project was to delineate the effect of benzalkonium chloride (BAK) and ethylenediaminetetraacetic acid (EDTA) on the absorption promoting properties of chitosan, when used in conjunction. Although BAK and EDTA are commonly included in ophthalmic formulations as a preservative system, they also possess penetration enhancing properties. Corneal absorption of atenolol, timolol, levobunolol, betataxol, befunolol has been reported to increase in the presence of EDTA (161, 162). BAK has also been demonstrated to increase corneal permeability of various compounds such as fluorescein (163), horseradish peroxide (164), prednisolone phosphate (165), dexamethasone, pilocarpine (166) and ketrolac (167). Literature reports indicate that BAK and EDTA up to a concentration of 0.01% and chitosan up to a concentration of 1.5% is well tolerated by the corneal cells (115, 168, 169). The concentrations of BAK, EDTA and chitosan in this study were selected on the basis of these and other reports.

3.3. Materials

Acyclovir was obtained from Hawkins Inc (Minneapolis, USA). BAK, EDTA and Chitosan (low molecular weight) were purchased form Sigma (St. Louis, Missouri, USA). New Zealand White rabbits were procured form Myrtle's Rabbitry (Thompson Station, TN). All other chemicals were obtained from Sigma (St. Louis, Missouri, USA). All solvents were of analytical grade and were obtained from Fisher Scientific (St.Louis, Missouri, USA)

3.4. Methods

3.4.1. Animal Studies

Experiments using rabbits conformed to the tenets of the Association for Research in Vision and Ophthalmology (ARVO) statement on the Use of Animals in Ophthalmic and Vision Research.

3.4.2. Corneal Permeation studies

New Zealand albino rabbits were used for the determination of *in vitro* corneal permeability. Rabbits were anesthetized using ketamine / xylazine administered intramuscularly and were then euthanized with an over dose of pentobarbital, injected into the marginal ear vein. The cornea's were excised with some scleral portion adhered to the cornea which helped to secure the membrane in place between the diffusion half-cells during the course of a transport study. After removal, the cornea was washed with ice cold DPBS (Dulbecco's Phosphate Buffer Saline, pH 7.40) to remove traces of blood and was mounted on a side-bi-side diffusion half cell (PermeGear Inc., Bethlehem, PA, USA) with the epithelial side facing the donor chamber (Figure 3-1). Temperature of the half-cells, and its contents, were maintained at 34°C with the help of a circulating water bath. A slight difference in the donor and receiver chamber volumes (3.2 mL DPBS was added to the receiver chamber and 3.0 mL DPBS was added to the donor chamber of the side-bi-side apparatus) maintained the normal shape of the cornea through marginally elevated hydrostatic pressure. DPBS added to the donor side contained ACV (1 mM)

alone or ACV in combination with chitosan, BAK and/or EDTA. The contents of both the chambers were stirred continuously with a magnetic stirrer Aliquots, 200 µl, were withdrawn from the receptor chamber at appropriate time intervals and an equal volume of DPBS was immediately replaced. Samples were stored at -80°C until further analysis.

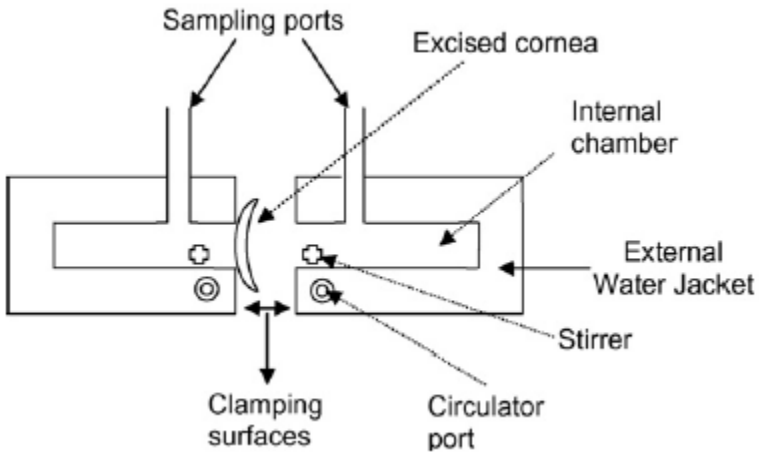

Figure 3-1: Schematic representation of side-bi-side diffusion apparatus

Chitosan stock solution was prepared in DPBS containing 2% acetic acid (pH 6.00 ± 0.20) and desired chitosan concentrations were obtained by diluting the stock solution with DPBS containing 2% acetic acid (pH 6.00 ± 0.20). For experiments involving chitosan, donor solutions were prepared by dissolving ACV, BAK and/or EDTA in the respective chitosan solutions. Transcorneal permeation rates of ACV from a solution containing ACV dissolved in DPBS containing 2% acetic acid (pH 6.00 ± 0.20) was used as a control for these experiments. In all transport studies the receiver chamber contained DPBS pH 7.40.

3.4.3. Analytical procedures

Samples were analyzed using an HPLC system which comprised of Waters 717 plus autosampler, Waters 2487 Dual λ Absorbance detector, Waters 600 controller pump and Agilent

3395 integrator. A Symmetry®C18 4.6 X 250 mm column was used and the mobile phase consisted of 15mM phosphate buffer (pH 2.50) with 1-2% Acetonitrile. The wavelength (λ) and flow rate was set at 254 nm and 1 mL/min, respectively.

3.4.4. Data Analysis

Rate of ACV transport across excised rabbit cornea was obtained from the slope of a "cumulative amount of ACV transported" versus "time" plot. Steady-state flux (SSF) were determined by dividing the rate of transport by the surface area as described in equation (1)

$$\text{Flux (J)} = (dM/dt)/A \quad (1)$$

Where, M is the cumulative amount of drug transported and A is the corneal surface area exposed to the permeant.

Corneal membrane permeability was determined by normalizing the SSF to the donor concentration, C_d according to equation (2)

$$\text{Permeability } (P_{app}) = \text{Flux}/C_d \quad (2)$$

All experiments were conducted at least in quadruplicate and results are expressed as mean ± standard deviation. Data obtained was subjected to statistical analysis using Student's t-Test. A difference between mean values was considered to be statistically significant when the p-value was ≤ 0.05.

3.5. Results:

3.5.1. Effect of chitosan on transcorneal permeation of ACV.

Chitosan stock solution (0.2% w/v) was prepared in DPBS containing 2% acetic acid (pH 6.00 ± 0.20). The desired chitosan concentrations (0.1 and 0.02 %) were obtained following appropriate dilutions with DPBS containing 2% acetic acid (pH 6.00 ± 0.20). ACV was then

dissolved in the chitosan solutions obtained to yield a final ACV concentration of 1 mM. The controls for these studies were prepared by dissolving ACV in the transport medium (DPBS containing 2% acetic acid (pH 6.00 ± 0.20)). Figure 3-2 depicts transport of ACV across the excised rabbit cornea, as a function of time, alone or in the presence of 0.02%, 0.1% and 0.2% w/v chitosan. Transcorneal permeability of ACV (Figure 3-3) in the presence of 0.2 % w/v (7.61 $x10^{-6}$ cm/s) and 0.1% w/v chitosan (4.1 $x10^{-6}$ cm/s) were almost 5.8- and 3.1-folds greater compared to that of ACV alone (1.32 x 10^{-6} cm/s). However, when used at a concentration of 0.02% w/v chitosan could only produce a slight, but statistically insignificant, increase in corneal permeation of ACV. Permeability of ACV in the presence of 0.02% chitosan was 2. 34 x 10^{-6} cm/s (Figure 3-3), a 1.77-fold increase, compared to that of ACV alone.

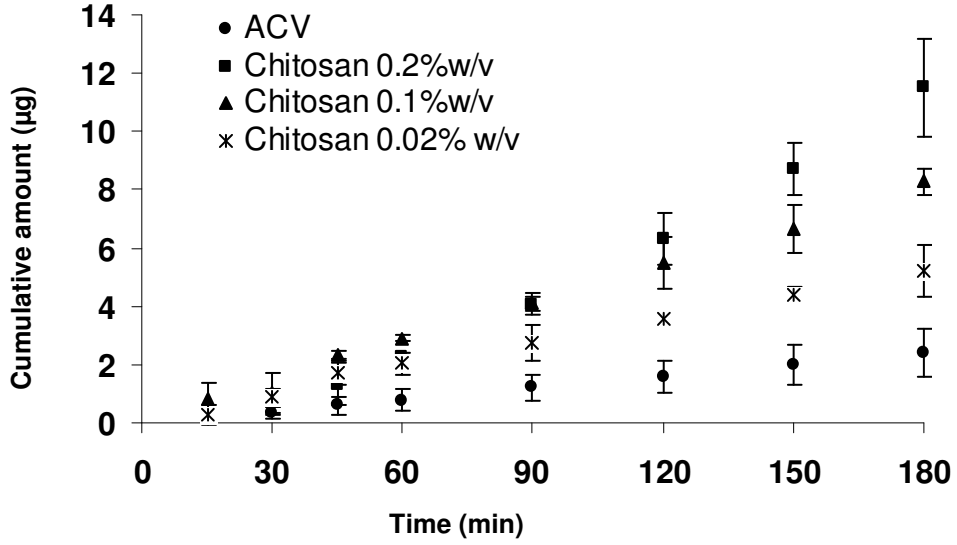

Figure 3-2: Transport of acyclovir (ACV), alone or in the presence of various concentrations of chitosan, across the isolated rabbit cornea. Values represent mean ± S.D. (n=4).

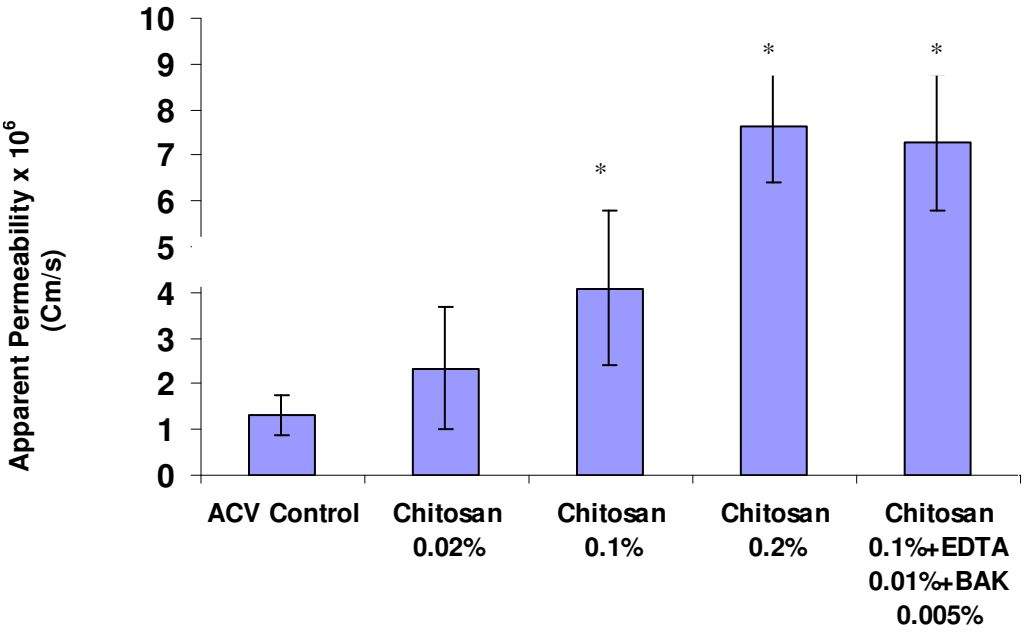

Figure 3-3: Transcorneal permeability of acyclovir (ACV), alone (control) or in the presence of chitosan and disodium ethylendiaminetetraacetic acid (EDTA). Values represent mean ± S.D. (n=4). * indicates $p<0.05$ (statistically significantly different from the control)

3.5.2. Effect of BAK on permeation of ACV across excised rabbit cornea.

In these studies the donor solution consisted of ACV (1 mM) alone or in the presence of BAK (0.01% or 0.005% w/v). The transport medium consisted of DPBS pH 7.40. BAK produced a concentration dependent increase in the transcorneal permeability of ACV. In the presence of 0.005% w/v BAK the cumulative amount of ACV transported over time increased from 4.24 x 10^{-5} mg/min to 11.95 x 10^{-5} mg/min. When the concentration of BAK was increased

to 0.01% w/v, cumulative amount of ACV transported across the cornea over time increased to 44.6 x 10^{-5} mg/min (Figure 3-4). The apparent permeability of ACV increased from 3.56 x 10^{-6} to 10.4 x 10^{-6} cm/s, a 3-fold increase, in the presence of 0.005% w/v BAK, and from 3.56 x 10^{-6} to 37.4 x 10^{-6} cm/s in the presence of 0.01% w/v BAK, a 10.5-fold increase (Figure 3-5).

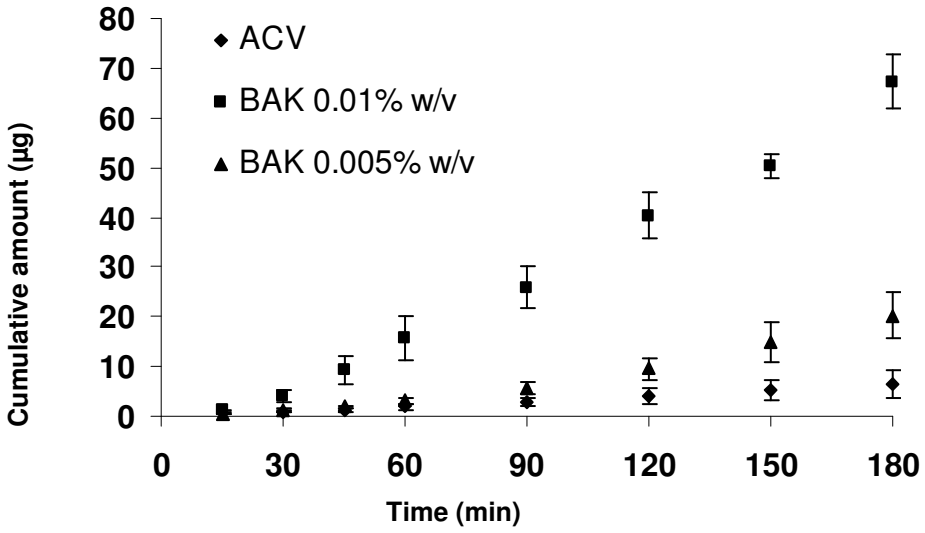

Figure 3-4: Transport of acyclovir (ACV), alone or in the presence of various concentrations of benzalkonium chloride (BAK), across the isolated rabbit cornea. Values represent mean ± S.D. (n=4).

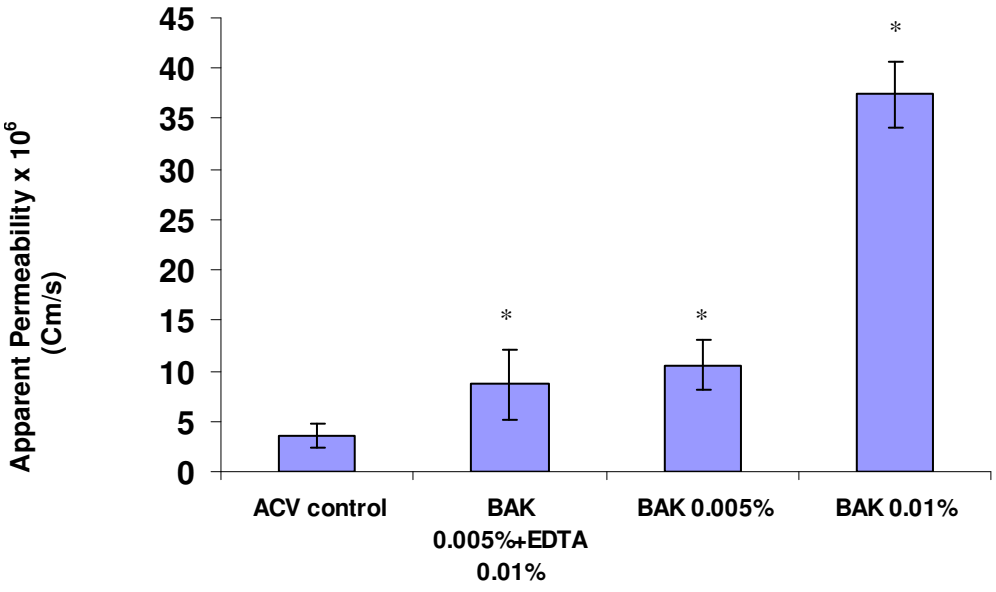

Figure 3-5: Transcorneal permeability of acyclovir (ACV), alone (control) or in the presence of benzalkonium chloride (BAK) and disodium ethylendiaminetetraacetic acid (EDTA). Values represent mean ± S.D. (n=4). * indicates p<0.05 (statistically significantly different from the control)

3.5.3. Effect of BAK in combination with EDTA on transcorneal permeation of ACV

These studies were undertaken to evaluate the effect of BAK and EDTA, in combination, on the transcorneal penetration of ACV. Donor solutions contained ACV (1 mM), BAK (0.005% w/v) and EDTA (0.01 % w/v) in DPBS pH 7.40. The flux and corneal permeation profiles of ACV alone, or in the presence of BAK and EDTA, across the excised rabbit cornea are depicted in Figures 3-5 and 3-6**.** BAK and EDTA, in combination, resulted in a 2.5-fold increase in ACV's permeability. The difference in the transcorneal permeability of ACV in the presence of BAK 0.005% or BAK (0.005%) and EDTA (0.01%) was not statistically significant (Figure 3-5).

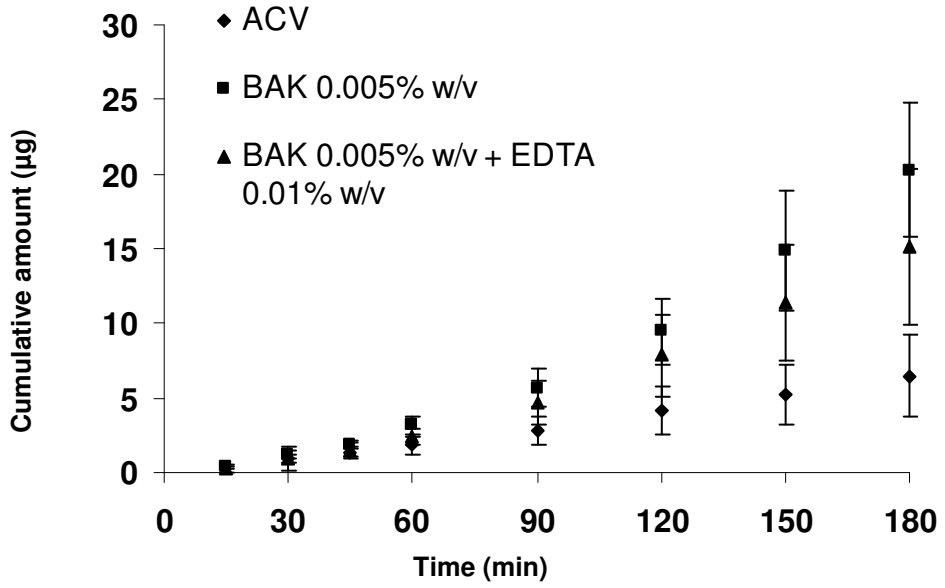

Figure 3-6: Transport of acyclovir (ACV), alone or in the presence of benzalkonium chloride (BAK) and disodium ethylendiaminetetraacetic acid (EDTA), across the isolated rabbit cornea. Values represent mean ± S.D. (n=4).

3.5.4. Effect of Chitosan, BAK and EDTA, in combination, on transcorneal permeability of ACV

Solutions containing chitosan (0.1%), ACV (1 mM), BAK (0.005%) and EDTA (0.01%) were prepared in DPBS containing 2% acetic acid (pH 6.00 ± 0.20). Control solutions contained ACV (1 mM) in the transport medium. In the combined presence of chitosan, BAK and EDTA, transcorneal permeation of ACV increased from 1.32 x 10^{-6} cm/s to 7.3 x 10^{-6} cm/s, a 5.5-fold increase (Figure 3-3).

3.5.5. Reversibility of the permeation enhancing effect of BAK, EDTA and Chitosan:

These experiments were undertaken to evaluate whether the corneal epithelial integrity was re-established following withdrawal of the permeation enhancing agents. For this purpose, at

the end of three hours donor and receiver solutions were removed from the side-bi-side diffusion cells and both chambers were washed with the respective transport buffer two times. A transfer pipette was used for this purpose. Following this, transport buffer containing ACV (1 mM) was added to the donor chamber and transport buffer was added to the receiver side. The transport studies were continued for another 3 h at 34^{o}C. Similar protocols were followed for the control set also, ACV (1 mM) alone, to ensure that the experimental procedure was not damaging the corneal epithelial cell layer integrity. The observed permeability coefficients of ACV during the initial 3 h transport study, in the presence or absence (control) of the permeation enhancers, and during the second 3 h study period, in the absence of any enhancer, were not significantly different (data not shown) suggesting that there was no regeneration of tight junctions. The control also did not exhibit any statistically significant change in permeability values.

3.6. Discussion

The objective of this study was to evaluate the effect of chitosan, alone and in combination with BAK and EDTA, on transcorneal permeation of ACV. ACV is a potent anti HSV agent and thus has a lot of therapeutic potential in the treatment of HSV induced corneal keratitis. However, since ACV is a hydrophilic molecule, transcorneal penetration of this therapeutic agent is restricted by the tight junction expressing corneal epithelial cells. This limits the therapeutic utility of ACV to superficial corneal herpetic keratitis. In recent reports, peptide transporter targeted ACV prodrugs such as valacyclovir and val-val-acyclovir have been reported to enhance ACV's corneal permeability by 3- and 5-fold respectively. However, these ACV prodrugs are rapidly hydrolyzed in aqueous solution, with valacyclovir and val-val-acyclovir

displaying T_{90}'s (time required for the drug content to decrease by 10%) of 2.6 and 16 h, respectively, at pH 7.40 (170). At pH 5.60 valacyclovir displays a T_{90} of 11 h. The study duration was too short to determine the half-life of val-val-acyclovir at pH 5.60 (170). Thus, at ophthalmologically relevant pH values, formulations containing these ACV prodrugs will probably not yield a product with adequate shelf-life. Other transporter targeted ACV prodrugs also demonstrate similar aqueous stability issues (171). Consequently, the utility of these prodrugs in ophthalmic formulations could be limited. Additionally, from a broad point of view, the applicability of this transporter targeted approach would only be limited to compounds that are amenable to corneal peptide transporter prodrug derivatization. Development of a generic approach to enhance transcorneal penetration of hydrophilic agents would, on the other hand, significantly improve ocular drug delivery options.

Chitosan was selected for this study based on reports establishing the reversible tight junction disrupting capability of this polymer. Chitosan can also slightly modulate the apical membrane characteristics which may aid in transcellular permeation of lipophilic compounds. Additionally, its mucoadhesive (155) and antimicrobial properties could also provide several advantages in the design of ocular dosage forms. Earlier studies demonstrate that chitosan based microspheres can enhance corneal penetration of cyclosporine A (155). In another study, Di Colo et al. reported that inclusion of chitosan microspheres in erodible bioadhesive ocular inserts of ofloxacin (154) and dexamethasone (157) increased penetration of the therapeutic agents into the aqueous humor. In the latter study (157), the authors observed that chitosan microspheres did not enhance transcorneal permeability of tobramycin but increased corneal permeability of dexamethasone. Tobramycin and dexamethasone were used as paracellular and transcellular

diffusion markers, respectively. The results led the author's to conclude that chitosan does not affect the tight junctions of the corneal epithelial cells (157). However, these results are in sharp contrast to other reports on chitosan's effect on epithelial tight junctions. Several reasons could probably explain this anomaly. Since chitosan nanospheres are actively internalized by corneal epithelial cells (156) it is probable that the enhanced permeation of dexamethasone or ofloxacin observed was as a result of co-internalization with chitosan. Following internalization, a lipophilic drug can diffuse out of the intracellular compartment and thus overall transmembrane permeability of such agents would increase. On the other hand, a hydrophilic agent would get trapped in the aqueous environment of the cytosol, following cellular internalization. Thus permeability of hydrophilic agents, through the transcellular route, would not increase in the presence of chitosan. Additionally, chitosan is known to affect only the apical membrane and not the basolateral cell membrane (103), limiting chitosan's ability to enhance transcellular diffusion of hydrophilic compounds. Studies conducted by Schipper et al. (103) suggest that chitosan needs to bind to the epithelial cell surface through charge-charge interactions which induces changes in cellular F-actin and ZO-1 organization. Prevention of this interaction by using oppositely charged heparin resulted in chitosan not affecting paracellular transport. Since, in the studies conducted by Di Colo et al. (157), topically applied chitosan was not in solution state it is possible that the chitosan molecules did not get sufficient time to interact with and disrupt the tight junctions. Surface exposure of charged moieties from the chitosan microspheres, dissolution of the chitosan microspheres in the tear fluid as well as spreading of the dissolved chitosan over the corneal epithelium (since the inserts are placed in the conjunctival cul-de-sac the) are other factors that can diminish the ability of chitosan to interact with and disrupt the

corneal epithelial tight junction proteins, when administered in the form of microspheres. Consequently, corneal permeation of hydrophilic agents from such formulations may not show a significant increase as in such cases chitosan probably cannot initiate a charge-charge interaction with the epithelial cell surface. On the other hand, ophthalmic formulations containing chitosan in solution has a much better chance of enhancing paracellular transport.

In this study we observe that chitosan increases the permeability of a hydrophilic molecule, ACV, across the corneal membrane. It is well established that ACV permeates the corneal membrane by passive paracellular diffusion (158). This increase in ACV's permeability indicates that chitosan does disrupt the corneal tight junctions. Chitosan displayed a dose dependent increase in the permeability of ACV with concentrations of 0.1 and 0.2% w/v chitosan producing 3.1- and 5.8-folds increase in permeability. At concentrations of 0.02% chitosan, the effect was not statistically significant. In these studies, the permeability enhancing effect of chitosan could be observed within 30 min of the start of the experiment. Our results are consistent with reports by Dodane et al. wherein chitosan was shown to initiate a reduction of TEER values in Caco-2 cells within 15 min (98). The slightly longer time taken in the current study could be as a result of the multiple epithelial layers of the cornea in comparison to the Caco-2 cell monolayers.

BAK also produced marked increase in transcorneal ACV permeation. At 0.01% w/v BAK increased ACV permeability by almost 10.5 fold whereas at 0.005% w/v permeability was increased 3.0 fold. These results are consistent with other reports investigating the absorption

enhancing effect of BAK. EDTA on the other hand, when used in conjunction with BAK, did not demonstrate any synergistic effect on the transcorneal permeation enhancing property of BAK. This was in contrast to earlier studies which report EDTA's permeation enhancing properties. The difference can probably be explained by the fact that in almost all such earlier studies EDTA was present in a calcium free donor solution (168, 169, 172). On the other hand, in the present study, both donor and recipient solutions contained calcium in the form of calcium chloride. Consequently, the calcium chelating property of EDTA, and hence its effect on tight junctions and paracellular permeability, would be markedly greater in the experiments conducted in the absence of calcium rather than in those wherein calcium is present (incidentally tear contains calcium). The membrane fluidization property of EDTA (173) would probably be overshadowed by the activity of BAK. These results are in agreement with those of Scholz et al. (174) wherein EDTA was not observed to influence transcorneal permeability of another hydrophilic molecule, pilocarpine-HCl.

A synergistic effect was observed when chitosan, BAK and EDTA were used in combination. Whereas, 0.1% w/v chitosan could produce only a 3.1-fold increase in ACV's corneal permeability, chitosan at the same concentration in the presence of BAK and EDTA generated a 5.5-fold increase in transcorneal penetration of ACV. Interestingly, osmolality of the transport buffer that was employed for the chitosan studies was 328 ± 6 whereas that of DPBS (used for the BAK and EDTA studies) was 270 ± 6. Osmolality was measured using Osmette S, model 4002 (Precision Systems Inc., Natick, MA). This increase in osmolality led to a 2.7-fold decrease in transcorneal ACV permeation (from 3.5×10^{-6} to 1.3×10^{-6} cm/s), which is consistent with the findings of Scholz et al. (174).

We also investigated the recovery of the corneal epithelial barrier properties following termination of exposure to the penetration enhancer compounds. This is probably the first study of this kind involving the isolated rabbit cornea. The results clearly indicate that a 3 h period was not sufficient for the corneal epithelial cellular integrity to be re-established. We conducted some additional studies in which ACV permeability was studied for five hours following a one hour exposure to BAK 0.005%. In these studies also no change in permeability was observed following withdrawal of BAK. Earlier studies with Caco-2 cell lines have demonstrated that following a 30 min exposure to chitosan the tight junction proteins need to be re-synthesized *de novo* (99)**.** Smith et al. also demonstrated membrane internalization of the ZO-1 and occludin proteins in Caco-2 cells following exposure to chitosan (100). Further, Dodane et al. established that if protein synthesis was inhibited during the recovery phase, following exposure to chitosan, then regeneration of the tight junctions was hampered. Results from these earlier studies indicate that Caco-2 cells require approximately 24 h to completely recover its barrier properties. In all these studies investigating tight junction recovery, following exposure to chitosan, the cell lines were re-incubated in the culture medium, which is enriched with vital cellular nutrients that enable the cells to synthesize essential proteins and maintain homeostasis, during the recovery phase. However, in the present study using excised rabbit corneas, the corneal epithelial cells did not have access to these vital nutrients. This could probably be a reason behind the lack of any signs of recovery of the corneal epithelial tight junctions. Further studies investigating the reversibility of chitosan's effect on corneal permeability of hydrophilic agents and epithelial barrier integrity are warranted.

In conclusion, results from this study indicate that chitosan does increase paracellular transcorneal diffusion of hydrophilic agents. Ophthalmic formulations of ACV, and probably other small hydrophilic agents, containing chitosan can demonstrate significantly greater corneal penetration and thus lead to increased therapeutic efficacy. BAK exhibits a synergistic effect on the permeation enhancing property of chitosan. Judicial combination of chitosan, BAK and EDTA, in ophthalmic solutions, can lead to significant improvements in ocular bioavailability.

"Reprinted with permission from Elsevier. Majumdar S, Hippalgaonkar K and Repka M.A. Effect of chitosan, benzalkonium chloride and ethylenediaminetetracetic acid on permeation of acyclovir across isolated rabbit cornea Int J of Pharm. 2008; 348 (1-2): 175-178".

CHAPTER 4

EFFECT OF MODIFIED CYCLODEXTRINS ON SOLUBILITY, STABILITY AND TRANSCORNEAL PERMEABILITY OF DELTA-8-TETRAHYDROCANNABINOL

4.1. Abstract

The purpose of this study was to investigate the effect of cyclodextrins (CDs) on aqueous solubility, stability and *in vitro* corneal permeability of delta-8-Tetrahydrocannabinol (Δ^8-THC). Phase solubility of Δ^8-THC was studied in the presence of 2-hydroxypropyl-β-cyclodextrin (HPβCD), randomly methylated-β-cyclodextrin (RMβCD) and sulfobutyl ether-β-cyclodextrin sodium salt (SβCD). Stability of Δ^8-THC in 5% w/v aqueous CD solutions, as a function of pH, was studied following standard protocols. *In vitro* corneal permeation of Δ^8-THC (with and without CDs) across excised rabbit cornea was also determined. Phase solubility profile of Δ^8-THC in the presence of both HPβCD and RMβCD was of the A_P type, whereas, with SβCD an A_L type was apparent. Aqueous solubility of Δ^8-THC increased to 1.65, 2.4 and 0.64 mg/mL in the presence of 25% w/v HPβCD, RMβCD and SβCD, respectively. Significant degradation of Δ^8-THC was not observed within the study period at the pH values studied, except for at pH 1.20. Transcorneal permeation of Δ^8-THC was dramatically improved in the presence of CDs. The results demonstrate that CDs significantly increase aqueous solubility, stability and transcorneal permeation of Δ^8-THC. Thus, topical ophthalmic formulations containing Δ^8-THC and modified beta CDs may show markedly improved ocular bioavailability.

4.2. Introduction

Cannabinoids have attracted a great deal of attention as a potential new class of antiglaucoma agents (118, 175). Delta-9-tetrahydrocannabinol (Δ^9-THC), the biologically active chemical component of *Cannabis Sativa* (marijuana), is responsible for a majority of the plant's pharmacological effects. Currently, Δ^9-THC is marketed in the USA as Marinol® for the control of nausea and vomiting caused by antineoplastic drugs, and to retard weight reduction syndrome associated with HIV/AIDS (176). However, Δ^9-THC is gaining recognition as a treatment option for a host of other medical disorders including glaucoma (177). Earlier studies demonstrate that smoking of marijuana and intravenous and oral administration of Δ^9-THC and Δ^8-THC (delta-8-tetrahydrocannabinol) reduces the intraocular pressure (IOP), in animals and in humans (178). However, since the mechanism surrounding their effect on IOP was initially thought to involve the central nervous system, issues such as psychoactivity and side effects associated with these routes of administration hindered progress. Recent discovery of CB1 receptor expression in various ocular tissues, has renewed interest in the study of topical administration of cannabinoids in the treatment of glaucoma (118, 175). A number of pharmacological and histological studies strongly suggest direct role of ocular CB1 receptors in the lowering of the IOP by the cannabinoids (118, 175). Additionally, Δ^9-THC has also been reported to reduce glutamate and N-methyl-D-aspartate induced retinal ganglionic cell death through its CB1 agonist activity (118, 175, 176, 179-182). Moreover, the antioxidant property of Δ^9-THC protects neurons against oxidative stress associated with glutamate-induced excitotoxicity (118, 181, 182). Therefore, in contrast to currently available drugs, topical administration of Δ^9-THC would not only reduce the IOP but would also protect the retinal ganglionic cells against glutamate and N-methyl D-

aspartate induced neurotoxicity. However, Δ^9-THC is psychotropic, poorly soluble in aqueous media and has undesirable side effects (183, 184). Moreover, susceptibility to oxidation, hydrolysis, thermal and photolytic degradation in the solution form make the design of Δ^9-THC ophthalmic formulations a challenging task (184-187).

Δ^8-THC, an isomer of Δ^9-THC, has also been shown to be pharmacologically active as an antiglaucoma agent (175, 188). The stereochemistry and *in vivo* and *in vitro* metabolism profiles of both compounds (Δ^8-THC and Δ^9-THC) are similar. However, Δ^8-THC is easier and less expensive to prepare and is considered to be less psychotropic than Δ^9-THC (188-191). Additionally, Δ^8-THC is chemically more stable, does not undergo oxidation to cannabinol and has a much longer shelf life than Δ^9-THC (188). Moreover, it has been shown to exhibit negligible side effects when administered prior to antineoplastic therapy in cancer patients (191). Taking this into consideration, Δ^8-THC may be a better choice for topical glaucoma therapy.

Although more stable, utility of Δ^8-THC as a topical ophthalmic agent is limited, just like Δ^9-THC by its lipophilicity, low aqueous solubility, and resinous nature. Additionally, a host of physiological factors limit ocular bioavailability of topically administered compounds (125, 126, 175). The multilayered and varied corneal structure severely limits penetration of xenobiotics across the corneal membrane. For efficient transcorneal permeation, the therapeutic agents must possess optimum hydrophilic and hydrophobic characteristics (175). Moreover, adsorption of cannabinoids to glass and plastics poses a significant challenge in formulation, analysis and topical delivery of these drugs (192-196).

In recent years, cyclodextrins (CDs) have been used in ophthalmics for the delivery of water insoluble drugs (126, 175). CDs are a group of cyclic oligosaccharides with a relative

lipophilic central cavity and a hydrophilic outer surface. The hydrophobic central cavity is able to form non-covalent inclusion complexes with various drug molecules. CDs have been reported to increase the aqueous solubility, chemical stability and bioavailability of ophthalmic drugs. Moreover, inclusion of CDs in ophthalmic formulations has been shown to reduce drug induced ocular irritation. Complexation with CDs also improves the ocular permeability of lipophilic drugs, without affecting their inherent permeability, by making greater concentration of the free drug available at the surface of cornea (126, 175). Additionally, modified beta CDs such as sulfobutyl ether-β-cyclodextrin sodium salt (SβCD) and 2- hydroxypropyl-β-cyclodextrin (HPβCD) have been reported to be safe for ocular application, even at concentrations as high as 10% and 45% w/v, respectively (126, 135, 136). Furthermore, topical eye drop formulations containing CDs and drugs (HPβCD/ Indomethacin, randomly methylated-β-cyclodextrin (RMβCD)/ chloramphenicol) are commercially available in the European market (197).

Till date there are no, literature reports with respect to the interaction of CDs with Δ^8-THC. Therefore, the objectives of this project were to determine the physiochemical characteristic of Δ^8-THC and to investigate the effect of three different modified CDs (HPβCD, RMβCD and SβCD) on aqueous solubility, stability and *in vitro* corneal permeability of Δ^8-THC.

4.3. Materials

Δ^8-THC was isolated from a mixture of Δ^9-THC and Δ^8-THC which was produced when Δ^9-THC was exposed to acidic conditions. HPβCD and RMβCD were purchased form Sigma Chemical Co (St Louis, MO, USA) with a degree of substitution of 0.6 and 1.7, respectively. SβCD (degree of substitution 6.6), clear glass vials 20 mL and 5 mL were procured from Fisher

Scientific (St.Louis, Missouri, USA). One mL clear HPLC vials and polypropylene inserts 200 µL were purchased from Waters Corporation (Milford, MA, USA). Ultra-high grade polypropylene micro centrifuge tubes 1.6mL was obtained from MidSci (St.Louis, Missouri, USA). Polyethylene inserts 250 µL were obtained from VWR International (West Chester, PA, USA). All glass vials used in this study conformed to USP type I standards (Table 1). HPLC grade solvents and other chemicals (analytical grade) were obtained from Fisher Scientific (St.Louis, Missouri, USA). Whole eyes from male albino New Zealand rabbits were obtained from Pel-Freez Biologicals (Rogers, AK). Eyes were shipped overnight in solution (Hanks' Balanced Salt Solutions) over wet ice and were used immediately on receipt.

4.4. Methods

4.4.1. Binding of Δ^8 THC to glass and plastics

Binding of Δ^8-THC to glass and plastics was studied at two different concentrations. Δ^8-THC in ethanolic stock was spiked in deionized water to yield Δ^8-THC concentrations of 0.5µg/mL and 0.15µg/mL. Final concentration of ethanol, in these primary stock solutions, was 5% v/v and 0.5% v/v, respectively. Primary stock solutions were sampled immediately for analysis and also transferred into glass and plastic containers for binding studies (Table 4-1). The solutions were exposed to the containers for a period of 30 minutes at room temperature and then analyzed for drug content. Care was taken to avoid contact with the caps. The container type, their capacity and approximate nominal and fill volumes are described in Table 4-1. Each experiment was carried out in sets of six. Change in Δ^8-THC concentration in the samples from the corresponding initial assay of the primary stock solution was determined. To avoid

evaporation of ethanol, the surface-to-volume ratio in the glass and plastic containers were minimized and the vials were tightly capped. As a control, the drug content in the primary stock solution was also monitored as a function of time.

Table 4-1: Container types, capacity and approximate nominal and fill volumes in the binding studies.

Type of containers	Purchased from	Volume	Volume Filled
Polyethylene inserts	VWR International	250 µl	200 µl
Polypropylene inserts	Waters Corporation	200 µl	150 µl
Ultra high grade Polypropylene	MidSci	1.6 ml	1.5 ml
Clear glass vial	Fisher Scientific	20 ml	19 ml
Clear glass vial	Fisher Scientific	5 ml	4 ml
HPLC vials	Waters Corporation	1 ml	0.8 ml

4.4.2. Saturation solubility studies

Saturation solubility studies were carried out using standard shake flask method. Briefly, Δ^8-THC (in hexane) was purged with nitrogen to evaporate the hexane. Water or the respective buffers were then added to dried sample and capped. The samples were continuously agitated at 100 rpm for 24 h at 25˚C in a reciprocating water bath. At the end of 24 h, the samples were centrifuged and the supernatant was analyzed for drug content. Solubility studies were carried out in water and in buffers at four pH values: phosphate (pH 3.00 and 7.40), acetate (pH 5.00) and borate (pH 9.00) buffers (buffer strength and ionic strength were15mM and 0.03, respectively)

4.4.3. Stability in aqueous solutions

Stability of Δ^8-THC as a function of pH was studied in the buffer solutions described above. Aliquots (19 mL) of the buffer were placed in glass vials and were allowed to equilibrate at 25 °C. Δ^8-THC stock solution in ethanol (1mL) was added to the buffers, such that the final concentration of ethanol was 5% v/v. From these aliquots, 900 µL were added to several one mL HPLC vials (USP type I glass). The HPLC vials were tightly sealed to avoid any evaporation of ethanol and stored in a vertical position at 25 °C. At predetermined intervals these vials were taken out and analyzed for Δ^8-THC content. Additionally, using a similar protocol, stability of Δ^8-THC at 40°C in phosphate buffer (pH 7.40) was also investigated. Experiments were conducted at least in triplicate. Log percent drug remaining was plotted against time and the apparent degradation rate constants were calculated from the slope of the line of best-fit. Stability of Δ^8-THC was also determined in buffer solutions containing 5% w/v CDs and 5% v/v ethanol.

4.4.4. Determination of octanol-water partition co-efficient and Ionization constant

Predicted values of mlog P (Moriguchi log P) and pKa of Δ^8 THC were determined using ACD Lab/I-Lab web service (ACD/Log P 8.02, ACD/Pka 8.03).

4.4.5. Phase solubility Studies

Complexation of Δ^8-THC with various CDs was determined using phase-solubility studies according to the method of Higuchi and Connors (198). Excess amount of Δ^8-THC was added to 5 mL aqueous solutions, in screw-capped vials, containing increasing concentrations of CDs. The concentrations ranged from 0.72 mM to 181 mM for HPβCD; 0.76 mM to 190 mM for

RMβCD; and 0.46 mM to 116 mM for SβCD. The resulting suspensions were shaken at 25 °C for 24 h in a reciprocating water bath. Following equilibration, the suspensions were centrifuged at 13,000 rpm for 20 minutes at 4 ºC and the supernatant thus obtained was analyzed using an HPLC system. Phase-solubility profile was obtained by plotting the solubility of Δ^8-THC against the concentration of CDs used. Each experiment was carried out at least in triplicate, and the binding constants ($K_{1:1}$) for the drug-cyclodextrin complex were calculated from the linear region of the solubility curves using equation (1)

$$K_{1:1} = \text{slope} / S_0 (1\text{-slope}) \quad (1)$$

Where, S_0 = Intrinsic solubility of the drug.

4.4.6. *In vitro* corneal permeation studies

Corneas excised from whole eyes, obtained from Pel-Freez Biologicals (Roger, AK), were used for the determination of *in vitro* transcorneal permeability. Whole eyes were shipped overnight in Hanks' Balanced Salt Solution, over wet ice, and were used immediately upon receipt. The corneas were excised with some scleral portion adhering to help secure the membrane between the diffusion half-cells during the course of a transport study. After excision, the corneas were washed with ice cold DPBS (Dulbecco's Phosphate Buffer Saline, pH 7.40) and mounted on side-bi-side diffusion half-cells (PermeGear Inc., Bethlehem, PA, USA) with the epithelial side facing the donor chamber. Temperature of the half-cells, were maintained at 34°C with the help of a circulating water bath. Excess Δ^8-THC was pre-equilibrated, for 24 h at 25°C, with DPBS containing 5% w/v of HPβCD, RMβCD or SβCD, separately. The supernatants were analyzed for drug content and 3 mL of these solutions were added to the donor chamber of the diffusion apparatus, in separate sets of experiment. The receiver chamber contained 3.2 mL of

the respective 5% w/v HPβCD, RMβCD or SβCD in DPBS solutions. CDs were added to the receiver chamber to maintain sink condition throughout the duration of the experiment. Additionally, *in vitro* corneal permeability of a Δ^8-THC suspension formulation (200 µg/mL) was also determined as a control. In this case, the donor solution consisted of 3mL of a 200 µg/mL Δ^8-THC suspension and the receiver chamber contained 3.2 mL of a 5% HPβCD in DPBS solution. A slight difference in the donor and receiver chamber volumes maintained the normal shape of the cornea through marginally elevated hydrostatic pressure. The contents of both chambers were stirred continuously with a magnetic stirrer. Aliquots, 600 µL, were withdrawn from the receiver chamber at predetermined time points (30, 60, 90, 120, 150 and 180 min), and replaced with an equal volume of the respective CD solutions. Samples were analyzed immediately for drug content. All experiments were carried out at least in quadruplicates.

.

4.4.7. Data Analysis

Rate of Δ^8-THC transport across excised rabbit cornea was obtained from the slope of a "cumulative amount of Δ^8-THC transported" versus "time" plot. Steady-state flux (SSF) were determined by dividing the rate of transport by the surface area as described in equation (2)

$$\text{Flux (J)} = (dM/dt)/A \qquad (2)$$

Where, M is the cumulative amount of drug transported and A is the corneal surface area exposed to the permeant.

Corneal membrane permeability was determined by normalizing the SSF to the donor concentration, C_d according to equation (3)

$$\text{Permeability } (P_{app}) = \text{FLUX}/C_d \qquad (3)$$

4.4.8. Analytical Method

Samples were analyzed for drug content using an HPLC system which comprised a Waters 717 plus autosampler, Waters 2487 Dual λ Absorbance detector, Waters 600 controller pump and Agilent 3395 integrator. A Symmetry® C18 4.6 X 250 mm column was used and the mobile phase consisted of 20% of a 25 mM phosphate buffer (pH 3.00) with 0.1% Triethylamine(TEA) mixture and 80% acetonitrile. The wavelength (λ) and flow rate was set at 215 nm and 1.5 mL/min, respectively. The limit of detection and limit of quantification of Δ^8-THC was 5 ng /mL and 10 ng /mL, respectively, and the precision RSD at the limit of quantification was 4%.

4.5. Results

4.5.1. Binding of Δ^8 THC to glass and plastics

The majority of research laboratories and pharmaceutical companies use glass that conforms to USP type I standards (199). Therefore binding of THC to USP type I glass and plastic containers was investigated. Binding was evaluated at two different Δ^8-THC concentrations (0.5 µg/mL and 0.15 µg/mL). The solutions were exposed to the containers (Table 4-1) for a period of 30 minutes at room temperature and analyzed for drug content. Chemical degradation of the drug was not observed in the 30 minute study period and any change in Δ^8-THC content was attributed to sticking of the compound to the walls of the glass vials or plastic containers. Table 4-2 summarizes the percentage loss of Δ^8-THC in the different containers at the two different concentrations studied. Δ^8-THC demonstrated greatest binding to

the plastic containers at 0.15 µg/mL, with the polyethylene and polypropylene inserts not showing any detectable Δ^8-THC levels at the end of 30 minutes. Δ^8-THC concentration was below the limit of quantification in four out of the six polyethylene inserts used when the primary stock solution concentration was 0.5 µg/mL. In the remaining two polyethylene inserts, the concentration of Δ^8-THC remaining was only 0.07 µg/mL and 0.12 µg/mL. About 78.7 percent and 41.2 percent losses in drug content were observed in the polypropylene inserts and ultra high grade polypropylene containers, respectively, at the 0.5 µg/mL drug concentration within 30 min. At 0.15 µg/mL Δ^8-THC, 47% drug loss was observed in the ultra high grade polypropylene containers. Δ^8-THC did not stick to glass vials meeting the USP Type I standards at the concentrations tested, 0.15 µg / mL and 0.5 µg / mL. The percent drug loss in the glass vials was observed to be within the RSD of the analytical method. The surface-to-volume ratio of the vials, however, had an impact on the binding of Δ^8-THC to glass (data not provided). On the basis of these results, further studies were carried out in glass vials meeting USP type I specifications only.

Table 4-2: Loss of Δ^8 THC in different containers at two different concentrations.

Type of container	% Drug loss in 30min (0.5µg/ml, 5%v/v Ethanol)	% Drug loss in 30min (0.15µg/ml, 0.5% v/v Ethanol)
Polyethylene inserts	86.4 and 76.0 (n=2)	ND
Polypropylene inserts	78.7 ± 8.1	ND
Ultra high grade Polypropylene	41.2 ± 4.7	47.0 ± 2.37
Clear glass vial (20 mL)	2.14 ± 1.69	2.9 ± 1.35
Clear glass vial (5 mL)	0.99 ± 2.14	2.65 ± 1.42
HPLC vials (1 mL)	0	2.94 ± 1.80

ND: not detectable

4.5.2. Saturation Solubility studies

Saturation solubility of Δ^8-THC in water and as a function of pH is illustrated in Figure 4-1. These studies were carried out at 25 °C for 24 h in a reciprocating water bath. Aqueous solubility of Δ^8-THC was observed to be 0.26 ± 0.03 µg/mL. The pH dependent solubility studies (pH 3.00 - pH 9.00) indicated that solubility of Δ^8-THC was independent of solution pH.

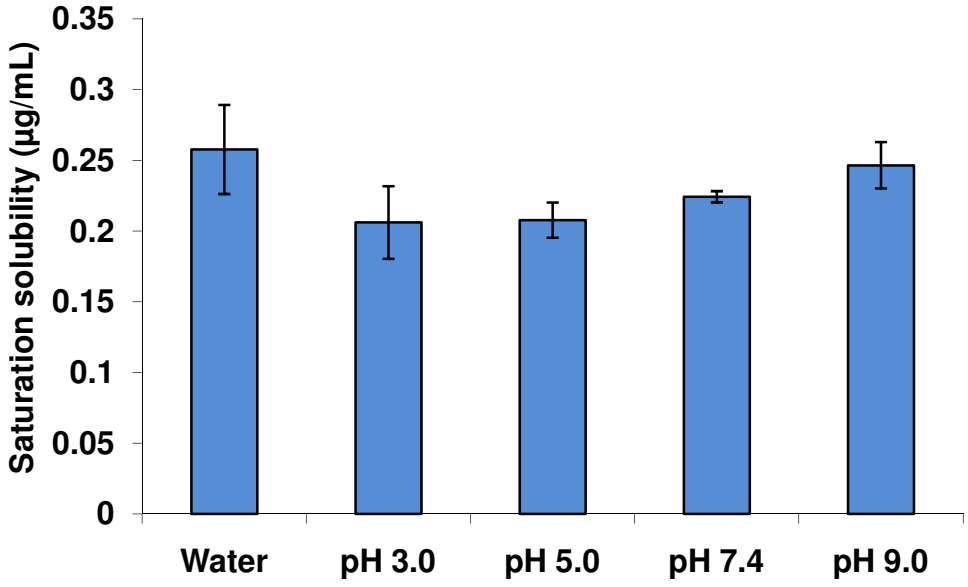

Figure 4-1: Solubility of Δ^8-THC in water and as a function of pH. Values are represented as mean ± SD (n=3).

4.5.3. Stability in aqueous solutions

Aqueous stability of Δ^8-THC was determined within the pH range of 1.2 to 9.0 at 25 °C. Δ^8-THC exhibited pseudo-first order degradation kinetics at all the pH values tested. Half-lives of Δ^8-THC in pH 5.00, 7.40 and 9.00 were 195.0 ± 4.2, 266.5 ± 14.0 and 105.0 ± 1.2 h, respectively. In pH 1.20 and pH 3.00 buffers, the half-lives were 84.0 ± 2.6 and 94.0 ± 5.4, h, respectively (Figure 4-2). A 1.5-fold increase in the degradation rate (from 0.0027 ± 0.00026 hr^{-1} to 0.0042 ± 0.00016 hr^{-1}) of Δ^8-THC was observed when the studies were carried out at 40° C in phosphate buffer pH 7.40.

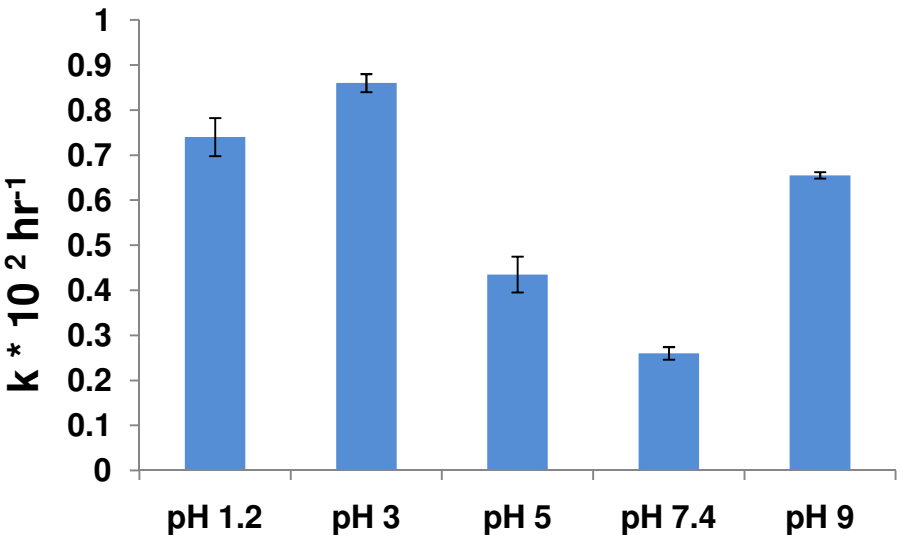

Figure 4-2: Apparent first order degradation rate constant (k x 10^2, hr^{-1}) of Δ^8-THC at 25°C as a function of pH. Results are depicted as mean ± SD (n=3).

4.5.4. pH stability profile in the presence of cyclodextrins

Table 4-3 depicts the pH-stability profile of Δ^8-THC in the presence of 5 % w/v CDs. HPβCD, RMβCD and SβCD were tested for their ability to improve the solution stability of Δ^8-THC. Stability was determined in buffer solutions containing 5% w/v CDs at five pH values: pH 1.20, 3.00 and 7.40 (phosphate), pH 5.00 (acetate) and pH 9.00 (borate). The buffers also contained 5% v/v ethanol since preparation of the Δ^8-THC controls needed 5% v/v ethanol. All three beta cyclodextrins tested dramatically improved the chemical stability of Δ^8-THC at all the pH values tested. Significant degradation of Δ^8-THC was not observed for a period of 2 months (last time point tested) in pH 3.00, 5.00, 7.40 and 9.00 buffers. However, at pH 1.20, 20.0 % and 75% of Δ^8-THC degraded in the 5% w/v SβCD and HPβCD solutions, respectively

Table 4-3: Effect of pH on the degradation of Δ^8-THC in the absence or in the presence of CDs. Results are depicted as mean ± SD (n=3).

pH	Percent delta-8-Tetrahydrocannabinol (Δ^8-THC) degraded			
	Without CD in 4 days	In the presence of 5% w/v HPβCD in 2 months	In the presence of 5% w/v RMβCD in 2 months	In the presence of 5%w/v SβCD in 2 months
1.20	53.0±1.2	20.0 ±2.3	0	75 ± 4.0
3.00	63.0± 2.1	4.0 ±0.8	0	0
5.00	40.0 ± 0.8	2.8 ±1.2	0	0
7.40	36.0 ± 1.2	3.0 ±0.6	0	0
9.00	54.0 ± 0.9	3.0 ±1.8	0	0

4.5.5. Determination of octanol-water partition co-efficient and Ionization constant

Predicted values of mlog P (Moriguchi log P) and pKa determined using ACD Lab/I-Lab web service (ACD/Log P 8.02, ACD/Pka 8.03, respectively) were 7.53 ± 0.36 and 9.83 ± 0.6, respectively.

4.5.6. Phase solubility Studies

The phase solubility studies are useful for studying the complexation of poorly soluble drugs with CDs because it not only determines the solubilizing capacity of the CDs but also provides an insight into the stoichiometry of the inclusion complexes formed. Figure 4-3 represents the phase-solubility diagrams of Δ^8-THC with HPβCD, , respectively. Phase-solubility studies were conducted for a period of 24 h. Binding constants (Table 4-4) were calculated from the slopes of the linear phase-solubility plots using equation 1. All the CDs tested, dramatically improved the aqueous solubility of Δ^8-THC. A 8,250-fold (1.65 mg/mL) and 12,000-fold (2.4 mg/mL) increase in solubility was observed in the presence of 25% w/v HPβCD and RMβCD, respectively. In the presence of 25 % w/v SβCD, aqueous solubility of Δ^8-THC was 640 µg/mL. Phase solubility data of Δ^8-THC with both HPβCD and RMβCD resulted in an A_P type Higuchi plot. The curve showed positive deviation from linearity, indicating the formation of higher order complexes (Figures 4-3a and 4-3b). In contrast, aqueous solubility of Δ^8-THC increased linearly as a function of SβCD concentration (A_L type plot) indicating the stoichiometry of Δ^8-THC: SBCD complex is probably 1:1 (Figure 4-3c). The binding constant values were 11555 M^{-1}, 12200 M^{-1} and 31000 M^{-1} for HPβCD, RMβCD and SβCD, respectively.

Figure 4-3a

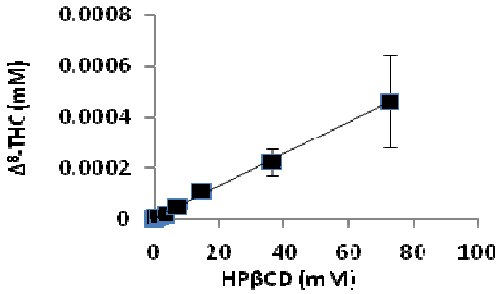
0.0008
0.0006
0.0004
0.0002
0
Δ8-THC (mM)
0
20
40
60
80
100
HPβCD (mM)

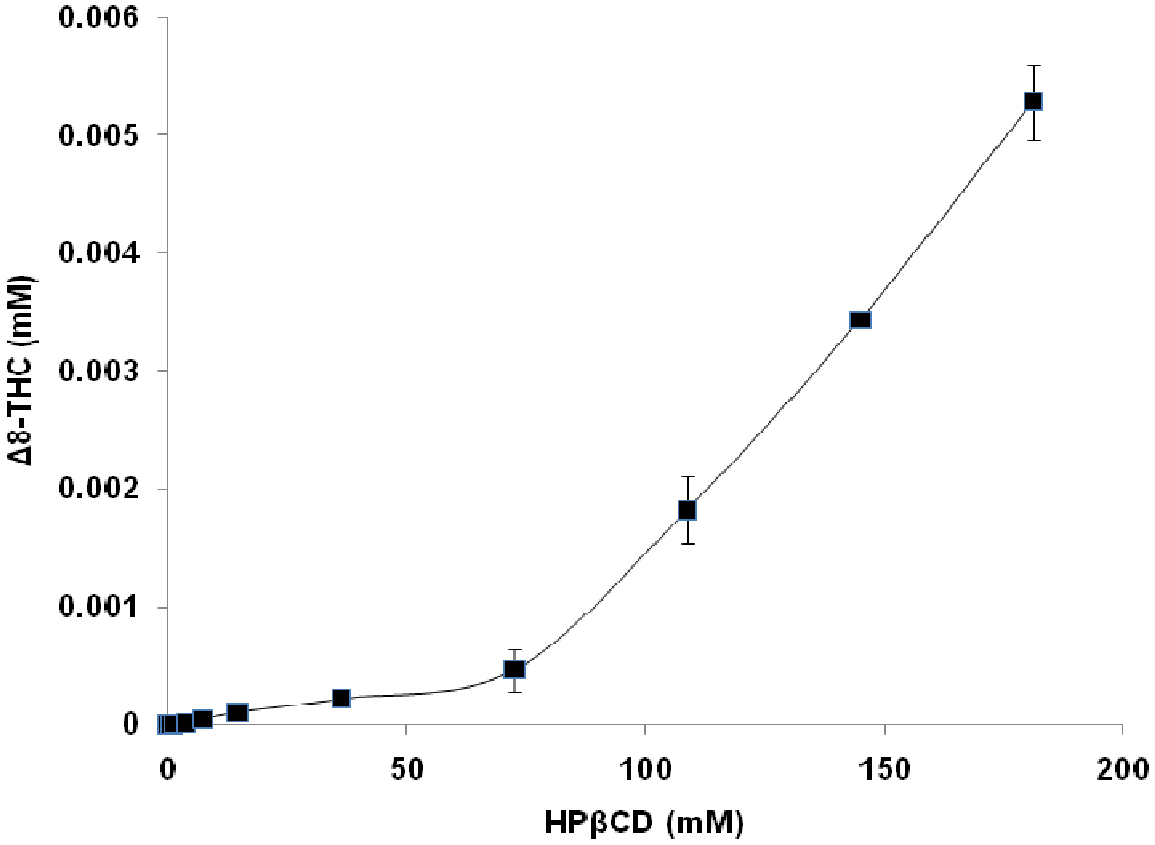
0.006
0.005
0.004
0.003
0.002
0.001
0
Δ8-THC (mM)
0
50
100
150
200
HPβCD (mM)

Figure 4-3b

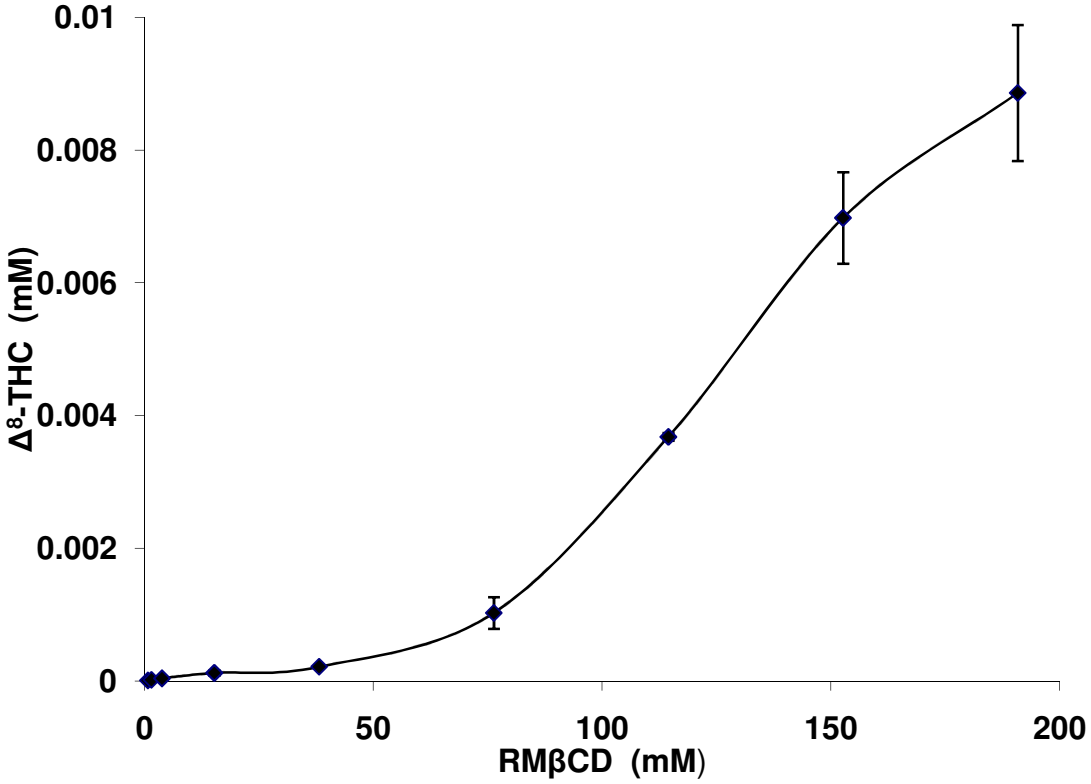

Figure 4-3c

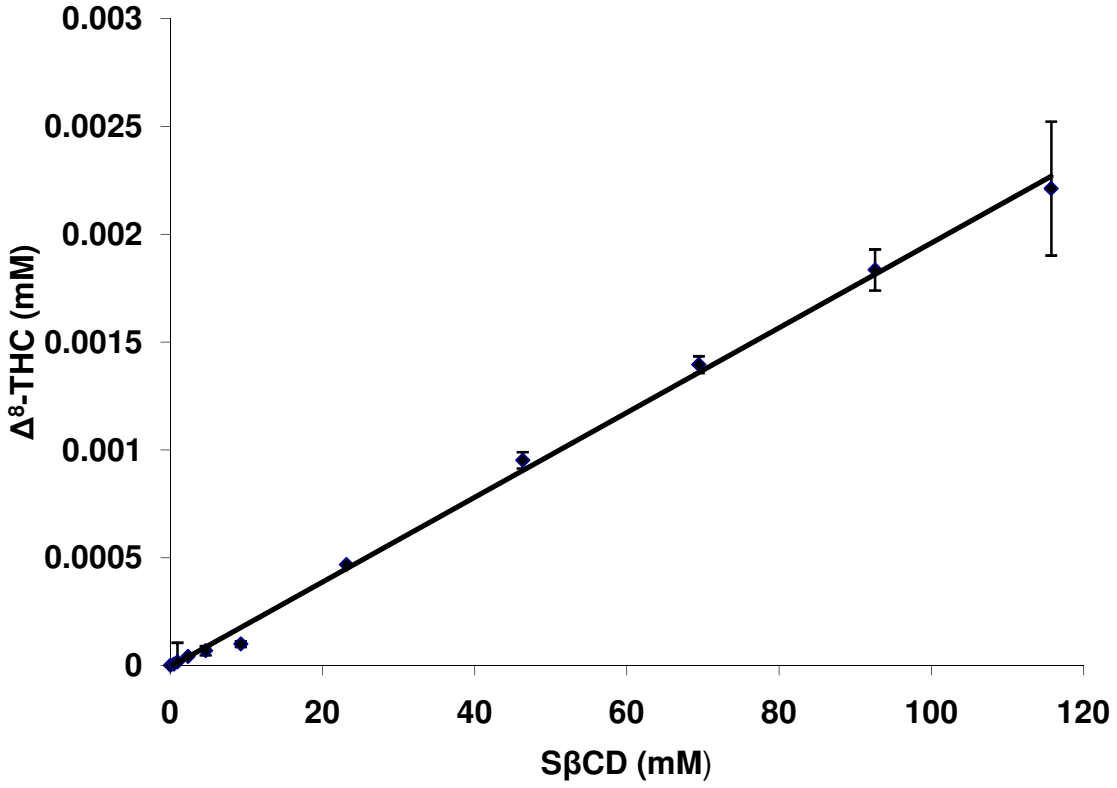

Figure 4-3: Phase solubility of Δ^8-THC in the presence of (a) HPβCD, (b) RMβCD and (c) SβCD. Insert in (a) represents that the phase solubility of Δ^8-THC in the presence of HPβCD as A_L type up to a concentration of 80 mM HPβCD. Each point represents mean ± SD (n=6).

Table 4-4: Slope, apparent stability constant ($K_{1:1}$) and correlation coefficient (R^2) determined from the Δ^8-THC: HPβCD, Δ^8-THC: RMβCD and Δ^8-THC: SβCD aqueous phase solubility diagrams.

Cyclodexrins	Slope x 10^6	$K_{1:1}$ (M^{-1})	R^2
HPβCD	7.36	11555	0.997
RMβCD	7.76	12200	0.994
SβCD	19.20	31000	0.998

4.5.7. *In vitro* corneal permeation studies

In these studies, the donor solution (3.0 mL) consisted of supernatants of Δ^8-THC solutions, pre-equilibrated for 24 h at 25 °C in DPBS (pH 7.40) containing 5% w/v HPβCD, RMβCD or SβCD. The receiver chamber contained 3.2 mL of the respective solutions of 5% HPβCD, 5% RMβCD or 5% SβCD in DPBS. The supernatants of the 5% w/v HPβCD, RMβCD and SβCD in DPBS contained 86 µg/ mL, 70 µg/mL and 168 µg/mL of Δ^8-THC, respectively. The permeability of Δ^8-THC, with or without CDs across the excised rabbit cornea is depicted in Figure 4-4. In the case of the Δ^8-THC suspension, the drug was not detectable in the receiver chamber till the last time point tested (3 h). However, corneal permeation of the resinous, unstable and poorly soluble Δ^8-THC was dramatically improved in the presence of CDs. The apparent permeability of Δ^8-THC in the presence of 5%w/v HPβCD, RMβCD and SβCD was determined to be 7.6 ± 0.6 x 10^{-6} cm/s, 6.3 ± 1.3 x 10^{-6} cm/s and 4.0 ± 0.6 x 10^{-6} cm/s, respectively.

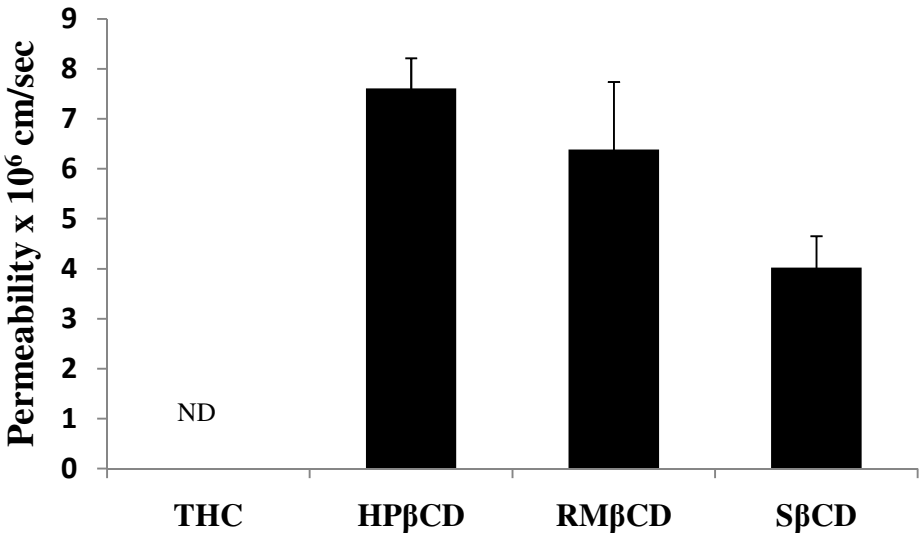

Figure 4-4: Transcorneal permeation of Δ^8-THC from Δ^8-THC suspension and Δ^8-THC in the presence of 5% w/v cyclodextrin formulation. ND: not detectable.

4.6. Discussion:

The goal of this study was to determine the physiochemical characteristic of Δ^8-THC and to evaluate the effect of CD on the solubility, stability and corneal permeation of Δ^8-THC. Δ^8-THC, an isomer of Δ^9-THC, has shown promise as an antiglaucoma agent (175, 188). However, similar to Δ^9-THC, the utility of Δ^8-THC as a topical ophthalmic agent is limited by its lipophilic nature, poor aqueous solubility, and resinous nature.

Highly lipophilic compounds can adsorb to glass and plastic containers and cause difficulties in handling and processing and lead to significant loss of content on storage. Additionally, adsorption can cause misinterpretation of the data and lack of reproducibility. The results from this study indicate that the extent of Δ^8-THC adsorption to polyethylene is significantly greater than its adsorption to polypropylene surfaces. The most striking observation

was that Δ^8-THC did not stick to glass vials meeting the USP Type I standards at the drug concentrations tested. (Table 4-2). The percentage loss of Δ^8-THC in the glass vials was observed to be within the RSD of the method. Therefore, glass that met USP type I specification were used in the subsequent studies. The surface-to-volume ratio of the vials (data not provided), consistent with earlier reports on Δ^9-THC by Blanc et. al (196), had an impact on binding of Δ^8-THC to glass. Increase in the surface-to-volume ratio (low fill volumes in the vials) resulted in a significantly greater loss of Δ^8-THC in comparison to vials that had a low surface-to-volume ratio (high fill volumes).

Solubility is an important parameter affecting drug permeation across biological membranes. Δ^8-THC demonstrated very low aqueous solubility (0.26 ± 0.03 µg/mL), consistent with its high hydrophobicity (Log P 7.53 ± 0.6). Wide ranges of aqueous solubility (1-2.8 µg/mL) and n-octanol/ water partition (6000- 9440000) coefficient have been reported for Δ^9-THC (195, 200). This variation can be attributed to the difficulty in uniformly dissolving the resinous molecule, adsorption to glass and plastics, and analytical techniques used for quantification. Δ^8-THC demonstrated pH independent solubility within the pH range tested (pH 1-9) (Figure 4-1) which was expected since the drug is known to be weakly acidic in nature and exists predominantly in the unionized state below pH 9.00.

Δ^8-THC demonstrated linear pseudo-first order degradation kinetics in aqueous solutions. In earlier studies with Δ^9-THC, by Garrett et.al (201), Δ^9-THC was found to exhibit a biphasic semilogarithmic degradation profile with time, in acidic aqueous solutions below pH 4.00, and followed a first order decay above pH 4.00. These studies, however, were carried out at a temperature of 60.8 °C and at such high temperatures there is a possibility of multiple

degradation mechanisms operating in conjunction. In the present study, hydrolysis of Δ^8-THC in an acidic pH range was observed to be much faster than that in neutral and basic buffers (Figure 4-2). Expectedly, a 1.5-fold increase in the degradation rate (from 0.0027 ± 0.00026 h^{-1} to 0.0042 ± 0.00016 h^{-1}) was observed when the studies were carried out at 40° C in phosphate buffer of pH 7.40.

Effect of increasing concentration of CDs on aqueous solubility of the therapeutic agent is usually determined using phase-solubility studies according to the method of Higuchi and Connors (122, 202). A-type phase-solubility profiles are obtained when apparent solubility of the therapeutic agent increases with increasing concentration of CDs. When the complex is first order with respect to CDs then A_L- type phase-solubility (linear increase in solubility of the compound as a function of CDs concentration) profiles are obtained. If the complex is first order with respect to therapeutic agent, but second or higher order with respect to the CDs then A_P type curve is obtained (positive deviation from linearity with increasing concentration of CDs) (122, 202). Phase-solubility studies demonstrate that HPβCD, RMβCD and SβCD, through their ability to form inclusion complexes, dramatically improved the solubility of Δ^8-THC (Fig 4-3a, 4-3b and 4-3c). The plots suggest that SβCD forms a 1:1 inclusion complex (A_L type) with Δ^8-THC. With HPβCD or RMβCD the results from this study suggest formation of higher order complexes and depict an A_P-type phase solubility curve. Recently Mannila et al. (203) demonstrated that Δ^9-THC yields an A_L type phase solubility curve with HPβCD, indicating the formation of 1:1 inclusion complexes between HPβCD and Δ^9-THC. Besides differences in the chemical structure a possible reason for the variations observed in the phase solubility plots could be differences in the experimental protocol. While Mannila and coworkers used HPβCD in

the concentration range of 0-80mM with a 72 h equilibration period, in the current study the HPβCD concentration ranged from 0-181mM with a 24 hour of equilibration time. If concentrations up to 80 mM were to be considered both studies demonstrate an A_L-type phase solubility plot (Figure 4-3a, insert). Phase solubility studies with RMβCD indicate the formation of higher order complexes with Δ^8-THC, which is consistent with an earlier report by Hazekamp and Verpoorte with Δ^9-THC (204). However, the observed solubility of Δ^8-THC (2.8 mg/mL) in the presence of RMβCD (190mM) and the stability constant ($K_{1:1}$) (12200 M^{-1}) were significantly less than the values reported for Δ^9-THC by Hazekamp and Verpoorte (14 mg/mL in the presence of 187mM RMβCD and $K_{1:1}$= 15,600 M^{-1}). This drastic difference could be attributed to differences in experimental protocols between the two studies. In the latter study, ethanolic stock solutions of both Δ^9-THC and RMβCD were used to prepare the complex and the equilibration time was 72 h. Additionally, Δ^8-THC and Δ^9-THC may interact differently with RMβCD. The binding constant of Δ^8-THC was greater with SβCD than with HPβCD or RMβCD (Table 4-4) suggesting that SβCD forms more stable inclusion complexes with Δ^8-THC. These results are consistent with the reports by Okimoto et al. (205) wherein neutral drugs were shown to exhibit greater binding constant with SβCD than with HPβCD.

Stability in aqueous solution is critical for topical ophthalmic formulation(126). The ability of CDs to reduce hydrolysis, oxidation and enzymatic decomposition of drugs is well documented (206). In this study, Δ^8-THC exhibited dramatically improved chemical stability at almost all pH values in the presences of CD. (Table 4-3). Δ^8-THC, in the presence of 5% w/v HPβCD, RMβCD and SβCD demonstrated insignificant degradation in pH 3.00, 5.00, 7.40 and 9.00 buffers up to a period of 2 months (last point tested) at room temperature. However, at pH

1.20, 5% w/v SBCD and 5% w/v HPβCD failed to prevent the degradation of Δ^8-THC which could be due to chemical instability of these CDs under strongly acidic conditions (207). The mechanism of enhanced stability of Δ^8-THC in the presence of 5% w/v RMβCD, at pH 1.20, is unknown at this point but may be explained by strong steric hindrance created by RMβCD complexation or by greater inclusion of Δ^8-THC in the RMβCD cavity at pH 1.20.

Cornea is the major pathway for intraocular penetration of topically instilled medications(175). *In vitro* corneal permeability data suggests that the complexation of Δ^8-THC with HPβCD, RMβCD and SβCD significantly improves transcorneal diffusion of Δ^8-THC. Complexation of Δ^8-THC with HPβCD resulted in a 2-fold increase (from 3.77 x 10^{-6} cm/s to 7.6 x 10^{-6} cm/s) in corneal permeability compared to that of Δ^8-THC: SβCD complex. Lower corneal permeability of Δ^8-THC in the presence of SβCD can be attributed to the higher magnitude of the binding constant with SβCD (Table 4-4). A number of reports indicate that the magnitude of the binding constant plays an important role in oral bioavailability of drug-cyclodextrin complexes (208). A very high binding constant value can lead to the presence of decreased free drug fraction at the corneal surface, leading to reduced membrane permeability. Statistically significant difference in the corneal permeability of Δ^8-THC from Δ^8-THC: HPβCD complex (7.6 ± 0.6 x 10^{-6} cm/s), and Δ^8-THC: RMβCD complex (6.3 ± 1.3 x 10^{-6} cm/s) was not observed. This observation could be attributed to almost similar binding constants of Δ^8-THC with HPβCD and RMβCD (Table 4-4). Recently, Kearse and Green (117) evaluated transcorneal permeability of Δ^9-THC, *in vitro,* from various vehicles including light mineral oil (LMO) (117). With LMO as the vehicle, corneal permeability of Δ^9-THC was only 0.018 x 10^{-6} cm/s, which is extremely poor and could explain the observed lack of any IOP lowering effect *in vivo* (209,

210). Incidentally, the authors observed that transcorneal permeation of Δ^9-THC in the presence of 30 % HPβCD was only 0.033 x 10^{-6} cm/s. In the present study Δ^8-THC demonstrated a 230-fold higher permeability (7.6 x 10^{-6} cm/s) in the presence of 5% w/v HPβCD (Figure 4-4).

Osmolality of DPBS containing 5% w/v HPβCD was 293 ± 4 mOsm/kg H_20 (Osmette S, model 4002 (Precision Systems Inc., Natick, MA)). This solution is isotonic indicating that corneal integrity would not be affected on exposure to this solution, which is consistent with results from previous report from our laboratory (135), wherein Trans-epithelial electrical resistance (TEER) values of corneas exposed to DPBS alone or in presence of 5% w/v HPβCD for a period of 3 h were observed to be similar. Additionally, transcorneal transport of [^{14}C]mannitol, a paracellular marker, and [^{3}H]diazepam, a transcellular marker in the presence of DPBS alone or in the presence of 5% w/v HPβCD remained the same indicating the integrity and viability of the corneal tissues are maintained during the experimental protocol (135). Osmolality of DPBS containing 5% w/v SβCD and 5% w/v RMβCD were 316 ± 4, 366 ± 4 mOsm/kg H_20, respectively. Although the RMβCD solutions were hypertonic, compared to that of HPβCD, which could affect the corneal integrity, the transcorneal permeation of Δ^8-THC was similar or less than that of HPβCD. RMβCD was thus not studied any further. However, further studies evaluating the integrity of cornea in the presence of RMβCD and SβCD are warranted.

In conculsion, ocular bioavailability of Δ^8-THC is low because of its lipophilicity, resinous nature, and its limited aqueous solubility and stability. Therefore, there is a need for solubility and stability enhancing agents to deliver Δ^8-THC into the deeper ocular tissues. Till date there are no reports on interaction of CDs (which can act as a solubilizer as well as stabilizer) with Δ^8-THC. Results from this study demonstrate that all the CDs tested dramatically

increase the aqueous solubility, stability and transcorneal permeation of Δ^8-THC. Thus, topical ophthalmic formulations containing Δ^8-THC and CDs may show markedly greater ocular bioavailability and IOP lowering activity and could add to the treatment options in glaucoma. However, further studies evaluating the effect of RMβCD and SβCD on corneal integrity are warranted

Acknowledgement

The project was partially supported by grant number 5P20RR021929 from the National Center for Research Resources. The content is solely the responsibility of the authors and does not necessarily represent the official views of the National Center for Research Resources.

Reprinted with permission from Springer. "Hippalgaonkar K, Gul W, ElSohly M.A, Repka M.A. and Majumdar S. Enhanced Solubility, Stability and Transcorneal Permeability of Delta-8-Tetrahydrocannabinol in the Presence of Modified Cyclodextrins. AAPSPharmscitech 2011 (PMID: 21637944)."

CHAPTER 5

INDOMETHACIN LOADED SOLID LIPID NANOPARTICLES FOR OCULAR DELIVERY: DEVELOPMENT, OPTIMIZATION AND IN VITRO EVALUATION

5.1. Abstract

The goal of this study was to develop, optimize using face-centered central composite design (FCCD) and evaluate indomethacin loaded solid lipid nanoparticles (IN-SLNs (0.1% w/v)) for ocular delivery. IN-SLNs were prepared using hot homogenization method. Type of lipid, homogenization pressure, number of homogenization cycles, fraction of Tween 80 in the mixture of surfactants (Poloxamer 188 and Tween 80) while keeping total surfactant concentration at 1% w/v, and pH were investigated for the preparation of IN-SLNs. Two factors (type of lipid and homogenization pressure) were pre-screened and selected to simplify the experimental design and focus on optimization of the other parameters using a three-factor, three-level FCCD aimed to minimize the particle size, maximize entrapment efficiency and maximize zeta potential. *In vitro* transcorneal permeation of indomethacin from the IN-SLNs was compared with that of indomethacin-solution formulation (IN-SOL) (29.3 % w/v propylene glycol and 1% w/v Polysorbate 80) and indomethacin-2-hydroxypropyl-β-cyclodextrin (HPβCD) inclusion complex formulation using a side-bi-side diffusion apparatus at 34°C. pH and

indomethacin content in all the formulations were 6.8 and 0.1 % w/v, respectively. Corneas excised from male New Zealand albino rabbit eyes, obtained from Pel-Freez Biologicals (Roger, AK), were used for the determination of *in vitro* transcorneal transport. Stability of IN-SLNs was also evaluated following sterilization (110° C for 30 min) and on storage (40°C, 25°C and 4°C). Indomethacin exhibited higher partition coefficient and solubility in Compritol 888® ATO and the latter was thus selected as the lipid phase for the preparation of the IN-SLNs. Homogenization at 15,000 psi for 6 cycles resulted in smaller particle size. The best predicted model for particle size and entrapment efficiency was a quadratic model without any significant lack of fit. Neither quadratic model nor any other model were significant for zeta potential indicating that zeta potential was not significantly affected by the experimental conditions used in this study. *In vitro* transcorneal permeability of indomethacin from IN-SOL and IN-HPβCD formulations was $2.8 \pm 0.48 \times 10^{-6}$ and $4.0 \pm 0.9 \times 10^{-6}$ cm/sec, respectively. IN-SLN formulation demonstrated a 4-fold and 3- fold increase in transcorneal permeation of indomethacin ($12.2 \pm 1.85 \times 10^{6}$ cm/sec), compared to that of IN-SOL and IN-HPBCD formulations, respectively. IN-SLNs were physically and chemically stable post sterilization and on storage at all the tested temperatures for a period of one month (last time point tested). Results from this study suggest that solid lipid nanoparticles (SLNs) can be used to improve the ocular bioavailability of indomethacin.

5.2. Introduction

Ocular inflammation is a common eye disorder. Indomethacin, 2-[1-{(4-chlorophenyl}carbonyl}-5-methoxy-2-methyl-1*H*-indol-3-yl]acetic acid, is a nonsteroidal anti-inflammatory drug which inhibits prostaglandin biosynthesis by the inhibition of cyclooxygenase

and therefore has analgesic, anti-inflammatory and antipyretic actions (211). A number of reports demonstrate that ocular administration of indomethacin is effective in treating ocular surface and anterior segment inflammation, including post-operative inflammation after cataract surgery (212-214). However, formulation of indomethacin as topical ophthalmic agent is limited by its poor solubility and stability in aqueous solutions (213). Currently, to the best our knowledge, topical ophthalmic formulation of indomethacin is not commercially available in the United States. Indocollyre® 0.1% eye drops (a topical extemporaneously prepared hydro-PEG 400 solution of indomethacin) commercially available in other continents has been reported to induce side-effects, such as irritation , superficial punctuate keratitis and local pain, and also to exhibit poor ocular bioavailability (212, 215).

In the past, a number of strategies attempting to improve the ocular bioavailability and to reduce the side effects of indomethacin have been investigated. These include the use of nanocapsules, surfactants, oils, polymeric nanoparticles and emulsions (213, 214, 216-218). However, the use of oils is limited due to their irritation potential, difficulty in sterilization and their influence on intraocular pressure (117, 118). On the other hand, the potential of emulsions for topical delivery of indomethacin is limited by its physical instability which can lead to agglomeration, drug expulsion and eventual cracking of the emulsions (119). In ophthalmology, topical polymeric nanoparticles, primarily developed for intravenous administration, have demonstrated promising results over the last 10 years. These systems are able to protect the drug against chemical and enzymatic degradation, improve tolerance, reduce systemic side effects and increase corneal uptake and intraocular half-live. However, issues such as cytotoxicity of polymers before or after internalization into the cells, lack of suitable large scale production

method and formation of toxic degradation products hindered progress in the development of polymeric nanoparticles (120).

In recent years, solid lipid nanoparticles (SLNs) have attracted a lot of attention for the delivery of water insoluble drugs. SLNs were especially developed to deliver lipophilic drugs, combining the advantages of the traditional colloidal systems (emulsions, liposomes and polymeric micro- and nano-particles) while avoiding some of their major disadvantages (119). These particulates are in the submicron size range (50-1000 nm) and are made up of biocompatible and biodegradable materials. All the excipients used in their manufacture have approved 'Generally Regarded as Safe' (GRAS) status and are free from the risk of acute or chronic toxicity (139-141). A striking advantage of these particles is that large scale production can be undertaken in a cost-effective and relatively simple manner using a high pressure homogenizer (139-141). The use of a solid lipid matrix also provides greater flexibility with respect to modifying drug release and improving drug stability by protecting the encapsulated ingredients from chemical degradation. SLN colloidal dispersions can be administered as eye drops. Such formulations will not lead to blurred vision or pose any ocular comfort issues due to their small particulate size (144). Moreover, the small size and muco-adhesive characteristics (141) of SLNs would lead to enhanced ocular bioavailability by increasing their residence time in the cul-de-sac and promoting uptake into corneal or conjunctival tissues through endocytotic mechanisms (143).

In the preparation, development and optimization of drug loaded SLNs, many formulation variables and parameters appear to have a marked influence on mean particle size, drug loading, drug entrapment efficacy, and zeta potential of these lipid nanoparticles (121).

Therefore, it is imperative to have a clear understanding of how process conditions and potential interaction between process variables affect the physicochemical properties of the drug loaded SLNs.

Response surface methodology (RSM) using a central composite design has been extensively used to determine the operation parameters that optimize a specific manufacturing process (219, 220). RSM is a collection of mathematical and statistical techniques based on the fit of a polynomial equation to experimental data for experimental design, modeling and analysis of problems composed matrices of variables (219-223). RSM overcomes the limitation of classical or empirical methods such as one-factor-at-a-time-method which is a time-consuming process and is incapable of searching global optimal conditions, especially when interaction between independents exist (221). Additionally, a relatively small number of runs are required in RSM to determine the mathematical trends that allow the prediction of final process parameters needed for a specific, optimized outcome (220).

Thus, the objective of the present investigation was to develop and optimize indomethacin loaded SLNs (IN-SLNs, 0.1% w/v) for ocular drug delivery. Response surface methodology (RSM) using the face-centered central composite design (FCCD) was used to optimize IN-SLNs formulations. Another objective of this project was to compare the *in vitro* permeation characteristics of indomethacin across isolated rabbit cornea from three formulations: IN-SLNs, indomethacin-solution formulation (IN-SOL, 0.1% w/v) and indomethacin-hydroxypropyl-beta-cyclodextrin formulation (IN-HPβCD, 0.1% w/v).

5.3. Materials

Compritol 888®ATO (glyceryl behenate) and Precirol ®ATO 5 (glyceryl palmitostearate) were kindly supplied by Gattefossé (Paramus, NJ, USA). Dynasan ® 118 (glyceryl tristerate), Dynasan ® 114 (glyceryl trimyristate) and Softisan® 154 (hydrogenated palm oil) were obtained as gift samples from Salsol Germany GmbH (Anckelmannsplatz , Hamburg, Germany). 2-hydroxypropyl-β-cyclodextrin (HPβCD) (average MW: 1380, degree of substitution 0.6) was procured from Sigma Chemical Co (St Louis, MO, USA). HPLC grade solvents, Amicon® ultra centrifugal filter device with regenerated cellulose membrane (MWCO 100kD), Poloxamer 188, Tween 80, indomethacin and all other chemicals (analytical grade) were obtained from Fisher Scientific (St.Louis, Missouri, USA). Whole eyes from male albino New Zealand rabbits were obtained from Pel-Freez Biologicals (Rogers, AK). Eyes were shipped overnight in solution (Hanks' Balanced Salt Solutions) over wet ice and were used immediately on receipt.

5.4. Methods

5.4.1. pH- Saturation Solubility

Saturation solubility studies as a function of pH were carried out following standard shake flask method. An excess amount of indomethacin was added to screw-capped glass vials containing various buffers. To achieve uniform mixing, samples were constantly agitated at 100 rpm for 24 hours at 25˚C in a reciprocating water bath (Fisher Scientific, USA). At the end of 24 hours, the samples were centrifuged (AccuSpin 17R, Fisher Scientific, USA) and the supernatant was analyzed for drug content. Solubility studies were carried out in buffers: phosphate (pH 1.20, 3.00, 6.80 and 7.40) and acetate (pH 5.00) with a buffer strength and ionic strength of 15 mM and 0.03, respectively.

5.4.2. Formulations

5.4.2.1. Indomethacin solution formulation (IN-SOL)

IN-SOL (100 mL) was prepared by mixing indomethacin (0.1 % w/v) with Tween 80 (1% w/v) and propylene glycol (29.3% w/v). To this mixture 1 N NaOH (prepared in bidistilled and 0.2 µM filtered water), was added in small increments under continuous mixing and stirring to dissolve the drug. NaOH was added until the pH reached 6.80. Finally, phosphate buffer (pH 6.80) was added to bring the final volume to 100 mL.

5.4.2.2. Indomethacin loaded solid lipid nanoparticles (IN-SLNs)

5.4.2.2.1. Preparation of indomethacin loaded solid lipid nanoparticles (IN-SLNs)

IN-SLNs were prepared using hot homogenization method as previously described (141, 224). Accurately weighed Compritol 888® ATO (2% w/v) was melted and indomethacin (0.1% w/v) was dissolved therein to obtain a clear lipid phase. Simultaneously, aqueous phase, containing surfactants (Poloxamer 188 and/or Tween 80) and glycerin (2.25 % w/v), in bidistilled water was heated. The hot aqueous phase was then added to the melted lipid phase under stirring (magnetic stirrer) to form a premix (600 rpm, 1-2 min). The premix was then subjected to emulsification at 16000 rpm for 6 min using T 25 digital Ultra-Turrax (IKA® Works, Inc., Willmington, NC, USA) to from a hot pre-emulsion. The obtained pre-emulsion, after adjusting to the required volume, was subjected to high pressure homogenization (at 15000 psi) using thermostated Emulsiflex C5 (Avestin Ottawa, Canada) to result in the formation of a hot emulsion dispersion. The temperature during the entire process was maintained at 80 ± 2 °C. The obtained hot emulsion was slowly cooled to room temperature to form IN-SLNs.

5.4.2.2.2. Experimental design for optimization of IN-SLNs

In the present study, the factors investigated in the preparation of IN-SLNs were lipid type, homogenization pressure, number of homogenization cycles, fraction of Tween 80 in the mixture of surfactants (Poloxamer 188 and Tween 80) at constant total surfactant concentration (1% w/v), and pH. Two factors, type of lipid and homogenization pressure, were pre-screened and only three factors were used for constructing face-centered central composite design (FCCD).

5.4.2.2.2.1. Screening Study

5.4.2.2.2.1.1. Selection of Lipid

5.4.2.2.2.1.1.1. Partitioning of indomethacin between lipids and phosphate buffer

Partitioning of indomethacin between lipids (Compritol 888® ATO (melting point (MP) :70-72°C), Precirol ® ATO 5 (MP: 56 °C) Dynasan® 116 (MP: 61-65°C), Dynasan ® 118 (MP: 70-73°C), Softisan 154 (MP: 53-55°C)) and phosphate buffer (15 mM. pH 6.80) was determined as described previously (225). Briefly, indomethacin (5mg) was dispersed in a mixture of melted lipids (500 mg) and 2 ml of hot phosphate buffer. The mixture was constantly agitated at 100 rpm for 30 minutes at 10 °C above the melting point of lipids in a reciprocating water bath. At the end of 30 minutes the mixture was cooled and centrifuged (13,000 rpm for 20 min) (AccuSpin 17R, Fisher Scientific, USA), the aqueous phase was analyzed for drug content. All experiments were carried out at least in quadruplicates. The apparent partition coefficient (K_{app}) of indomethacin was determined using equation (1)

$$K_{app} = (A_{IND} - A_{INDA}) / A_{INDA} \quad (1)$$

Where A_{IND} is the amount of indomethacin added (5mg) and A_{INDA} is the amount of indomethacin determined in the aqueous phase.

5.4.2.2.2.1.1.2. Solubility of indomethacin in different lipids

Indomethacin, 100 mg, was added to 2 g or 5 g of Compritol 888® ATO, Precirol ®ATO 5, Dynasan ® 116, Dynasan ® 118 or Softisan ® 154 and the samples were incubated at 10°C above the melting points of lipid for 15 minutes. Samples showing good solubility were cooled at room temperature for 24 h and were observed for the presence of crystals using light microscopy.

5.4.2.2.2.1.2. Selection of Homogenization Pressure

Three different homogenization operating pressures were evaluated for the preparation of IN-SLNs. The hot pre-emulsion was passed through the high pressure homogenizer at 7,500 psi, 15,000 psi or 20,000 psi for 5 cycles. The formulation used for the preparation of the pre-emulsion in this study consisted of 0.1% w/v indomethacin, 2% w/v Compritol 888® ATO, 2.25% w/v glycerin, 1% w/v surfactant (0.75% w/v Tween 80 and 0.25% w/v Poloxamer 188). All experiments were performed in triplicates. The surfactant composition was arbitrarily selected in this particular study.

5.4.2.2.2.2. Face-centered Central Composite Design (FCCD)

A three-factor, three-level FCCD was used to optimize the preparation process of the IN-SLNs. The three independent factors chosen for the optimization study were number of homogenization cycles, fraction of Tween 80 in the surfactant mixture (Tween 80/ Poloxamer 188 + Tween 80) while keeping the total surfactant concentration constant at 1% w/v and pH. These three independent factors were coded as A, B and C, respectively. These three factors and the levels of these factors in coded or actual values, along with the dependent variables, are defined in Table 5-1. The range for A, B and C were 1 to 10 cycles, 0 to 1 and 4 to 7.4, respectively (Table 5-1). Design-expert software (Version 8.0.5, Stat-Ease Inc., Minneapolis, U.S.A.) was used to generate the representative combinations of these factors at different levels. The entire software generated design consisted of 20 experimental runs (Table 5-2). The design consisted of 6 axial points, 8 factorial points and 6 replicates of center point for estimation of pure error sum of squares. Using this design, we are able to choose the best model among the linear, two-factor interaction, and quadratic model from results of analysis of variance (ANOVA). The effects of these factors on responses (dependent variables) were studied: Y_1 = particle size; Y2 = entrapment efficiency (%) and Y_3 = zeta potential. The responses were modeled following polynomial equations, equation (2), to evaluate the linear, quadratic and interactive effects of independent variables on the response.

$$Y = B_0 + \sum B_i X_i + \sum B_{ii} X_i^2 \sum B_{ij} X_i X_j \qquad (2)$$

Where Y is predicted response (s), B_0 is intercept, B_i, B_{ii}, B_{ij}, are model regression coefficients and Xi, Xj (i=1, 2 and 3, j=1, 2 and 3 and $i \neq j$) are independent variables/factors of the model in coded or actual values.

To determine if the factors and the interaction between the factors were significant and whether the terms in the regression model were statistically significant ($p<0.05$) the results of these experiments were compared using ANOVA. The coefficient of multiple determinations which measured the proportionate reduction of total variation in Y associated with the use of the set of X variables was denoted by $R^{2.}$ The validity of the regression model was assessed according to statistical assumptions and lack of fit test. Effect of the variables on each response variable was studied by generating response surface plots. All the statistical analyses were performed using Design-expert software (Version 8.0.4, Stat-Ease Inc., Minneapolis,U.S.A.).

Table 5-1: Coded and actual values of factors used in Face Centered central composite design (FCCD).

Factors (Independent Variables)	**Coded Symbol**	**Levels**		
		Low (-1)	Medium(0)	High (+1)
Number of Homogenization Cycles	A	1	6	10
Fraction of Tween 80 in mixture of surfactant (Tween 80/Tween 80+ poloxamer 188) (Total surfactant concentration 1% w/v)	B	0	0.5	1
pH	C	4.00	5.50	7.40
Dependent Variables		**Constraints**		
Y_1= Particle size (nm)		Minimize		
Y_2=Entrapment Efficiency (%)		Maximize		
Y_3 =Zeta Potential (mV)		Maximize		
pH		6.80		

Table 5-2: Experimental runs generated by Design Expert software and the observed responses in face centered central composite design for optimization of IN-SLNs.

	Factors			Responses		
Runs	Number of Homogenization Cycles (A)	Fraction of Tween 80, total surfactant concentration, 1% w/v (Tween 80/ Tween 80+ Poloxamer 188) (B)	pH (C)	Particle size (nm) Y_1	Entrapment Efficiency (%) Y_2	Zeta Potential (mV) Y_3
1	6	0.5	5.50	130	80	-22
2	10	1	4.00	251	100	-21
3	10	1	7.40	251	72	-22
4	6	0	5.50	104	74	-21
5	6	0.5	5.50	135	81	-21
6	6	0.5	5.50	138	80	-20
7	6	0.5	5.50	122	81	-22
8	6	0.5	4.00	128	90	-22
9	6	0.5	5.50	127	79	-21
10	10	0	4.00	101	86	-21
11	1	0	4.00	572	86	-21
12	6	1	5.50	319	96	-21
13	6	0.5	5.50	128	80	-22
14	1	1	4.00	1030	100	-20
15	10	0	7.40	100	43	-21
16	1	0.5	5.50	672	80	-20
17	6	0.5	7.40	128	52	-22
18	1	1	7.40	1030	72	-20
19	1	0	7.40	540	43	-21
20	10	0.5	5.50	138	81	-21

5.4.2.2.3. Optimization and experimental validation.

Optimized formulation was selected using Design-expert software (Version 8.0.5, Stat-Ease Inc., Minneapolis, U.S.A.) on the basis of small particle size, higher entrapment efficiency, high zeta potential with good desirability. The targeted pH of the optimized IN-SLNs formulation was selected as 6.80 during the development of the optimized criteria because Indocorylle® (commercial indomethacin formulation is Europe) is marketed at this pH.

Three new batches of the optimized formulation with the predicted levels of the process/formulation parameters were prepared to confirm the validity of the optimization procedure. These batches were used for further studies.

5.4.2.3 Indomethacin HPβCD formulation (IN-HPβCD)

To investigate the influence of indomethacin ionization on complexation with HPβCD, and to formulate the drug using HPβCD, phase solubility studies at different pH values were conducted.

5.4.2.3.1 Phase-solubility studies

Phase-solubility studies of indomethacin were carried out in buffered HPβCD containing solutions according to the method described by Higuchi and Connors (198). The solutions were buffered at four pH values: phosphate buffer (3.00, 6.80 and 7.40) and acetate buffer (pH 5.00). The buffer strength and ionic strength were 15 mM and 0.03, respectively. An excess amount of indomethacin was added to 5 mL of the buffered cyclodextrin solution, in screw capped glass

vials, containing increasing concentrations of HPβCD (0 - 145 mM). The resulting suspensions were shaken at 25 °C for 24 hours in a reciprocating water bath. Following equilibration, the suspensions were centrifuged at 13,000 rpm for 20 minutes at 4 ºC and the supernatant thus obtained was analyzed for drug content. Each experiment was carried out at least in triplicate, and the binding constants ($K_{1:1}$) for the drug-cyclodextrin complex were calculated from the linear region of the solubility curves using the following equation:

$K_{1:1}$= slope/ S_0 (1-slope) (3)

Where, S_0 = Intrinsic solubility of the drug at different pH values.

5.4.2.3.2 IN- HPβCD formulation preparation

For the preparation of IN- HPβCD formulation, indomethacin (0.1 % w/v) was dissolved in 2.5% w/v HPβCD solution prepared in phosphate buffered saline (pH 6.80). The final pH of the IN-HPβCD solution was selected as 6.80 because Indocorylle® is marketed at this pH.

5.4.3. Particle size and zeta potential measurement

The mean particle size and the polydispersity index (PI) of the SLN dispersion was determined by photon correlation spectroscopy using Zetasizer Nano ZS Zen3600 (Malvern Instruments Inc., Westborough, MA, USA) at 25°C and 173° backscatter detection in disposable folded capillary clear cells. The measurements were obtained using a He-Ne laser of 633 nm and the particle size analysis data were evaluated using volume distribution. Zeta potential measurements were carried out at 25°C in folded capillary cells using the same instrument. The

zeta potential values were obtained from the electrophoretic mobility using the Smoluchowski equation. For measurement of particle size distribution and zeta potential SLNs samples were diluted (1: 500) with water and 10 mM HEPES buffer (pH 6.80), respectively. Bidistilled and 0.2 µM filtered waters was used for these measurements. All measurements were performed at least in quadruplicates.

5.4.4. Assay and entrapment efficiency

The lipid in the IN-SLN dispersion was precipitated using 190 proof alcohol and the drug content in the supernatant,t after centrifugation (13000 rpm for 20 min), as such or on further dilution with 190 proof alcohol, was measured using a HPLC system. Indomethacin content in IN-SOL and IN-HPβCD were also measured after dilution with 190 proof alcohol.

The percentage of indomethacin entrapped in the SLNs (Entrapment efficiency (% EE)) was determined by measuring the concentration of free drug in the aqueous phase of undiluted IN-SLN dispersion. The EE was evaluated by ultra filtration technique with a 100 kDa centrifugal filter device composed of regenerated cellulose membrane (Amicon® Ultra). An aliquot, 500 µL, of undiluted IN-SLN was added to the sample reservoir and centrifuged at 5000 RPM for 10 min. The obtained filtrate was further diluted with alcohol (190 proof) and analyzed for drug content using HPLC. The EE was estimated using equation (4)

$$EE\ (\%) = ((W_i - W_f)/ (W_i)) \times 100 \text{-------} (4)$$

Where W_i = Total drug content W_f = amount of free drug in aqueous phase

5.4.5. Osmolality and pH measurement

Osmolality was measured by the freezing-point depression method using an Osmette S, model 4002 (Precision Systems Inc., Natick, MA). After calibration of the osmometer with reference standards (100 and 500 mOsm/kg H_20) the osmolality was measured (2 ml sample vials were used). The pH was measured using a calibrated Mettler Toledo Seven Easy pH meter (Fisher Scientific, St.Louis, Missouri, USA)

5.4.6. Sterilization and stability of the formulations

Three batches of optimized IN-SLNs were evaluated for physical and chemical stability after autoclaving (110°C for 30 min) and on storage (40°C, 25°C and 4°C). The stability parameters evaluated were particle size, polydisperisity index, zeta potential, entrapment efficiency, pH and drug content. Initial values for the parameters mentioned above were determined 24 hours post-preparation and post-sterilization. IN-SLNs were subjected to moist heat sterilization at 110°C for 30 min using a Tuttnauer Brinkmann 3545 EP autoclave (Fisher Scientific, St.Louis, Missouri, USA). The samples were then subjected to stability studies at 40°C, 25°C and 4°C for a period of one month (last point tested). Additionally, the drug content in the IN-HPβCD and IN-SOL formulation was also monitored post sterilization (110°C for 30 min) and on storage (40°C, 25°C and 4°C).

5.4.7. *In vitro* drug release studies

The *in vitro* release/diffusion of indomethacin from IN-HPβCD, IN-SOL and IN-SLN formulations was determined using dialysis cassettes (Slide-A-Lyser® G2, 10k MWCO Cellulose

membrane, Thermo Scientific, Rockford, IL). The dialysis cassettes, containing 2 mL of one of the formulations, were placed in glass vessels filled with 200 mL of phosphate buffer (15 mM, pH 6.80). The samples were then continuously agitated at at 37˚C in a reciprocating water bath (100 rpm). Aliquots, 500 µL, were withdrawn from the receiver chamber at predetermined time points, and replaced with an equal volume of fresh phosphate buffer (15 mM, pH 6.80) to maintain sink conditions. Samples were analyzed for drug content using HPLC. All experiments were carried out at least in triplicates.

5.4.8. Powder X-ray diffraction (pXRD) studies

pXRD measurements were carried out with a Bruker D8 Advanced X-ray diffractometer with a SOL-X detector The 2θ scan range was 5°-50° with a step scan of 0.30. pXRD patterns were recorded for indomethacin, compritol 888® ATO, physical mixture (indomethacin and compritol 888® ATO) and lyophilized IN-SLNs . The ratios of drug and lipids used in these set of studies were similar to the weight ratio in the IN-SLNs. Lyophilization was carried out using Labconco Freeze Dry systems/Freezone 2.5.

5.4.9. Fourier transform infrared spectroscopy (FTIR) studies

A Perkin-Elmer spectrum 100-FTIR spectrometer (Perkin-Elmer Life and Analytical Sciences, Shelton, CT, USA) equipped with universal attenuated total reflection sampling accessory was used for recording infrared spectra of samples. FTIR studies were carried out on indomethacin, compritol 888® ATO, physical mixture (indomethacin and compritol 888® ATO)

blank IN-SLNs and lyophilized IN-SLNs. The spectrum was collected for each sample within the wave number region 4000-650 cm^{-1}. The spectra were evaluated for absence or shift in the wave number of the characteristic peaks. The ratios of drug and lipids used in these set of studies were similar to the weight ratios in IN-SLNs

5.4.10. Differential Scanning Calorimetry (DSC) analysis

The Differential Scanning Calorimetry (DSC) analysis was carried out using a Diamond Differential Scanning Calorimeter (Perkin-Elmer Life and Analytical Sciences, Shelton, CT, USA). The samples were weighed and heretically sealed in aluminum pans and were heated from 20°C to 200°C at a heating rate of 10°C/min under nitrogen purge (20 mL/min). An empty aluminum pan was used as the reference.

The DSC analysis was carried out on the following samples: (1) indomethacin (~0.5 mg); (2) HPβCD; (3) physical mixture (indomethacin and HPβCD); (4) lyophilized IN-HPβCD; (5) lyophilized IN-SLNs formulation; (6) lyophilized blank SLNs; (7) physical mixture (indomethacin and Compritol 888® ATO). Additionally, hyper DSC studies (20 to 200°C at heating rate of 200 °C /min) on lyophilized IN-SLNs, and physical mixture (indomethacin and Compritol 888® ATO) were also performed. Approximately 10 mg of lyophilized IN-SNL, blank SLNs and IN-HPβCD was used for the DSC analysis. The physical mixture consisted of ~0.5 mg indomethacin and ~9.5 mg of HPβCD/or Compritol 888® ATO. The ratios of drug and lipids, and drug and HPβCD used in these set of studies were similar to the weight ratios in IN-SLNs and IN-HPβCD, respectively.

5.4.11. *In vitro* corneal permeation studies

Corneas excised from whole eyes, obtained from Pel-Freez Biologicals (Roger, AK), were used for the determination of *in vitro* trans-corneal permeability. Whole eyes were shipped overnight in Hanks' Balanced Salt Solution, over wet ice, and were used immediately upon receipt. The corneas were excised with some scleral portion adhering to help secure the membrane between the diffusion half-cells during the course of a transport study. After excision, the corneas were washed with ice cold DPBS (Dulbecco's Phosphate Buffer Saline, pH 7.40) and mounted on side-bi-side diffusion half cells (PermeGear Inc., Bethlehem, PA, USA) with the epithelial side facing the donor chamber. Temperature of the half-cells, were maintained at 34°C with the help of a circulating water bath.

Two mL of the optimized IN-SLNs (pre- and post-sterilization), or IN-SOL or, IN-HPβCD was diluted with 1 mL of 3 mM acyclovir (ACV) solution (in DPBS pH 7.40) and immediately added to the donor chamber after adjusting the pH to 6.80. The indomethacin content in all the formulations was 0.1 % w/v. The receiver chamber medium consisted of 3.2 mL of HPβCD (2.5 % w/v) in DPBS (pH 7.40) solution for all the transport studies. A slight difference in the donor and receiver chamber volumes helped maintain the normal shape of the cornea through marginally elevated hydrostatic pressure. The contents of both chambers were stirred continuously with a magnetic stirrer. Aliquots, 400 µL, were withdrawn from the receiver chamber at predetermined time points (30, 60, 90, 120, 150 and 180 min), and replaced with an equal volume of the 2.5% w/v HPβCD in DPBS (pH 7.40). Samples were stored at -80°C until further analysis of indomethacin and acyclovir content. ACV was added to monitor the integrity

of the corneal epithelium in the presence of the formulation components. Transcorneal permeation of ACV alone (control) was also evaluated as described above except that in this study the donor solution consisted of one mL of ACV (3 mM in DPBS pH 7.40) diluted with two mL of DPBS (pH 6.80). Additionally, permeation of indomethacin through the cornea from IN-HPβCD was also monitored in the presence of surfactants (0.75% w/v Tween 80 and 0.25% w/v Poloxamer 188). All experiments were carried out at least in quadruplicate. ACV content in the donor chamber was analyzed using ultra filtration technique (Amicon® Ultra 100 kDa centrifugal filter device). An aliquot (200 µL) of ACV containing IN-SLN dispersion sample was added to the sample reservoir and centrifuged at 5000 RPM for 10 min. The obtained filtrate was further diluted with water and analyzed for ACV content using HPLC.

In order to evaluate the effect of the addition of ACV on the physiochemical properties of the IN-SLNs during the transport experiment additional experiments were undertaken. In these experiments, 1 mL of 3 mM ACV solution (in DPBS pH 7.40) was added to 2 mL of the formulation and at the end of three hours osmolality, zeta potential, particle size, and entrapment efficiency or IN-SLNs were determined.

5.4.12. Data Analysis

Rate of indomethacin and ACV transport across excised rabbit cornea was obtained from the slope of a "cumulative amount of indomethacin or ACV transported" versus "time" plot. Steady-state flux (SSF) were determined by dividing the rate of transport by the surface area as described in equation (5)

$$\text{Flux (J)} = (dM/dt)/A \quad (5)$$

Where, M is the cumulative amount of drug transported and A is the corneal surface area exposed to the permeant.

Corneal membrane permeability was determined by normalizing the SSF to the donor concentration, C_d according to equation (6)

$$\text{Permeability } (P_{app}) = \text{Flux}/C_d \quad (6)$$

5.4.13. Analytical method:

Samples were analyzed for indomethacin and acyclovir content using an HPLC system comprised of Waters 717 plus autosampler, Waters 2487 Dual λ Absorbance detector, Waters 600 controller pump and Agilent 3395 integrator. A Symmetry® C_{18} 4.6 X 250 mm column was used for both compounds. Mobile phase for acyclovir consisted of 20 mM phosphate buffer (pH 2.50) and acetonitrile (98:2) and for indomethacin the mobile phase used was methanol, water and orthophosphoric acid (70:29.05:0.05). The λ_{max} for indomethacin and acyclovir were 270 and 254 nm respectively. The flow rate was set at 1 mL/min for both compounds.

5.5. Results

5.5.1. pH- Saturation Solubility:

Figure 5-1 illustrates the saturation solubility of indomethacin as a function of pH. These studies were carried out at 25 °C for 24 hours in a reciprocating water bath. Solubility of indomethacin was observed to be highly dependent on solution pH. Solubility of the drug in an acid pH (pH 1.20, 3.00, and 5.00) was observed to be significantly lower than that in the neural buffers (pH

6.80 and 7.40). Aqueous solubility of indomethacin at pH 7.40, pH 6.80, pH 5.00, pH 3.00 and pH 1.20 was 732.0 ± 20.0 µg/mL, 340.0 ± 10.0 µg/mL, 10.0 ± 0.06 µg/mL, 1.5 ± 0.05 µg/mL and 0.3 ± 0.03 µg/mL, respectively.

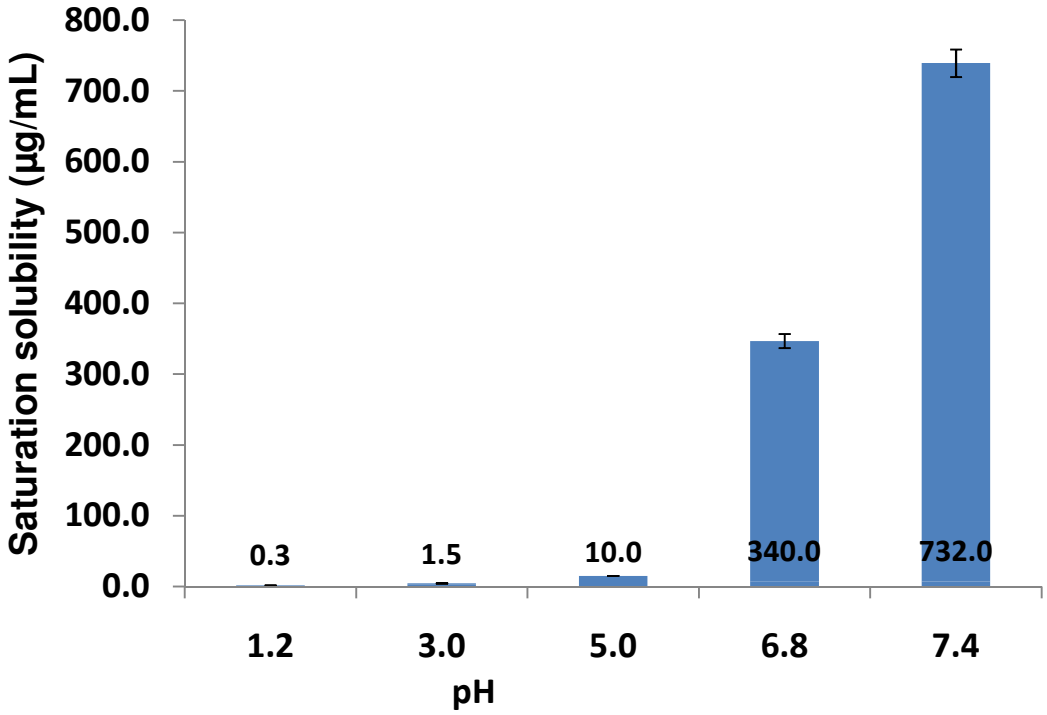

Figure 5-1: Solubility of indomethacin at 25 °C as a function of pH. Results are depicted as mean ± SD (n=3).

5.5.2. Experimental design

Five factors i.e. type of lipid, homogenization pressure, number of homogenization cycles, fraction of Tween 80 in a mixture of surfactants (Poloxamer 188 and Tween 80, total surfactant concentration 1% w/v) and pH were investigated for optimization of the IN-SLNs

preparation process. Two factors, type of lipid and homogenization pressure, were pre-screened and only three factors were used to construct face-centered central composite design (FCCD).

5.5.2.1. Screening study: Selection of Lipid

Figure 5-2 illustrates the apparent partition coefficient (K_{app}) of indomethacin in various lipids. Partitioning behavior of indomethacin between lipid and phosphate buffer (pH 6.80) was determined by measuring the free concentration remaining in the aqueous phase. The K_{app} was calculated using equation 1. The K_{app} of indomethacin in Compritol 888® ATO, Precirol®ATO 5, Dynasan® 114, Softisan 154 and Dynasan ® 118, were 10.2 ± 0.70, 5.1 ± 0.66, 2.71 ± 0.54, 2.71 ± 0.31 and 2.50 ± 0.26, respectively. Solubility of indomethacin (100 mg) in 2 g and 5g of lipid was evaluated by incubating the drug with the lipid, at a temperature 10°C above the melting points of lipid, for 15 minutes. Indomethacin remained undissolved and drug crystals were observed in 2 g of Precirol®ATO 5, Dynasan® 114, Softisan 154 and Dynasan ® 118. Indomethacin was soluble in 5 gm of Precirol®ATO 5, Dynasan® 114, Softisan 154 and Dynasan ® 118, however, drug crystals were observed in these lipids after 24 hours under light microscopy. However, Indomethacin exhibited good solubility (clear yellow lipid melt) in 2 g or 5 g of Compritol 888® ATO and no drug crystals were observed on cooling to room temperature and after 24 hours under light microscopy.

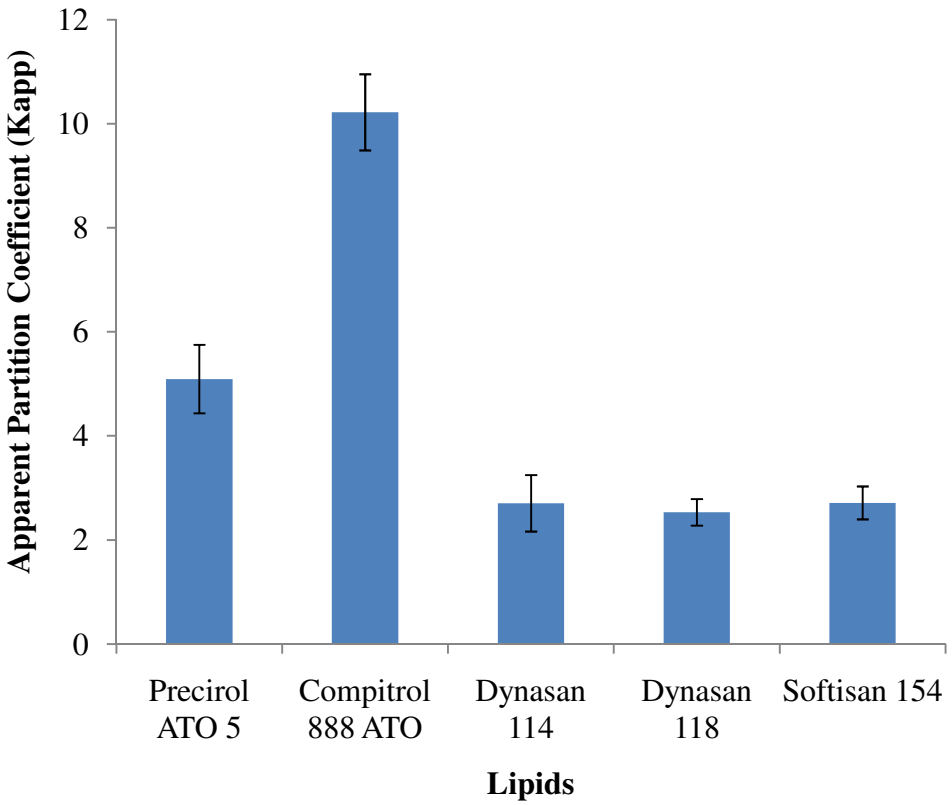

Figure 5-2: Partition Coefficient of Indomethacin in various lipids.

5.5.2.2. Screening study: Selection of homogenization pressure

For selection of the optimum homogenization pressure the pre-emulsion was passed through the high pressure homogenizer at three different homogenization pressures (7,500 psi, 15,000 psi and 20,000) for 5 cycles. Figure 5-3 illustrates the mean particle size of the IN-SLNs obtained at the three different homogenization pressures. The mean particle size of the IN-SLNs at 7500 psi, 15000 psi and 20,000 psi were 300 ± 10 nm, 180 ± 4 nm and 178 ± 10 nm, respectively. In these studies Compritol 888® ATO (2% w/v) was employed as the lipid phase, based on the lipid prescreening experiments, and the surfactant (0.75% w/v of Tween 80 and 0.25 % w/v of Poloxamer 188) was used to prepare the IN-SLNs

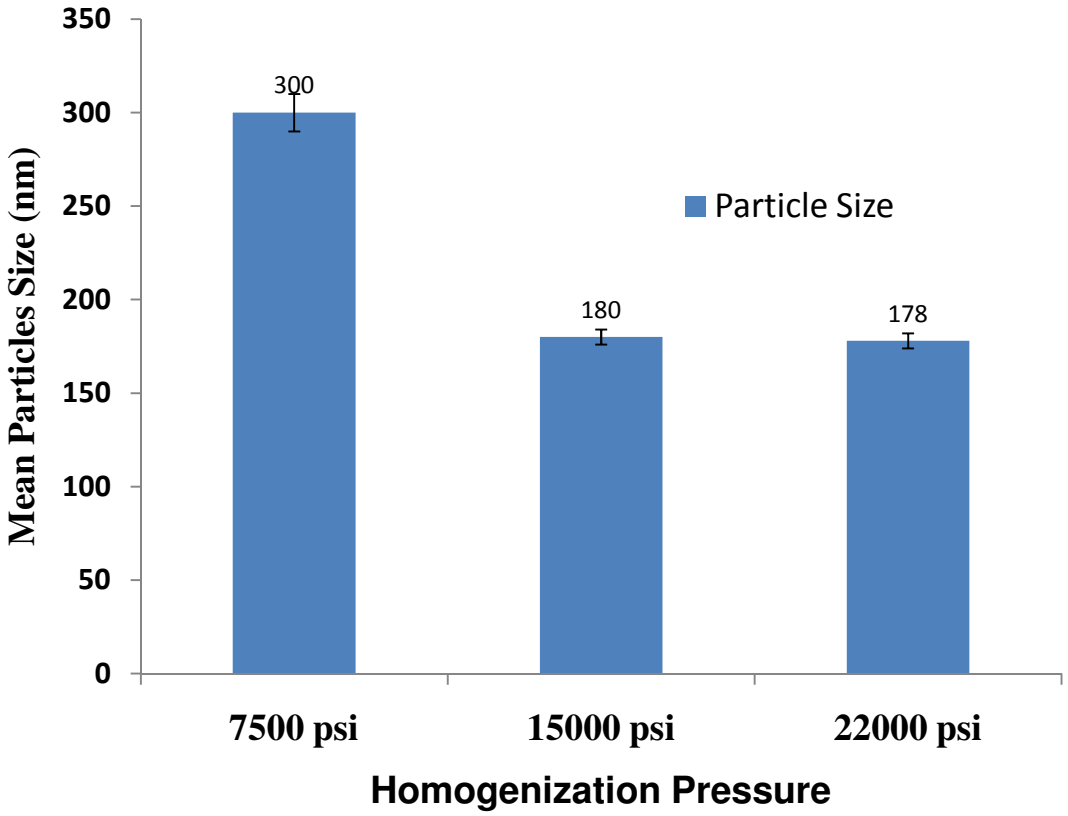

Figure 5-3: Effect of homogenization pressure on the mean particle size of the IN-SLNs.

5.5.2.3. Face-centered Central Composite Design (FCCD)

A three-factor, three-level FCCD was used to optimize the IN-SLN formulation process parameters with respect to the number of homogenization cycles (A), fraction of Tween 80 in the mixture of Poloxamer 188 and Tween 80, while keeping the total surfactant concentration at 1% w/v (B), and pH (C) (Independent Variables/factors). The experimental runs and the responses (Y_1 = particle size; Y2 = entrapment efficiency and Y_3 = zeta potential) are provided in Table 5-2. Compritol 888® ATO (2% w/v), indomethacin (0.1% w/v) and glycerin (2.25% w/v) were

used as the other formulation components and a homogenization pressure of 15,000 psi was used to carry out the experimental runs illustrated in Table 5-2. Compritol 888® ATO and the homogenization pressure of 15,000 psi were selected based on the results of the pre-screening experiments (Section 5.4.2.1 and 5.4.2.2). The ranges of the responses Y_1, Y_2, and Y_3 were 100 to 1030 nm, 43 to100% and -20 to -22 mV, respectively (Table 5-2). Table 5-3 represents the ANOVA results with respect to the different models for each dependent variable Y_1, Y_2, and Y_3. The linear and quadratic models for the response variable Y_1 demonstrated an F-value of 10.20 and 998.96, respectively. The p-value for the linear and quadratic models for the response variable Y_2 were <0.0004 and <0.0001, respectively. For response variable Y_3, p values of 0.3415, 0.4678 and 0.0870 were observed for linear, 2FI, and quadratic models, respectively. The fitted quadratic model equation generated by the design expert software for the responses Y_1, Y_2, and Y_3 are given in Table 5-4. Tables 5-5, 5-6 and 5-7 represents the ANOVA results for the fitted quadratic model for particle size (Y_1), entrapment Efficiency (%) (Y_2) and zeta potential (Y_3), respectively. Where liner terms A, B and C represents homogenization pressure, Tween 80 fraction in the mixture of surfactants (Tween 90 and Poloxamer 188, total surfactant concentration 1% w/v) and pH, respectively. Terms AB, BC and AC represent interaction terms and A^2, B^2 and C^2 represent quadratic terms.

Table 5-3: Analysis of variance results of different models for each response.

Dependent Variable	Model	Sum of Squares	df	Mean Square	F-Value	p-value Prob > F
Particle size (Y_1)	Linear	10718.04	3	3572.68	10.20	0.0005*
	2FI	172.6968	3	57.57	0.14	0.9356
	Quadratic	5412.205	3	1804.07	998.96	< 0.0001*
Entrapment Efficiency (%) (Y_2)	Linear	4406.5	3	1468.83	56.67	< 0.0004*
	2FI	112.5	3	37.50	1.61	0.2344
	Quadratic	296	3	98.67	159.14	< 0.0001*
Zeta Potential (Y_3)	Linear	1.80	3	0.60	1.20	0.3415
	2FI	1.38	3	0.46	0.90	0.4678
	Quadratic	3.09	3	1.03	2.92	0.0870

2FI: Two factor interaction model; *p<0.05

Table 5-4: Fitted Quadratic model equations for particle size (Y_1), entrapment efficiency (Y_2), and zeta potential (Y_3) as the responses.

Response	Fitted Quadratic Model Equation
Particle size (Y_1)	$(Y_1)^{0.68} = 81.13 - 20.60\,A + 5.33B + 4.66\,C - 2.05AB + 1.27A^2 + 32.60B^2 - 0.42C^2$
Entrapment Efficiency (Y_2)	$Y_2 = 40.13 - 21.54\,B + 24.07C + 4.41BC + 18\,B^2 - 3.3C^2$
Zeta Potential (Y_3)	$Y_3 = -28.11 - 0.36\,A + 0.68B + 2.8\,C - 0.17A - 0.016AC - 0.14BC + 0.04A^2 + 1.27B^2 - 0.23C^2$

Table 5-5: Analysis of variance results of fitted quadratic model for particle size response (Y_1)

Source	Sum of Squares	df	Mean Square	F-Value	P-value
Model	16300.9	7	2328.7	1387.7	< 0.0001
A	8665.9	1	8665.9	5164.0	< 0.0001
B	2051.2	1	2051.2	1222.3	< 0.0001
C	0.9	1	0.9	0.5	0.4731
AB	170.6	1	170.6	101.7	< 0.0001
A^2	2121.5	1	2121.5	1264.2	< 0.0001
B^2	205.7	1	205.7	122.6	< 0.0001
C^2	4.1	1	4.1	2.5	0.1422
Residual	20.1	12	1.7		
Lack of Fit	16.7	7	2.4	3.5	0.0927
Pure Error	3.4	5	0.7		
Cor Total	16321.0	19			

Table 5-6: Analysis of variance results of fitted quadratic model for percentage entrapment efficiency (Y_2).

Source	Sum of Squares	df	Mean Square	F-Value	P-value
Model	4814.9	5	963.0	2139.96	< 0.0001
B	1166.4	1	1166.4	2592	< 0.0001
C	3240.0	1	3240	7200	< 0.0001
BC	112.5	1	112.5	250	< 0.0001
B^2	64.8	1	64.8	144	< 0.0001
C^2	288.8	1	288.8	641.78	< 0.0001
Residual	6.3	14	0.45		
Lack of Fit	3.5	9	0.39	0.68	0.7107
Pure Error	2.8	5	0.57		
Cor Total	4821.2	19			
Model	4814.9	5	963.0	2134.0	< 0.0001
Cor Total	16321.0	19			

Table 5-7: Analysis of variance results of fitted quadratic model for zeta potential (Y_3).

Source	Sum of Squares	df	Mean Square	F-Value	P-value
Model	6.3	9	0.7	2.0	0.1528
A	1.6	1	1.6	4.5	0.0592
B	0.1	1	0.1	0.3	0.6064
C	0.1	1	0.1	0.3	0.6064
AB	1.1	1	1.1	3.2	0.1047
AC	0.1	1	0.1	0.4	0.5652
BC	0.1	1	0.1	0.4	0.5652
A^2	1.8	1	1.8	5.2	0.0556
B^2	0.3	1	0.3	0.8	0.3956
C2	1.3	1	1.3	3.6	0.0863
Residual	3.5	10	0.4		
Lack of Fit	0.2	5	0.0	0.1	0.9961
Pure Error	3.3	5	0.7		
Cor Total	9.8	19			

The fitted quadratic models for Y_1 and Y_2 responses demonstrated an insignificant lack of fit with p-value of 0.0927 and 0.7107, respectively (Table 5-5 and Table 5-6). On the other hand, the fitted quadratic model for Y_3 exhibited a significant lack of fit with F-value of 0.1 and p-value of 0.9961, respectively (Table 5-7). ANOVA results of the fitted quadratic model for response Y_1 demonstrated that linear terms (A, B), interaction terms (AB) and quadratic terms (A^2, B^2) were significant (Table 5-5) while the linear terms B and C, interaction term BC and quadratic terms B^2 and C^2 were significant in ANOVA results for response Y_2 (Table 5-6). None of the terms were significant in the fitted quadratic model for response Y_3 (Table 5-7). Table 5-8 summaries the results of the regression analysis for responses Y_1, Y_2 and Y_3 for fitting to the quadratic model equations given in Table 5-4. The R^2, adjusted R^2 and predicted R^2 were > 0.9956 for response Y_1 and Y_2. On the contrary, the R^2, adjusted R^2 and predicted R^2 for response Y_3 were 0.6394, 0.3148 and 0.2047, respectively.

Table 5-8: Summary of results of regression analysis for responses Y_1, Y_2 and Y_3 for fitting to quadratic model equations given in Table 5-4

Quadratic model	R^2	Adjusted R^2	Predicted R^2
Response Y_1	0.9988	0.9980	0.9956
Response Y_2	0.9987	0.9982	0.9974
Response Y_3	0.6394	0.3148	0.2047

The three-dimensional (3D) plots, based on the fitted quadratic model to assess the change of the response surface, depicting the effect of homogenization cycles (A) and ratio of Tween 80 (B) on particle size of IN-SLNs is shown in Figure 5-4. The response surface plot from interaction of pH (C) and fraction of Tween 80 (B) on percentage entrapment efficiency of IN-SLNs is presented in Figure 5-5. In these plots (Figure 5-4 and Figure 5-5) the fraction of Tween 80 in the mixture of surfactants (Tween 80 and Poloxamer 188) was varied while keeping the total surfactant concentration at 1% w/v. Particle size of IN-SLNs rapidly decreased as the number of homogenization cycle (A) increased (Figure 5-5). As the fraction of Tween 80 (B) increased in the formulation an increase in the particle size of the IN-SLNs was observed. However, increase in Tween 80 (B) in the formulation led to a significant increase in the percentage entrapment of indomethacin in the SLNs at all the pH (C) values tested (Figure 5-5). Figures 5-6 and 5-7 represent the 3D response surface plots of effect of homogenization cycle (A), fraction of Tween 80 (B) and pH (C) on zeta potential (Y_3). Significant changes in the zeta potential values were not observed, as indicated by straight plots, with a change in A, B or C.

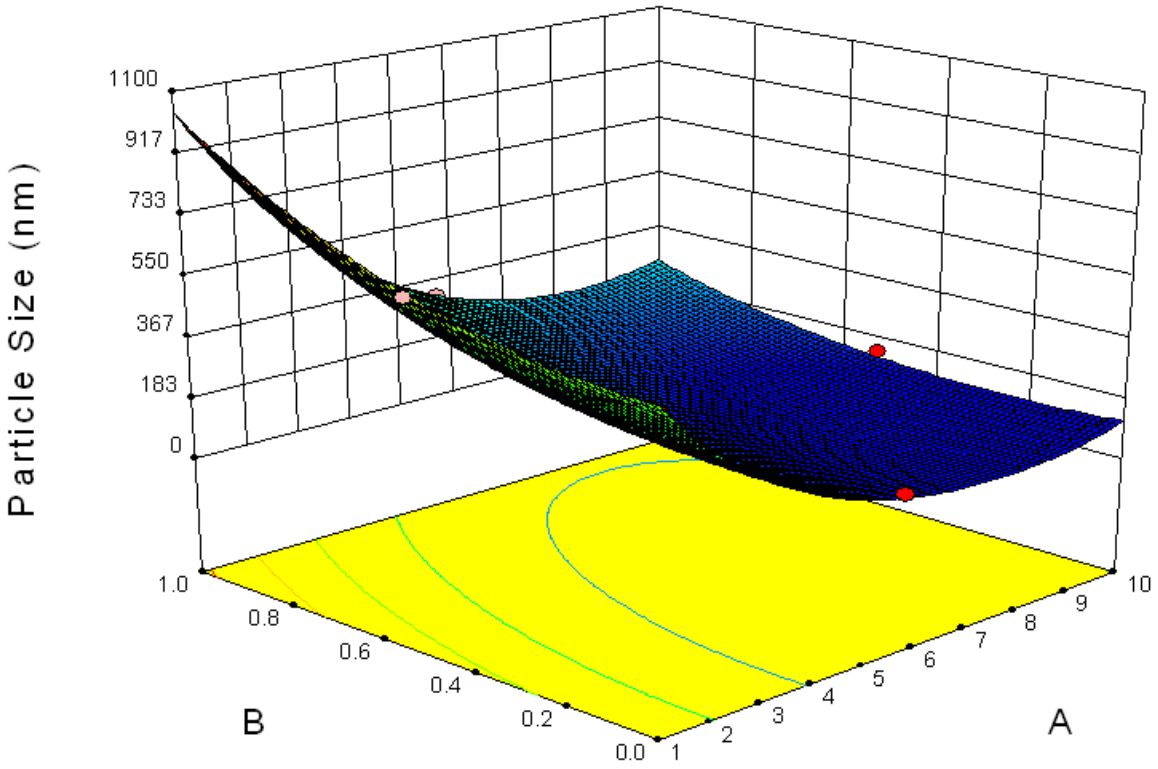

Figure 5-4: Response surface plot of effect of A: homogenization cycles; and B: fraction of Tween 80 in the mixture of surfactants (Poloxamer 188 and Tween 80, total concentration 1% w/v) on response particle size (Y_1).

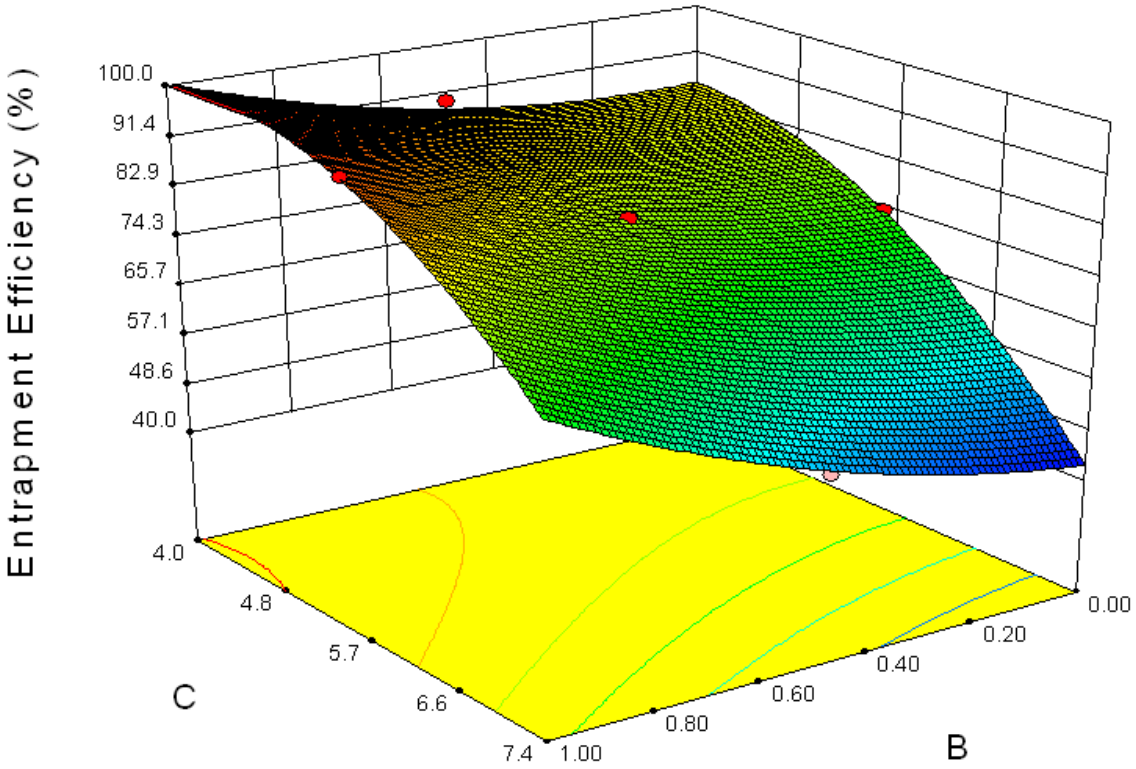

Figure 5-5: Response surface plot of effect of B: fraction of Tween 80 in the mixture of surfactants (Poloxamer and Tween 80, total concentration 1% w/v); and C: pH on response entrapment efficiency (Y_3).

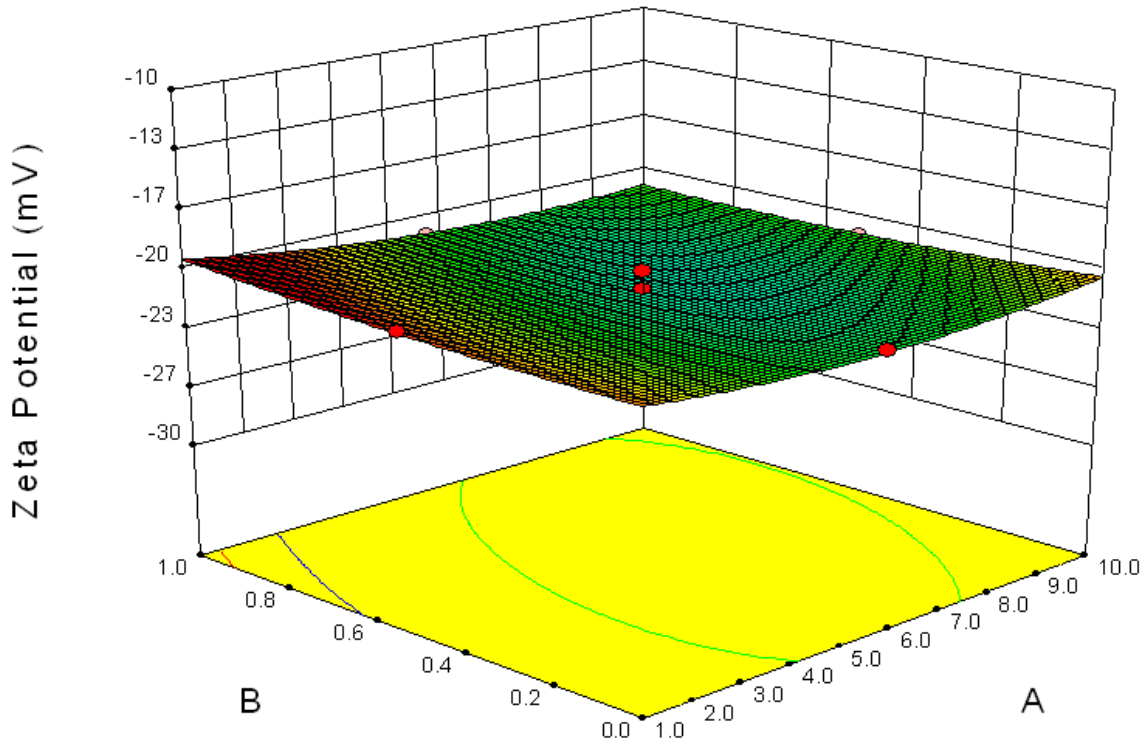

Figure 5-6: Response surface plot of effect of A: homogenization cycle; and B: fraction of Tween 80 in the mixture of surfactants (Poloxamer and Tween 80, total concentration 1% w/v), on response zeta potential (Y_3).

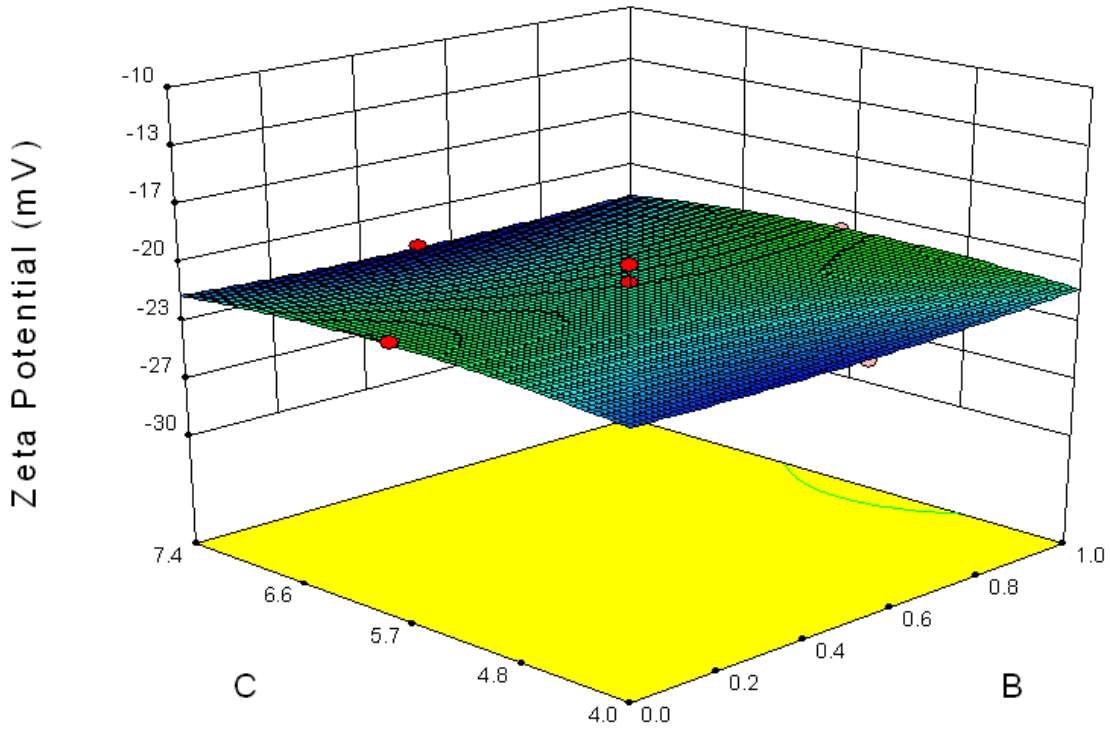

Figure 5-7: Response surface plot of effect of B: fraction of Tween 80 in the mixture of surfactants (Poloxamer and Tween 80, total concentration 1% w/v), and C: pH, on response zeta potential (Y_3).

5.5.2.4. Optimization and experimental validation

By analyzing the response surface plots, constraints (Table 5-1) and by solving the fitted quadratic model equation optimization of the IN-SLNs formulation was achieved using Design-expert software (Version 8.0.5, Stat-Ease Inc., Minneapolis, U.S.A.). The optimum level for the homogenization cycle, fraction of Tween 80 in the mixture of surfactants (Tween 80 and Poloxamer, total surfactant concentration 1% w/v) and pH were determined to be 6 cycles, 0.75

and 6.80, respectively. Based on the prescreening experimental data Compritol 888®ATO and the homogenization pressure of 15,000 psi were chosen for optimization of IN-SLNs manufacturing process. Table 5-9 represents the quantitative composition of the optimized IN-SLN formulation. At these levels of the independent variables, predicted IN-SLNs particle size, percentage entrapment efficiency and zeta potential were calculated to be 144 nm, 72 % and – 22 mV, respectively.

Table 5-9: Optimized IN-SLNs formulation using Design expert software.

Components	Percentage (w/v)
Indomethacin	0.1
Compritol 888® ATO	2
Poloxamer 188	0.25
Tween 80	0.75
Glycerin	2.25
pH	6.80

.

In order to validate the experimental model, triplicate batches of IN-SLNs were prepared by using the statistically optimized conditions. Table 5-10 represents a comparison of the predicted and observed responses for the optimized formulation. The observed responses for

particle size (Y_1), percentage entrapment efficiency (Y_2) and zeta potential (Y_3) were 140 ± 5 nm, 72 ± 5% and -21 ± 1.8 mV, respectively. The values were within 5% of the predicted error.

Table 5-10: Comparative levels of predicted and observed responses for optimized formulation.

Response	Observed (O)	Predicted (P)	Predicted error (%) ((O-P)/P)*100
Y_1 (nm)	140 ± 5	144	-2.78
Y_2 (%)	72 ± 5	72	0
Y_3 (mV)	-21 ± 1.8	-22	- 4.5%

5.5.3. Phase solubility Studies

Phase solubility studies are useful for studying the complexation of poorly soluble drugs with CD. Figure 5-8 represents the phase-solubility diagrams of indomethacin with HPβCD in a buffered solution. The solutions were buffered at four pH values: 3.00, 6.80 and 7.40 (phosphate buffer) and 5.00 (acetate buffer). Table 5-11 depicts the binding constants of indomethacin: HPβCD complexes at different pH values. Phase-solubility studies were conducted for a period of 24 hours. Binding constant was calculated from the slopes of the linear phase-solubility plots using equation 3. HPβCD dramatically improved the aqueous solubility of indomethacin at all the pH values tested. A 180-fold (from 1.5 µg/mL to 272 µg/mL) and a 81-fold (from 10 µg/mL to 810 µg/mL) increase in solubility of indomethacin was observed in the presence of 20% w/v (144 mM) HPβCD at pH 3.20 and pH 5.00, respectively. At pH 6.80 and pH 7.40 an 8.0-fold (from 0.34 mg/mL 2.7 mg/mL) and a 5.2-fold (from 0.73 mg/mL to 5.2 mg/mL) increase in

solubility was observed in the presence of 20% w/v HPβCD. In pH 3.20 and pH 5.00 buffers aqueous solubility of indomethacin increased linearly as a function of HPβCD concentration (A_L type plot). On the other hand, at neutral pH (pH 6.80 and pH 7.40), the phase solubility plots showed negative deviation from linearity (A_N type plot) at higher concentrations of HPβCD (Figure 5-8). The binding constants of indomethacin: HPβCD complexes were 1192 M^{-1}, 715 M^{-1} and 126 M^{-1} and 77 M^{-1} for HPβCD at pH 3.00 and pH 5.00, pH 6.80 and pH 7.40, respectively (Table 5-11)

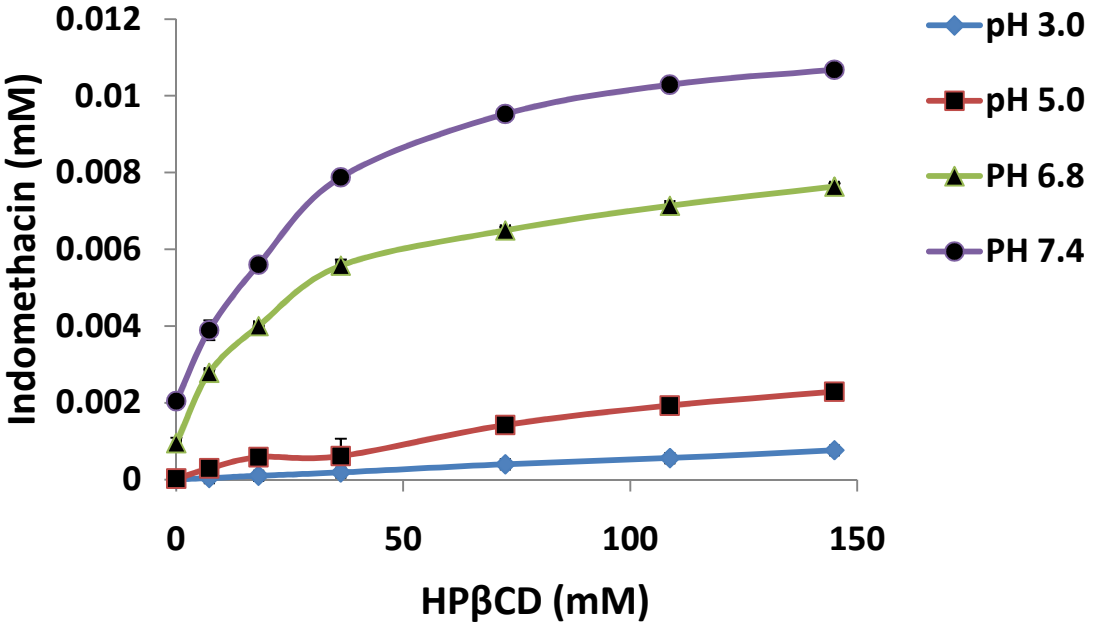

Figure 5-8: Phase solubility plots of indomethacin in the presence of HPβCD at 25°C as a function of pH, following 24 hours equilibration. Each point represents mean ± SD (n=6).

Table 5-11: Slope, apparent stability constant ($K_{1:1}$) and correlation coefficient (R^2) determined from the linear portion of Indomethacin: HPβCD aqueous phase solubility diagrams at different pH values. Solubility of indomethacin (Intrinsic solubility (S_0)) in the absence of HPβCD at different pH values are also given.

pH	S_0 X 10^5 (mM)	Slope x 10^5	$K_{1:1}$ (M^{-1})	R^2
7.40	204.0	15.6	77	0.977
6.80	95.0	12.0	126	0.945
5.00	2.5	1.8	715	0.992
3.00	0.4	0.5	1192	0.999

5.5.4. Effect of sterilization and storage:

Three batches of the optimized IN-SLN formulation were sterilized by autoclaving (110°C for 30 min) and were subjected to storage stability studies at 40°C, 25°C and 4°C for a period of one month. Table 5-12 represents the effect of sterilization on the physical parameters of the IN-SLNs. These parameters were evaluated one day after sterilization. Post-sterilization the mean particle size, polydispersity index (PI), zeta potential, pH and percentage entrapment efficiency of the IN-SLNs were observed to be 149 ± 5.0 nm, 0.17 ± 0.03, -22 ± 0.8 mV, 6.65 ± 0.1 and 71.0 ± 0.2, respectively. Significant difference in all the parameters tested after sterilization was not observed.

Table 5-12: Effect of sterilization (110°C, 30 min) on mean particle size, PI, zeta potential, pH and entrapment efficiency on optimized IN-SLNs formulation.

Evaluated Parameters	Pre-Sterilization	Post-Sterilization
Mean Particle Size (nm)	140 ± 5	149 ± 5.0
PI	0.16 ± 0.01	0.17 ± 0.03
Zeta Potential (mV)	-21 ± 1.8	-22 ± 0.8
pH	6.80 ± 0.10	6.65 ± 0.10
Entrapment Efficiency (%)	72.0 ± 1.5	71.0 ± 0.2

Figure 5-9 represents the effect of sterilization and storage on indomethacin drug content in IN-SLNs, IN-HPβCD and IN-SOL formulations. In the case of IN-SLNs a significant decrease in drug content was not observed post-sterilization and on storage under the test conditions for a period of one month (last time point tested) (Figure 5-9 (A)). However, post-sterilization indomethacin content in the IN-HPβCD and the IN-SOL formulations decreased from 100 % to 84.0 ± 0.3% and 87.7 ± 0.25%, respectively (Figure 5-9 (B), Figure 5-9 (C)). Additionally, further decrease in drug content was observed in IN-HPβCD and IN-SOL formulation on storage. At 40°C, 25°C and 4°C drug content in the IN-HPβCD formulation decreased (from 84.0 ± 0.3%) to 67.0 ± 1.0 %, 72.0 ± 0.5 % and 76.0 ± 0.3%, respectively, at the end of one month (Figure 5-9 (B)). In the case of IN-SOL formulation, at the end of one month the drug content decreased (from 87.7 ± 0.25%) to 73.0 ± 0.9 %, 79.0 ± 0.5 % and 81.0 ± 0.3% at 40°C, 25°C and 4°C, respectively (Figure 5-9 (C)).

Figure 5-9 (A)

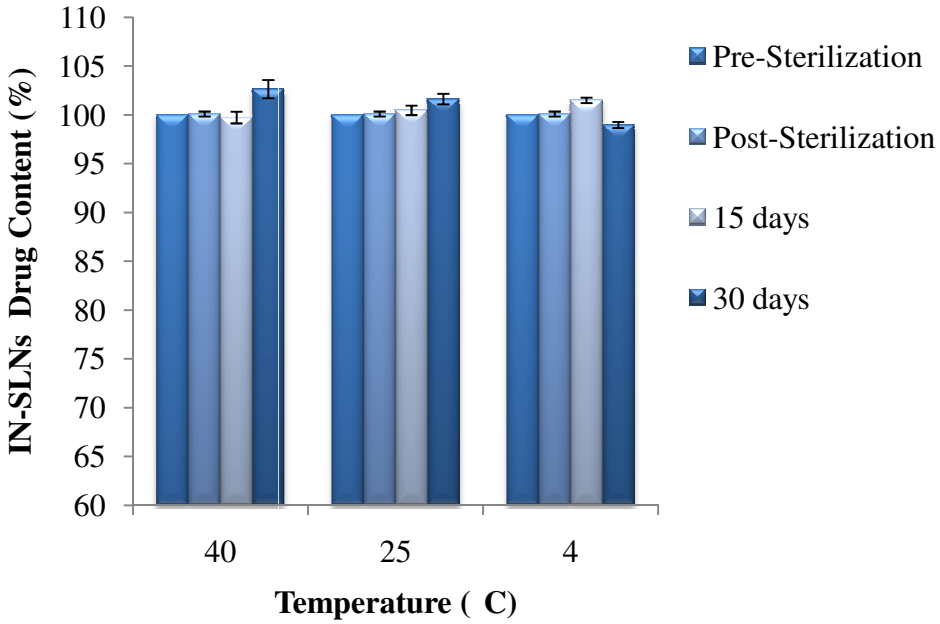

Figure 5-9 (B)

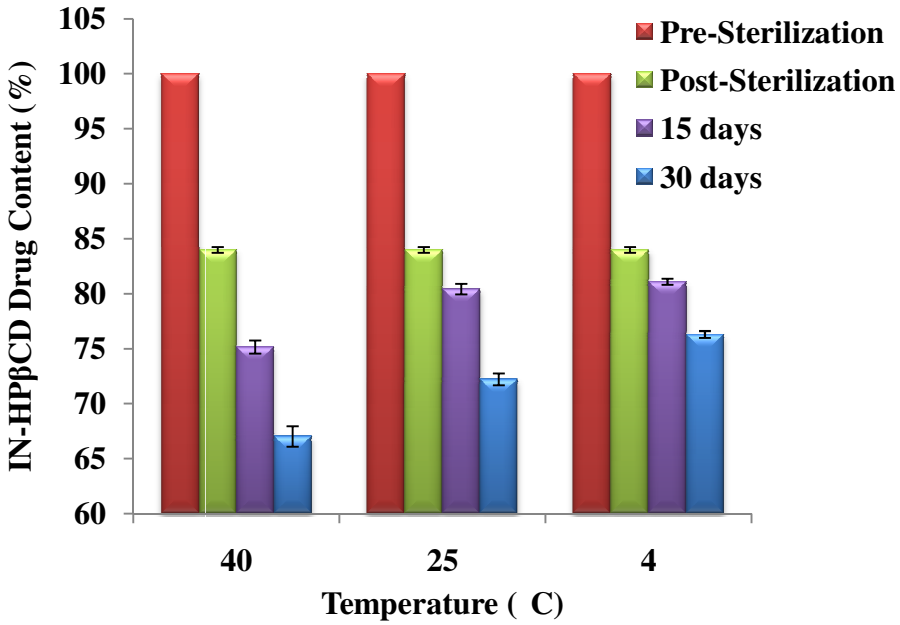

Figure 5-9 (C)

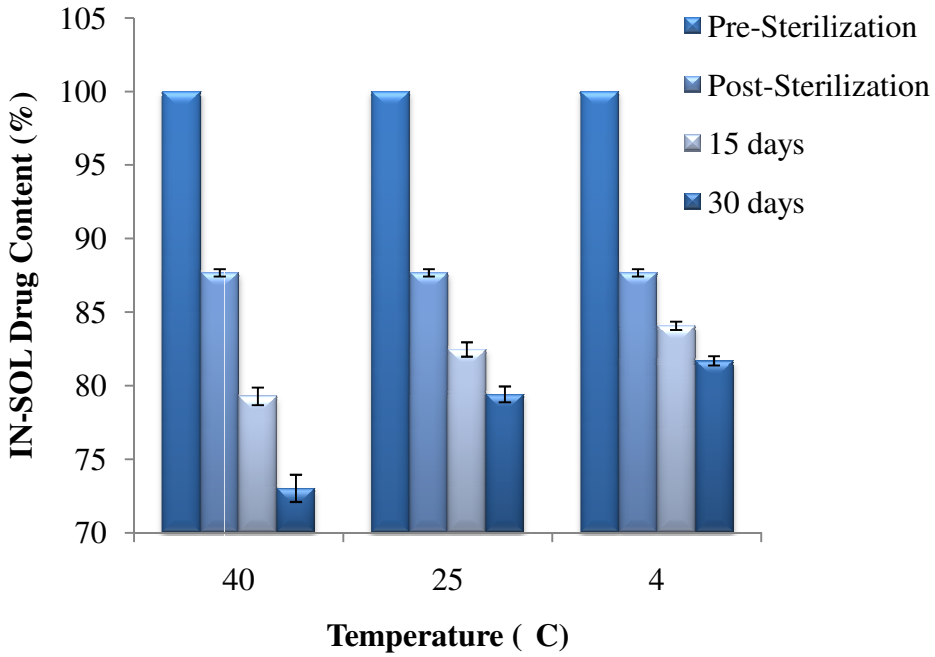

Figure 5-9: Effect of sterilization and one month storage under the test conditions on drug content in IN-SLNs (A), IN-HPβCD (B) and IN-SOL(C) formulations.

Figure 5-10 (A)

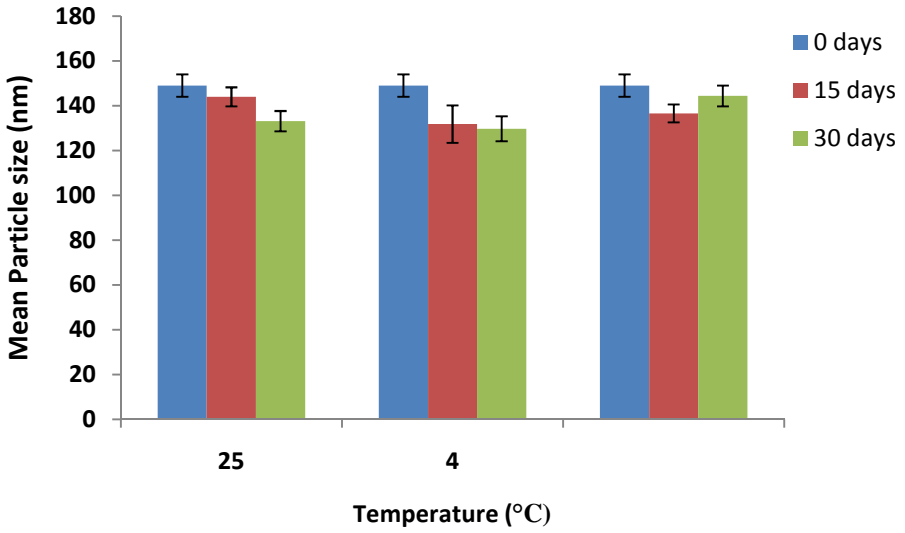

Figure 5-10 (B)

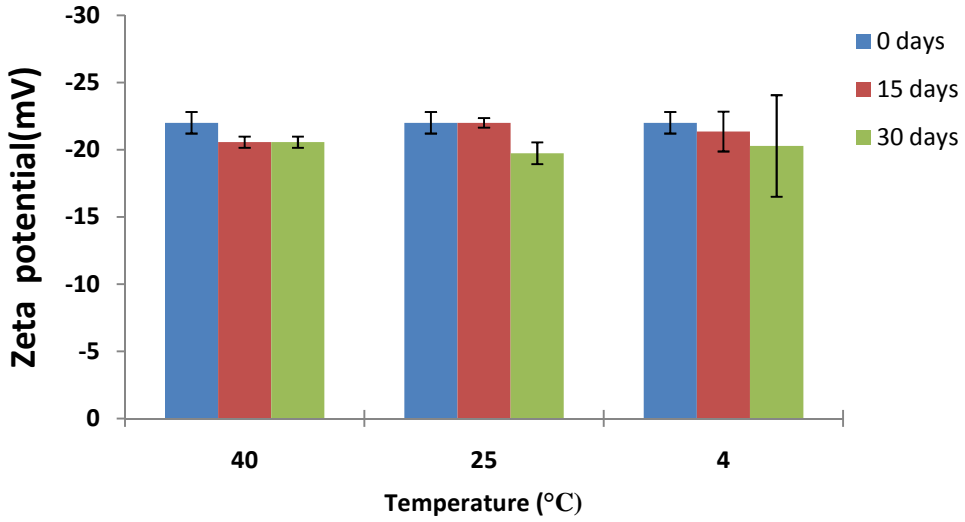

Figure 5-10 (C)

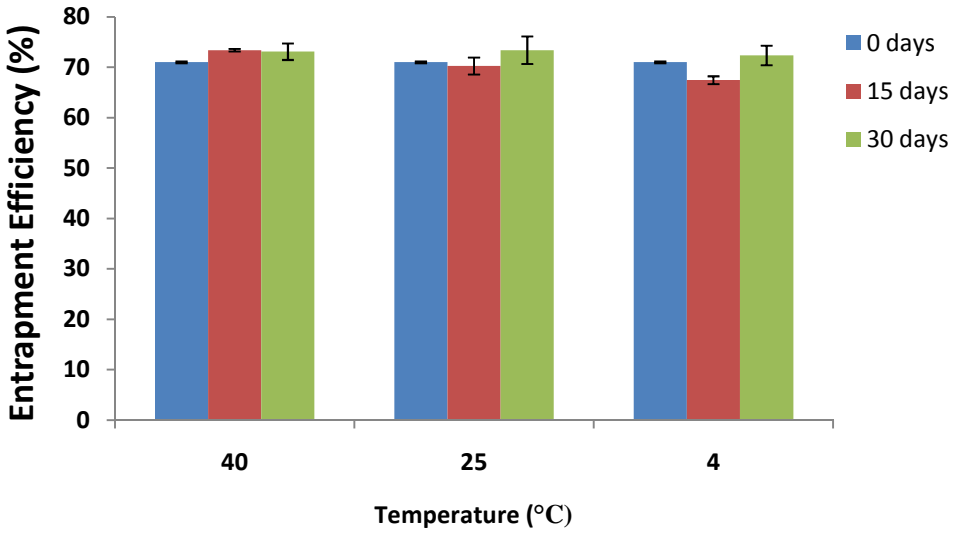

Figure 5-10 (D)

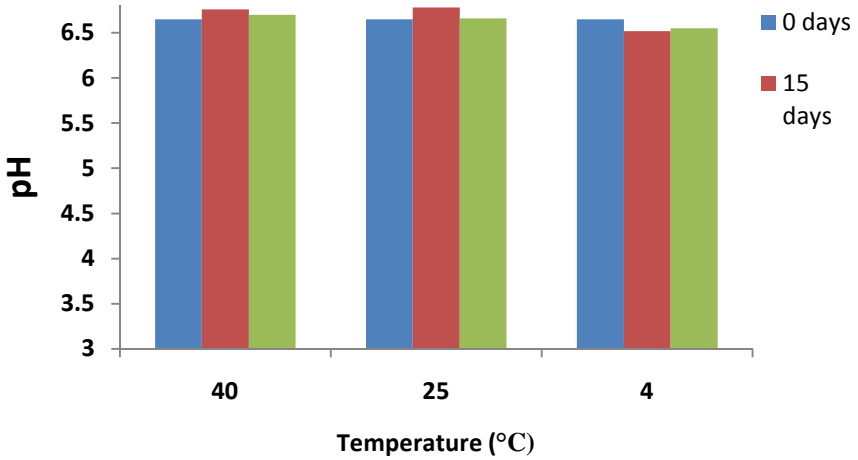

Figure 5-10 represents the effect of storage at 40°C, 25°C and 4°C on the mean particle size, zeta potential, entrapment efficiency and pH of the IN-SLNs. A significant change was not observed with respect to any of these parameters on storage for up to a period of one month (last point tested) under any of the test conditions.

5.5.5. *In vitro* drug release studies

Figure 5-11 represents the *in vitro* cumulative percent release/diffusion of indomethacin from IN-HPβCD, IN-SOL and IN-SLN formulations. These studies were carried out using dialysis cassettes and the receptor compartment consisted of 15 mM phosphate buffer, pH 6.80 maintained 37˚C. At all time points tested a significant decrease in the net release/diffusion of drug from the IN-SLN dispersion was observed compared to IN-HPβCD and IN-SOL formulation. Around 80% of indomethacin was released / diffused across the membrane from the IN-HPβCD and IN-SOL formulations in 3 hours. In contrast, only 60 % of drug was released / diffused across the membrane from the IN-SLN formulation in the same period. These results suggest that release of indomethacin could be modified by using the IN-SLNs.

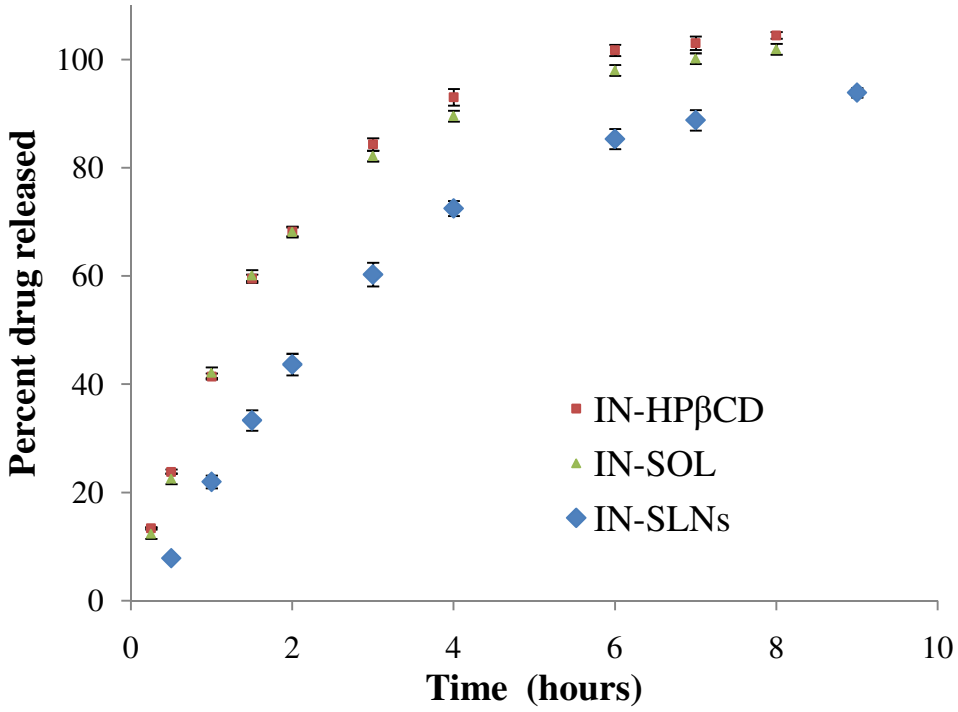

Figure 5-10: Comparative cumulative percent release of indomethacin from IN-HPβCD, IN-SOL and IN-SLNs formulations. Results are depicted as mean ± SD (n=3).

5.5.6. pXRD Studies

Figure 5-12 represents the overlaid X-ray diffractograms of indomethacin, compritol 888® ATO, physical mixture (indomethacin and compritol 888® ATO), and lyophilized IN-SLNs. The X-ray diffraction pattern of indomethacin demonstrated four sharp peaks at 2θ angles of about 19, 21, 26 and 29°. The diffraction patterns of compritol 888® ATO was similar to that of the physical mixture and showed two peaks at 2θ angles of about 21 and 23°. However, the X-ray diffractogram of the lyophilized IN-SLNs showed three peaks at 2θ angles of about 19, 21, and 23°. The difference in the diffraction pattern of compritol 888® ATO in bulk lipid and IN-SLNs could be attributed to stress experienced during lyophilization which may have led to transformation of the metastable β' form to β_i form resulting in appearance of the third peak (226).

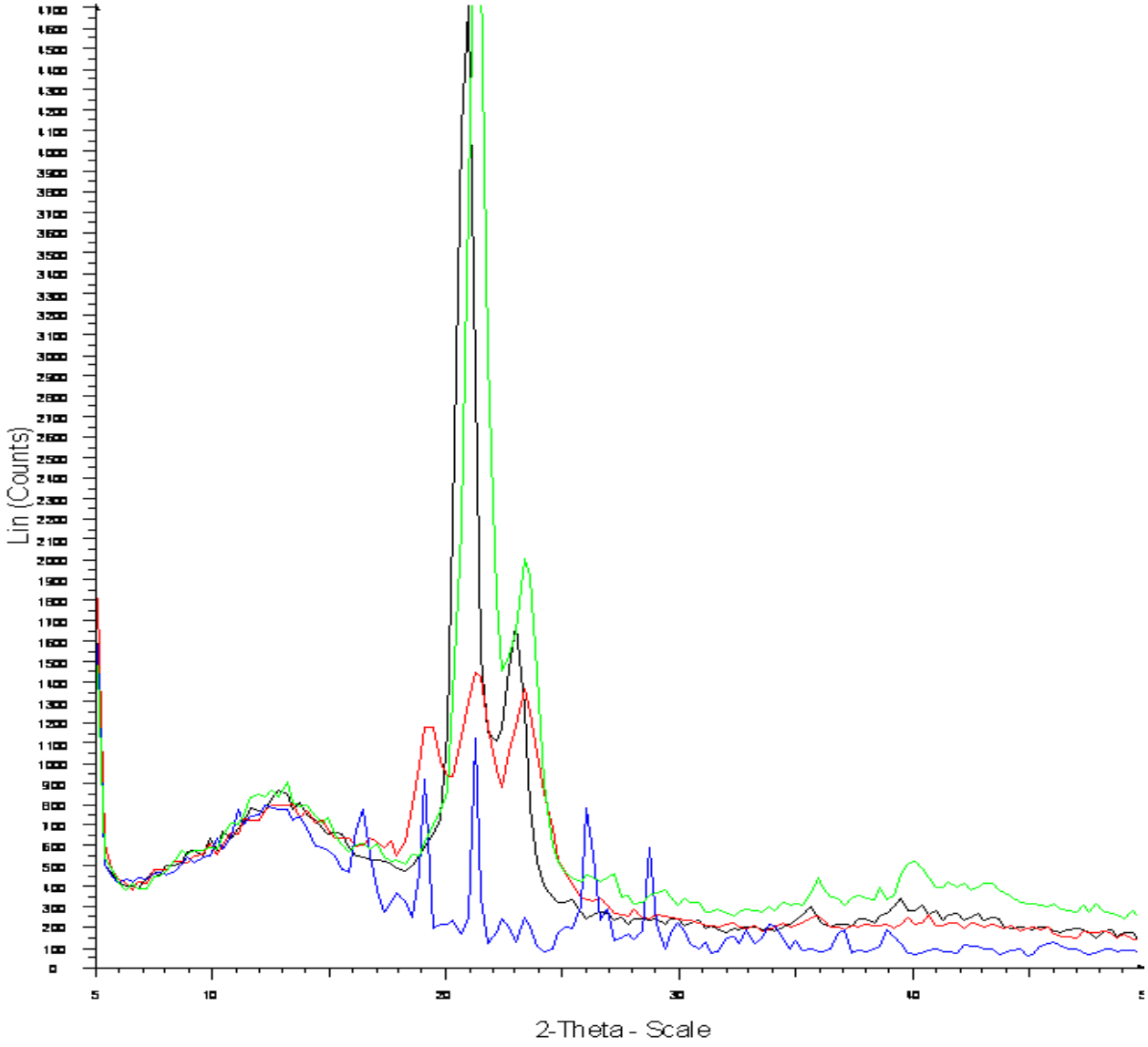

Figure 5-11: pXRD diffractograms of indomethacin (blue), compritol 888® ATO (black), physical mixture of indomethacin and compritol 888® ATO (green) and lyophilized IN-SLNs (red).

5.5.7. FTIR studies:

Overlaid FTIR spectra of indomethacin, compritol 888® ATO, lyophilized blank IN-SLNs, and lyophilized IN-SLNs are shown in Figure 5-13. The FTIR spectra of indomethacin indicated characteristic stretching bands at 1689.32 cm^{-1} and 1711.82 cm^{-1} corresponding to carbonyl groups. Peak at 1689.32 cm^{-1} and 1711.82 cm^{-1} correspond to benzoyl and acid carbonyl stretch, respectively. The presence of peak at 1711.82 could be related to the existence of indomethacin in the γ form (227-229). The compritol demonstrated characteristic peaks related to C=O (1736.04 cm^{-1}) stretching and C-H stretching (2915.94cm^{-1}/2848.97cm^{-1}). The FTIR spectrums of the physical mixture, lyophilized blank IN-SLNs, lyophilized IN-SLNs were similar to that of bulk compritol 888 ® ATO and demonstrated no shift in the wave number of the characteristic peaks. The, sharp crystalline bands of indomethacin were absent in the physical mixture (Figure 5-14).

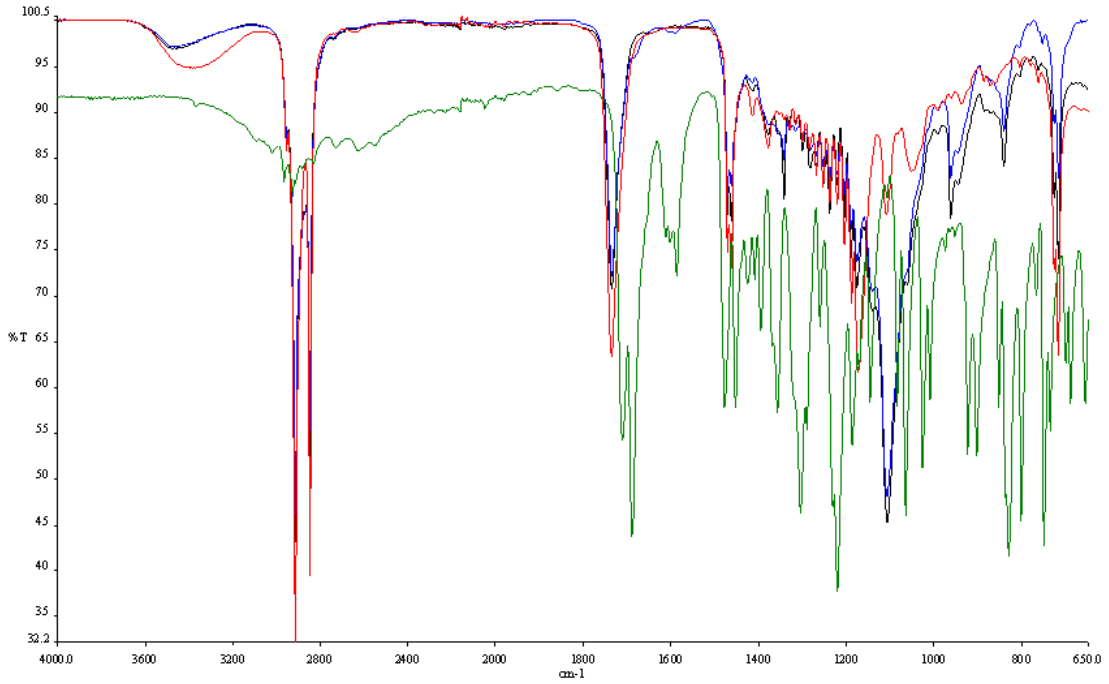

Figure 5-12: Fourier transform infrared spectra of indomethacin (green), compritol 888® ATO (red), lyophilized blank IN-SLNs (black) and lyophilized IN-SLNs (blue).

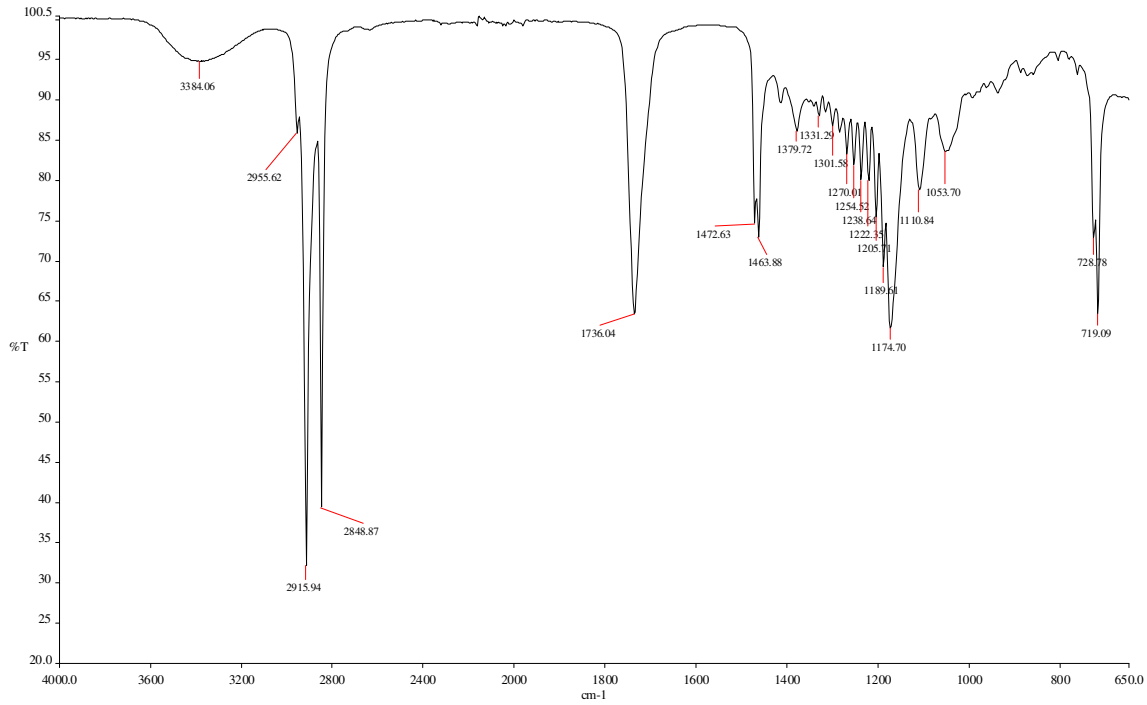

Figure 5-13: Fourier transform infrared spectra of physical mixture of indomethacin and compritol 888® ATO

5.5.8. Differential Scanning Calorimetry (DSC)

Perkin-Elmer Diamond DSC was used to investigate the complexation of indomethacin with HPβCD, and to study the melting and recrystallization behavior of the SLNs. Figure 5-15 represents the overlaid thermograms of indomethacin, HPβCD, physical mixture of Indomethacin and HPβCD and lyophilized IN-HPβCD. DSC thermograms of indomethacin, Compritol 888® ATO, physical mixture (indomethacin and Compritol 888® ATO), lyophilized blank SLNs and lyophilized IN-SLNs formulation are presented in Figure 5-16. Indomethacin exhibited an endotherm corresponding to its melting point at ~159°C and HPβCD exhibited no melting endotherm within the temperature range tested. The drug melting transition was

observed in the physical mixture of indomethacin and HPβCD while it was absent in the IN-HPβCD complex. The thermal curve of the bulk Compritol 888® ATO and physical mixture (indomethacin and Compritol 888® ATO) exhibited an endothermic peak at ~71°C. The melting endoderm of Compritol 888® ATO in lyophilized blank SLNs and IN-SLNs formulation was observed at 69.03°C and 67.06°C, respectively. Additionally, an endotherm at 50-55°C corresponding to melting point of Poloxamer 188 was also observed in blank SLNs and In-SLNs. Hyper DSC thermograms (20 to 200°C at heating rate of 200 °C /min) of physical mixture of indomethacin and bulk lipid exhibited a melting endotherm corresponding to melting of indomethacin at ~ 158°C, which was absent in IN-SLNs (Figure 5-17).

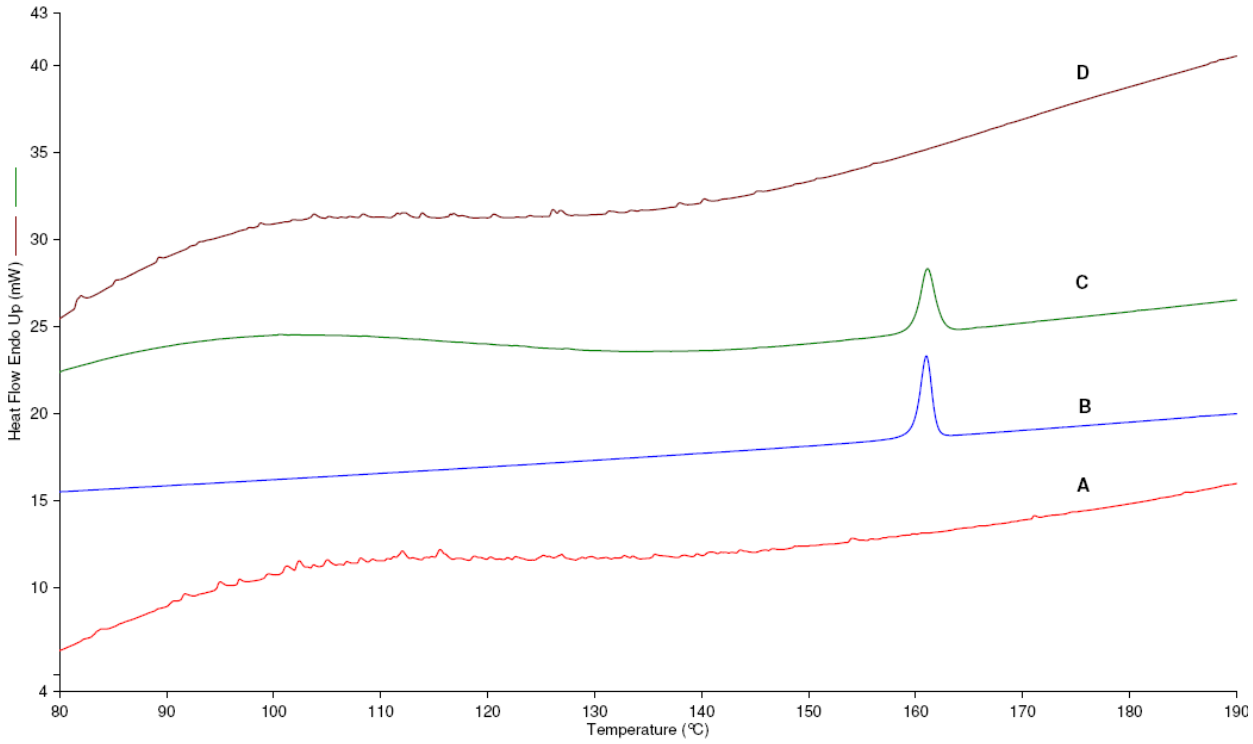

Figure 5-14: DSC thermograms of A: HPβCD; B: Indomethacin; C: physical mixture of Indomethacin and HPβCD; and D: lyophilized IN-HPβCD formulation.

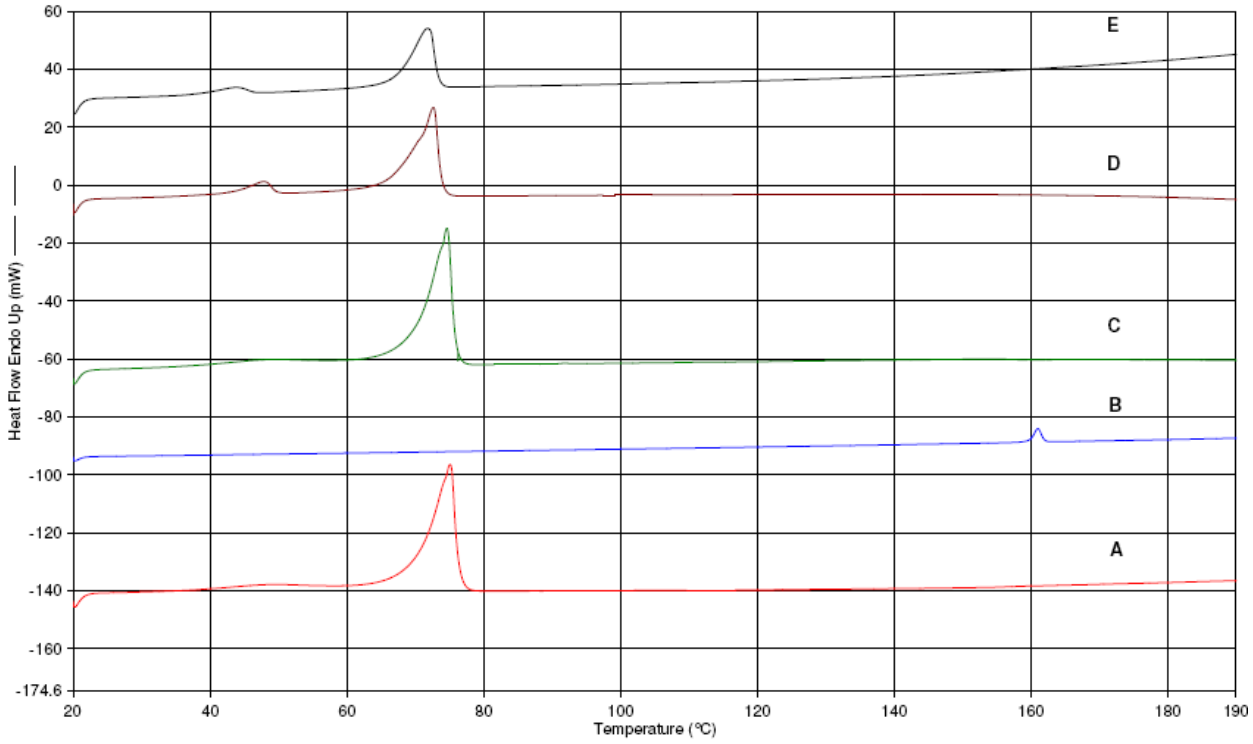

Figure 5-15: DSC thermograms of A: Compritol 888® ATO; B: Indomethacin; C: physical mixture (indomethacin and Compritol 888® ATO);D: lyophilized blank SLNs; and E: lyophilized IN-SLNs formulation

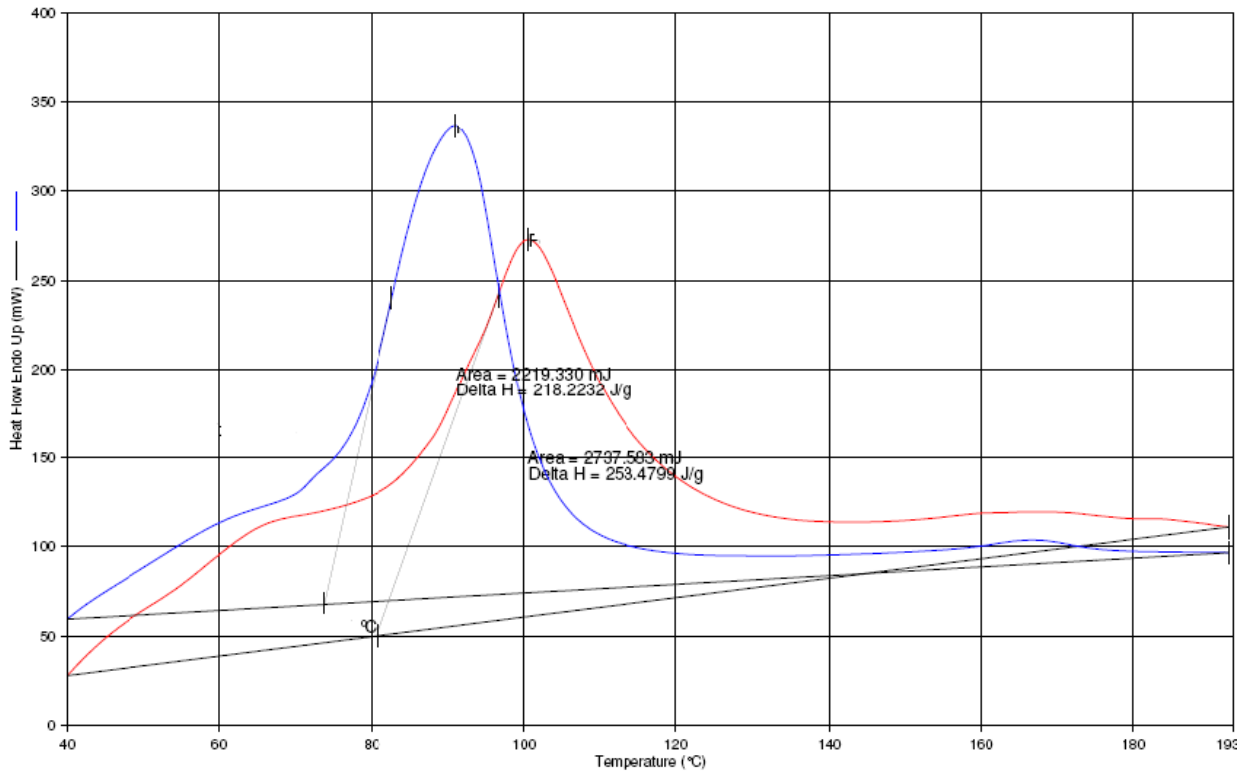

Figure 5-16: Hyper DSC thermograms of physical mixture (indomethacin and Compritol 888® ATO) and lyophilized IN-SLNs formulation

5.5.9. *In vitro* corneal permeation studies

In these studies, the donor solution consisted of 2 mL of the formulation (optimized IN-SLNs (0.1% w/v indomethacin content) (pre- and post-sterilization) or IN-SOL (0.1% w/v indomethacin content) or IN-HPβCD (0.1% w/v indomethacin content)) diluted with 1mL of 3 mM acyclovir (ACV) solution (in DPBS pH 7.40). The pH of the solution, immediately after dilution, was adjusted to 6.80 and the transport experiments were conducted. The receiver chamber solution contained 3.2 mL of 2.5% HPβCD in DPBS (pH 7.40) in all cases. The transcorneal permeability coefficients of indomethacin, from all formulations tested, are depicted

in Figure 5-18. The *in vitro* transcorneal permeability of indomethacin from IN-SOL and IN-HPβCD formulations was 2.8 ± 0.48 x 10^{-6} cm/sec and 4.0 ± 0.9 x 10^{-6} cm/sec, respectively. IN-SLNs formulation demonstrated a 4.3-fold and a 3-fold increase in transcorneal permeability of indomethacin (12.2 ± 1.85 x 10^{-6} cm/sec), compared to that of IN-SOL and IN-HPβCD formulations, respectively Transcorneal permeability of indomethacin from the IN-SLNs formulation post-sterilization was observed to be 13.2 ± 0.8 x 10^{-6} cm/sec). Figure 5-19 represents the permeation of acyclovir through the cornea, alone (control) or in the presence of IN-SOL, IN-HPβCD and IN-SLNs (pre- and post-sterilization). One mL of ACV (3 mM in DPBS pH 7.40) was added to two ml of pH 6.80 DPBS (control) or to 2 mL of the formulations. The final pH of all formulations was adjusted to 6.80 before conducting transcorneal permeation. ACV was added to monitor/compare the integrity/tightness of the corneal tissues in the presence of the formulations and during the course of the experiments. The transcorneal permeability of ACV alone (control) and in the presence of IN-SOL, IN-HPβCD, pre-sterilized IN-SLNs and post-sterilized IN-SLNs was observed to be 2.2 ± 0.2 x 10^{-6} cm/sec, 2.0 ± 0.7 x 10^{-6} cm/sec, 2.6 ± 0.4 x 10^{-6} cm/sec, 2.4 ± 0.5 x 10^{-6} cm/sec, and 2.4 ± 0.67 x 10^{-6} cm/sec, respectively. The mean particle size, zeta potential, pH, PI and osmolality of the IN-SLN formulation before and after dilution with ACV were similar (Table 5-13). Additionally, on dilution with ACV a significant difference in the osmolality of IN-SOL, IN-HPβCD or IN- SLNs were not observed (Table 5-14). However, on dilution with ACV, at the end of three hours a 36 % decrease in the entrapment efficiency (from 72.0 ± 1.5 % to 46 ± 4.0 %) with the IN-SLN formulation was observed (Table 5-13). Figure 5-20 represents transcorneal permeability of indomethacin from IN-HPβCD in the absence or in the presence of surfactants (0.75% Tween 80 and 0.25%

Poloxamer). Transcorneal permeation of indomethacin from IN-HPβCD in the absence of and in the presence of surfactants was determined to be 4.02 ± 0.84 x 10^6 cm/sec and 4.45 ± 0.33 x 10^6 cm/sec, respectively.

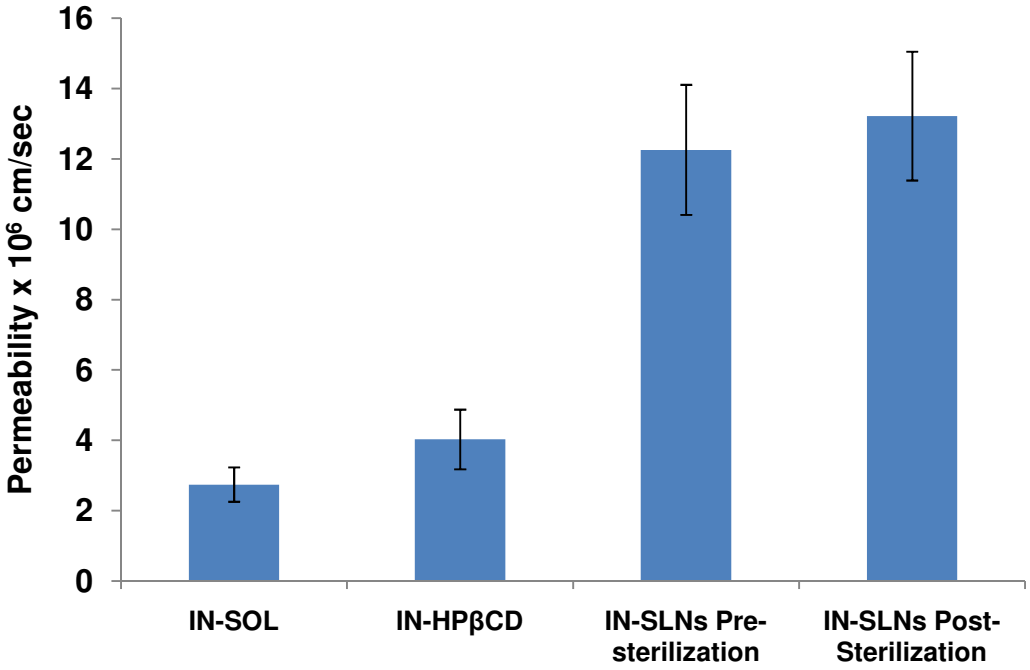

Figure 5-17: Transcorneal permeation of indomethacin from IN-SOL (0.1% w/v), IN-HPβCD (0.1% w/v) and IN-SLNs (pre-and post-sterilization) (0.1% w/v) formulations. Two mL of the formulations were diluted with one mL of ACV (3 mM in DPBS pH 7.40) solution. The pH of all the final solutions was adjusted to 6.80 before conducting transcorneal permeation studies. Results are depicted as mean ± SD (n=6).

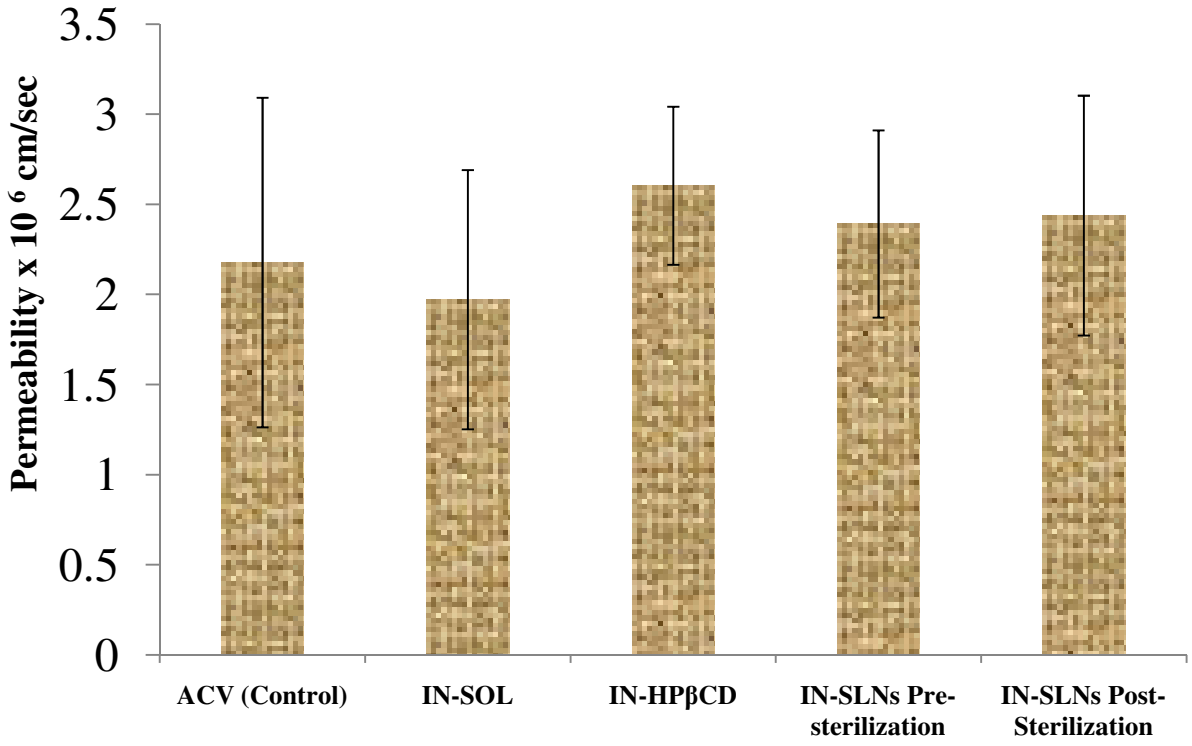

Figure 5-18: Transcorneal permeation of acyclovir (ACV), alone (control) or in the presence of IN-SOL, IN-HPβCD and IN SLNs (before and after sterilization) formulations. One mL of ACV (3 mM in DPBS pH 7.40) was added to two ml of pH 6.80 DPBS (control) or to 2 mL of the formulations. The pH of the final solutions was adjusted to 6.80 before conducting the transcorneal permeation experiments. Results are depicted as mean ± SD (n=6).

Table 5-13: Effect of dilution of formulations with 1mL of acyclovir solution (3mM) on mean particles size, PI, zeta potential, pH and entrapment efficiency of pre-sterilized IN-SLNs

Evaluated Parameters	IN-SLN	IN-SLNs post dilution
Mean Particle Size (nm)	140 ± 5	144 ± 10
PI	0.16 ± 0.01	0.17 ± 0.003
Zeta Potential (mV)	-21 ± 1.8	-22 ± 1.9
pH	6.80 ± 0.1	6.80 ± 0.10
Entrapment Efficiency (%)	72.0 ± 1.5	46 ± 4.0

Table 5- 14: Effect of dilution of formulations with 1mL of acyclovir solution (3mM in DPBS pH 7.40) on osmolality of IN-HPβCD and IN-SLNs formulations

Formulations	Osmolality (mOsm/kg H_20)	
	No Dilution	After dilution
IN-HPβCD	285 ± 6	285 ± 5
IN-SLNs (Pre-sterilization)	278 ± 4	278 ± 3
IN-SLNs (Post-sterilization)	280 ± 3	280 ± 5

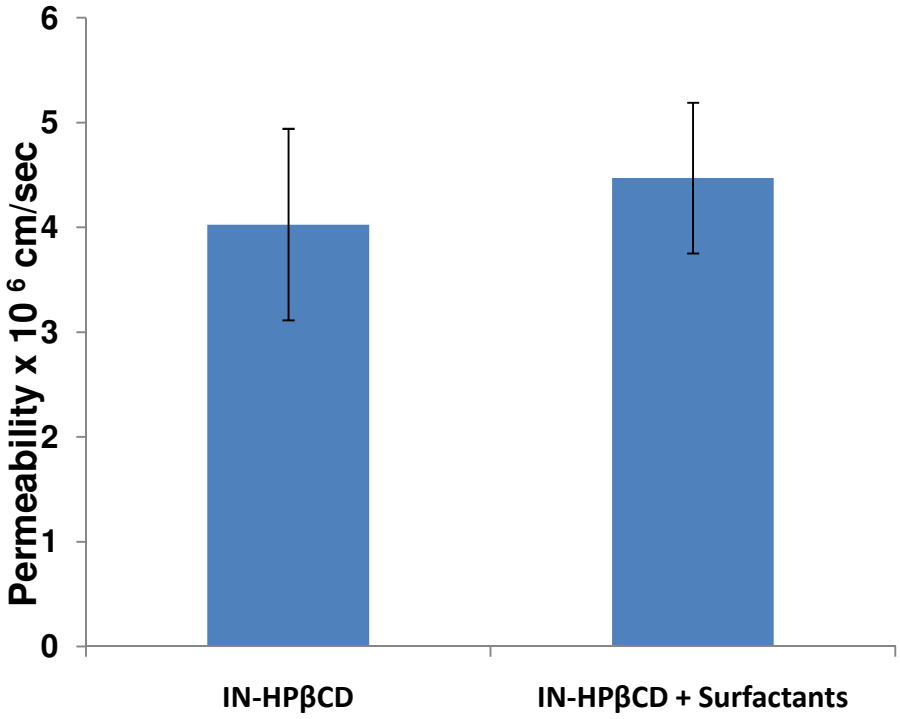

Figure 5-19: Transcorneal permeability of indomethacin from IN-HPβCD and IN-HPβCD containing 0.75% Tween 80 and 0.25% poloxomer 188 formulations. Results are depicted as mean ± SD (n=6).

5.6. Discussion

The goal of this study was to develop and optimize the preparation of IN-SLNs (0.1% w/v) using face-centered central composite design (FCCD) and to compare corneal permeation of indomethacin from IN-SLNs, IN-SOL (0.1% w/v) and IN-HPβCD (0.1% w/v) formulations. The final indomethacin content in all the formulation was maintained at 0.1 % w/v because Indocollyre®, a topical extemporaneously prepared hydro-PEG 400 solution of indomethacin, a commercial indomethacin formulation is available in Europe at this concentration. Five factors i.e. type of lipid, homogenization pressure, number of homogenization cycles, fraction of Tween 80 in the mixture of surfactants (Poloxamer 188 and Tween 80) while the keeping total surfactant concentration at 1% w/v, and pH were investigated for preparation of IN-SLNs. Two factors (type of lipid and homogenization pressure) were pre-screened and pre-selected to simplify the experimental design and focus on optimization of the other parameters using FCCD.

Solubility and entrapment efficiency of the drug, determinants of the loading capacity of the drug in the lipids, are the two major factors that drive the selection of the lipid phase for the preparation of the SLNs. Indomethacin exhibited highest partition coefficient of 10.2 ± 0.70 in Compritol 888® ATO (Figure 5-2). Additionally, in contrast to all the other lipids tested, indomethacin exhibited good solubility (clear yellow lipid melt) in Compritol 888® ATO (2 g and 5 g) and drug crystals were not observed under light microscopy 24 h after cooling to room temperature. Significantly higher entrapment efficiency and drug solubility in Compritol 888® ATO could be attributed to differences in the lipid crystalline structure related to the chemical nature of the lipid and arrangement of the drug molecules in the lattice. Compritol 888® ATO is a

mixture of mono-, di- and tri-glycerides and produces less ordered lipid crystals and with lattice defects which helps in accommodating the drug molecules compared to the other triglycerides tested (Dynasan 114, Dynasan 118, and Softisan 154). Although, Precirol®ATO 5 (glyceryl palmitostearate) is also a mixture of mono-, di- and triglycerides, higher solubility and entrapment of the drug in Compritol 888 ATO (glyceryl behenate) could be attributed to differences in the chemical composition of the lipids. Therefore, Compritol 888® ATO was selected as the lipid phase for the preparation of the IN-SLNs. The concentration of the lipid in all further formulations tested was maintained as 2 % w/v because an increase in the lipid content in the formulation could result in larger particle size with broader size distribution (121). Cavitational forces in the homogenization gap are responsible for the reduction in the particle size of the lipid nanoparticles (230). Increase in the homogenization pressure from 7,500 psi to 15,000 psi resulted in a decrease in the mean particle size of the IN-SLNs. Increase in the homogenization pressure did not result in any further decrease in the mean particle size of the IN-SLNs (Figure 5-3). Therefore, 15,000 psi was considered as the optimum homogenization pressure for preparation of IN-SLNs.

A three-factor, three-level FCCD was used to further optimize the preparation of the IN-SLNs. The three independent factors chosen for the optimization study were: number of homogenization cycles (A); fraction of Tween 80 in the mixture of surfactants (Poloxamer 188 and Tween 80) while keeping the total surfactant concentration at 1% w/v (B); and pH (C). Compritol 888® ATO (2% w/v) and homogenization pressure (15000 psi), selected on the basis of the results of the pre-screening experiments, were used to carry out the experimental runs. Variation in the particle size of the IN-SLNs was observed as a function of number of

homogenization cycles and fraction of Tween 80 in the surfactant mixture (Table 5-2). Minimum particle size of the IN-SLNs (100 nm) was achieved in run No 15 and the maximum particle size of 1030 nm was observed in run number 14 and 18 (Table 5-2). The ratio of maximum to minimum particle size was 10.3. A ratio greater than 10 indicates that transformation is required. Transformation is needed if the error, (residuals) is a function of magnitude of response and the choice of transformation depends on statistical considerations. In this study power transformation was chosen to transform the particle size to stabilize variance and to make the data follow normal distribution. Box-cox plot provided in design expert software was used to choose the appropriate power transformation (0.68) (Table 5-4, equation Y_1). Analysis of variance (ANOVA) results, calculated by Design-expert software, were used to choose the best model equation to fit the particle size response (Y_1) from among linear, two-factor interaction model (2FI) and quadratic model. Quadratic second-order polynomial model was found to be most appropriate for particle size response (Y_1). This model was highly statistically significant, with F-value 998.96 and p-value < 0.0001, when compared to other models (Table 5-3). Additionally, the quadratic model demonstrated insignificant lack of fit for Y_1 ($F= 3.5$; $P>0.05$) (Table 5-5). Two linear (homogenization cycles (A), fraction of Tween 80 in the surfactant mixture (B)), one interaction (homogenization cycles and fraction of Tween 80 AB), A^2 and B^2 terms were significant ($p<0.05$) (Table 5-5) and were included in the quadratic model equation for response Y_1 (Table 5-4, equation Y_1). Other terms were not significant ($p>0.05$) and were thus not included in the quadratic equation. Although, the linear term C (pH) was not significant and had no effect on the particle size (Y_1) of the IN-SLNs it was included in the quadratic model equation to ensure that the model was hierarchical (Table 5-5). Positive sign before a factor in polynomial equation

indicates that the response increases with the factor and negative sign indicates that the response decreases with the factor (231). Particle size response (Y_1) (Table 5-4, equation Y_1) of the IN-SLNs is directly related to the number of homogenization cycles (positive sign before A), while an inverse relationship exists with the fraction of Tween 80 (-ve sign before B) in the mixture of surfactants (Tween 80 and Poloxamer (total surfactant concentration constant at 1% w/v)). The coefficient of determination (R^2) and adjusted R^2 values were 0.9988 and 0.9980, respectively (Table 5-8) indicating that the quadratic model equation for the particle size response (Table 5-4, equation Y_1) could explain 99.88% variability in the particle size response. Additionally, close agreement between the predicted (0.9956) and adjusted R^2 (0.9980) indicates the accuracy and general ability of the polynomial model to predict the particle size response (Y_1) (Table 5-8).

Response surface plots indicated that the homogenization cycles (A) and fraction of Tween 80 in the mixture of surfactants (Poloxamer and Tween 80, total concentration 1% w/v) (B) had a significant effect on the particle size response (Y_1) (Figure 5-4). Increase in the number of homogenization cycles, at all tested fractions of Tween 80 in the formulation, led to a decrease in the particle size of the IN-SLNs. In high pressure homogenization the fluid is accelerated at high velocity and pressure through the narrow gap. Very high shear stress and cavitational forces during each pass breaks the particle down to a small size. Thus, higher the number of times the fluid is passed through the homogenizer greater the reduction in droplet size. However, at all homogenization cycles, IN-SLNs stabilized with only Tween 80 as the emulsifier demonstrated highest particle sizes. As the fraction of Tween 80 in the formulation decreased, particle size of the IN-SLNs was observed to decrease with all homogenization cycles. This observation is consistent with other reports wherein different emulsifier compositions required different

homogenization parameters to reduce the particle size of the SLNs due to a difference in the velocity of coverage of the new lipid surfaces created (143). At a particular cycle number, the observed differences in the particle size of the IN-SLNs stabilized using different combinations of surfactants could be explained by the different HLB values of Tween 80 (HLB 18), Poloxamer 188 (HLB 29) and the combination of Tween 80 and Poloxamer, which could lead to different surface absorption and packing properties of the surfactants (232, 233).

In the case of percentage entrapment efficiency response (Y_2), the quadratic model equation (Table 5-4, equation Y_2) was found to be significant based on the F value of 159.14 ($p< 0.001$) (Table 5-3). Additionally, lack of fit for the selected quadratic model was not significant (F=0.68; P=0.7107) (Table 5-6). The terms pH (C) and fraction of Tween 80 in the mixture of surfactants (B) were significant (Table 5-6) and were therefore included in the equation (Table 5-4, equation Y_2). All other terms that were not significant were excluded from the equation. Similarity between the predicted (0.9956) and adjusted R^2 (0.9980) indicates the ability of the quadratic model to predict the percentage entrapment efficiency response (Table 5-8). In addition to solubility of the drug in the lipid phase, physiochemical properties of the drug and processing factors can affect the amount of drug incorporated into the delivery systems (234, 235). As indicated by the response surface plot, both the fraction of Tween 80 in the formulation and the formulation pH had a significant effect on the percentage of indomethacin incorporated within the IN-SLNs (Figure 5-5). Indomethacin (pKa of 4.5) demonstrated a pH dependent entrapment efficiency, consistent with the pH dependent solubility (Fig 5-1),which was expected because the drug is known to be weakly acid in nature and exists predominately in the ionized form above pH 4.5, which will promote localization in the aqueous phase. However, at all pH values, IN-

SLNs stabilized by only Tween 80 (no Poloxamer 188), demonstrated higher entrapment efficiency. As the fraction of Tween 80 in the formulation decreased, a significant decrease in the entrapment of indomethacin in the SLNs was observed at all pH values. Decrease in the entrapment with an increase in the concentration of Poloxamer 188 in the formulation could be attributed to the higher solubilization of the drug by Poloxamer 188 in the aqueous phase. The results are in agreement with the observation regarding the incorporation of diazepam and prednisolone in the SLNs where the solubility of the drug in the aqueous-emulsifier phase was a determining factor for entrapment efficiency (235, 236).

The fitted quadratic model equation for the zeta potential response is given in Table 5-4 (equation Y_3). Neither the quadratic model (F value 2.92 ($p = 0.087$) nor any other model were significant indicating that the independent variables A, B and C were not related to response variable zeta potential (Y_2) (Table 5-3). Additionally, the change in the zeta potential may not be predicted by the process factors and by the quadratic model because all the terms in the equation (Table 5-4, equation Y_2) were statistically insignificant (Table 5-7) and because of the low R^2 value of 63.94% (Table 5-8). Moreover, disagreement between the predicted (0.2047 and adjusted R^2 (0.3148 (Table 5-8) indicates the inability of the quadratic polynomial model to predict the zeta potential response. This suggests that the zeta potential was not significantly affected by the experimental variables used in this study. The surface response plots (Fig 5-6 and Fig 5-7) for zeta potential of the IN-SLNs as a function of the number of homogenization cycles (A), fraction of Tween 80 in the mixture of surfactants (B) and pH (C) also showed no curvature indicating that the zeta potential was not dependent on any of the independent variables used in this study.

By analyzing the response surface plots, constraints (Table 5-1) and by solving fitted quadratic model equation, optimization of the IN-SLN formulation was achieved with 15,000 psi, 6 cycles, indomethacin (0.1% w/v), Compritol 888 ATO (2% w/v), Tween 80 (0.75% w/v), Poloxamer 188 (0.25% w/v), glycerin (2.25% w/v) and pH 6.80 (Table 5-9). The targeted pH of the optimized IN-SLN formulation was selected as 6.8 during setting of optimization criteria because Indocorylle® (commercial indomethacin formulation is Europe) is marketed at this pH. The observed values from the triplicate batches prepared were similar to the predicted values and were within 5% of the predicted error (Table 5-10). The close agreement between the observed and predicted values confirms the validity of the experimental model. Additionally, the mean particle size, zeta potential and entrapment efficiency of the three batches were similar indicating precision, batch to batch uniformity and controlled experimental conditions (Table 5-10).

Phase solubility studies demonstrate that HPβCD through its ability to form inclusion complexes dramatically improved the solubility of indomethacin at all pH value tested. The aqueous solubility of indomethacin increased linearly as a function of HPβCD concentration (A_L type plot) at pH 3.20 and pH 5.00 indicating the formation of a 1:1 complex at this pH. On the other hand, the phase solubility curve showed a negative deviation from linearity (A_N type plot) at higher concentrations of HPβCD at neutral pH (pH 6.80 and pH 7.40) (Figure 5-8). The difference in the phase solubility behavior of indomethacin (pKa 4.5) as a function of pH could be attributed to the difference in interaction of ionized and unionized indomethacin with HPβCD. A_N type of phase solubility curves of indomethacin with HPβCD at pH 7.40 have been reported previously (237). The binding constants of indomethacin ($K_{1:1}$) was also observed to be pH

dependent indicating significant effect of ionization on indomethacin/ HPβCD interaction (Table 5-11). Highest and lowest binding constant values was observed at pH 3.00 and 7.40, respectively. At pH 3.00, indomethacin exists predominately in the unionized form, and this form being more lipophilic forms more stable inclusion complexes with HPβCD. The decrease in stability constant with the increase of pH above 3.00 could be explained by increased drug hydrophilicity as a result of ionization, which probably reduces the affinity for the lipophilic HPβCD cavity (238, 239). These findings are consistent with literature reports wherein increase in solution pH resulted in a decrease in the stability constants of indomethacin/ HPβCD, flenamic acid/ β-CD and flenamic acid/tri-O-methyl-β-cyclodextrin inclusion complexes (237, 240).

In this study, the pH and indomethacin content of the IN-HPβCD formulation was targeted to 6.80 and 1 mg/mL, respectively. Several reports indicate that maximum ocular permeation and bioavailability is achieved only when just enough cyclodextrins (<15%) is added to the vehicle to solubilize the available drug. Presence of excess amounts of cyclodextrins will decrease the ocular bioavailability due to retention of the drug molecule in the lipophilic central cavity of the cyclodextrins (46, 116, 125, 126). The saturation solubility of indomethacin in 2.5 % w/v HPβCD at pH 6.80 was determined to be 1.1 mg/ml (Figure 5-2). Thus, to avoid excess cyclodextrins in the formulation, IN-HPβCD was formulated using 2.5 % w/v HPβCD.

All ophthalmic products should be sterile, and physically and chemically stable on storage (241). Indomethacin has been reported to undergo pH dependent hydrolysis to 5-methoxy-2methyl-indol-3-acetic acid and p-cholorobenzoic acid (237, 242). The ability of SLNs to reduce hydrolysis, oxidation and photo-degradation of drugs as a result of incorporation into solid lipid matrices is well documented (119) In this study, incorporation of indomethacin within

the SLNs dramatically improved chemical stability of indomethacin. A significant decrease in the drug content was not observed with the IN-SLN formulations on sterilization (110°C, 30 min) and on storage for up to a period of 1 month (last point tested) under the conditions tested (40°C, 25°C and 4°C) (Figure 5-9 (A)). Additionally, the mean droplet size, zeta potential, entrapment efficiency and pH of the IN-SLNs remained unaltered post-sterilization and on storage (Figure 5-10). However, dramatic loss of indomethacin content from the IN-HPβCD and IN-SOL formulations was observed post-sterilization and on storage under the conditions tested (Figure 5-9 (B) and Figure 5-9 (C)).

The IN-SLNs were further characterized to evaluate for molecular interaction using pXRD, FTIR and DSC. The inclusion complex of indomethacin and HPβCD was characterized using DSC. Compritol 888® ATO and physical mixture (indomethacin and Compritol 888® ATO) exhibited similar pXRD diffraction patterns and FTIR spectrum. Additionally, the characteristic sharp crystalline peaks of indomethacin were also not observed in the pXRD diffractogram and the FTIR spectrum of the physical mixture. Moreover, significant shift or lowering of intensity of the FTIR spectrum and pXRD diffraction patterns of the physical mixture was not observed (Figure 5-12, Figure 5-13 and Figure 14). This could be due to lower ratio of drug and lipids used in physical mixture in these set of studies (similar to weight ratio in IN-SLNs), which would result in the masking of the indomethacin peaks in the pXRD and FTIR studies by the bulk lipid in physical mixture.

In the case of the DSC studies, the melting endotherm of indomethacin was not observed in the physical mixture of indomethacin and Compritol 888® ATO because enough time was given for the drug to get solubilized in the bulk lipid which melts at ~71°C (Figure 5-16).

However, in contrast to lyophilized IN-SLNs, when a physical mixture of indomethacin and Compritol 888® ATO was subjected to hyper DSC (20 to 200°C at heating rate of 200 °C /min) a melting endotherm corresponding to melting of indomethacin at ~ 158°C was observed (Figure 5-17). This clearly indicates the presence of indomethacin in an amorphous state after entrapment within the SLNs. Additionally, the melting endotherm of bulk Compritol 888® ATO in blank SLNs shifted to lower temperatures (from ~71°C to ~ 69°C). The decrease in melting point of the bulk lipid core in SLNs has been attributed to the small size of the SLNs, the dispersed state of the lipid and the presence of surfactants (235, 243-246). The depression in the melting point of the bulk lipid in the IN-SNLs (67.06°C) compared to that of blank SLNs (69.03°C) indicates increased lattice defects, resulting from the incorporation of indomethacin, which in-turn reduces the degree of crystallinity and hence the melting point of bulk lipid (Figure 5-16). Similar decrease in melting point of the bulk lipid due to incorporation of drug was previously observed (247). The disappearance of the endothermic melting peak of the drug in the lyophilized IN-HPβCD suggests molecular encapsulation of drug in the cyclodextrin cavity (Figure 5-15).

Cornea is the major pathway for intraocular penetration of topically instilled medications (175) *In vitro* corneal permeability data suggests that incorporation of indomethacin in the SLNs led to a significant increase in the transcorneal diffusion of the drug. A 4.3-fold (from 2.8 ± 0.48 x 10-$^{-6}$ cm/sec to 12.2 ± 1.85 x 10^{-6} cm/sec) and a 3-fold (from 4.0 ± 0.9 x 10^{-6} cm/sec to 12.2 ± 1.85 x 10^{-6} cm/sec) increase in corneal permeability of indomethacin from the IN-SLN formulations was observed compared to that from the IN-SOL and IN-HPβCD formulations, respectively (Figure 5-18). Significant difference in the transcorneal transport of indomethacin

from the pre-and post-sterilized IN-SLN formulations was not observed which was expected since the physiochemical parameters of indomethacin remained unaltered on sterilization (Figure 5-18 and Table 5-12). In contrast to IN-HPβCD formulations which did not contain any surfactants, IN-SLN formulations were stabilized with 0.75% Tween 80 and 0.25% Poloxamer 188, and these surfactants could be responsible for the observed increase in corneal permeation of indomethacin. To test this hypothesis corneal permeation of indomethacin from the IN-HPβCD formulation was carried out in the presence of surfactants. Results demonstrate that permeation of indomethacin through the cornea was not modified in the presence of surfactants (Figure 5-20). The transcorneal permeability of ACV (a positive control) in the presence of the formulations was not statistically significantly different from that of the control, indicating that the integrity of the corneal epithelium was not affected by the formulation components (Figure 5-19) Additionally, the mean particle size, zeta potential, pH, PI and osmolality of the IN-SLN formulation before and after dilution were similar indicating that ACV did not affect the physical characteristics of the IN-SLNs during the transport experiments (Table 5-13 and Table 5-14). A significant decrease in the entrapment efficiency of the drug in the IN-SLNs was not observed on storage at all the temperatures tested for a period of one month (last time point tested) (Figure 5-10). However, on dilution with 1 mM ACV solution, a 36% decrease in entrapment efficiency of the drug was observed at the end of three hours (Table 5-13) indicating that the release of indomethacin from the IN-SLNs was majorly affected by partitioning of the drug between the lipid and the external aqueous phase. These results are consistent with the report by Calvo et.al wherein rapid release of the encapsulated indomethacin (85% in two hours), due to partitioning effect, from various colloidal formulations on dilution in phosphate buffered medium (pH 7.40)

was observed (217). Calvo et.al also evaluated the transcorneal permeability of indomethacin, *in vitro*, from various colloidal systems and Indocollyre®. The transcorneal permeability of indomethacin from Indocollyre®, emulsions, nanocapsules and nanoparticles was observed to be $0.75 \pm 0.04 \times 10^{-6}$ cm/sec, $2.74 \pm 0.49 \times 10^{-6}$ cm/sec, $3.57 \pm 0.73 \times 10^{-6}$ cm/sec and $3.80 \pm 1.81 \times 10^{-6}$ cm/sec, respectively. In the present study, indomethacin permeability from the IN-SLNs ($12.2 \pm 1.85 \times 10^{-6}$ cm/sec) was 16.2-fold higher compared to that of Indocollyre and 3.0-fold higher compared to that of the colloidal systems (217).

Conclusions

In this study RSM was used to develop and optimize the process parameters for the preparation of indomethacin loaded SLNs for ocular drug delivery. Mathematical analysis of the quadratic model equation revealed that the number of homogenization cycles and fraction of Tween 80 in the formulation had a significant effect on the particle size of the IN-SLNs. Amount of Tween 80 and pH of the formulation were predicted to be affect the entrapment of indomethacin in the SLNs. However, none of the factors investigated had a significant quadratic relationship with zeta potential. The optimized formulation was achieved using indomethacin (0.1% w/v), Compritol 888 ATO (2% w/v), Tween 80 (0.75% w/v), Poloxamer 188 (0.25% w/v), glycerin (2.25% w/v), 15000 psi, 6 cycles and pH 6.80. The observed responses were close to the predicted values of the optimized formulation. The optimized IN-SLNs were physically stable during sterilization and on storage for a period of one- month (last point tested) at all the storage temperatures (40°C, 25°C and 4°C) tested. Incorporation of indomethacin in the SLNs dramatically improved chemical stability of the drug. Significantly higher *in vitro* transcorneal

permeability of indomethacin from the IN-SLN formulation compared to that from IN-SOL, IN-HPβCD and the reported corneal permeability of a commercial formulation (Indocollyre®), indicates that the formulation of indomethacin in the SLNs could significantly improve the ocular bioavailability of the drug. Future experiments are aimed at evaluating the *in vivo* efficacy of these IN-SLNs.

Acknowledgement

This project was supported by the National Eye Institute, National Institutes of Health (NIH) [Grant EY018426-02] and HRSA [Grant DIBT16663]. The content is solely the responsibility of the authors and does not necessarily represent the official views of the National Institutes of Health.

CHAPTER 6

EFFECT OF TOPICALLY CO-ADMINISTERED P-GP SUBSTRATES/MODULATORS ON VITREAL KINETICS OF INTRAVITREALLY ADMINISTERED QUINIDINE IN RABBITS

6.1. Abstract

The purpose of this study was to investigate whether topically administered P-glycoprotein (P-gp) substrates/modulators can alter vitreal kinetics of intravitreally administered quinidine. Male New Zealand rabbits were used under anesthesia. Vitreal kinetics of intravitreally administered quinidine (0.75 μg dose) was determined alone and in the presence of verapamil (co-administered topically/intravitreally) or prednisolone hemisuccinate sodium (PHS, co-administered topically). In the presence of topically instilled verapamil (1% w/v), elimination half-life ($t_{1/2}$) (176 ± 7 min), apparent elimination rate constant (λ_z) (0.0039 ± 0.0001 min^{-1}) and mean retention time (MRT) (143 ± 30 min) of intravitreally administered quinidine were significantly different from that of the control (105 ± 11 min, 0.0066 ± 0.0007 min^{-1} and 83 ± 13 min, respectively). A 2-fold increase in the $t_{1/2}$ with a corresponding decrease in λ_z and a 1.5-fold increase in the MRT of quinidine was observed in the presence of topically co-administered 2% w/v PHS. Intravitreal co-administration of quinidine and verapamil resulted in a significant

increase in the $t_{1/2}$ (159 ± 9 min) and a decrease in the λ_z (0.0043 ± 0.0002 min^{-1}) of quinidine. The vitreal pharmacokinetic parameters of sodium fluorescein, alone or in the presence of topically instilled verapamil, did not show any statistically significant difference, indicating that ocular barrier integrity was not affected by topical verapamil administration. Results from this study suggest that topically applied P-gp substrates/modulators can alter vitreal pharmacokinetics of intravitreally administered P-gp substrates, possibly through the inhibition of P-gp expressed on the basolateral membrane of the retinal pigmented epithelium.

6.2. Introduction:

The retina is the primary target for most posterior segment ocular disorders such as age-related macular degeneration, diabetic macular edema, retinitis pigmentosa, endophthalmitis and proliferative vitreoretinopathy (79). Drug delivery to the posterior chamber ocular tissues is, however, challenged by various physiological barriers such as the cornea, conjunctiva, sclera and the blood-ocular-barriers (52, 56, 57, 158, 248, 249). The retinal pigmented epithelium (RPE), which forms the outer blood-retinal-barrier, limits vitreal penetration of drugs administered by the systemic and trans-scleral routes (36, 71, 75). P-glycoprotein (P-gp), a 170 kDa ATP dependent membrane bound efflux protein, expressed on the RPE plays a major role in restricting diffusion of P-gp substrates from the choroidal stroma into the neural retina across the RPE (68, 69).

P-gp displays broad specificity, accepting many structurally, functionally and mechanistically unrelated compounds (72), and its role in limiting drug penetration across biological barriers is well established. P-gp mediated drug efflux at the blood-brain-barrier is a

major factor behind poor penetration of chemotherapeutic agents, that are P-gp substrates, into the brain following systemic administration (250, 251). A number of reports also illustrate intestinal P-gp's role in limiting systemic bioavailability of orally administered agents. Moreover, upregulation of P-gp expressed by tumor cells is considered to be a major mechanism behind multidrug resistance (60, 252-254). Additionally, it has also been demonstrated that P-gp expressed on the canalicular membrane of the hepatocytes and the luminal surface of the proximal kidney tubule cells, including nephrons, expedite hepatic and renal elimination of substrates.

Generally, P-gp is expressed on the apical membrane of epithelial cells, preventing drug transport from the lumen into the systemic circulation (e.g. intestinal epithelium) or from the systemic circulation into the brain (endothelial cells of the Blood-Brain-Barrier) (60). An earlier report, however, suggests that P-gp is expressed on both apical as well as basal membranes of the RPE cells (69). P-gp on the RPE cells may thus affect permeation of substrates from the vitreous humor into the systemic circulation, and vice versa (56, 57), and could be a major factor behind the inability of systemic, periocular and transscleral routes of administration to generate and maintain therapeutic concentrations of P-gp substrates in the retina. Thus, factors/agents that can modulate the efflux activity of RPE P-gp could probably alter ocular pharmacokinetics of P-gp substrates.

In the past, a number of strategies attempting to modulate the activity or expression of efflux proteins on various mammalian tissues have been investigated. These include the use of chemosensitisers, prodrugs, polymers, nanoparticles, transcriptional regulators and monoclonal antibodies (149-151). Surprisingly, there are only three studies, to our knowledge, investigating

the effect of drug-drug interaction at the level of the RPE P-gp and its effect on ocular drug pharmacokinetics *in vivo*. These recent reports evaluated the effect of systemic/systemic, systemic/intravitreal or intravitreal/intravitreal co-administration of substrates or inhibitors on ocular pharmacokinetics (71, 152, 153). However, so far, the effect of topically administered P-gp substrates/inhibitors on the functional activity of P-gp expressed on the RPE has not been reported.

Topical eye drops containing antimicrobial and anti-inflammatory agents, steroids and other therapeutic compounds are routinely administered to treat various ocular infections and disorders. Many of these agents are P-gp substrates/inhibitors and can diffuse into the RPE. The objective of this study was to determine whether topically administered P-gp substrates could modulate the functional activity of RPE P-gp and alter the vitreal pharmacokinetics of another P-gp substrate, quinidine, administered intravitreally. Erythromycin (60) prednisolone (P-gp substrates commonly applied topically) (255) and verapamil (a P-gp inhibitor used in earlier reports investigating inhibition of RPE P-gp) were administered topically. Quinidine, used in an earlier study to evaluate functional activity of RPE P-gp (71), was used as a model P-gp substrate in this study and its pharmacokinetic parameters were evaluated.

6.3. Materials:

Microdialysis probes (CMA/20; 20,000 Dalton molecular weight cut-off and 10 mm shaft) were obtained from CMA/Micro-dialysis Inc (North Chelmsford, MA, USA). Erythromycin, prednisolone hemisuccinate sodium (PHS), verapamil hydrochloride, fluorescein sodium and quinidine hydrochloride were purchased form Sigma Chemical Co. (St Louis, MO,

USA). Ketamine hydrochloride and Xylazine were procured from Fort Dodge Animal Health (Fort Dodge, IA, USA) and Lloyd Laboratories (Shenandoah, IA, USA), respectively. Pentobarbital was obtained from Virbac AH, Inc. (Fort Worth, TX, USA). Solvents used were purchased from Fisher Scientific (St. Louis, Missouri, USA).

New Zealand male albino rabbits (NZW) were procured from Myrtle's Rabbitry (Thompson Station, TN, USA). Experiments conformed to the tenets of the Association for Research in Vision and Ophthalmology (ARVO) statement on the Use of Animals in Ophthalmic and Vision Research and followed the University of Mississippi IACUC approved protocols

6.4. Methods:

6.4.1. *In vitro* probe recovery

Probe recovery was determined by placing the probe in an isotonic phosphate buffered saline (IPBS) solution, pH 7.40, at 37 ºC, containing a known concentration of quinidine (equivalent to an intravitreal dose of 0.75 µg) alone or in the presence of verapamil or PHS. The probe was perfused with sterile IPBS (with or without verapamil) at a flow rate of 2 µL/min, and the dialysate was collected every 20 minutes. Relative recovery was calculated using equation 1.

$$\text{Recovery}_{\textit{in vitro}} = C_d / C_s \qquad (1)$$

C_d = Dialysate quinidine concentration.

C_s = Quinidine concentration in IPBS.

The concentration of quinidine in the vitreous humor samples was calculated by dividing the dialysate concentration with the *in vitro* recovery factor obtained as described above.

6.3.2. Probe implantation

Rabbits (weighing 2-2.5 Kg) were anesthetized using ketamine (35 mg/kg) / xylazine (3.5 mg/kg) administered intramuscularly and were maintained under anesthesia throughout the duration of the experiment (ketamine / xylazine administered intramuscularly every 40 minutes). Prior to probe implantation, 1% tropicamide was applied topically to dilate the pupil. A 22G needle was then inserted into the posterior chamber of the eye .The point of insertion was approximately 3 mm below the corneal-scleral limbus. The needle was withdrawn, and the vitreal probe was implanted immediately. The position of the probe was adjusted so that the semipermeable membrane was in the mid-vitreous section. The probes were continuously perfused with sterile IPBS (pH 7.40) at a flow rate of 2 µL/min using a CMA/100 microinjection pump (CMA/Micro-dialysis Inc). Following probe implantation, animals were allowed to stabilize for a period of 2 hours prior to drug administration. Vitreal samples were collected every 20 minutes for a period of 9 hours. Samples were collected in microcentrifuge tubes and stored at -20 ºC until further analysis. At the end of the study, animals were euthanized, under deep anesthesia, with an overdose of sodium pentobarbital administered through the marginal ear vein.

6.4.3. Drug administration

Quinidine was administered intravitreally (0.75 µg dose in 50 µL of IPBS). Studies were carried out with quinidine administered alone (control) or in the presence of topically co-administered erythromycin (0.2% w/v, pH 7.40), verapamil (0.5% w/v and 1% w/v, pH 6.00) and PHS (1% w/v and 2% w/v, pH 7.40). One hundred microliters of the inhibitor solution was instilled in the conjunctival sac. In the preliminary studies, erythromycin (0.2% w/v) was applied

topically at 0, 2 and 4 hours post intravitreal quinidine injection. Subsequently, the topical P-gp substrate/inhibitor administration time was modified to 2, 4 and 6 hours post quinidine administration, to prolong the residence of the topically applied agent in the RPE tissue. Further studies with verapamil and PHS were carried out with topical instillation at 2, 4 and 6 hours post intravitreal administration. All solutions were prepared in sterile IPBS.

Vitreal pharmacokinetics of quinidine (0.75 µg) was also studied in the presence of intravitreally administered verapamil (100 µg). In this study, verapamil was co-administered intravitreally with quinidine (injection volume 50 µL; co-dissolved), following the probe stabilization period. Additionally, IPBS (pH 7.40) containing verapamil (1 mg/mL) was continuously perfused through the concentric probes to maintain high verapamil levels in the vitreous humor throughout the duration of the experiment.

6.4.4. Fluorescein kinetics

Vitreal kinetics of intravitreally administered fluorescein (dose - 10µg, injection volume 50 µL), alone or in the presence of topically co-administered verapamil (1% w/v, IPBS pH 6.00), were studied to ensure preservation of the barrier properties of the RPE in the presence of topical verapamil (1% w/v). In these experiments, 100µL of 1%w/v verapamil solution was applied at 2, 4 and 6 hours post intravitreal fluorescein administration.

6.4.5. Distribution of prednisolone hemisuccinate sodium (PHS) and verapamil in ocular tissues following topical or intravitreal application

In a separate set of studies, verapamil (1% w/v, pH 6.00) or PHS (2% w/v, pH 7.40) was applied topically in the cul-de-sac of the rabbit's eye at 2, 4, and 6 hours post probe stabilization. At the end of 7 hours (for the verapamil studies) and 9 hours (for the PHS studies), rabbits were euthanized, eyes were enucleated and ocular tissues were collected and analyzed for drug content using an HPLC system. Additionally, ocular tissue concentrations of verapamil at the end of 7 hours, following intravitreal administration, as described earlier, was also determined.

6.4.6. Bioreversion of PHS to Prednisolone

PHS, a hemisuccinate ester prodrug of prednisolone, (256) requires hydrolysis (chemical or enzymatic) of the ester bond to generate free prednisolone. The presence of esterase activity in rabbit ocular tissues has been demonstrated and well documented with ester prodrugs of pilocarpine, dipivefrin, gancyclovir and acyclovir (257-259). Bioreversion of PHS was studied in vitreous humor and in the ocular tissues such as the cornea, iris-ciliary body and RPE/choroid as previously described (258). Vitreous humor was centrifuged, and the supernatant was used. All the other ocular tissues were homogenized in 5 mL chilled IPBS with a tissue homogenizer (Tissuemiser, Fisher Scientific, St Louis, USA) for periods of 30 seconds, with 1 minute intervals, in an ice bath. The homogenates were centrifuged at 13,000 rpm for 10 min at 4°C, and the supernatants were used for the PHS enzymatic hydrolysis studies. Protein content in the

supernatant was measured using the Bradford Protein estimation kit (Sigma Chemical Co, St Louis, MO), and the final protein content was adjusted to 1 mg/mL with IPBS.

Hydrolysis studies were carried out in triplicate at 37°C in a shaking water bath (75 reciprocations per min). One Hundred (100) µL of PHS stock solution was added to the required volume of the tissue homogenates and to vitreous humor to obtain a final PHS concentration of 10 µg/mL. At predetermined time points, 100 µL samples were withdrawn, and an equal volume of ice cold methanol was immediately added to the sample to arrest the enzymatic degradation process. Stability of PHS (10 µg/mL) in IPBS was also studied as a control.

6.4.7. Analytical procedures

6.4.7.1. Sample preparation

For studies involving distribution of PHS and verapamil in ocular tissues following topical or intravitreal application, enucleated eyes were rinsed with ice cold IPBS, to remove any traces of blood, and blotted dry using Kimwipes®. Aqueous and vitreous humor samples were collected using a 27G needle attached to a 1 mL tuberculin syringe. Eyes were then dissected and iris-ciliary bodies, lenses and retina/choroid tissues were isolated and weighed. Tissues were homogenized in ice cold IPBS using a Tissuemiser. Homogenates were diluted with an equal volume of ice cold acetonitrile:methanol (50:50) mixture, and centrifuged at 13,000 rpm for 20 minutes at 4°C. The supernatant was analyzed for drug content. Aqueous and vitreous humor samples were used as such, or diluted with IPBS, and taken for analysis. Extraction efficiency of PHS and verapamil from the ocular tissues was almost 100%.

6.4.7.2. Chromatography

Quinidine and verapamil were analyzed using an HPLC system comprised of a Waters 717 Plus autosampler, Waters 2475 multi λ Fluorescence detector, Waters 600 controller pump and Agilent 3395 integrator. A Symmetry® C_{18} (4.6 x 250 mm) column was used, and the flow rate was set at 1 mL/min for both the compounds. Quinidine analysis was carried out using 20 mM phosphate buffer (pH 2.50) with 20% acetonitrile as the mobile phase, at an excitation wavelength of 250 nm and emission wavelength of 440 nm. Verapamil quantification was performed at an excitation wavelength of 280 nm and emission wavelength of 320 nm using acetonitrile and 0.07% v/v o-phosphoric acid in deionized water (33:67) as the mobile phase. Fluorescein and prednisolone analyses were performed using reversed phase HPLC procedures as previously described (Macha and Mitra, 2001; Chang Y. Cho, 2003)

6.4.8. Data analysis:

Vitreal pharmacokinetic parameters of quinidine were determined by non-compartmental analysis using WinNonlin, version 5.2 (Pharsight; Mountain View, CA). Terminal slopes of the vitreous concentration-time profile were estimated by the log-linear regression, and the apparent elimination rate constant (λ_z) was derived from the slope. Elimination half-life ($t_{1/2}$) was calculated from the equation: $t_{1/2} = 0.693/\lambda_z$. The area under the vitreal concentration-time curve from time "0" to time "t" and from time "300" to time "540" was calculated by linear trapezoidal method and extrapolated to infinity

according to Eq 2.

$$AUC_{0-\infty} = AUC_{0-t} + \frac{C_v}{\lambda_z} \qquad (2)$$

The area under the statistical moment curve ($AUMC_{0-\infty}$) was calculated using Eq 3.

$$\sum_{t_{n-1}}^{t_n} \frac{(C_{n-1} \cdot t_{n-1} + C_n \cdot t_n)}{2} \cdot (t_n - t_{n-1}) + \frac{C_v \cdot t_{last}}{\lambda_z} + \frac{C_v}{\lambda_z^2} \qquad (3)$$

where, is the quinidine concentration at last time point (540 min). The mean retention time (MRT) was calculated using the equation: MRT = $AUMC_{0-\infty}$ / $AUC_{0-\infty}$. The total clearance was calculated as: CL= Dose/$AUC_{0-\infty}$. $CL_{300-540}$ = Dose/$AUC_{300-540}$. The apparent volume of distribution at steady-state V_{ss} = (Dose x $AUMC_{0-\infty}$)/ $(AUC_{0-\infty})^2$.The time course of fluorescein after a single intravitreal bolus dose was described by a biexponential profile (260) as expressed in Eq 4.

$$C = Ae^{-\alpha t} + Be^{-\beta t} \qquad (4)$$

In which A and B are zero time concentration coefficients, t the time (min) and α and β are the disposition rate constants of the initial and terminal phase, respectively. Vitreous humor was considered as part of the apparent central compartment and all other exchanging compartments including, the anterior chamber, were considered as part of the apparent peripheral compartment. Elimination was assumed to take place through plasma from the apparent central compartment. This model is illustrated as follows:

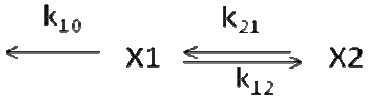

Quinidine is administered into the vitreous humor (X1), and the variables X1 and X2 represent the amount of the drug in the vitreous humor and other exchanging compartments, respectively. A similar model has been used to describe the kinetics of intravitreally administered fluorescein and other drugs (260-262) . In the open two-compartment model represented by equation 4, the

rate constant of drug transfer from the apparent peripheral to the apparent central compartment (k_{21}) was calculated according to Eq 5.

$$k_{21} = \frac{\alpha B + \beta A}{A + B} \quad (5)$$

The elimination rate constant of fluorescein from the apparent central compartment (k_{10}) was determined using Eq 6.

$$k_{10} = \frac{\alpha\beta}{k_{21}} \quad (6)$$

Rate constant of fluorescein transfer from the apparent central compartment to the apparent peripheral compartment (k_{12}) was calculated using Eq 7.

$$k_{12} = \alpha + \beta - (k_{21} + k_{10}) \quad (7)$$

Data obtained was subjected to statistical analysis using Students t-test. A p value ≤ 0.05 was considered to denote a statistically significant difference.

6.5. Results:

6.5.1. Effect of topically applied erythromycin on vitreal kinetics of intravitreally administered quinidine

Vitreal kinetics of intravitreally administered quinidine (0.75 µg dose, 50 µL injection volume) was studied either alone or in the presence of topically co-administered erythromycin (100 µL of a 0.2% w/v solution in IPBS, pH 7.40). The erythromycin solution was administered either at 0, 2 and 4 hours or at 2, 4 and 6 hours following intravitreal quinidine administration.

When erythromycin was applied at 0, 2 and 4 hours, vitreal pharmacokinetic parameters i.e. $t_{1/2}$ (104 ± 7 min), CL (0.0086 ± 0.0030 mL.min^{-1}) and λ_z (0.0066 ± 0.0004 min^{-1}) were not significantly different from that of the control values (105 ± 11 min, 0.0048 ± 0.0012 mL.min^{-1} and 0.0066 ± 0.0007 min^{-1}, respectively). A change in the topical erythromycin dosing times to 2, 4 and 6 hours following intravitreal quinidine administration also did not produce a significant difference in the pharmacokinetic parameters. Higher doses of erythromycin, in a solution form, could not be administered due to the limited aqueous solubility (2 mg/mL) of erythromycin.

6.5.2. Effect of topically co-administered verapamil on intravitreal kinetics of quinidine

Effect of topically co-administered verapamil (100 µL applied at 2, 4 and 6 hours) on the intravitreal kinetics of quinidine (0.75 µg) was examined at two different verapamil concentrations (0.5% w/v & 1% w/v). Verapamil had limited solubility at pH 7.40 (1 mg/mL) (71). Thus, verapamil solutions used in this study were prepared in IPBS pH 6.00 ± 0.10. The concentration-time profiles of quinidine following intravitreal administration, alone or in the presence of topically co-administered verapamil (0.5% w/v & 1% w/v), are illustrated in Figures 6-1A and 6-1B. The vitreal pharmacokinetic parameters have been provided in Table 6-1. At a concentration of 0.5% w/v, verapamil did not produce any significant change in the vitreal kinetics of quinidine. However, at 1% w/v, topical verapamil produced a 1.7-fold decrease in the λ_z (from 0.0066 ± 0.0007 to 0.0039 ± 0.0001 min^{-1}), a 1.7-fold increase in $t_{1/2}$ and a 1.7-fold increase in the MRT. Statistically significant differences between the mean vitreal quinidine concentrations of the 1% verapamil treated group and the control group was observed from the

360 minute time point onwards (Fig. 6-1B). Significant differences in $AUC_{0-\infty}$ and CL were not observed from those of the control. However, when partial areas were taken into account a 1.7-fold increase in $AUC_{300-540}$ and a 1.7-fold decrease in $CL_{300-540}$ were observed.

Figure 6-1A

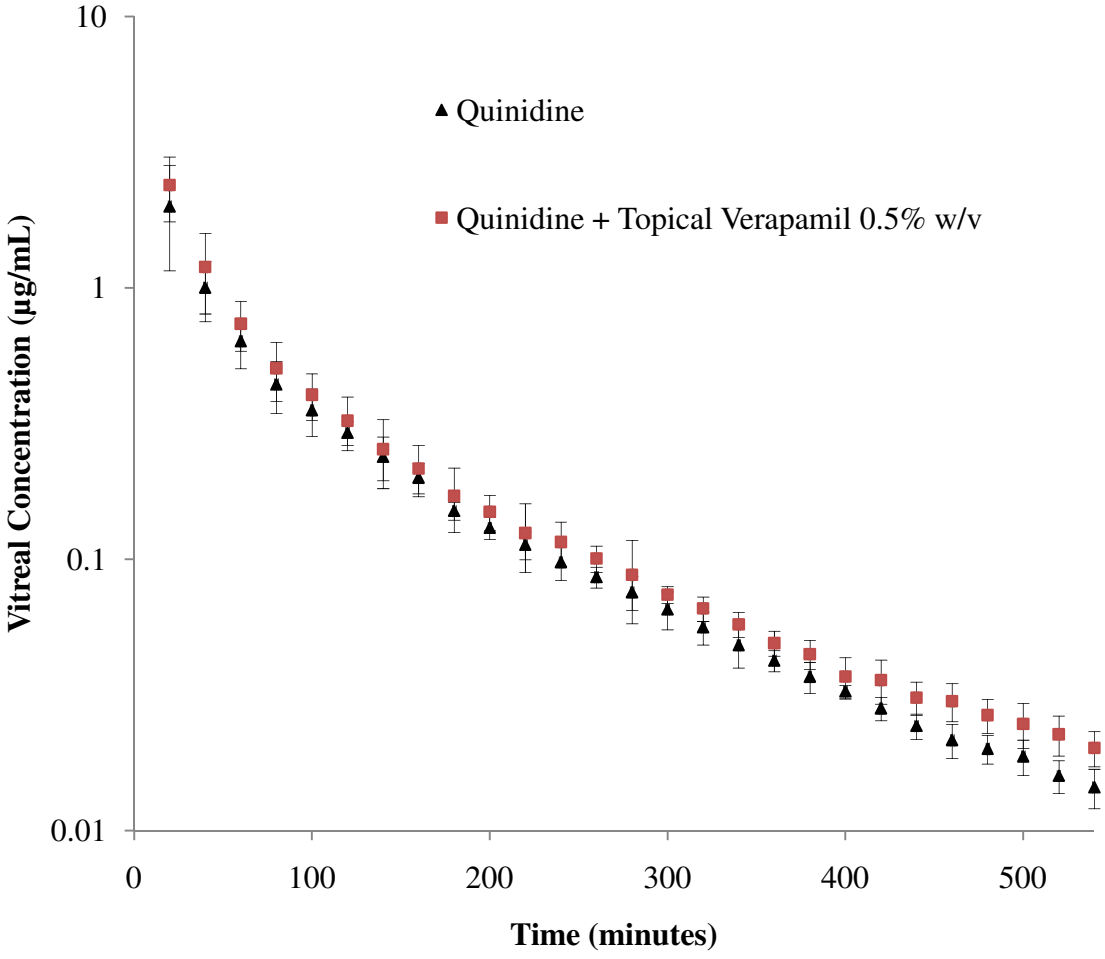

Figure 6-1B

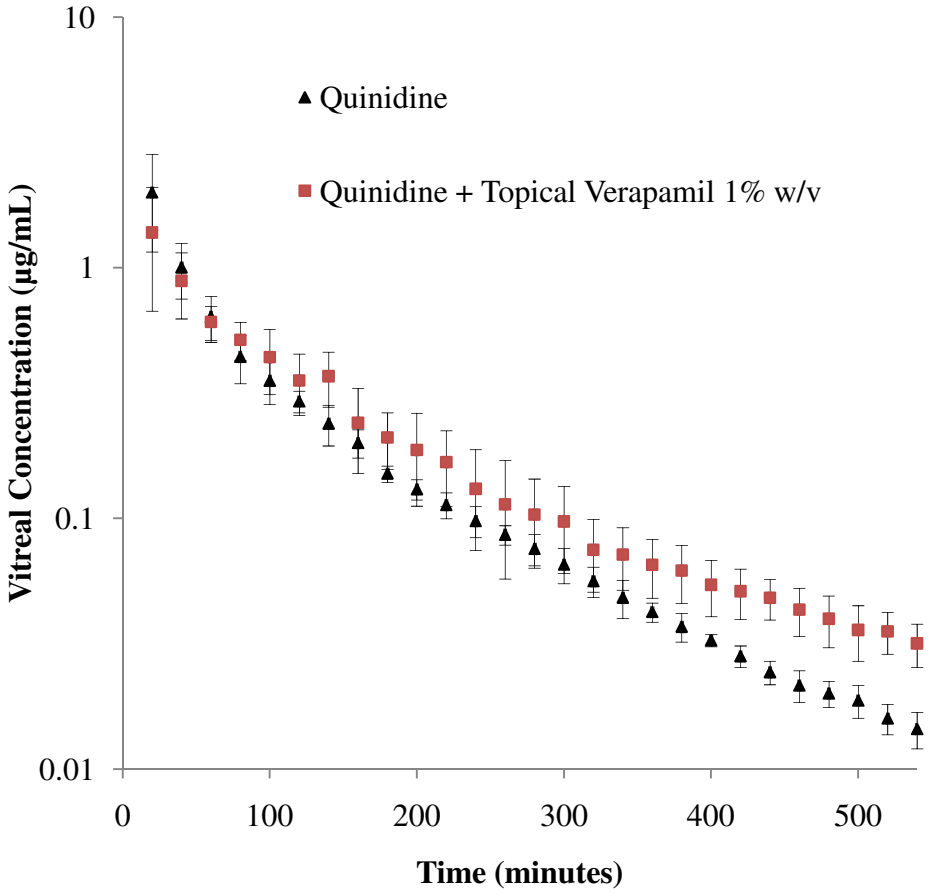

Figure 6-1: Vitreal concentration-time profile of quinidine (0.75 µg) alone (control) or in the presence of topically co-administered (A) verapamil 0.5% w/v and (B) verapamil 1% w/v Data points represent mean ± standard deviation of four determinations.

Table 6-1: Vitreal pharmacokinetic parameters of intravitreally administered quinidine (0.75 µg dose) alone or in the presence of topically co-administered verapamil (0.5% w/v or 1% w/v). Verapamil was administered at 2, 4 and 6 hours after intravitreal quinidine administration

Kinetic Parameters	Quinidine	Quinidine + Verapamil (0.5% w/v)	Quinidine + Verapamil (1% w/v)
λ_z (min^{-1})	0.0066± 0.0007	0.0066 ± 0.0010	0.0039 ± 0.0001 ***
$AUC_{0-\infty}$ (µg x min/mL)	168 ± 56	180 ± 41	158 ± 37
CL (mL/min)	0.0048 ± 0.0012	0.0043 ± 0.0008	0.0049 ± 0.0012
V_{SS} (mL)	0.41 ± 0.14	0.37 ± 0.12	0.72 ± 0.30
MRT_{∞} (min)	83 ± 13	84 ± 13	143 ± 30 **
$AUC_{300-540}$ (µg x min/mL)	7.73 ± 1.32	9.05 ± 0.38	12.86 ± 1.25*
$CL_{300-540}$ (mL/min)	0.099 ± 0.017	0.080 ± 0.004	0.060 ± 0.013*

.

6.5.3. Vitreal kinetics of quinidine in the presence of intravitreally administered verapamil

The effect of intravitreal co-administration of verapamil (100 µg) on the vitreal kinetics of quinidine was also examined. In these studies the microdialysis probe perfusion solution contained verapamil, (1 mg/mL) to maintain a significantly higher verapamil/quinidine ratio in the vitreous humor. Figure 6-2 represents the vitreous concentration-time profile of quinidine in the presence of intravitreally co-administered verapamil. A 1.6-fold increase in MRT (from 83 ±

13 min to 131± 16 min), a 1.5-fold decrease in λ_z (from 0.0066 ± 0.0007 min^{-1} to 0.0043 ± 0.0002 min^{-1}) and a corresponding 1.5-fold increase in $t_{1/2}$ (from 105 ± 11 min to 159 ± 9 min) of quinidine were observed in the presence of intravitreally co-administered verapamil (Table 6-2). Statistically significant differences between the mean vitreal quinidine concentrations of the treated and control groups were observed from the 100 minute time point onwards (Fig. 6-2).

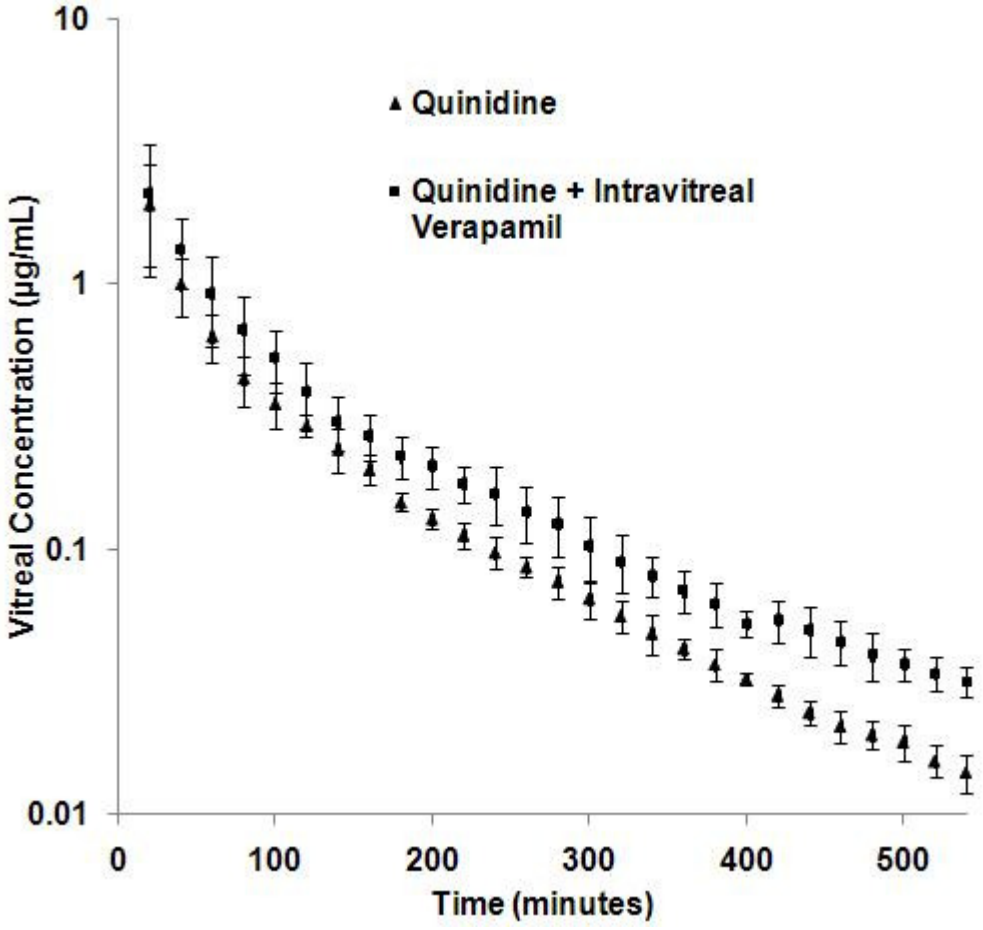

Figure 6-2: Vitreal concentration-time profile of quinidine (0.75 µg) alone (control) or in the presence of intravitreally co-administered verapamil (100 µg, administered along with quinidine). Data points represent mean ± standard deviation of four determinations.

Table 6-2: Vitreal kinetic parameters of quinidine (0.75 µg dose) alone or in the presence of intravitreally co-administered verapamil (100 µg). Verapamil solution (1 mg/mL in IPBS) was used as the perfusate. Values represented as mean ± standard deviation (n=4). *p<0.05, **p<0.01, ***p<0.001

Kinetic Parameters	Quinidine	Quinidine + Intravitreal Verapamil
λ_z (min^{-1})	0.0066± 0.0007	0.0043 ± 0.0002 ***
$AUC_{0-\infty}$ (µg x min/mL)	168 ± 56	180 ± 72
CL (mL/min)	0.0048 ± 0.0012	0.0046 ± 0.0014
V_{SS} (mL)	0.41 ± 0.14	0.63 ± 0.27
MRT_{∞} (min)	83 ± 13	131 ± 16 **
$AUC_{100-540}$ (µg x min/mL)	40 ± 0.03	56 ± 11*
$AUC_{300-540}$ (µg x min/mL)	7.73 ± 1.32	13.31 ± 2.28**
$CL_{300-540}$ (mL/min)	0.099 ± 0.017	0.057 ± 0.009**

6.5.4. Effect of topical prednisolone hemisuccinate sodium (PHS) on vitreal kinetics of quinidine

Prednisolone is practically insoluble in water (Karssen et al., 2002), and therefore its water soluble derivative PHS was used in this study. The effect of topically administered PHS (1% w/v and 2% w/v) on the vitreal kinetics of intravitreally administered quinidine was studied

(Table 6-3 and Figs. 6-3A & 6-3B). One hundred microliters of a 1% or 2% w/v PHS solution were instilled at 2, 4 and 6 hours following quinidine administration. Topical co-administration of PHS 1% w/v resulted in a 1.4-fold increase in the $t_{1/2}$ and a 1.4-fold decrease in the λ_z of quinidine. However, statistically significant changes in $AUC_{300\text{-}540}$ and $CL_{300\text{-}540}$ were not observed at this dose. Co-administration of 2% w/v PHS produced a 2.0-fold increase in the $t_{1/2}$ and a 2-fold decrease in the λ_z of quinidine. A 1.4-fold increase in $CL_{300\text{-}540}$ and $AUC_{300\text{-}540}$ were also observed. Moreover, a 1.6-fold increase in MRT of quinidine was observed when compared to that of the control. Statistically significant differences between the mean vitreal quinidine concentrations of the 2% PHS treated group and the control group was noted from the 360 minute time point onwards (Fig. 6-3B).

Figure 6-3A

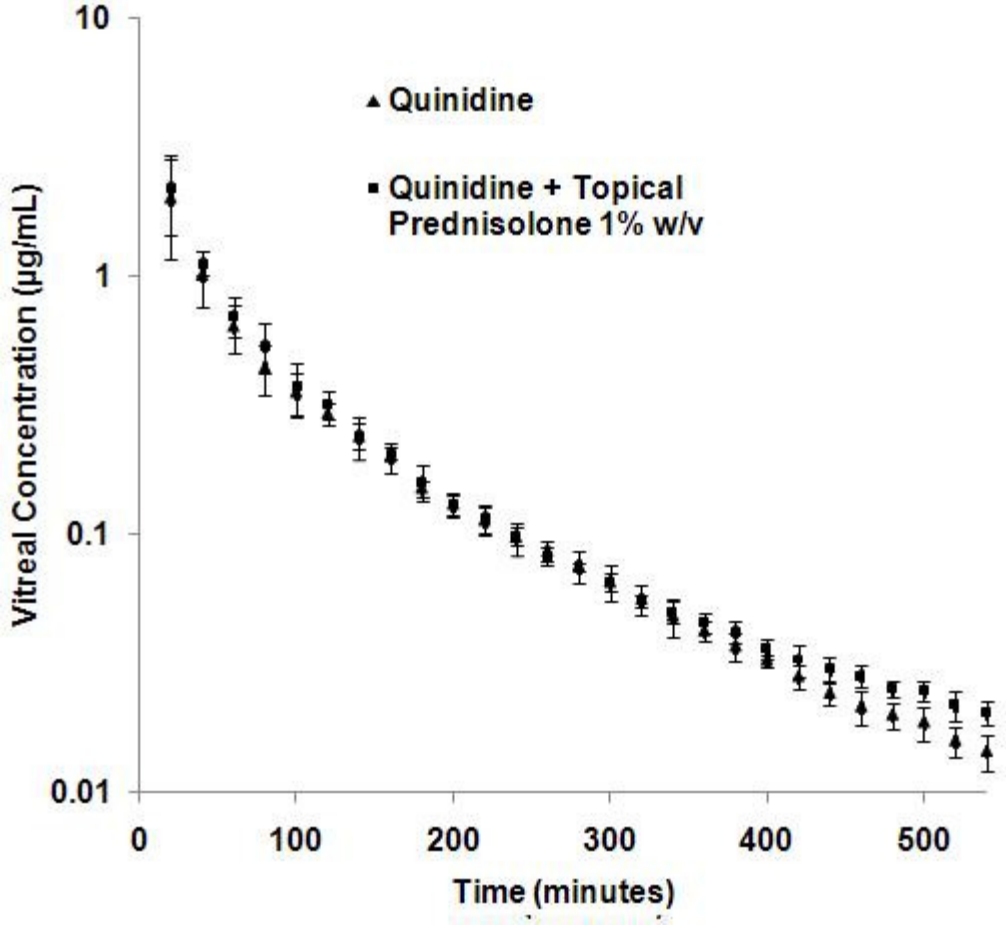
10
1
0.1
0.01
Vitreal Concentration (µg/mL)
Quinidine
Quinidine + Topical Prednisolone 1% w/v
0
100
200
300
400
500
Time (minutes)

Figure 6-3B

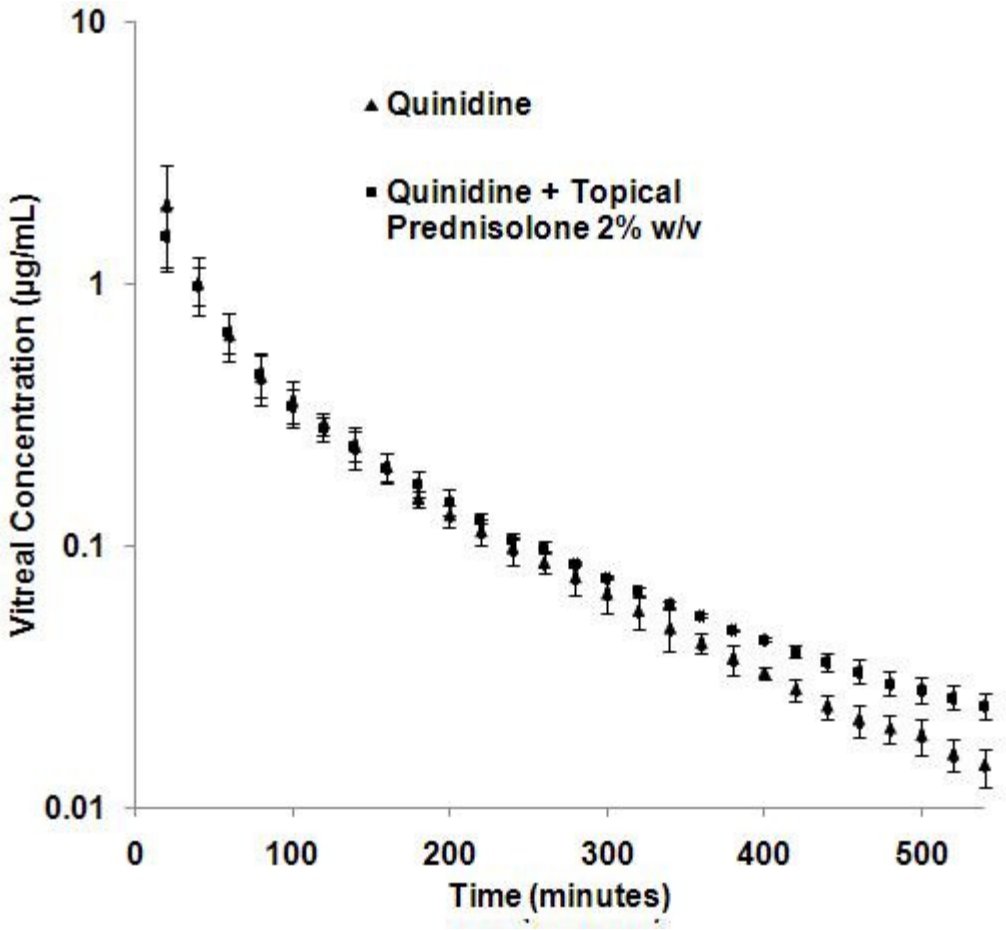

Figure 6-3: Vitreal concentration-time profile of quinidine (0.75 µg) alone (control) or in the presence of topically co-administered predinisolone hemisuccinate sodium (A) 1% w/v (B) 2% w/v. Data points represent mean ± standard deviation of four determinations.

Table 6-3: Vitreal pharmacokinetic parameters of quinidine (0.75 µg dose), following intravitreal administration in the presence and absence of topically co-administered prednisolone hemisuccinate sodium (PHS). Values represented as mean ± standard deviation (n=4).

Kinetic Parameters	Quinidine	Quinidine + PHS 1% w/v	Quinidine + PHS 2% w/v
λ_z (min^{-1})	0.0066± 0.0007	0.0048 ± 0.0004**	0.0033 ± 0.0004***†
$AUC_{0-\infty}$ (µg x min/mL)	168 ± 56	191 ± 42	151 ± 21.6
CL (mL/min)	0.0048 ± 0.0012	0.0040 ± 0.0009	0.0050 ± 0.0007
V_{SS} (mL)	0.41 ± 0.14	0.37 ± 0.14	0.65 ± 0.20
MRT_{∞} (min)	83 ± 13	87 ± 16	129 ± 21**†
$AUC_{300-540}$(µg x min/mL)	7.73 ± 1.32	8.70 ± 0.79	11.76 ± 0.40*†
$CL_{300-540}$(mL/min)	0.099 ± 0.017	0.087 ± 0.008	0.063 ± 0.002*†

*, **, *** indicates statistical significant difference between quinidine (control) and treated groups (Quinidine+ PHS 2% w/v and Quinidine + PHS 1% w/v); *p<0.05, **p<0.01, ***p<0.001

† indicates statistical significant difference between Quinidine + PHS 2% w/v and Quinidine + PHS 1% w/v; †p<0.05

6.5.5. Ocular tissue distribution of verapamil and PHS

Table 6-4 represents ocular tissue concentrations of verapamil (post topical and intravitreal administration) and PHS sodium (following topical administration). Topical and intravitreal routes of administration generated similar verapamil concentrations in the RPE/choroid at the end of 7 hours. The 7 hour time point was selected for verapamil since the effect of topical verapamil on the vitreal quinidine kinetics became evident at around this time (significant change in the mean vitreal concentrations between the treated and control groups) in the pharmacokinetic profile (Fig. 6-1A). Very low/insignificant verapamil concentrations were observed in the vitreous humor following topical verapamil administration, indicating that the 2 hours stabilization period was sufficient to seal the scleral port created during probe implantation. PHS tissue concentrations were evaluated at the end of the experiment (9 h). Interestingly, following topical administration, the fraction of PHS sodium appearing in the vitreous humor (concentration in the vitreous humor as a percentage of the topically administered dose) was significantly higher than that observed with verapamil.

Table 6-4: Ocular distribution of verapamil and PHS. Verapamil tissue concentrations were determined 7h after topical (100 µL of a 1% w/v solution applied 2, 4 and 6 h post intravitreal quinidine administration) and intravitreal administration (dose: 100 µg). Ocular distribution of topically-applied PHS (100 µL of a 2% w/v solution applied at 2, 4 and 6 h post intravitreal quinidine administration) was determined 9 h after intravitreal quinidine administration, and the values have been reported for both intact PHS and free prednisolone concentrations observed. Values represent mean ± standard deviation (n=4).* Generated as a result of bioreversion of PHS in the ocular tissues

Tissues	Verapamil concentration		PHS Topical application (2% w/v)	
	Topical Application	Intravitreal Administration	Intact PHS concentration	Concentration of free Prednisolone *
Aqueous Humor (µg/mL)	7.9 ± 3.2	1.5 ± 0.3	10.2 ± 1.1	5.0 ± 1.4
Iris-Ciliary Body (µg/gm)	4.4 ± 1.6	27.0 ± 10.0	7.0 ± 1.5	13.3 ± 4.3
Lens (µg/gm)	6.3 ± 1.2	45.1 ± 4.2	-	-
Vitreous Humor (µg/mL)	0.086 ± 0.003	31.5 ± 1.4	0.64 ± 0.21	0.49 ± 0.29
Retina-Choroid (µg/gm)	47.0 ± 8.1	52.0 ± 12.2	8.8 ± 1.2	16.7 ± 1.6

6.5.6. Bioreversion of PHS

Table 6-5 depicts the apparent pseudo-first-order degradation rate constants and half-lives of PHS in ocular tissue homogenates (1 mg/mL protein content), including vitreous humor. Tissue homogenates were prepared in IPBS pH 7.40. PHS was hydrolyzed to the parent drug, prednisolone, suggesting the role of esterases in the bioreversion of PHS. Degradation rate constants were obtained from log concentration of PHS remaining versus time plots. Hydrolysis rate constant obtained from the control (PHS in IPBS) were subtracted from the overall observed rate constants to estimate rate constants for the enzyme mediated hydrolytic process.

Table 6-5: Apparent first order degradation rate constants (k) x 10^3, min^{-1} and half-lives ($t_{1/2}$, min), of PHS (prednisolone hemisuccinate sodium) in ocular tissue homogenates (1 mg/mL protein content). Values represent mean ± standard deviation (n=4).

Drug / Kinetic parameters		Control	Cornea	Vitreous humor	Iris-ciliary	RPE/Choroid
PHS	K x 10^3 (min^{-1})	0.33 ± 0.05	0.81 ± 0.07	3.06 ± 0.34	2.00 ± 0.06	1.20 ± 0.05
	$t_{1/2}$ (min)	2118 ± 333	852 ± 74	228 ± 28	347 ± 10	578 ± 27

6.5.7. Intravitreal kinetics of fluorescein in the presence of topically applied verapamil

Figure 6-4 illustrates the vitreous concentration-time profile of fluorescein, alone or in the presence of topically co-administered verapamil. Vitreal fluorescein concentration-time data could be best fitted to a two-compartment open model. One hundred microliters of verapamil (1% w/v, pH 6.00) was applied topically at 2, 4 and 6 hours after fluorescein administration to evaluate the effect of topical verapamil administration on the barrier properties of the RPE. The vitreal pharmacokinetic parameters of fluorescein, such as elimination half-life, CL, AUC, steady-state volume of distribution and apparent elimination rate constant, remained unchanged in the presence of topically co-administered verapamil (Table 6-6).

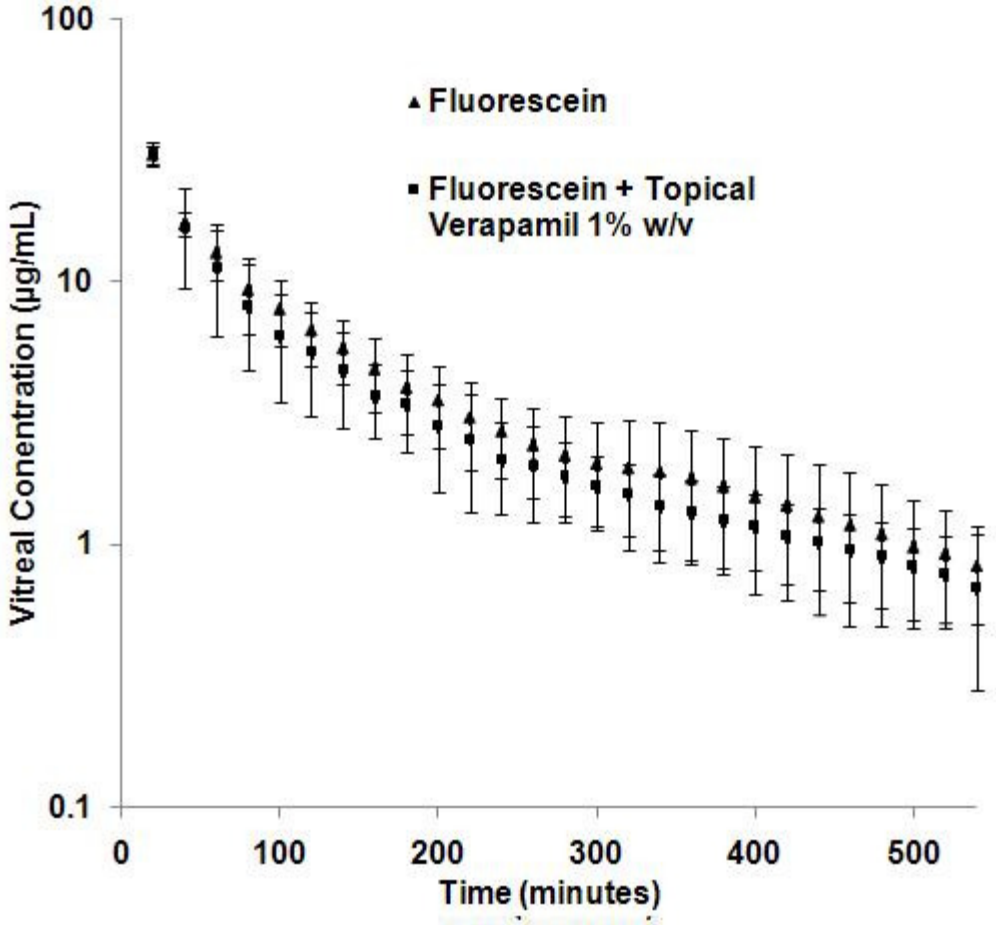

Figure 6-4: Vitreal concentration-time profile of fluorescein (10.0 µg) alone or in the presence of topically co-administered verapamil (1%w/v, 100 µL administered at 2, 4 and 6 h after intravitreal fluorescein administration). Data points represent mean ± standard deviation of four determinations

Table 6-6: Vitreal kinetics of intravitreally administered fluorescein (10 µg). Values represent mean ± standard deviation (n=4).

Kinetic Parameters	Fluorescein
k_{10} (min^{-1})	0.021 ± 0.01
k_{12} (min^{-1})	0.02 ± 0.01
k_{21} (min^{-1})	0.0135 ± 0.004
AUC (µg x min/mL)	3272 ± 632
K_{10} $t_{½}$ (min)	38.6 ± 20.3
CL (mL/min)	0.003 ± 0.0005
MRT_{∞} (min)	124 ± 49
V_{SS} (mL)	0.37 ± 0.1
β (min^{-1})	0.0049 ± 0.0009
β $t_{½}$ (min)	122 ± 39

6.6. Discussion

The goal of this novel study was to evaluate whether a drug-drug interaction could occur between intravitreally and topically co-administered P-gp substrates and its effect on the ocular pharmacokinetics of the intravitreally administered compound.

Duvvuri et.al demonstrated that intravitreal co-administration of verapamil and quinidine resulted in increased vitreal elimination of quinidine. Moreover, when quinidine was administered systemically and verapamil was co-administered intravitreally, the vitreal AUC of quinidine increased significantly (71). In another *in vivo* study, Senthikumari et al. reported a

significant increase in the ocular tissue concentrations of intravitreally administered rhodamine-123 in the presence of a P-gp inhibitor applied intravenously (Senthilkumari et al., 2008a). The authors hypothesized that the increased vitreal rhodamine-123 concentrations were probably the result of inhibition of efflux mediated by P-gp expressed on the ocular tissues. In a subsequent study, the investigators studied systemic co-administration of both compounds (rhodamine-123 and the inhibitor) but did not observe an increase in vitreal rhodamine-123 concentrations, probably because of inadequate inhibitor concentrations at the target site (Senthilkumari et al., 2008b).

The above three studies, to our knowledge the only published reports investigating *in vivo* RPE P-gp mediated efflux, evaluated the effect of either intravitreal or systemically co-administered inhibitors on vitreal kinetics of P-gp substrates. From a therapeutic point of view, with respect to delivery of P-gp substrates to the posterior chamber ocular tissues, the use of an intravitreal inhibitor is not feasible considering that high intravitreal levels of the inhibitor can only be maintained through multiple intravitreal injections. On the other hand, the use of systemic inhibitors is not attractive because of nonspecific systemic exposure to the inhibitor and the limited, clinically relevant, inhibitor dose that can be administered.

A hitherto uninvestigated and novel alternative approach that could be therapeutically effective as well as minimize systemic exposure would be modulation of efflux mediated by P-gp expressed on the RPE through topical substrate/inhibitor application. As discussed earlier, several therapeutic agents that are P-gp substrates are currently administered topically. Literature also suggests that a fraction of topically administered agents may reach the RPE (263-267). Taking both factors into consideration, this study was undertaken to evaluate the feasibility of

modulating ocular kinetics of intravitreally administered substrates through local application of P-gp substrates/inhibitors.

Erythromycin, 0.2% w/v, applied at 0, 2 and 4 hours or at 2, 4 and 6 hours following intravitreal quinidine administration, did not significantly affect the pharmacokinetic parameters of quinidine. Higher doses of erythromycin were not tested because of limited aqueous solubility. Topical verapamil, at a concentration of 0.5% w/v, also did not produce any significant change in the vitreal quinidine kinetics. The inability of 0.5% w/v verapamil and 0.2% w/v erythromycin to affect the pharmacokinetic parameters of quinidine could be due to insufficient inhibitor concentrations at the RPE, at these doses. Co-administration of topical verapamil 1% w/v resulted in a significant decrease in the apparent elimination rate constant and an increase in the vitreal half-life and mean retention time of quinidine in the posterior chamber (Table 6-1). Significant differences in $AUC_{0-\infty}$ and CL, from those of the control, were not observed possibly because the inhibitory effect of the topically administered agents becomes significant only when vitreal quinidine concentrations reduce to the low levels observed at the midpoint of the study, or, because adequate inhibitor concentrations are achieved at the RPE at that point of time. Consistent with the findings with verapamil and erythromycin, PHS demonstrated a dose-dependent effect on the vitreal pharmacokinetic parameters of quinidine (Table 6-3). At a concentration of 2% w/v, PHS produced a much more significant change compared to 1% w/v, probably because of higher concentrations of prednisolone generated at the target site, the RPE.

In the studies involving topical application of 1% verapamil (Figure 6-1B) and 2% PHS (Figure 6-2B), statistically significant difference between the mean vitreal quinidine

concentrations of the control and the treated groups were observed from the 360 minute time point. In the case of 1% PHS a statistically significant difference between the means of the control and treated groups was observed only after 460 minutes. When partial areas were taken into account, significant differences in $AUC_{300\text{-}540}$ and $CL_{300\text{-}540}$ were observed in the 1% w/v verapamil and 2% w/v PHS treated groups, from that of control, demonstrating an interaction of topically administered P-gp substrates with RPE P-gp. These results illustrate the importance of the permeability kinetics of the topically applied agents.

Fluorescein has been used as a marker compound to monitor the integrity and tightness of the blood-retinal barriers. The vitreal pharmacokinetic parameters of fluorescein were not affected by topical co-administration of 1% w/v verapamil (Table 6-6), and the values obtained in this study were consistent with previously published values (260). The results thus strongly suggest that the observed effect of topical verapamil on the vitreal kinetics of quinidine is a result of verapamil interacting with RPE P-gp.

Since prednisolone rather than PHS is known to interact with P-gp, bioreversion of PHS to prednisolone is necessary. *In vitro* metabolism studies confirmed bioreversion of PHS, to generate free prednisolone, in the ocular tissues (Table 6-5). At higher topical doses of PHS, greater quantities of PHS would be reaching the RPE, and thus greater concentrations of prednisolone would be generated. Interestingly, the ocular tissue distribution studies, following topical administration of verapamil and PHS, revealed that significantly higher fractions of the topically administered PHS dose reached the vitreous humor (almost 5-fold higher) compared to verapamil. Cheruvu et al. indicated that compounds with high logP values demonstrate lower trans-scleral permeability, possibly because of an interaction with the proteins expressed on the

Bruch's membrane (268). The higher vitreal PHS concentrations observed could be a result of greater aqueous solubility of PHS at physiological pH ranges, favoring greater diffusion across the Bruch's membrane and/or because of changes in the binding affinity with the Bruch's membrane proteins. The ocular tissue concentration data (Table 6-4) also suggests that verapamil and PHS migrate laterally along the cornea/aqueous humor route, and possibly also across the conjunctiva, into the sclera. The results further demonstrate that following topical administration, sufficient verapamil and PHS concentrations can accumulate in the choroid/RPE tissue and inhibit P-gp on the basolateral membrane of RPE. In fact, the concentration of verapamil in the RPE /choroid tissue 7 hours post topical verapamil instillation was similar to that obtained after intravitreal administration. Insignificant vitreal concentrations, however, suggest that very little verapamil could traverse across the RPE into the neural retina.

The elimination rate of quinidine from the vitreous humor was observed to decrease in the presence of intravitreally administered verapamil (Table 6-2), suggesting functional involvement of P-gp expressed on the basolateral membrane of the RPE, or apical membrane of the retinal endothelial cells. These results are contrary to that of Duvvuri et al. wherein quinidine elimination was observed to increase in the presence of intravitreal verapamil. The authors had suggested P-gp expressed on the neural retina, facing the vitreous, probably influences elimination of P-gp substrates from the vitreous humor. However, there are no other reports corroborating P-gp expression on the neural retina. Besides P-gp expression on the apical membrane of the retinal endothelial cells, most *in vitro and ex vivo* studies suggest functional activity of P-gp is localized on the basolateral membrane of the RPE. A study by Steuer et.al demonstrated higher permeability of verapamil (2.6-fold) and rhodamine (3.5-fold) across

isolated RPE in the neural retina to choroid direction compared to the choroid to neural retina direction, demonstrating the significance of P-gp localized on the basolateral membrane (choroidal side) of the RPE (Steuer et al., 2005). The results by Senthilkumari et al. also suggest functional expression of P-gp on the basolateral membrane of the RPE (Senthilkumari et al., 2008a). Biochemical and functional studies carried out by Kennedy et al. is the only study, to our knowledge, that suggests expression of P-gp on the apical membrane of the RPE. However, the authors postulated that P-gp localized on the apical RPE probably serves additional functions such as modulation of volume sensitive chloride efflux or functions as lipid translocase, etc. (69). However, since the intravitreal verapamil dose administered was not mentioned by the authors (71), there is a possibility that the verapamil dose administered in the earlier study was sufficient to inhibit P-gp on the neural retina but not interact with P-gp expressed on the basolateral membrane of the RPE.

Taken together, the above results demonstrate that topically administered P-gp substrates can migrate along the corneal-scleral pathway and possibly across the conjunctiva into the sclera and significantly alter elimination profiles of intravitreally administered P-gp substrates. This interaction can be used to modulate drug elimination from the posterior chamber of the eye. The impact of this strategy might be significantly more marked with topical and systemic co-administration (currently under investigation), considering the low plasma concentrations of the P-gp substrates generated compared to the vitreous humor concentrations obtained following intravitreal administration. This technique may also help modulate efflux activity of other transporters, such as the multidrug resistant proteins, expressed on the RPE. Further investigation of this novel approach is warranted.

Acknowledgements

We appreciate the support and technical help extended by the Univeristy of Mississippi animal facility staff, in particular Dr. Harry Fyke (University Veterinarian) and Ms. Penni Bolton (Animal Care Supervisor). This project was supported by the National Eye Institute, National Institutes of Health (NIH) [Grant EY018426-02]. The content is solely the responsibility of the authors and does not necessarily represent the official views of the National Institutes of Health.

CHAPTER 7

INTERACTION BETWEEN TOPICALLY AND SYSTEMICALLY CO-ADMINISTERED P-GLYCOPROTEIN SUBSTRATES/INHIBITORS: EFFECT ON VITREAL KINETICS

7.1. Abstract

The objective of the present study was to investigate the effect of topically co-administered P-glycoprotein (P-gp) substrates/inhibitors on the vitreal kinetics of a systemically administered P-gp substrate. Anesthetized male rabbits were used in these studies. Concentration time profile of quinidine in the vitreous humor, following intravenous administration, was determined alone and in the presence of topically co-administered verapamil, prednisolone sodium phosphate (PP), and erythromycin. The vitreal pharmacokinetic parameters of quinidine in the presence of verapamil (apparent elimination rate constant (λ_z): 0.0027 ± 0.0002 min^{-1}; clearance (CL_F): 131 ± 21 mL/min; area under curve ($AUC_{0-\infty}$): 39 ± 7.0 µg.min/mL; mean residence time (MRT): 435 ± 20 min) were significantly different from that of the control (0.0058 ± 0.0006 min^{-1}, 296 ± 46 mL/min, 17 ± 3 µg.min/mL, and 232 ± 20 min, respectively). A 1.7-fold decrease in the vitreal λ_z and a 1.5-fold increase in the vitreal AUC of quinidine were

observed in the presence of topical PP. Statistically significant differences between the vitreal profiles of the control and erythromycin treated group were also observed. Plasma concentration time profiles of quinidine, alone or in the presence of the topically instilled compounds, remained unchanged indicating uniform systemic quinidine exposure across groups. This study demonstrates an interaction between topically and systemically co-administered P-gp substrates, probably through the modulation of P-gp on the basolateral membrane of the retinal pigmented epithelium, leading to changes in the vitreal kinetics of the systemically administered agent.

7.2. Introduction

Drug delivery to the back-of-the eye through the systemic route is a challenging task (269). The blood-retinal barrier (BRB), consisting of the inner and outer BRB, prevents access of xenobiotics from the systemic circulation into the back-of-the eye (52). The retinal pigmented epithelium (RPE), which constitutes the outer BRB, acts as a major barrier to not only systemically administered agents but also to compounds administered by the periocular routes (270). The RPE is a single layer of hexagonal epithelial cells that forms the outermost layer of the retina and is separated from the choroid by the Bruch's membrane (268). It carries out essential biochemical functions such as phagocytosis of photoreceptor outer segments, transport regulation between the photoreceptors and the choriocapillaries and the uptake and conversion of the retinoids (55). However, the RPE also presents a significant barrier to the ocular penetration of many therapeutic agents (270).

Following systemic administration therapeutic moieties can easily diffuse out of the leaky choroiocapillaries into the choroidal stroma (52, 56, 57). The tight junctions of the RPE,

however, regulates further diffusion of hydrophilic and macro molecules from the choroidal stroma into the retina (57). Furthermore, P-glycoprotein (P-gp), a membrane bound protein involved in the efflux of many hydrophobic molecules, expressed on the basolateral membrane of the RPE (henceforth referred to as RPE P-gp), plays a vital role in RPE's barrier properties towards lipophilic compounds. The physiological role of this efflux protein is to protect the eye from harmful toxic substances. However, through their protective action, RPE P-gp severely limits ocular penetration of many systemically, as well as periocularly, administered drugs (270). Thus, modulation of the activity of RPE P-gp could alter the penetration of substrates from the systemic circulation into the vitreous humor and subsequent elimination from the posterior chamber. This could significantly alter the ocular pharmacokinetic parameters of the systemically administered P-gp substrate.

Effect of a drug-drug interaction at the level of the RPE P-gp, and its effect on ocular drug pharmacokinetics *in vivo,* has attracted attention only in recent years. Literature reports the effect of systemic/systemic, systemic/intravitreal or intravitreal/intravitreal co-administration of inhibitors and model marker compounds on ocular pharmacokinetics (71, 152, 153). In the previous chapter (Chapter 6, we demonstrated, for the first time, an interaction between topically and intravitreally co-administered P-gp substrates wherein the topically administered P-gp modulators altered the vitreal kinetics of an intravitreally administered P-gp substrate, quinidine (270).

The objective of the current research project was to determine the effect of topical P-gp inhibitors on the vitreal kinetics of a systemically co-administered P-gp substrate. For this purpose, two currently marketed ophthalmic formulations, erythromycin ophthalmic ointment

(USP, 0.5%) and prednisolone sodium phosphate (USP, 1%, (PP)), were administered topically. Additionally, a 1% verapamil solution was also prepared for topical administration. Erythromycin and PP are routinely administered topically to control ocular infections and inflammation, respectively, and are well established P-gp inhibitors (270, 271). Verapamil is another well known P-gp substrate/inhibitor (71). Quinidine, which was used in our previous study (Chapter 6) as the marker compound (270), was used as a model P-gp substrate in this study also and its vitreal and plasma pharmacokinetic parameters were determined.

7.3. Materials

Verapamil hydrochloride and quinidine hydrochloride were obtained from Sigma-Aldrich (St Louis, MO, USA). Prednisolone sodium phosphate (PP) ophthalmic solution (USP, 1%) and erythromycin ophthalmic ointment (USP, 0.5%), were procured from Butler Animal Health Supply (Dublin, OH, USA). Ketamine hydrochloride and Xylazine were purchased from Fort Dodge Animal Health (Fort Dodge, IA, USA) and Lloyd Laboratories (Shenandoah, IA, USA), respectively. Pentobarbital was obtained from Virbac AH, Inc. (Fort Worth, TX, USA). HPLC grade solvents and other chemicals (analytical grade) were obtained from Thermo Fisher Scientific (Waltham. MA, USA). Microdialysis concentric probes (CMA/20; 20000 Dalton cut-off, 0.5 X 10 mm polyarylethersulphone membrane and 14 mm shaft), used for sampling the vitreous chamber, were purchased from CMA/Micro-dialysis (North Chelmsford, MA, USA).

New Zealand male albino rabbits (NZW) were procured from Myrtle's Rabbitry (Thompson Station, TN, USA). All the animal experiments conformed to the tenets of the Association for Research in Vision and Ophthalmology (ARVO) statement on the Use of

Animals in Ophthalmic and Vision Research and followed the University of Mississippi IACUC approved protocols.

7.4. Methods:

7.4.1. Microdialysis probe implantation and recovery studies

7.4.1.1. *In vivo* Probe implantation

Rabbits (weighing 2-2.5 Kg) were anesthetized using ketamine (35 mg/kg) / xylazine (3.5 mg/kg) administered intramuscularly and were maintained under anesthesia throughout the duration of the experiment (ketamine / xylazine administered intramuscularly every 40 min). Before probe implantation, the median ear artery of the rabbit was cannulated using a 24G X 3/4'' SURFLO® Teflon I.V. Catheter with an injection plug (Terumo ®, Somerset, NJ, USA) for collection of blood samples. Following cannulation, microdialysis probe implantation was carried out as previously described (270). Briefly, eyes were proptosed, after dilating the pupil with 1% tropicamide solution, and a 22G needle was carefully inserted into the vitreous chamber. The point of insertion was approximately 3 mm below the corneal-scleral limbus. The needle was retracted, and the vitreal probe was implanted immediately. The position of the probe was adjusted so that the semipermeable membrane was in the mid-vitreous section. The probes were continuously perfused with sterile Isotonic phosphate buffer saline (IPBS ; pH 7.4) at a flow rate of 2 µL/min using microdialysis pump control module and syringe drives (Bioanalytical Systems, Inc. Mount Vernon, IN, USA). Following probe implantation, animals were allowed to stabilize for a period of 2 h before drug administration. Vitreal samples were collected every 20 min for a period of 9 h. Samples were collected in microcentrifuge tubes and

stored at -20 ºC until further analysis. At the end of the study, animals were euthanized with an overdose of sodium pentobarbital administered through the marginal ear vein. A limitation of the anaesthetized rabbit model, accompanied with microdialysis, is that only a limited number of terminal elimination half-lives may be reached, particularly for compounds with long half-lives, which could affect half-life calculations. However, considering the goals of this research project, which is to investigate if the vitreal elimination kinetics are altered, this model and experimental protocol serves the purpose.

7.4.1.2. *In vitro* probe recovery

Probe recovery values were determined by placing the probe in an IPBS solution, pH 7.40, at 37ºC, containing a known concentration of quinidine. The probe was continuously perfused with sterile IPBS at a flow rate of 2 µL/min, and the dialysate samples were collected every 20 min. Recovery of quinidine was calculated using eq (1):

$$\text{Recovery}_{\textit{in vitro}} = C_d / C_s \qquad (1)$$

where, C_d is the quinidine concentration in the dialysate and C_s is the quinidine concentration in IPBS.

The actual concentrations of quinidine in the vitreous humor during the *in vivo* pharmacokinetic study were calculated using eq (2):

$$\text{Quinidine concentration in the vitreous humor} = C_q / \text{Recovery}_{\textit{in vitro}} \qquad (2)$$

where, C_q is concentration of quinidine in the dialysate.

In all the studies, $\text{Recovery}_{\textit{in vitro}}$ was determined prior to and at the end of *in vivo* experiment and average $\text{Recovery}_{\textit{in vitro}}$ values were used to determine the actual concentration of quinidine in the vitreous humor.

7.4.2. Drug administration

After the probe stabilization period, quinidine hydrochloride, formulated in propylene glycol/IPBS (40:60, pH 7.40), was administered intravenously through the marginal ear vein (5 mg/kg BW). Vitreal kinetics of quinidine following intravenous administration was studied alone (control) or in the presence of the topically applied substrates/inhibitors; verapamil (1%, pH 6.00), erythromycin 0.5% ophthalmic ointment and PP (1%). Four animals were studied on each treatment day and the animals were dosed sequentially by groups (control followed by inhibitor groups). One hundred microliters of verapamil and PP were instilled in the conjuctival sac 2, 4 and 6 h after intravenous quinidine administration. In the case of the erythromycin study, a single dose of 0.5 mg erythromycin (100 mg ointment) was applied in the conjunctival sac 2 h after the intravenous quinidine injection. Verapamil solution was prepared by dissolving verapamil hydrochloride in sterile IPBS (pH 6.00) to yield a 1% solution; PP and erythromycin ophthalmic formulations were used as such. Verapamil and PP were dosed three times based on the data from and as a continuation of our previous work (Chapter 6) (270), wherein we demonstrated the effect of topical inhibitor on the vitreal kinetics of an intravitreally administered substrate. Erythromycin was dosed only once since an ointment formulation was used.

In our previous study (Chapter 6) (270), to delineate the effect of the vehicle on the ocular tissue barrier properties we had studied the vitreal kinetics of intravitreally administered fluorescein (marker compound to monitor the integrity and tightness of blood-retinal barrier), alone or in the presence of topically co-administered verapamil (1% w/v, vehicle: IPBS pH

6.00). The vitreal pharmacokinetic parameters of fluorescein remained unchanged in the presence of topically co-administered verapamil (270) indicating tightness and integrity of the blood-retinal barrier was not altered. None of the other components of the vehicle would interact with P-gp. Since the vehicle used in the current study is the same, a separate vehicle control was thus not included.

Vitreal microdialysis samples were collected every 20 min for a period of 9 h. Blood samples (0.5mL) were also collected concurrently, in both control and inhibition studies groups, from the catheter implanted in the central ear artery of each rabbit. Blood samples were drawn and then collected in heparinized vials at approximately 10, 15, 30, 60, 90, 120, 240, 360 and 480 min after intravenous quinidine administration. The exact time of blood collection was noted and a plasma concentration time profile was constructed accordingly. Plasma was separated from the whole blood by centrifugation at 13000 rpm for 10 min at 4 ºC (Accuspin Micro 17R, Thermo Fisher Scientific (Waltham. MA, USA)) and was stored at -20 ºC until further analysis.

7.4.3. Distribution of prednisolone/prednisolone sodium phosphate (PP) and erythromycin in the ocular tissues following topical administration

In a separate set of studies, following the probe stabilization period, PP and erythromycin ophthalmic ointment were applied topically in the conjuctival sac of the rabbit eye at 2, 4 and 6 h and at 2 h, respectively. At the end of 9 h, post quinidine administration, animals were euthanized, eyes were enucleated and ocular tissues were collected and analyzed for drug content. No further attempts were made to understand the time course of levels of inhibitors in plasma, vitreous and other ocular tissues following topical application.

7.4.4. Enzymatic conversion of PP to prednisolone

Prednisolone rather than PP, a phosphate ester of prednisolone, is known to interact with P-gp. Therefore, bioreversion rates of PP to prednisolone were determined in the aqueous humor, vitreous humor, lens, RPE/choroid and iris-ciliary body following previously described procedures (135, 270). Studies were carried out in triplicate at 37°C in a shaking water bath (75 reciprocations per min). One hundred (100) µL of PP stock solution was added to the required volume of the tissue homogenates and aqueous and vitreous humor to obtain a final PP concentration of 5 µg/mL. The protein content in the tissue homogenates was determined using the Bradford method (272). At predetermined time points, 100 µL aliquots were withdrawn, and an equal volume of ice cold methanol was immediately added to the sample to arrest the enzymatic degradation process. Stability of PP (5 µg/mL) in IPBS was also studied as a control and the values were subtracted from the overall reaction rates to estimate the enzyme mediated degradation rates. The bioreversion rates were normalized to the protein content in the tissue homogenates.

7.4.5. Analytical procedures:

7.4.5.1. Ocular tissue collection and sample preparation

With respect to studies involving ocular distribution of PP and erythromycin following topical application, vitreous and aqueous humor were collected as previously described (270). Ocular tissues such as iris-ciliary bodies, lens and retina/choroid, were weighed and homogenized in ice cold IPBS or methanol using a Tissuemiser (Thermo Fisher Scientific (Waltham. MA, USA)). Homogenates were further diluted with ice cold acetonitrile:methanol

(50:50) mixture, centrifuged and analyzed for drug content. Centrifugation was carried out at 13,000 rpm for 20 min at 4°C. Aqueous and vitreous humor samples were used as such, or diluted with methanol, and taken for analysis. Extraction efficiency of PP and erythromycin from ocular tissues was > 95%.

7.4.5.2. HPLC Analysis

Microdialysis and plasma samples were analyzed for quinidine content using a reverse phase HPLC procedure as previously described (71). The HPLC system comprised of Waters 717 plus autosampler, Waters 2475 multi λ Fluorescence detector, Waters 600 controller pump and Agilent 3395 integrator. A Symmetry® C18 4.6 X 250 mm column was used and the mobile phase consisted of 20 mM phosphate buffer (pH 2.50) with 12 % acetonitrile at a flow rate of 1 mL/min. Excitation and emission wavelength were set at 250 nm and 440 nm, respectively. Microdialysis samples were directly injected into the HPLC. Plasma samples were analyzed after dilution with ice-cold acetonitrile:methanol (50:50) mixture and centrifugation. For quantification of quinidine in microdialysis samples calibration standards (2 ng/mL to 200 ng/mL) were prepared in IPBS. For analysis of quinidine in plasma samples, calibration curve (15 ng/mL to 3000 ng/mL) was prepared by spiking the blank rabbit plasma with known concentrations of quindine in IPBS, followed by protein precipitation with acetonitrile:methanol (50:50) mixture. The standard curves generated coefficient of determination (r^2) values greater than 0.9999. The limit of quantification of quinidine in the microdialysis and plasma samples was 2 ng/ mL and 10 ng/ mL, respectively. The percentage relative standard deviation (intra-day and inter-day) for quinidine QC samples in IPBS and rabbit plasma were below 2% and 5.8%, respectively. Quinidine samples were analyzed in a single run or in groups. QC samples in IPBS

(2, 5, 15, 100 and 160 ng/mL) and plasma (spiked concentration: 25, 75, 1000 and 2000 ng/mL) were always included in the runs after every 25-30 samples. The accuracy (intra-day and inter-day) at different concentrations were within range of 99.9-101.4% and 98.0-105.0% for QC samples in IPBS and rabbit plasma, respectively. Prednisolone and PP content in the bioreversion and ocular disposition studies were determined using reversed phase HPLC procedure as previously described with minor modification (273). Analysis was carried out using Waters 2487 Dual λ Absorbance detector. The mobile phase consisted of isopropanol and 0.2 % v/v o-phosphoric acid in deionized water (25: 75, pH 3.00). A YMC-Pack J'sphere ODS-M80 (4.6 x 250 mm) column was used for separation, and the flow rate and wavelength (λ) were set at 0.8 mL/min and 245 nm, respectively.

7.4.5.3. Liquid Chromatography/Mass spectrometry (LC-ESI-TOF) analysis

Erythromycin content in the ocular tissues, including vitreous and aqueous humor, were determined using Liquid chromatography/Mass spectrometry (LC-ESI-TOF). Primary stock solution of erythromycin and internal standard, roxithromycin, (IS) were prepared in 100% methanol and secondary stock solutions were prepared in IPBS. Calibration curve was prepared by spiking known concentration of erythromycin in blank ocular tissues, vitreous humor and aqueous humor. The samples were allowed to stand for 30 min and then were homogenized in methanol using a Tissuemiser to produce calibration standards (10 to 500 ng/mL) of erythromycin.

The liquid chromatograph used was an Agilent Series 1100 comprised of the following modular components: quaternary pump, a vacuum solvent microdegasser, an autosampler with

100-well tray. The mass spectrometric analysis was performed by using the LC-ESI-TOF (Model #G1969A, Agilent Technologies, Palo Alto, CA, USA) equipped with an ESI source. All acquisitions were performed under positive ionization mode with a capillary voltage of 3500 V. Nitrogen was used as the nebulizer gas (30 psig) as well as the drying gas at 11 L/min at a temperature of 350 ºC. The voltage of PMT, fragmentor and skimmer was set at 850V, 100V and 60V respectively. Full scan mass spectra were acquired from *m/z* 200-1000. Data acquisition and processing was done using the Analyst^{TM} QS software (Agilent Technologies, Palo Alto, CA, USA).

Separation was achieved on a synergi Hydro-RP; 100 x 2.0 mm I.D.; 4 µm particle size (Phenomenex, Torrance, CA, USA). The column was equipped with a guard column (Supelco, Bellefonte, PA, USA). The mobile phase consisted of water with 0.1 % formic acid (A), and acetonitrile with 0.1 % formic acid (B) at a flow rate of 0.3 mL/min, with the following gradient elution: 0 min, 75 % A/25 % B to 20% A/80 % B over 10 min. Each run was followed by a 5 min wash with 100 % B and an equilibration period of 11 min with 75 % A/25 % B. The total run time for analysis was 10 min. Ten microliters of the sample was injected and peaks were assigned with respect to the mass of the compounds and comparison of the retention times. The limit of detection of Erythromycin was 0.05 ng/mL and each sample contained 100 ng/mL IS. This method involved the use of the $[M+H]^+$ ions in the positive ion mode with extractive ion monitoring (EIM). In the positive ion mode, the protonated species $[M+H]^+$ at *m/z* 734.4680 for erythromycin and 837.5324 for IS were observed

7.4.6. Data analysis

Non-compartmental pharmacokinetic analysis was carried out for the quinidine concentration time profile in the vitreous humor using WinNonlin, version 5.2 (Pharsight; Mountain View, CA). The pharmacokinetic parameters were calculated using the formulae described earlier (270). Briefly, terminal slopes of the vitreous concentration-time profile were estimated by log-linear regression, and the apparent elimination rate constant (λ_z) was then derived from the slope. Elimination half-life ($t_{1/2}$) was calculated from the equation: $t_{1/2} = 0.693/\lambda_z$. The area under the vitreal concentration-time curve ($AUC_{0-\infty}$) and the area under the moments curve ($AUMC_{0-\infty}$) were estimated by the trapezoidal rule. The mean residence time (MRT) was calculated using the equation: $MRT = AUMC_{0-\infty} / AUC_{0-\infty}$. The total clearance was calculated as: $CL = Dose/AUC_{0-\infty}$. The peak vitreal concentration (C_{max}) and the time to reach the peak concentration (t_{max}) were determined from the observed values

The time course of plasma quinidine concentration, after a single systemic dose was best described by a two-compartment open model as expressed in eq (3).

$$C = Ae^{-\alpha t} + Be^{-\beta t} \quad (3)$$

In which A and B are zero time concentration coefficients, t the time (min) and α and β are the disposition rate constants of the initial and terminal phase, respectively. The rate constant of drug transfer from the apparent peripheral to the apparent central compartment (k_{21}), elimination rate constant from the apparent central compartment (k_{10}) and rate constant of quinidine transfer from the apparent central compartment to the apparent peripheral compartment (k_{12}) were calculated as previously described (270). Data obtained was subjected to statistical analysis using one-way

analysis of variance (ANOVA) followed by the post-hoc Dunnett's test for multiple comparison (JMP software (SAS Institute Inc, Cary, NC)). Homogeneity of variances between the groups was checked using Bartlett's test before performing ANOVA. Results were considered statistically significant if p value was ≤ 0.05**.**

7.5. Results

7.5.1. Effect of topically applied verapamil on the vitreal kinetics of systemically administered quinidine

The vitreal concentration-time profile of quinidine after systemic administration (5 mg/kg) alone (control) or in the presence of topically administered verapamil is illustrated in Figure 7-1, and the pharmacokinetic parameters have been provided in Table 7-1. Verapamil HCl displayed low solublility at pH 7.40 (1 mg/mL), and therefore solutions were prepared in sterile IPBS at pH 6.00**.** With respect to the vitreal pharmacokinetic parameters of intravenously administered quinidine*,* topically instilled **v**erapamil (100 µL of 1 % w/v), administered at 2, 4 and 6 h after systemic quinidine administration, produced a 1.9-fold increase in the MRT (from 232 ± 20 to 435 ± 20 min), a 2.2-fold decrease in the λ_z (from 0.0058 ± 0.0006 min^{-1} to 0.0027 ± 0.0002 min^{-1}) and a 2.3-fold increase in the $AUC_{0-\infty}$ of quinidine in the vitreous humor.

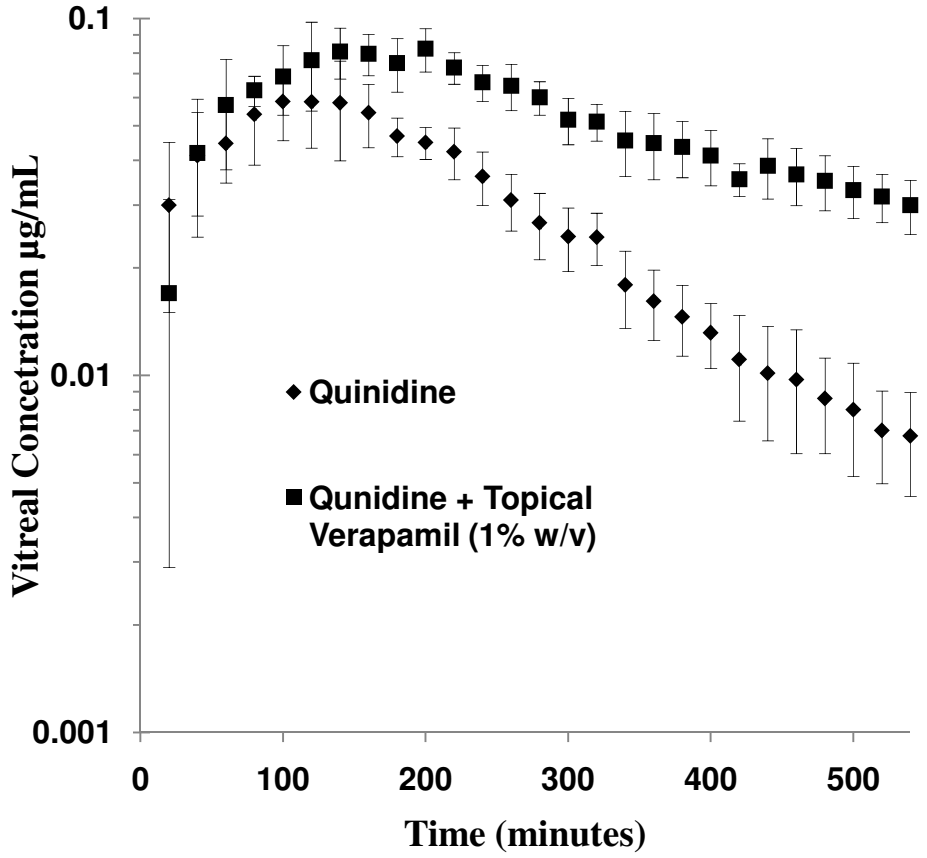

Figure 7-1: Vitreal concentration-time profile of quinidine (5 mg/kg, systemic administration) alone (control) or in the presence of topically co-administered verapamil 1% w/v (100 µL administered at 2, 4 and 6 h after quinidine administration). Data points represent mean ± standard deviation of four determinations.

Table 7-1: Vitreal pharmacokinetic parameters of systemically administered quinidine (5 mg/kg) alone or in the presence of topically co-administered verapamil , prednisolone sodium phosphate ophthalmic solution, USP (1% w/v) and erythromycin ointment. Verapamil and prednisolone sodium phosphate were administered at 2, 4 and 6 h after systemic quinidine administration. Single dose of erythromycin ophthalmic ointment (100mg) was applied at 2 h after quinidine administration. Single control group (Quinidine) has been compared to each treatment group. Values represented as mean ± standard deviation (n=4). * p<0.05, **p<0.01, ***p<0.001 (difference from control)

Kinetic Parameters	Quinidine	Quinidine + Verapamil (1% w/v)	Quinidine + Prednisolone (1% w/v)	Quinidine + Erythromycin (0.5 % w/w)
λ_z (min^{-1})	0.0058 ± 0.0006	0.0027 ± 0.0002 ***	0.0035 ± 0.0001 **	0.0040 ± 0.0002 **
λ_z half-life (min)	120 ± 14	256 ± 24***	198 ± 21*	173 ± 11*
T_{max} (min)	115 ± 30	146 ± 23	120 ± 40	115 ± 30
C_{max} (µg/mL)	0.06 ± 0.02	0.08 ± 0.01	0.07 ± 0.007	0.08 ± 0.02
$AUC_{0-\infty}$ (µg x min/mL)	17 ± 3	39 ± 7.0**	26 ± 2.0*	32 ± 9*
AUC_{0-last} (µg x min/mL)	16 ± 2	28 ± 5.0*	22 ± 1.6*	28 ± 9*
VZ_F (mL)	50642 ± 2486	47661 ± 4490	47708± 5245	38592± 10690
CL_F (mL/min)	296 ± 46	131 ± 21***	193 ± 15*	161 ± 50**
$AUMC_{0-\infty}$ (µg x min^2/mL)	4024 ± 926	17225± 4230***	7519 ± 1289*	10328 ± 3424*
MRT_{∞} (min)	232 ± 20	435 ± 20***	288 ± 30*	310 ± 23**

7.5.2. Effect of topically applied prednisolone sodium phosphate (PP) on vitreal kinetics of systemically administered quinidine

PP is a phosphate ester of prednisolone and is currently marketed in the United States as an ophthalmic anti-inflammatory formulation. Therefore, effect of topically administered PP on the vitreal kinetics of systemically administered quinidine (5 mg/kg) was investigated (Fig. 7-2). One hundred microliters of a 1% w/v PP solution was instilled at 2, 4 and 6 h after quinidine administration. Table 7-1 presents the vitreal pharmacokinetic parameters of quinidine. Topical PP co-administration produced a 1.7-fold decrease in the λ_z (from 0.0058 ± 0.0006 to 0.0035 ± 0.0001 min^{-1}), a 1.7-fold increase in $t_{1/2}$ and a 1.3-fold increase in the MRT. Moreover, a 1.5-fold increase in the vitreal $AUC_{0-\infty}$ of quinidine, compared to that of the control, was observed when PP was co-administered.

7.5.3. Effect of topical erythromycin on vitreal kinetics of systemically administered quinidine

Vitreal kinetics of intravenous quinidine (5 mg/kg) was also studied either alone or in the presence of topically administered erythromycin in the form of the marketed erythromycin ophthalmic ointment. In these set of studies, 100 mg of the ointment (0.5% w/w) was applied topically two hours after systemic quinidine administration. Figure 7-3 depicts the vitreous concentration-time profile of quinidine alone or in the presence of topically administered erythromycin. The vitreal pharmacokinetic parameters have been presented in Table 7-1. In the control group, the λ_z for quinidine was found to be 0.0058 ± 0.0006 min^{-1} whereas in the presence of topical erythromycin it was found to be 0.0040 ± 0.0002 min^{-1}. A corresponding

1.5- fold increase in the vitreal elimination half-life ($t_{1/2}$) was also observed. Additionally, a significant increase in the $AUC_{0-\infty}$ and MRT of quinidine in the vitreous humor was also evident.

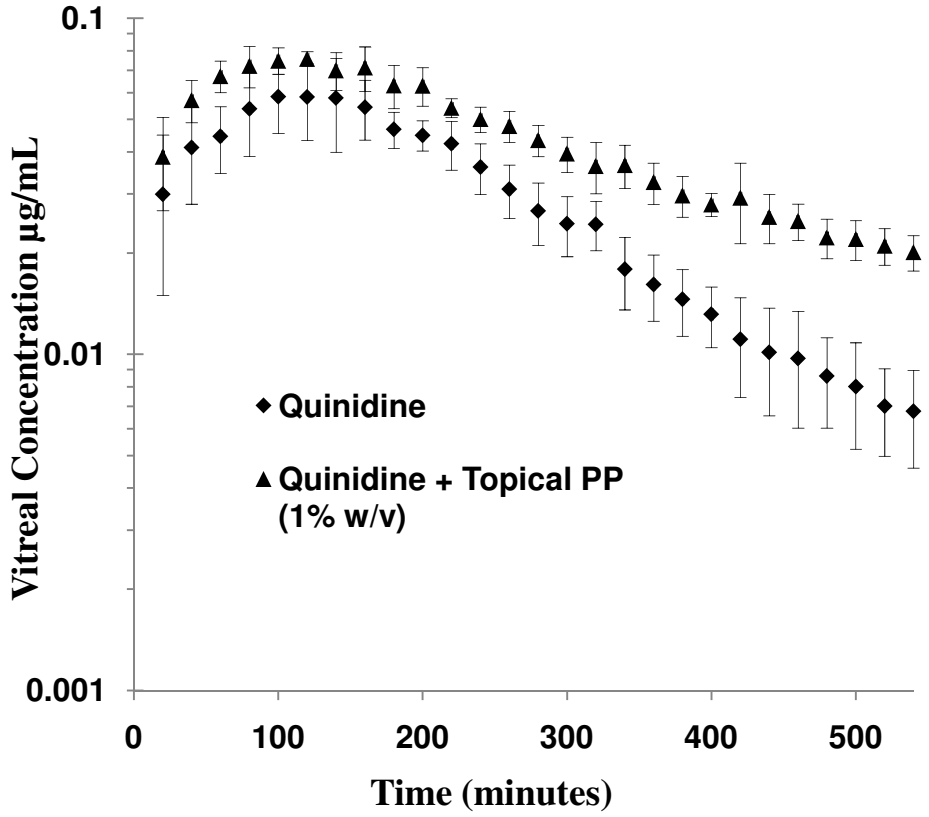

Figure 7-2: Vitreal concentration-time profile of quinidine (5mg/kg, systemic administration) alone (control) or in the presence of topically co-administered PP 1% w/v (100 µL administered at 2, 4 and 6 h after quinidine administration). Data points represent mean ± standard deviation of four determinations. Control group data is the same as that in Figure 7-1 and has been replotted to facilitate comparison.

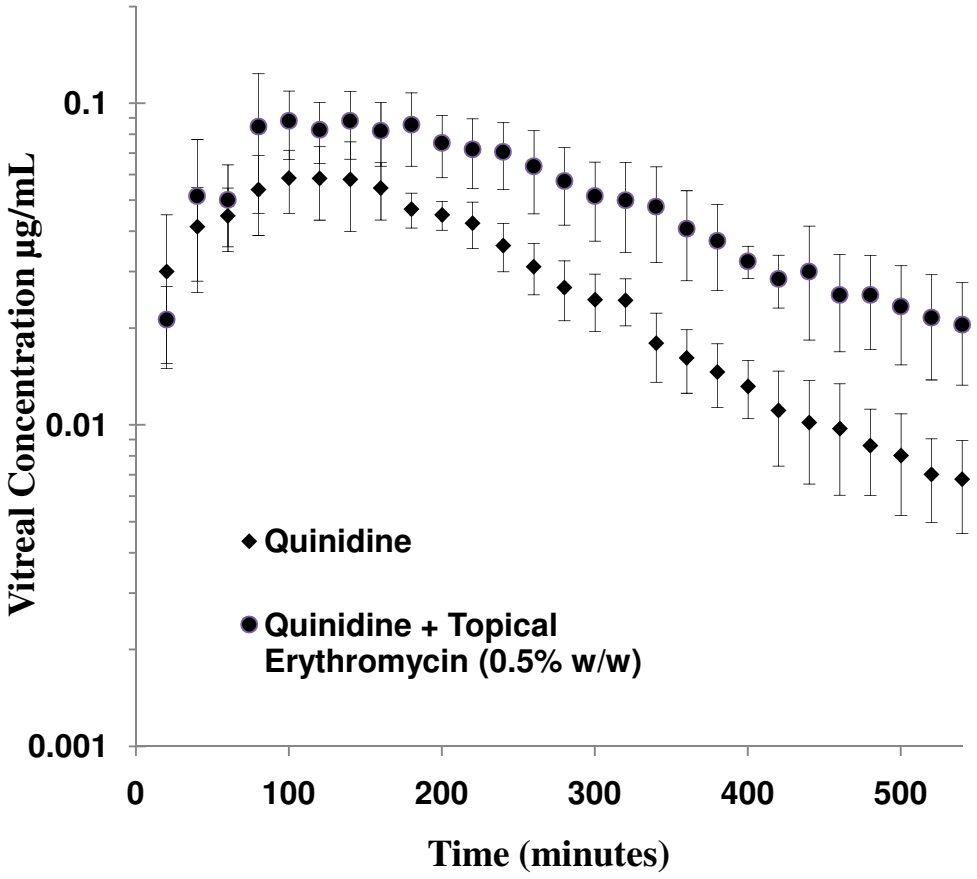

Figure 7- 3: Vitreal concentration-time profile of quinidine (5mg/kg) alone (control) or in the presence of topically co-administered erythromycin ophthalmic ointment, 0.5% w/w (100 mg, administered 2 h after quinidine administration). Data points represent mean ± standard deviation of four determinations. Control group data is the same as that in Figure 7-1 and has been replotted to facilitate comparison.

7.5.4. Plasma concentration time profile of quinidine in the presence and absence of topically applied inhibitors:

Plasma kinetics of systemically administered quinidine (5 mg/kg), alone or in the presence of topically co-administered verapamil, PP and erythromycin was determined and compared, to evaluate the effect of topical inhibitors on plasma kinetics of quinidine and to

ensure uniform systemic exposure in all study groups. Figures 7-4A, 7-4B and 7-4C, represent the plasma concentration time profiles of quinidine alone or in the presence of verapamil, PP and erythromycin, respectively. Quinidine plasma concentration time data, alone or in the presence of the inhibitors, was best explained by a two-compartment open model based on the Akaike Information criterion (AIC) and the Schwarz Bayesian Criterion (SBC) values (minimum for the 2 compartment model compared to 1 and 3 compartment models). Therefore, a two compartment open model was used to calculate the pharmacokinetic parameters. The plasma pharmacokinetic parameters of quinidine, such as elimination half-life, CL, AUC, k_{10} , k_{21} , k_{12}, steady-state volume of distribution and apparent elimination rate constant remained unchanged in the presence of the topically co-administered inhibitors (Table 7-2).

7.5.5. Ocular tissue distribution of PP and erythromycin following topical administration: Table 7-3 represents concentrations of PP and erythromycin in the aqueous humor, vitreous humor and other ocular tissues at the end of the experiment (9 h). Topical administration of PP generated significantly high concentrations of prednisolone (generated from PP by enzymatic action) in the ocular tissues. Erythromycin concentrations in all the ocular tissues were significantly lower compared to PP. However, significant levels of erythromycin were observed in the vitreous humor even at 7h post application. The lower concentrations of erythromycin generated in the ocular tissues compared to that of PP may be due to the differences in the dosing regimen. It should be noted that only a single dose of erythromycin, 100 mg of the 0.5% ointment, was applied 2 h after quinidine administration, whereas in the case of verapamil and PP, 100 µL of a 1% w/v solution was applied at 2, 4 and 6 h after quinidine administration.

Figure 7-4A

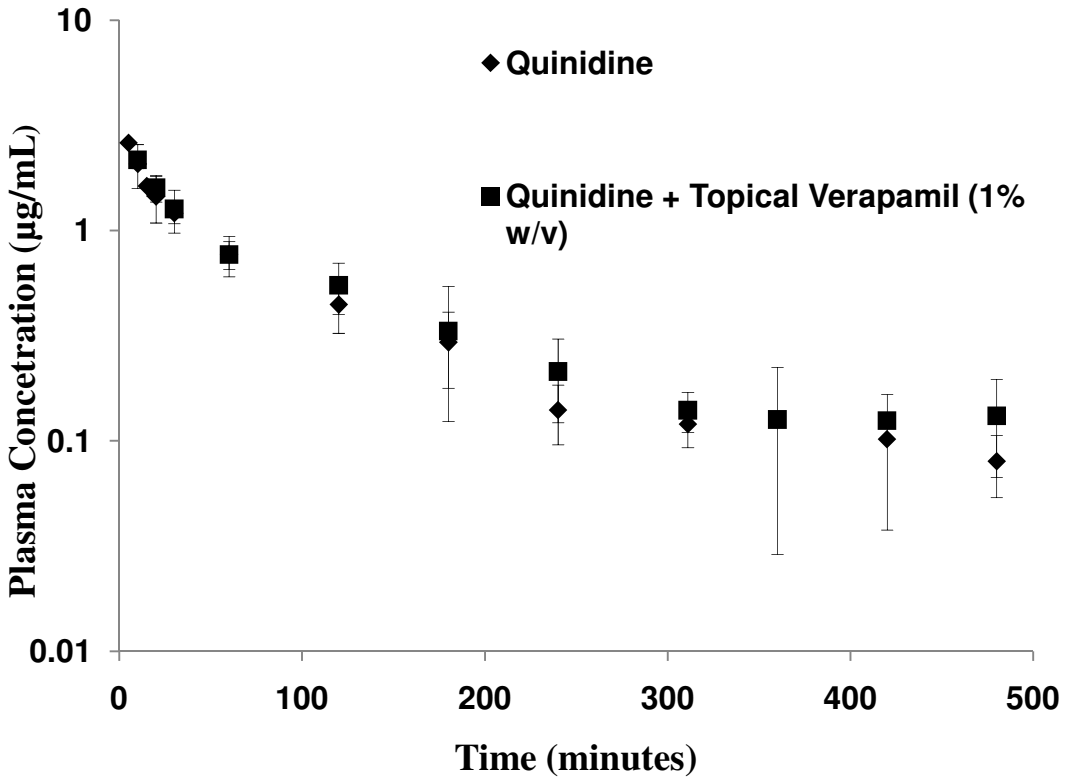
10
1
0.1
0.01
Plasma Concetration (µg/mL)
0
100
200
300
400
500
Time (minutes)
Quinidine
Quinidine + Topical Verapamil (1% w/v)

Figure 7-4B

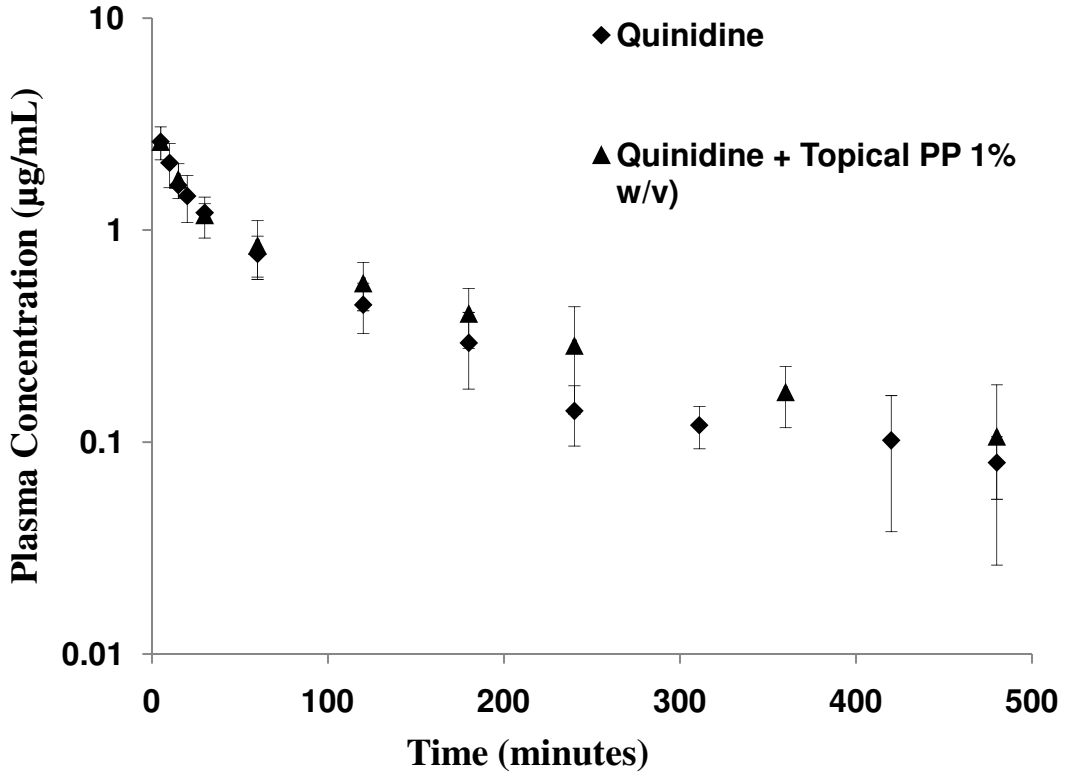
10
1
0.1
0.01
Plasma Concentration (µg/mL)
0
100
200
300
400
500
Time (minutes)
Quinidine
Quinidine + Topical PP 1% w/v)

Figure 7-4C

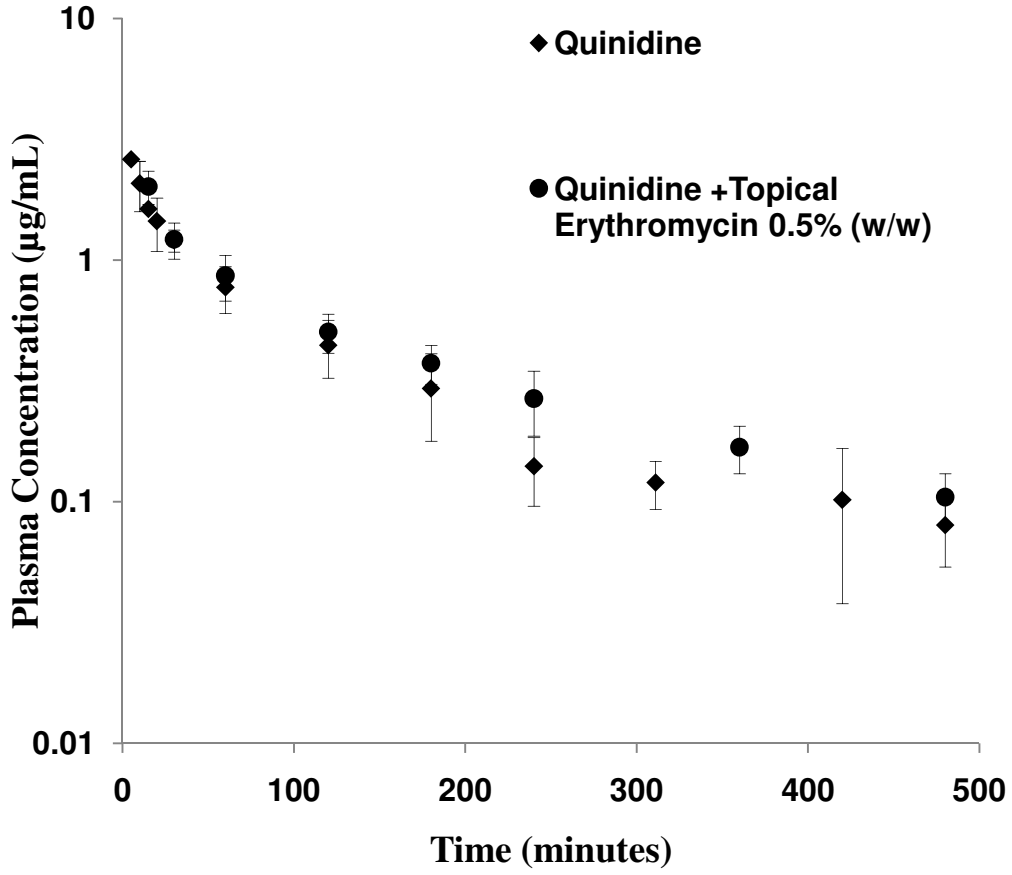

Figure 7-4: Plasma-time profile of quinidine (5 mg/kg, systemic administration) alone (control) or in the presence of topically co-administered (A) verapamil 1% w/v, (B) prednisolone sodium phosphate 1% w/v, (C) erythromycin ophthalmic ointment, 0.5% w/w Data points represent mean ± standard deviation of four determinations.

Table 7-2: Plasma pharmacokinetic parameters of systemically administered quinidine (5 mg/kg) alone or in the presence of topically co-administered verapamil , prednisolone sodium phosphate ophthalmic solution, USP (1% w/v) and erythromycin ointment. Verapamil and prednisolone sodium phosphate were administered at 2, 4 and 6 h after systemic quinidine administration. Single dose of Erythromycin ophthalmic ointment (100mg) was applied at 2 h after quinidine administration. No significant differences in the parameters were observed. Single control group (Quinidine) has been compared to each treatment group.

Kinetic Parameters	Quinidine	Quinidine + Verapamil (1% w/v)	Quinidine + Prednisolone (1% w/v)	Quinidine + Erythromycin (0.5 % w/w)
k_{10} (min^{-1})	0.015 ± 0.003	0.015 ± 0.007	0.015 ± 0.002	0.027 ± 0.02
k_{12} (min^{-1})	0.021 ± 0.015	0.027 ± 0.011	0.040± 0.009	0.047 ± 0.04
k_{21} (min^{-1})	0.024 ± 0.016	0.020 ± 0.007	0.031 ± 0.015	0.02 ± 0.004
AUC (µg x min/mL)	210 ± 20	233 ± 65	235 ± 54	231 ± 35
K_{10} $t_{½}$ (min)	52 ± 21	52 ± 20	48.5 ± 9	37 ± 15
CL (mL/min)	25 ± 3	23 ± 8	22 ± 5.5	22 ± 4
MRT_{∞} (min)	144 ± 58	170 ± 63	189 ± 44	142 ± 33
V_d (mL)	3756 ± 1636	3588 ± 487	3719 ± 1314	3196 ± 1276
β (min^{-1})	0.006 ± 0.001	0.0051 ± 0.002	0.0055 ± 0.001	0.0057 ± 0.001
β $t_{½}$ (min)	135 ± 83	142 ± 53	134 ± 38	124 ± 23

Table 7-3: Ocular distribution of verapamil, prednisolone sodium phosphate, and erythromycin ophthalmic ointment after topical administration.

Tissues	Topical Application of 1 % w/v Verapamil[#]	Topical Application of 0.5% w/w Erythromycin	Topical application of 1% w/v PP	
			Intact PP concentration	Concentration of free Prednisolone *
Aqueous Humor µg/mL	7.9 ± 3.2	4.7 ± 1.0	11 ± 5.4	76.0 ± 2.0
Iris-Ciliary Body µg/g	4.4 ± 1.6	1.53 ± 0.31	4.1 ± 0.6	32.0 ± 7.0
Lens µg/g	6.3 ± 1.2	0.26 ± 0.04	-	16.0 ± 4.0
Vitreous Humor µg/mL	0.086 ± 0.003	1.4 ± 0.15	1.8 ± 0.01	15.0 ± 2.0
Retina-Choroid µg/g	47.0 ± 8.1	1.74 ± 0.05	3.0 ± 1.2	43.0 ± 10.0

Prednisolone sodium phosphate (100 µL of a 1% w/v solution applied 2, 4 and 6 h post systemic administration) and erythromycin (100 mg of 0.5% w/w ointment applied at 2 h post systemic administration) tissue concentration were determined 9 h after topical administration. PP values have been reported for both intact PP and free prednisolone concentrations observed. Verapamil tissue concentrations were determined 7h after topical (100 µL of a 1% w/v solution applied 2, 4 and 6 h post intravitreal quinidine administration). Values represent mean ± standard deviation (n=4).

* Generated as a result of bioreversion of PP in the ocular tissues.

values from our previous study (Chapter 6) (270).

7.5.6. Enzymatic conversion of PP to prednisolone

Tissue homogenates were prepared in IPBS pH 7.4. Vitreous and aqueous humor were used as such. PP was rapidly hydrolyzed to the parent drug, prednisolone, by the ocular phosphatases. Table 7-4 depicts the apparent first order degradation rate constants and half-lives of PP in the ocular tissue homogenates (1 mg/mL protein content), including aqueous and vitreous humor. Degradation rate constants were obtained from the log concentration of PP remaining versus time plots. Hydrolysis rate constant obtained from the control (PP in IPBS) were subtracted from the overall observed rate constants to estimate rate constants for the enzyme mediated hydrolytic process.

Table 7-4: Apparent first order degradation rate constants (k) x 10^3, min^{-1} and half-lives ($t_{1/2}$, min), of PP (prednisolone sodium phosphate) in ocular tissue homogenates (1 mg/mL protein content). Values represent mean ± standard deviation (n=4).

Drug / Kinetic parameters		Control	Aqueous humor	Vitreous humor	Iris-ciliary	RPE/Choroid
PP	(k) x 10^3 (min^{-1})	0.36 ± 0.03	22.5 ± 4.0	0.83 ± 0.02	2.9 ± 0.09	3.17 ± 0.05
	$t_{1/2}$ (min)	1933 ± 160	31 ± 6.0	835 ± 17.0	239 ± 8.0	218 ± 4.0

7.6. Discussion

The role of RPE P-gp in limiting the penetration of systemically or periocularly administered substrates into the posterior chamber of the eye is well established (270). Surprisingly, very few studies have focused on strategies to overcome the efflux activity of this RPE P-gp. Duvvuri et al. reported that inhibition of the RPE P-gp, with the help of an intravitreal inhibitor (71). In another *in vivo* study, Senthikumari et al. demonstrated that systemically administered P-gp inhibitors significantly altered the ocular tissue concentrations of an intravitreally injected P-gp substrate (152). Both routes of inhibitor administration, however, suffer from major drawbacks such as concerns associated with intravitreal injections and nonspecific systemic exposure of the inhibitor from intravenous administration and the limited, clinically relevant, inhibitor dose that can be administered (270).

In our previous study (Chapter 6), exploring the feasibility of a novel approach for inhibiting the RPE P-gp, we demonstrated that topical inhibitors could decrease the elimination rate of intravitreally administered P-gp substrates (270). In the present study we carried this investigation further to examine the effect of a topical substrate/inhibitor administration on the ocular penetration of a systemically administered P-gp substrate. Although systemic administration of ophthalmic drugs also poses non-specific systemic exposure concerns, this novel topical substrate/inhibitor co-application approach could help decrease the systemic dose necessary to achieve ocular therapeutic response.

The C_{max} and T_{max} of quinidine in the vitreous humor were observed to be 0.06 ± 0.02 µg/mL and 115 ± 30 min, respectively. The vitreal AUC of quinidine was found to be 8% of the systemic AUC (Table 7-1 and 7-2). These results are consistent with previous literature reports

(71). Co-administration of topical verapamil and PP at 2, 4 and 6 h after systemic (i.v.) quinidine administration resulted in a significant decrease in the apparent vitreal λ_z and in an increase in the vitreal $t_{1/2}$ and MRT of quinidine (Table 7-1 and Fig. 7-1 and 7-2). Consistent with this, erythromycin also produced a significant decrease in the vitreal λ_z and an increase in the vitreal $t_{1/2}$ and MRT of quinidine (Table 7-1, Fig. 7-3). These findings strongly suggest that topically co-administered P-gp inhibitors interact with the RPE P-gp resulting in decreased vitreal elimination of the systemically administered P-gp substrate.

Duvvuri et al. reported a significant increase in the C_{max}, and the rate of entry of quinidine into the vitreous and a significant decrease in the T_{max} of quinidine following systemic administration of quinidine and intravitreal administration of the inhibitor (71). However, in the present study a statistically significant difference in the C_{max} and T_{max} of quinidine in the vitreous humor, on topical co-administration of the three inhibitors, was not observed (Table 7-1). This may be explained by the fact that Duvvuri et al. administered the intravitreal inhibitor 20 minutes prior to systemic quinidine administration whereas in the present study the inhibitors were applied 2 hours post quinidine administration, by which time the vitreal quinidine absorption phase would have been over.

Significant differences in the central compartment pharmacokinetic parameters of quinidine, in the presence and absence of topically co-administered verapamil, PP or erythromycin, were not observed (Table 7-2 and Fig. 7-4). These findings strongly suggest that the quinidine dose administered across groups were uniform and that the observed effect of the topically co-administered verapamil, PP and erythromycin, on the vitreal kinetics of quinidine was as a result of modulation of the efflux activity of RPE P-gp.

Topically co-administered verapamil produced a 1.7-fold decrease in the terminal elimination rate constant of intravitreally administered quinidine while $AUC_{0-\infty}$ and CL remained unchanged (270). Here, however, verapamil, with a similar dosing regimen, generated a greater (2.2-fold) decrease in the elimination rate constant of quinidine from the vitreous humor and also a significant increase in the vitreal $AUC_{0-\infty}$ and a decrease in CL. This is probably due to lower quinidine concentrations generated at the P-gp binding site in the RPE cytosol on intravenous administration. At the end of 2h, when the topical inhibitors were administered, the free plasma quinidine concentration was 0.05 µg/mL (considering almost 80-90% protein binding (274, 275)) and free vitreal quinidine concentration achieved was 0.06 µg/mL following systemic administration (current study), while vitreal free concentration of quinidine was 0.3 µg/mL (as estimated using microdialysis) following intravitreal injection. Assuming that similar verapamil concentrations were generated at the RPE/choroid following topical administration in both the studies (present and chapter 6), the verapamil to quinidine ratio would be significantly higher at the RPE P-gp binding site when quinidine is administered systemically. This results in greater inhibition and thus a significant decrease in the CL and elimination rate constant and a significant increase in the vitreal $AUC_{0-\infty}$ in the presence of verapamil, when compared to intravitreal administration (270).

Interestingly, 1% w/v PP produced a greater decrease in the vitreal λ_z compared to 1% w/v prednisolone hemisuccinate sodium (PHS) in our previous study (Chapter 6) (270). Additionally, a statistically significant difference in the $AUC_{0-\infty}$ and CL of quinidine was also observed in the presence 1% w/v PP. This can be explained by the low concentrations of quinidine generated in the vitreous humor (following systemic administration), rapid

bioreversion rates of PP to prednisolone and by the formulation components of the PP ophthalmic solution. Prednisolone and not PP is known to interact with P-gp (270). *In vitro* metabolism studies confirmed faster bioreversion of PP to prednisolone in the RPE/choroid ($t_{1/2}$: 218 min) compared to the hemisuccinate ester (PHS) ($t_{1/2}$: 578 min) (270). This is possibly as a result of differences in the phosphatase and esterase levels in the ocular tissues (276).

It is also interesting to note that topical PP (1%) generated significantly higher concentrations of prednisolone (15.0 ± 2.0 µg/mL) in the vitreous humor compared to the vitreal prednisolone levels achieved with topical 2% PHS (0.49 ± 0.29 µg/mL) (270). Moreover, 2 % PHS generated only 16.7 ± 1.6 µg/g of prednisolone in the RPE/choroid tissue (270) whereas 1% w/v PP generated 43 ± 10 µg/g (Table 7-3) of prednisolone. The higher levels of prednisolone obtained in the posterior segment ocular tissues supports our earlier observation that hydrophilic moieties on topical application tend to permeate to the back-of-the eye tissues better (270). Additionally, the PP formulation used in this study contains benzalkonium chloride (BAK, 0.01% w/v) and ethylenediaminetetraacetic acid (EDTA) as formulation components. The role of BAK and EDTA in enhancing corneal, conjunctival and scleral permeation of compounds is well documented (174, 277, 278). Thus PP might have diffused across the conjunctiva and into the sclera much more efficiently generating higher PP and prednisolone concentrations in the RPE/choroid. The significantly higher PP and prednisolone concentrations in the aqueous humor, lens and iris-ciliary body also supports enhanced transcorneal PP permeation in the presence of BAK and EDTA and rapid generation of prednisolone in the aqueous humor. Prednisolone being very lipophilic would then rapidly partition into the anterior segment ocular tissues and then laterally migrate along the iris-ciliary to the sclera and then the RPE and vitreous humor. Thus,

overall the results suggest that BAK and EDTA enhanced penetration of PP into the back-of-the eye tissues.

The levels of verapamil (approximately 0.2 µM) obtained in the vitreous humor (1 h after the last dose) (270) were much lower compared to PP (approximately 3.7 µM) and prednisolone (approximately 41 µM) in the vitreous humor even at 3 h after the last dose. Although similar concentrations of prednisolone (43 ± 10.0 µg/g; approximately 120 µM) and verapamil (47 ± 8.1 µg/g; approximately 95 µM) (270) were generated at the RPE/choroid in both studies the extent of RPE P-gp inhibition was less with prednisolone compared to verapamil (Table 7-1). This is probably because verapamil is a more potent P-gp inhibitor (prednisolone IC_{50} is 300 µM compared to an IC_{50} of 4.7 µM for verapamil; a 65-fold difference) (271, 279).

Further, in our previous study (Chapter 6), erythromycin, at a concentration of 0.2% w/v applied at 2, 4 and 6 h after intravitreal quinidine administration did not significantly affect the pharmacokinetic parameters of quinidine (270). On the contrary, in the present investigation erythromycin ophthalmic ointment produced a statistically significant difference in the vitreal λ_z , $AUC_{0-\infty,}$ CL and MRT of systemically administered quinidine. A single application of the ointment, 100 mg of 0.5% w/v applied 2 h after systemic quinidine administration, exhibited significant levels of erythromycin in the vitreous humor and RPE/choroid, even after 7h post erythromycin application, suggesting depot formation and sustained release of the drug from the residual formulation in the cul-de-sac. The observed effect on quinidine pharmacokinetics can probably be explained by the higher ocular tissue concentrations of erythromycin achieved in this study and the low concentrations of free quinidine in the plasma and RPE (as discussed earlier) and thus higher erythromycin to quinidine ratio in the RPE P-gp microenvironment.

Besides P-gp, the RPE is known to express other transporters (e.g. multi drug resistant proteins (MRPs), organic anion transporting polypeptides (OATPs)) (269) with which quinidine may interact (280-282). Though quinidine is a preferred substrate of P-gp and has been widely used as a P-gp substrate/inhibitor (71, 150, 283, 284) some involvement of other transporters cannot be ruled out completely. Future studies to optimize this approach will involve more specific P-gp/ MRP inhibitors and substrates. Additionally, the effect of the inhibitor type, concentration, time of application and time course of inhibitors in the vitreous, plasma and other ocular tissues following topical application on ocular kinetics of systemically/intravitreally administered P-gp substrates will also be the object of consideration in our future studies.

In conclusion, this study demonstrates for the first time that topically applied P-gp inhibitors can diffuse to the RPE and alter the elimination kinetics of a systemically administered P-gp substrate, probably through inhibition of the RPE P-gp. The degree of inhibition will depend on the physicochemical characteristics of the inhibitor and its affinity for P-gp and the concentration of the therapeutic agent in the plasma or vitreous humor. Formulation factors such as inclusion of permeation and viscosity enhancers may play a major role in yielding effective levels of the inhibitor at the RPE. This interaction may be used positively for drug delivery purposes through the use of potent, pharmacologically inactive, efflux inhibitors.

Acknowledgements

This project was supported by Grant Number EY018426-02 from the National Eye Institute (NIH/NEI). The content is solely the responsibility of the authors and does not necessarily represent the official views of the National Eye Institute, National Institutes of

Health. We also appreciate the support and technical help extended by the University of Mississippi animal facility staff, in particular Dr. Harry Fyke (University Veterinarian) and Ms. Penni Bolton (Animal Care Supervisor).

REFERENCES

1. Stjernschantz J, Astin M. Anatomy and Physiology of the Eye, Physiological Aspects of Ocular Drug Delivery. In: Edman P, editor. Biopharmaceutics of Ocular Drug Delivery: CRC Press, Inc.; 1993. p. 1-27.
2. Sunkara G, Kompella UB. Membrane Transport Process in the Eye. In: Mitra AK, editor. Ophthalmic Drug Delivery Systems. New York: Marcel Dekker, Inc.; 2003. p. 13-59.
3. Sasaki H, Yamamura K, Mukai T, Nishida K, Nakamura J, Nakashima M, et al. Enhancement of ocular drug penetration. Crit Rev Ther Drug Carrier Syst. 1999;16(1):85-146.
4. Majumdar S. Ocular Drug Delivery: Evaluation of Dipeptide Monoester Ganciclovir Prodrugs. Department of Pharmaceutical Sciences and Pharmacology [Dissertation]: The University of Missouri-Kansas City; 2005.
5. Rupenthal ID, Alany RG. Ocular Drug Delivery. In: Gad SC, editor. Pharmaceutical Manufacturing Handbook: Production and Processes. Hoboken, New Jersey: John Wiley and Sons, Inc.; 2008. p. 729-67.
6. Barar J, Javadzadeh AR, Omidi Y. Ocular novel drug delivery: impacts of membranes and barriers. Expert Opin Drug Deliv. 2008;5(5):567-81.
7. Kompella UB, Lee VHL. Barriers to Drug Transport in Ocular Epithelia. In: Amidon GL, Lee PI, Topp EM, editors. Transport Processes in Pharmaceutical Systems. New York: Marcel Dekker, Inc.; 2000. p. 317-77.
8. Hosoya K, Lee VHL, Kim K. Roles of the conjunctiva in ocular drug delivery: a review of conjunctival transport mechanisms and their regulation. Eur J Pharm Biopharm. 2005;60(2):227-40.
9. Kinsey VE. The chemical composition and the osmotic pressure of the aqueous humor and plasma of the rabbit. J Gen Physiol. 1951;34(3):389-402.
10. Candia OA. Electrolyte and fluid transport across corneal, conjunctival and lens epithelia. Exp Eye Res. 2004;78(3):527-35.
11. Koevary SB. Pharmacokinetics of topical ocular drug delivery: potential uses for the treatment of diseases of the posterior segment and beyond. Curr Drug Metab. 2003;4(3):213-22.
12. Ambati J, Adamis AP. Transscleral drug delivery to the retina and choroid. Prog Retin Eye Res. 2002;21(2):145-51.
13. Geroski DH, Edelhauser HF. Transscleral drug delivery for posterior segment disease. Adv Drug Deliv Rev. 2001;52(1):37-48.
14. Unlu N, Robinson JR. Scleral permeability to hydrocortisone and mannitol in the albino rabbit eye. J Ocul Pharmacol Ther. 1998;14(3):273-81.
15. Kao JC, Geroski DH, Edelhauser HF. Transscleral permeability of fluorescent-labeled

antibiotics. J Ocul Pharmacol Ther. 2005;21(1):1-10.
16. Hayreh SS. Segmental nature of the choroidal vasculature. Br J Ophthalmol. 1975;59(11):631-48.
17. Kiilgaard JF, Jesen PK. The Choroid and Optic Nerve Head. In: Fishbarg J, editor. The Biology of The Eye: Elsevier; 2006. p. 273-91.
18. Cour Ml, Tezel T. Retinal Pigmented Epithelium. In: Fishbarg J, editor. The Biology of The Eye: Elsevier; 2006. p. 244-71.
19. Rittenhouse KD, Pollack GM. Microdialysis and drug delivery to the eye. Adv Drug Deliv Rev. 2000;45(2-3):229-41.
20. Gaudana R, Ananthula HK, Parenky A, Mitra AK. Ocular drug delivery. AAPS J. 2010;12(3):348-60.
21. Loftsson T, Sigurdsson HH, Konradsdottir F, Gisladottir S, Jansook P, Stefansson E. Topical drug delivery to the posterior segment of the eye: anatomical and physiological considerations. Pharmazie. 2008;63(3):171-9.
22. Gibson M. Ophthalmic Dosage Forms. In: Gibson M, editor. Pharmaceutical Preformulation and Formulation: A practical guide from drug selection to commercial dosage form. Second ed: informa healthcare; 2009. p. 431-56.
23. Sasaki H, Yamamura K, Nishida K, Nakamura J, Ichikawa M. Delivery of Drugs to the Eye by Topical Application. Prog Retin Eye Res. 1996;15:583-620.
24. Järvinen K, Järvinen T, Urtti A. Ocular absorption following topical delivery. Adv Drug Deliv Rev. 1995;16(1):3-19.
25. Komai Y, Ushiki T. The three-dimensional organization of collagen fibrils in the human cornea and sclera. Invest Ophthalmol Vis Sci. 1991;32(8):2244-58.
26. Ahmed I, Patton TF. Disposition of timolol and inulin in the rabbit eye following corneal versus non-corneal absorption. Int J Pharm. 1987;38(1-3):9-21.
27. Ahmed I, Patton TF. Importance of the noncorneal absorption route in topical ophthalmic drug delivery. Invest Ophthalmol Vis Sci. 1985;26(4):584-7.
28. Hughes PM, Olejnik O, Chang-Lin J-E, Wilson CG. Topical and systemic drug delivery to the posterior segments. Advanced Drug Delivery Reviews. 2005;57(14):2010-32.
29. Hamalainen KM, Kananen K, Auriola S, Kontturi K, Urtti A. Characterization of paracellular and aqueous penetration routes in cornea, conjunctiva, and sclera. Invest Ophthalmol Vis Sci. 1997;38(3):627-34.
30. Hosoya K, Horibe Y, Kim KJ, Lee VH. Nucleoside transport mechanisms in the pigmented rabbit conjunctiva. Invest Ophthalmol Vis Sci. 1998;39(2):372-7.
31. Turner HC, Alvarez LJ, Bildin VN, Candia OA. Immunolocalization of Na-K-ATPase, Na-K-Cl and Na-glucose cotransporters in the conjunctival epithelium. Curr Eye Res. 2000;21:843-50.
32. Hosoya K-I, Horibe Y, Kim K-J, Lee VHL. Carrier-Mediated Transport of NG-Nitro-l-Arginine, a Nitric Oxide Synthase Inhibitor, in the Pigmented Rabbit Conjunctiva. J Pharmacol Exp Ther. 1998;285(1):223-7.
33. Hosoya K, Horibe Y, Kim KJ, Lee VH. Na(+)-dependent L-arginine transport in the pigmented rabbit conjunctiva. Exp Eye Res. 1997;65(4):547-53.
34. Davies NM. Biopharmaceutical Considerations In Topical Ocular Drug Delivery. Clinical and Experimental Pharmacology and Physiology. 2000;27:558-62.

35. Alonso MJ, Sanchez A. The potential of chitosan in ocular drug delivery. J Pharm Pharmacol. 2003;55(11):1451-63.
36. Ghate D, Edelhauser HF. Ocular drug delivery. Expert Opin Drug Deliv. 2006;3(2):275-87.
37. Gunda S, Hariharan S, Mandava S, Mitra AK. Barriers in Ocular Drug Delivery. In: Tombran-Tink J, Barnstable CJ, editors. Ophthalmology Research: Ocular Transporters in Ophthalmic Diseases and Drug Delivery. New Jersey: Humana Press; 2008. p. 399-413.
38. Järvinen T, Pate DW, Laine K. Cannabinoids in the treatment of glaucoma. Pharmacology & Therapeutics. 2002;95(2):203-20.
39. Yi X-j, Wang Y, Yu F-SX. Corneal Epithelial Tight Junctions and Their Response to Lipopolysaccharide Challenge. Invest Ophthalmol Vis Sci. 2000;41(13):4093-100.
40. Liaw J, Rojanasakul Y, Robinson JR. The effect of drug charge type and charge density on corneal transport. Int J Pharm. 1992;88(1-3):111-24.
41. Borchardt RT. Assessment of Transport Barriers Using Cell and Tissue Culture Systems. Drug Dev Ind Pharm. 1990;16(18):2595 - 612.
42. Ahmed I, Gokhale RD, Shah MV, Patton TF. Physicochemical determinants of drug diffusion across the conjunctiva, sclera, and cornea. J Pharm Sci. 1987;76(8):583-6.
43. Chien DS, Sasaki H, Bundgaard H, Buur A, Lee VH. Role of enzymatic lability in the corneal and conjunctival penetration of timolol ester prodrugs in the pigmented rabbit. Pharm Res. 1991;8(6):728-33.
44. Wang W, Sasaki H, Chien D-S, Lee VHL. Lipophilicity influence on conjunctival drug penetration in the pigmented rabbit: A comparison with corneal penetration. Curr Eye Res. 1991;10(6):571-9.
45. Loftssona T, Järvinen T. Cyclodextrins in ophthalmic drug delivery. Adv Drug Deliv Rev. 1999;36(1):59-79.
46. Loftsson T, StefÃnsson E. Effect of Cyclodextrins on Topical Drug Delivery to the Eye. Drug Dev Ind Pharm. 1997;23(5):473-81.
47. Rojanasakul Y, Wang LY, Bhat M, Glover DD, Malanga CJ, Ma JK. The transport barrier of epithelia: a comparative study on membrane permeability and charge selectivity in the rabbit. Pharm Res. 1992;9(8):1029-34.
48. Janoria KG, Hariharan S, Paturi D, Pal D, Mitra AK. Biotin uptake by rabbit corneal epithelial cells: role of sodium-dependent multivitamin transporter (SMVT). Curr Eye Res. 2006;31(10):797-809.
49. Sasaki H, Ichikawa M, Yamamura K, Nishida K, Nakamura J. Ocular membrane permeability of hydrophilic drugs for ocular peptide delivery. J Pharm Pharmacol. 1997;49(2):135-9.
50. Jumbe LN, Miller HM. Ocular Drug Transfer Following Systemic Drug Adminsitration. In: Mitra AK, editor. Ophthalmic Drug Delivery Systems: Marcel Dekker, Inc.; 2003. p. 109-35.
51. Hornof M, Toropainen E, Urtti A. Cell culture models of the ocular barriers. Eur J Pharm Biopharm. 2005;60(2):207-25.
52. Cunha-Vaz JG. The blood-retinal barriers system. Basic concepts and clinical evaluation. Exp Eye Res. 2004;78(3):715-21.
53. Cunha-Vaz JG. The blood-ocular barriers: past, present, and future. Documenta Ophthalmologica. 1997;93:149-57.

54. Russ P, Davidson M, Hoffman L, Haselton F. Partial characterization of the human retinal endothelial cell tight and adherens junction complexes. Invest Ophthalmol Vis Sci. 1998;39(12):2479-85.
55. Pitkanen L, Ranta VP, Moilanen H, Urtti A. Permeability of retinal pigment epithelium: effects of permeant molecular weight and lipophilicity. Invest Ophthalmol Vis Sci. 2005;46(2):641-6.
56. Dey S, Anand BS, Patel J, Mitra AK. Transporters/receptors in the anterior chamber: pathways to explore ocular drug delivery strategies. Expert Opin Biol Ther. 2003;3(1):23-44.
57. Duvvuri S, Majumdar S, Mitra AK. Drug delivery to the retina: challenges and opportunities. Expert Opin Biol Ther. 2003;3(1):45-56.
58. Ambudkar SV, Dey S, Hrycyna CA, Ramachandra M, Pastan I, Gottesman MM. Biochemical, cellular, and pharmacological aspects of the multidrug transporter. Annu Rev Pharmacol Toxicol. 1999;39:361-98.
59. Padowski JM, Pollack GM. Pharmacokinetic and pharmacodynamic implications of P-glycoprotein modulation. Methods Mol Biol. 2010;596:359-84.
60. Matheny CJ, Lamb MW, Brouwer KR, Pollack GM. Pharmacokinetic and pharmacodynamic implications of P-glycoprotein modulation. Pharmacotherapy. 2001;21(7):778-96.
61. Gottesman MM, Pastan I. Biochemistry of Multidrug Resistance Mediated by the Multidrug Transporter. Annual Review of Biochemistry. 1993;62(1):385-427.
62. Jones PM, George AM. Symmetry and structure in P-glycoprotein and ABC transporters what goes around comes around. Eur J Biochem. 2000;267(17):5298-305.
63. Rosenberg MF, Callaghan R, Ford RC, Higgins CF. Structure of the Multidrug Resistance P-glycoprotein to 2.5 nm Resolution Determined by Electron Microscopy and Image Analysis. J Biol Chem. 1997;272(16):10685-94.
64. Loo TW, Clarke DM. Recent progress in understanding the mechanism of P-glycoprotein-mediated drug efflux. J Membr Biol. 2005;206(3):173-85.
65. Gottesman MM, Pastan I. Biochemistry of multidrug resistance mediated by the multidrug transporter. Annu Rev Biochem. 1993;62:385-427.
66. Raviv Y, Pollard HB, Bruggemann EP, Pastan I, Gottesman MM. Photosensitized labeling of a functional multidrug transporter in living drug-resistant tumor cells. J Biol Chem. 1990;265(7):3975-80.
67. Higgins CF, Gottesman MM. Is the multidrug transporter a flippase? Trends Biochem Sci. 1992;17(1):18-21.
68. Steuer H, Jaworski A, Elger B, Kaussmann M, Keldenich J, Schneider H, et al. Functional characterization and comparison of the outer blood-retina barrier and the blood-brain barrier. Invest Ophthalmol Vis Sci. 2005;46(3):1047-53.
69. Kennedy BG, Mangini NJ. P-glycoprotein expression in human retinal pigment epithelium. Mol Vis. 2002;8:422-30.
70. Aukunuru JV, Sunkara G, Bandi N, Thoreson WB, Kompella UB. Expression of multidrug resistance-associated protein (MRP) in human retinal pigment epithelial cells and its interaction with BAPSG, a novel aldose reductase inhibitor. Pharm Res. 2001;18(5):565-72.

71. Duvvuri S, Gandhi MD, Mitra AK. Effect of P-glycoprotein on the ocular disposition of a model substrate, quinidine. Curr Eye Res. 2003;27(6):345-53.
72. Ambudkar SV, Kimchi-Sarfaty C, Sauna ZE, Gottesman MM. P-glycoprotein: from genomics to mechanism. Oncogene. 2003;22(47):7468-85.
73. Shah SS, Denham LV, Elison JR, Bhattacharjee PS, Clement C, Huq T, et al. Drug delivery to the posterior segment of the eye for pharmacologic therapy. Expert Rev Ophthalmol. 2010;5:75-93.
74. Iyer MN, He F, Wensel TG, Mieler WF, Benz MS, Holz ER. Clearance of intravitreal moxifloxacin. Invest Ophthalmol Vis Sci. 2006;47(1):317-9.
75. Janoria KG, Gunda S, Boddu SH, Mitra AK. Novel approaches to retinal drug delivery. Expert Opin Drug Deliv. 2007;4(4):371-88.
76. Maurice D. Review: practical issues in intravitreal drug delivery. J Ocul Pharmacol Ther. 2001;17(4):393-401.
77. Urtti A. Challenges and obstacles of ocular pharmacokinetics and drug delivery. Adv Drug Deliv Rev. 2006;58(11):1131-5.
78. Raghava S, Hammond M, Kompella UB. Periocular routes for retinal drug delivery. Expert Opin Drug Deliv. 2004;1(1):99-114.
79. Kim SH, Lutz RJ, Wang NS, Robinson MR. Transport barriers in transscleral drug delivery for retinal diseases. Ophthalmic Res. 2007;39(5):244-54.
80. de la Fuente M, Ravina M, Paolicelli P, Sanchez A, Seijo B, Alonso MJ. Chitosan-based nanostructures: a delivery platform for ocular therapeutics. Adv Drug Deliv Rev. 2010;62(1):100-17.
81. Ali M, Byrne ME. Challenges and solutions in topical ocular drug-delivery systems. Expert Rev Clin Pharmacol. 2008;1(1):145-61.
82. Kaur IP, Smitha R. Penetration enhancers and ocular bioadhesives: two new avenues for ophthalmic drug delivery. Drug Dev Ind Pharm. 2002;28(4):353-69.
83. Lee VH, Robinson JR. Topical ocular drug delivery: recent developments and future challenges. J Ocul Pharmacol. 1986;2(1):67-108.
84. Green K. The effect of preservatives on corneal permeability of drugs. In: Edman P, editor. Biopharmaceutics of Ocular Drug Delivery: CRC Press, Inc.; 1993. p. 43.
85. Chiou GCY, Chuang CY. Improvement of systemic absorption of insulin through eyes with absorption enhancers. J Pharm Sci. 1989;78(10):815-8.
86. Ismail IM, Chen CC, Richman JB, Andersen JS, Tang-Liu DD. Comparison of azone and hexamethylene lauramide in toxicologic effects and penetration enhancement of cimetidine in rabbit eyes. Pharm Res. 1992;9(6):817-21.
87. Merkus FWHM, Schipper NGM, Hermens WAJJ, Romeijn SG, Verhoef JC. Absorption enhancers in nasal drug delivery: efficacy and safety. J Control Release. 1993;24(1-3):201-8.
88. Chetoni P, Burgalassi S, Monti D, Saettone MF. Ocular toxicity of some corneal penetration enhancers evaluated by electrophysiology measurements on isolated rabbit corneas. Toxicol In Vitro. 2003;17(4):497-504.
89. Furrer P, Plazonnet B, Mayer JM, Gurny R. Application of in vivo confocal microscopy to the objective evaluation of ocular irritation induced by surfactants. Int J Pharm. 2000;207(1-2):89-98.

90. Rojanasakul Y, Liaw J, Robinson JR. Mechanisms of action of some penetration enhancers in the cornea: Laser scanning confocal microscopic and electrophysiology studies. Int J Pharm. 1990;66(1-3):131-42.
91. Majumdar S, Mitra AK. Chemical modification and formulation approaches to elevated drug transport across cell membranes. Expert Opin Drug Deliv. 2006;3(4):511-27.
92. Rinaudo M. Chitin and chitosan: Properties and applications. Prog Polym Sci. 2006;31(7):603-32.
93. Luessen HL, de Leeuw BJ, Langemeyer MW, de Boer AB, Verhoef JC, Junginger HE. Mucoadhesive polymers in peroral peptide drug delivery. VI. Carbomer and chitosan improve the intestinal absorption of the peptide drug buserelin in vivo. Pharm Res. 1996;13(11):1668-72.
94. Sinswat P, Tengamnuay P. Enhancing effect of chitosan on nasal absorption of salmon calcitonin in rats: comparison with hydroxypropyl- and dimethyl-beta-cyclodextrins. Int J Pharm. 2003;257(1-2):15-22.
95. Yu S, Zhao Y, Wu F, Zhang X, Lu W, Zhang H, et al. Nasal insulin delivery in the chitosan solution: in vitro and in vivo studies. Int J Pharm. 2004;281(1-2):11-23.
96. Senel S, Hincal AA. Drug permeation enhancement via buccal route: possibilities and limitations. J Control Release. 2001;72(1-3):133-44.
97. Sandri G, Rossi S, Ferrari F, Bonferoni MC, Muzzarelli C, Caramella C. Assessment of chitosan derivatives as buccal and vaginal penetration enhancers. Eur J Pharm Sci. 2004;21(2-3):351-9.
98. Dodane V, Amin Khan M, Merwin JR. Effect of chitosan on epithelial permeability and structure. Int J Pharm. 1999;182(1):21-32.
99. Ranaldi G, Marigliano I, Vespignani I, Perozzi G, Sambuy Y. The effect of chitosan and other polycations on tight junction permeability in the human intestinal Caco-2 cell line(1). J Nutr Biochem. 2002;13(3):157-67.
100. Smith J, Wood E, Dornish M. Effect of chitosan on epithelial cell tight junctions. Pharm Res. 2004;21(1):43-9.
101. Kerec M, Bogataj M, Veranic P, Mrhar A. Permeability of pig urinary bladder wall: the effect of chitosan and the role of calcium. Eur J Pharm Sci. 2005;25(1):113-21.
102. Kos MK, Bogataj M, Veranic P, Mrhar A. Permeability of pig urinary bladder wall: time and concentration dependent effect of chitosan. Biol Pharm Bull. 2006;29(8):1685-91.
103. Schipper NG, Olsson S, Hoogstraate JA, deBoer AG, Varum KM, Artursson P. Chitosans as absorption enhancers for poorly absorbable drugs 2: mechanism of absorption enhancement. Pharm Res. 1997;14(7):923-9.
104. Di Colo G, Zambito Y, Burgalassi S, Nardini I, Saettone MF. Effect of chitosan and of N-carboxymethylchitosan on intraocular penetration of topically applied ofloxacin. Int J Pharm. 2004;273(1-2):37-44.
105. Lehr C-M, Bouwstra JA, Schacht EH, Junginger HE. In vitro evaluation of mucoadhesive properties of chitosan and some other natural polymers. Int J Pharm. 1992;78(1-3):43-8.
106. Hassan EE, Gallo JM. A Simple Rheological Method for the in Vitro Assessment of Mucin-Polymer Bioadhesive Bond Strength. Pharm Res. 1990;7:491-5.
107. Felt O, Furrer P, Mayer JM, Plazonnet B, Buri P, Gurny R. Topical use of chitosan in ophthalmology: tolerance assessment and evaluation of precorneal retention. Int J Pharm.

1999;180(2):185-93.
108. Pangburn SH, Trescony PV, Heller J. Lysozyme degradation of partially deacetylated chitin, its films and hydrogels. Biomaterials. 1982;3(2):105-8.
109. Hirano S, Tsuchida H, Nagao N. N-acetylation in chitosan and the rate of its enzymic hydrolysis. Biomaterials. 1989;10(8):574-6.
110. Nordtveit RJ, Vårum KM, Smidsrød O. Degradation of fully water-soluble, partially N-acetylated chitosans with lysozyme. Carbohydrate Polymers. 1994;23(4):253-60.
111. Muzzarelli RAA. Biochemical significance of exogenous chitins and chitosans in animals and patients. Carbohydrate Polymers. 1993;20(1):7-16.
112. Muzzarelli RA. Human enzymatic activities related to the therapeutic administration of chitin derivatives. Cell Mol Life Sci. 1997;53(2):131-40.
113. Wang W, Xu D. Viscosity and flow properties of concentrated solutions of chitosan with different degrees of deacetylation. Int J Biol Macromol. 1994;16(3):149-52.
114. Mucha M. Rheological characteristics of semi-dilute chitosan solutions. Macromolecular Chemistry and Physics. 1997;198(2):471-84.
115. Felt O, Carrel A, Baehni P, Buri P, Gurny R. Chitosan as tear substitute: a wetting agent endowed with antimicrobial efficacy. J Ocul Pharmacol Ther. 2000;16(3):261-70.
116. Kaur IP, Kanwar M. Ocular preparations: the formulation approach. Drug Dev Ind Pharm. 2002;28(5):473-93.
117. Kearse EC, Green K. Effect of vehicle upon in vitro transcorneal permeability and intracorneal content of Delta9-tetrahydrocannabinol. Curr Eye Res. 2000;20(6):496-501.
118. Tomida I, Pertwee RG, Azuara-Blanco A. Cannabinoids and glaucoma. Br J Ophthalmol. 2004;88(5):708-13.
119. Muller RH, Mader K, Gohla S. Solid lipid nanoparticles (SLN) for controlled drug delivery - a review of the state of the art. Eur J Pharm Biopharm. 2000;50(1):161-77.
120. Wissing SA, Kayser O, Muller RH. Solid lipid nanoparticles for parenteral drug delivery. Adv Drug Deliv Rev. 2004;56(9):1257-72.
121. Mehnert W, Mader K. Solid lipid nanoparticles: production, characterization and applications. Adv Drug Deliv Rev. 2001;47(2-3):165-96.
122. Loftsson T, Jarho P, Masson M, Jarvinen T. Cyclodextrins in drug delivery. Expert Opin Drug Deliv. 2005;2(2):335-51.
123. Loftsson T, Brewster ME. Pharmaceutical applications of cyclodextrins. 1. Drug solubilization and stabilization. J Pharm Sci. 1996;85(10):1017-25.
124. Brewster ME, Loftsson T. Cyclodextrins as pharmaceutical solubilizers. Adv Drug Deliv Rev. 2007;59(7):645-66.
125. Loftsson T, Stefansson E. Cyclodextrins in eye drop formulations: enhanced topical delivery of corticosteroids to the eye. Acta Ophthalmol Scand. 2002;80(2):144-50.
126. Kaur IP, Chhabra S, Aggarwal D. Role of cyclodextrins in ophthalmics. Curr Drug Deliv. 2004;1(4):351-60.
127. Loftsson T, Frikdriksdóttir H, Sigurkdardóttir AM, Ueda H. The effect of water-soluble polymers on drug-cyclodextrin complexation. Int J Pharm. 1994;110(2):169-77.
128. Stella VJ, Rao VM, Zannou EA, Zia V. Mechanisms of drug release from cyclodextrin complexes. Adv Drug Deliv Rev. 1999;36(1):3-16.
129. Bary AR, Tucker IG, Davies NM. Considerations in the use of hydroxypropyl-[beta]-

cyclodextrin in the formulation of aqueous ophthalmic solutions of hydrocortisone. Eur J Pharm Biopharm. 2000;50(2):237-44.
130. Higuchi T, Connors KA. Phase solubility techniques. Adv Anal Chem Instr. 1965;4(117-212).
131. Loftsson T, Fririksdóttir H, Thórisdóttir S, Stefánsson E. The effect of hydroxypropyl methylcellulose on the release of dexamethasone from aqueous 2-hydroxypropyl-[beta]-cyclodextrin formulations. Int J Pharm. 1994;104(2):181-4.
132. Reer O, Bock TK, Muller BW. In vitro corneal permeability of diclofenac sodium in formulations containing cyclodextrins compared to the commercial product voltaren ophtha. J Pharm Sci. 1994;83(9):1345-9.
133. Reddy IK, Khan MA, Wu WM, Bodor NS. Permeability of a soft steroid, loteprednol etabonate, through an excised rabbit cornea. J Ocul Pharmacol Ther. 1996;12(2):159-67.
134. Loftsson T, StefÃ¡nsson E. Effect of Cyclodextrins on Topical Drug Delivery to the Eye. Drug Dev Ind Pharm. 1997;23(5):473-81.
135. Majumdar S, Srirangam R. Solubility, stability, physicochemical characteristics and in vitro ocular tissue permeability of hesperidin: a natural bioflavonoid. Pharm Res. 2009;26(5):1217-25.
136. Rajewski RA, Stella VJ. Pharmaceutical applications of cyclodextrins. 2. In vivo drug delivery. J Pharm Sci. 1996;85(11):1142-69.
137. Suhonen P, Jarvinen T, Lehmussaari K, Reunamaki T, Urtti A. Ocular absorption and irritation of pilocarpine prodrug is modified with buffer, polymer, and cyclodextrin in the eyedrop. Pharm Res. 1995;12(4):529-33.
138. Pomponio R, Gotti R, Fiori J, Cavrini V, Mura P, Cirri M, et al. Photostability studies on nicardipine-cyclodextrin complexes by capillary electrophoresis. J Pharm Biomed Anal. 2004;35(2):267-75.
139. Rawat M, Singh D, Saraf S. Lipid carriers: a versatile delivery vehicle for proteins and peptides. Yakugaku Zasshi. 2008;128(2):269-80.
140. Uner M, Yener G. Importance of solid lipid nanoparticles (SLN) in various administration routes and future perspectives. Int J Nanomedicine. 2007;2(3):289-300.
141. Manjunath K, Reddy JS, Venkateswarlu V. Solid lipid nanoparticles as drug delivery systems. Methods Find Exp Clin Pharmacol. 2005;27(2):127-44.
142. Müller RH, Mäder K, Gohla S. Solid lipid nanoparticles (SLN) for controlled drug delivery - a review of the state of the art. Eur J Pharm Biopharm. 2000;50(1):161-77.
143. Souto EB, Doktorovova S, Gonzalez-Mira E, Egea MA, Garcia ML. Feasibility of lipid nanoparticles for ocular delivery of anti-inflammatory drugs. Curr Eye Res. 2010;35(7):537-52.
144. Gokce EH, Sandri G, Bonferoni MC, Rossi S, Ferrari F, Guneri T, et al. Cyclosporine A loaded SLNs: Evaluation of cellular uptake and corneal cytotoxicity. Int J Pharm. 2008.
145. Kaur IP, Bhandari R, Bhandari S, Kakkar V. Potential of solid lipid nanoparticles in brain targeting. J Control Release. 2008;127(2):97-109.
146. Cavalli R, Gasco MR, Chetoni P, Burgalassi S, Saettone MF. Solid lipid nanoparticles (SLN) as ocular delivery system for tobramycin. Int J Pharm. 2002;238(1-2):241-5.
147. Gokce EH, Sandri G, Egrilmez S, Bonferoni MC, Guneri T, Caramella C. Cyclosporine a-loaded solid lipid nanoparticles: ocular tolerance and in vivo drug release in rabbit eyes.

Curr Eye Res. 2009;34(11):996-1003.
148. Attama AA, Reichl S, Muller-Goymann CC. Sustained release and permeation of timolol from surface-modified solid lipid nanoparticles through bioengineered human cornea. Curr Eye Res. 2009;34(8):698-705.
149. Nobili S, Landini I, Giglioni B, Mini E. Pharmacological strategies for overcoming multidrug resistance. Curr Drug Targets. 2006;7(7):861-79.
150. Jain R, Majumdar S, Nashed Y, Pal D, Mitra AK. Circumventing P-glycoprotein-mediated cellular efflux of quinidine by prodrug derivatization. Mol Pharm. 2004;1(4):290-9.
151. Katragadda S, Budda B, Anand BS, Mitra AK. Role of efflux pumps and metabolising enzymes in drug delivery. Expert Opin Drug Deliv. 2005;2(4):683-705.
152. Senthilkumari S, Velpandian T, Biswas NR, Saxena R, Ghose S. Evaluation of the modulation of P-glycoprotein (P-gp) on the intraocular disposition of its substrate in rabbits. Curr Eye Res. 2008;33(4):333-43.
153. Senthilkumari S, Velpandian T, Biswas NR, Sonali N, Ghose S. Evaluation of the impact of P-glycoprotein (P-gp) drug efflux transporter blockade on the systemic and ocular disposition of P-gp substrate. J Ocul Pharmacol Ther. 2008;24(3):290-300.
154. Di Colo G, Zambito Y, Burgalassi S, Serafini A, Saettone MF. Effect of chitosan on in vitro release and ocular delivery of ofloxacin from erodible inserts based on poly(ethylene oxide). Int J Pharm. 2002;248(1-2):115-22.
155. De Campos AM, Sanchez A, Alonso MJ. Chitosan nanoparticles: a new vehicle for the improvement of the delivery of drugs to the ocular surface. Application to cyclosporin A. Int J Pharm. 2001;224(1-2):159-68.
156. Enriquez de Salamanca A, Diebold Y, Calonge M, Garcia-Vazquez C, Callejo S, Vila A, et al. Chitosan nanoparticles as a potential drug delivery system for the ocular surface: toxicity, uptake mechanism and in vivo tolerance. Invest Ophthalmol Vis Sci. 2006;47(4):1416-25.
157. Zambito Y, Zaino C, Di Colo G. Effects of N-trimethylchitosan on transcellular and paracellular transcorneal drug transport. Eur J Pharm Biopharm. 2006;64(1):16-25.
158. Majumdar S, Gunda S, Mitra A. Functional expression of a sodium dependent nucleoside transporter on rabbit cornea: Role in corneal permeation of acyclovir and idoxuridine. Curr Eye Res. 2003;26(3-4):175-83.
159. Majumdar S, Nashed YE, Patel K, Jain R, Itahashi M, Neumann DM, et al. Dipeptide monoester ganciclovir prodrugs for treating HSV-1-induced corneal epithelial and stromal keratitis: in vitro and in vivo evaluations. J Ocul Pharmacol Ther. 2005;21(6):463-74.
160. Anand BS, Mitra AK. Mechanism of corneal permeation of L-valyl ester of acyclovir: targeting the oligopeptide transporter on the rabbit cornea. Pharm Res. 2002;19(8):1194-202.
161. Ashton P, Diepold R, Platzer A, Lee VH. The effect of chlorhexidine acetate on the corneal penetration of sorbitol from an arnolol formulation in the albino rabbit. J Ocul Pharmacol. 1990;6(1):37-42.
162. Mitra AK. Opthalmic Drug Delivery Systems. Second ,Revised and Expanded ed.: Marcel Dekker, Inc 2003.
163. Green K, Tonjum A. Influence of various agents on corneal permeability. Am J Ophthalmol. 1971;72(5):897-905.

164. Tonjum AM. Permeability of rabbit corneal epithelium to horseradish peroxidase after the influence of benzalkonium chloride. Acta Ophthalmol (Copenh). 1975;53(3):335-47.
165. Green K, Downs SJ. Prednisolone phosphate penetration into and through the cornea. Invest Ophthalmol. 1974;13(4):316-9.
166. Camber O, Edman P, Gurny R. Influence of sodium hyaluronate on the meiotic effect of pilocarpine in rabbits. Curr Eye Res. 1987;6(6):779-84.
167. Flach AJ, Jaffe NS, Akers WA. The effect of ketorolac tromethamine in reducing postoperative inflammation: double-mask parallel comparison with dexamethasone. Ann Ophthalmol. 1989;21(11):407-11.
168. Pawar PK, Majumdar DK. Effect of formulation factors on in vitro permeation of moxifloxacin from aqueous drops through excised goat, sheep, and buffalo corneas. AAPS PharmSciTech. 2006;7(1):E13.
169. Rathore MS, Majumdar DK. Effect of formulation factors on in vitro transcorneal permeation of gatifloxacin from aqueous drops. AAPS PharmSciTech. 2006;7(3):57.
170. Anand B, Nashed Y, Mitra A. Novel dipeptide prodrugs of acyclovir for ocular herpes infections: Bioreversion, antiviral activity and transport across rabbit cornea. Curr Eye Res. 2003;26(3-4):151-63.
171. Anand BS, Katragadda S, Nashed YE, Mitra AK. Amino acid prodrugs of acyclovir as possible antiviral agents against ocular HSV-1 infections: interactions with the neutral and cationic amino acid transporter on the corneal epithelium. Curr Eye Res. 2004;29(2-3):153-66.
172. Ahuja M, Dhake AS, Majumdar DK. Effect of formulation factors on in-vitro permeation of diclofenac from experimental and marketed aqueous eye drops through excised goat cornea. Yakugaku Zasshi. 2006;126(12):1369-75.
173. Kikuchi T, Suzuki M, Kusai A, Iseki K, Sasaki H, Nakashima K. Mechanism of permeability-enhancing effect of EDTA and boric acid on the corneal penetration of 4-[1-hydroxy-1-methylethyl]-2-propyl-1-[4-[2-[tetrazole-5-yl]phenyl]phenyl] methylimidazole-5-carboxylic acid monohydrate (CS-088). Int J Pharm. 2005;299(1-2):107-14.
174. Scholz M, Lin JE, Lee VH, Keipert S. Pilocarpine permeability across ocular tissues and cell cultures: influence of formulation parameters. J Ocul Pharmacol Ther. 2002;18(5):455-68.
175. Jarvinen T, Pate DW, Laine K. Cannabinoids in the treatment of glaucoma. Pharmacol Ther. 2002;95(2):203-20.
176. Thumma S, Majumdar S, Elsohly MA, Gul W, Repka MA. Chemical stability and bioadhesive properties of an ester prodrug of Delta(9)-tetrahydrocannabinol in poly(ethylene oxide) matrices: Effect of formulation additives. Int J Pharm. 2008;362(1-2):126-32.
177. Williamson EM, Evans FJ. Cannabinoids in clinical practice. Drugs. 2000;60(6):1303-14.
178. Porcella A, Maxia C, Gessa GL, Pani L. The synthetic cannabinoid WIN55212-2 decreases the intraocular pressure in human glaucoma resistant to conventional therapies. Eur J Neurosci. 2001;13(2):409-12.
179. Marquis RE, Whitson JT. Management of glaucoma: focus on pharmacological therapy. Drugs Aging. 2005;22(1):1-21.
180. Williams PB, inventor Novel Cannabinoids and method of use,WO/2007/130361 2007.

181. Crandall J, Matragoon S, Khalifa YM, Borlongan C, Tsai NT, Caldwell RB, et al. Neuroprotective and intraocular pressure-lowering effects of (-)Delta9-tetrahydrocannabinol in a rat model of glaucoma. Ophthalmic Res. 2007;39(2):69-75.
182. Szczesniak AM, Kelly ME, Whynot S, Shek PN, Hung O. Ocular hypotensive effects of an intratracheally delivered liposomal delta9-tetrahydrocannabinol preparation in rats. J Ocul Pharmacol Ther. 2006;22(3):160-7.
183. Repka MA, ElSohly MA, Munjal M, Ross SA. Temperature stability and bioadhesive properties of delta9-tetrahydrocannabinol incorporated hydroxypropylcellulose polymer matrix systems. Drug Dev Ind Pharm. 2006;32(1):21-32.
184. van Drooge DJ, Hinrichs WL, Wegman KA, Visser MR, Eissens AC, Frijlink HW. Solid dispersions based on inulin for the stabilisation and formulation of delta 9-tetrahydrocannabinol. Eur J Pharm Sci. 2004;21(4):511-8.
185. Mechoulam R. Marihuana chemistry. Science. 1970;168(936):1159-66.
186. Mechoulam R, Hanus L. A historical overview of chemical research on cannabinoids. Chem Phys Lipids. 2000;108(1-2):1-13.
187. Fairbairn JW, Liebmann JA, Rowan MG. The stability of cannabis and its preparations on storage. J Pharm Pharmacol. 1976;28(1):1-7.
188. Muchtar S, Almog S, Torracca MT, Saettone MF, Benita S. A submicron emulsion as ocular vehicle for delta-8-tetrahydrocannabinol: effect on intraocular pressure in rabbits. Ophthalmic Res. 1992;24(3):142-9.
189. Avraham Y, Ben-Shushan D, Breuer A, Zolotarev O, Okon A, Fink N, et al. Very low doses of delta 8-THC increase food consumption and alter neurotransmitter levels following weight loss. Pharmacol Biochem Behav. 2004;77(4):675-84.
190. Stinchcomb AL, Valiveti S, Hammell DC, Ramsey DR. Human skin permeation of Delta8-tetrahydrocannabinol, cannabidiol and cannabinol. J Pharm Pharmacol. 2004;56(3):291-7.
191. Valiveti S, Hammell DC, Earles DC, Stinchcomb AL. In vitro/in vivo correlation studies for transdermal delta 8-THC development. J Pharm Sci. 2004;93(5):1154-64.
192. Wong AS, Orbanosky MW, Reeve VC, Beede JD. Stability of delta-9-tetrahydrocannabinol in stored blood and serum. NIDA Res Monogr. 1982;42:119-24.
193. Johnson JR, Jennison TA, Peat MA, Foltz RL. Stability of delta 9-tetrahydrocannabinol (THC), 11-hydroxy-THC, and 11-nor-9-carboxy-THC in blood and plasma. J Anal Toxicol. 1984;8(5):202-4.
194. Christophersen AS. Tetrahydrocannabinol stability in whole blood: plastic versus glass containers. J Anal Toxicol. 1986;10(4):129-31.
195. Garrett ER, Hunt CA. Physiochemical properties, solubility, and protein binding of delta9-tetrahydrocannabinol. J Pharm Sci. 1974;63(7):1056-64.
196. Blanc JA, Manneh VA, Ernst R, Berger DE, de Keczer SA, Chase C, et al. Adsorption losses from urine-based cannabinoid calibrators during routine use. Clin Chem. 1993;39(8):1705-12.
197. Davis ME, Brewster ME. Cyclodextrin-based pharmaceutics: past, present and future. Nat Rev Drug Discov. 2004;3(12):1023-35.
198. Dollo G, Le Corre P, Chevanne F, Le Verge R. Inclusion complexation of amide-typed local anaesthetics with [beta]-cyclodextrin and its derivatives. ii. evaluation of affinity constants and in vitro transfer rate constants. Int J Pharm. 1996;136(1-2):165-74.

199. Mizutani T, Mizutani A. Estimation of adsorption of drugs and proteins on glass surfaces with controlled pore glass as a reference. J Pharm Sci. 1978;67(8):1102-5.
200. Grotenhermen F. Pharmacokinetics and pharmacodynamics of cannabinoids. Clin Pharmacokinet. 2003;42(4):327-60.
201. Garrett ER, Tsau J. Stability of tetrahydrocannabinols. I. J Pharm Sci. 1974;63(10):1563-74.
202. Brewster ME, Loftsson T. Cyclodextrins as pharmaceutical solubilizers. Adv Drug Deliv Rev. 2007;59(7):645-66.
203. Mannila J, Jarvinen T, Jarvinen K, Tarvainen M, Jarho P. Effects of RM-beta-CD on sublingual bioavailability of Delta9-tetrahydrocannabinol in rabbits. Eur J Pharm Sci. 2005;26(1):71-7.
204. Hazekamp A, Verpoorte R. Structure elucidation of the tetrahydrocannabinol complex with randomly methylated beta-cyclodextrin. Eur J Pharm Sci. 2006;29(5):340-7.
205. Okimoto K, Rajewski RA, Uekama K, Jona JA, Stella VJ. The interaction of charged and uncharged drugs with neutral (HP-beta-CD) and anionically charged (SBE7-beta-CD) beta-cyclodextrins. Pharm Res. 1996;13(2):256-64.
206. Challa R, Ahuja A, Ali J, Khar RK. Cyclodextrins in drug delivery: an updated review. AAPS PharmSciTech. 2005;6(2):E329-57.
207. Loftsson T, Masson M. Cyclodextrins in topical drug formulations: theory and practice. Int J Pharm. 2001;225(1-2):15-30.
208. Carrier RL, Miller LA, Ahmed I. The utility of cyclodextrins for enhancing oral bioavailability. J Control Release. 2007;123(2):78-99.
209. ElSohly MA, Harland EC, Benigni DA, Waller CW. Cannabinoids in glaucoma II: the effect of different cannabinoids on intraocular pressure of the rabbit. Curr Eye Res. 1984;3(6):841-50.
210. Green K, Roth M. Ocular effects of topical administration of delta 9-tetrahydrocannabinol in man. Arch Ophthalmol. 1982;100(2):265-7.
211. Backensfeld T, Müller BW, Wiese M, Seydel JK. Effect of Cyclodextrin Derivatives on Indomethacin Stability in Aqueous Solution. Pharmaceutical Research. 1990;7(5):484-90.
212. Gueudry J, Lebel H, Muraine M. Severe corneal complications associated with topical indomethacin use. British Journal of Ophthalmology. 2010;94::133-4.
213. Chetoni P, Panichi L, Burgalassi S, Benelli U, Saettone MF. Pharmacokinetics and anti-inflammatory activity in rabbits of a novel indomethacin ophthalmic solution. J Ocul Pharmacol Ther. 2000;16(4):363-72.
214. Yamaguchi M, Ueda K, Isowaki A, Ohtori A, Takeuchi H, Ohguro N, et al. Mucoadhesive properties of chitosan-coated ophthalmic lipid emulsion containing indomethacin in tear fluid. Biol Pharm Bull. 2009;32(7):1266-71.
215. Muchtar S, Abdulrazik M, Frucht-Pery J, Benita S. Ex-vivo permeation study of indomethacin from a submicron emulsion through albino rabbit cornea. Journal of Controlled Release. 1997;44(1):55-64.
216. Sanders DR, Goldstick B, Kraff C, Hutchins R, Bernstein MS, Evans MA. Aqueous penetration of oral and topical indomethacin in humans. Arch Ophthalmol. 1983;101(10):1614-6.
217. Calvo P, Vila-Jato JL, Alonso MJ. Comparative in vitro evaluation of several colloidal

systems, nanoparticles, nanocapsules, and nanoemulsions, as ocular drug carriers. J Pharm Sci. 1996;85(5):530-6.
218. Klang S, Abdulrazik M, Benita S. Influence of emulsion droplet surface charge on indomethacin ocular tissue distribution. Pharm Dev Technol. 2000;5(4):521-32.
219. Box GPE, Hunter WG, Hunter JS. Statistics for experimenters: An introduction to desing, data analysis and model building. New York: Wiley; 1978.
220. Zhang J, Fan Y, Smith E. Experimental design for the optimization of lipid nanoparticles. J Pharm Sci. 2009;98(5):1813-9.
221. Hamedi A, Vahid H, Ghanati F. Optimization of the medium composition for production of mycelial biomass and exo-polysaccharide by Agaricus blazei Muril Dpph 131 using response surface methodology. Biotechnology. 2007;6(4):456-64.
222. Molpeceres J, Guzman M, Aberturas MR, Chacon M, Berges L. Application of central composite designs to the preparation of polycaprolactone nanoparticles by solvent displacement. J Pharm Sci. 1996;85(2):206-13.
223. Zhang X, Liu J, Qiao H, Liu H, Ni J, Zhang W, et al. Formulation optimization of dihydroartemisinin nanostructured lipid carrier using response surface methodology. Powder Technology. 2010;197(1-2):120-8.
224. Mehnert W, Mäder K. Solid lipid nanoparticles: Production, characterization and applications. Advanced Drug Delivery Reviews. 2001;47(2-3):165-96.
225. Venkateswarlu V, Manjunath K. Preparation, characterization and in vitro release kinetics of clozapine solid lipid nanoparticles. Journal of Controlled Release. 2004;95(3):627-38.
226. Hamdani J, Moes AJ, Amighi K. Physical and thermal characterisation of Precirol and Compritol as lipophilic glycerides used for the preparation of controlled-release matrix pellets. Int J Pharm. 2003;260(1):47-57.
227. Borka L. The polymorphism of indomethacine. New modifications, their melting behavior and solubility. Acta Pharm Suec. 1974;11(3):295-303.
228. Honary S, Majidian A, Naghib F. The Effect of Different Surfactants on Dissolution Rate of Recrystallized Indomethacin. Iranian Journal of Pharmaceutical Research. 2007;6(1):25-33.
229. Bandi N, Wei W, Roberts CB, Kotra LP, Kompella UB. Preparation of budesonide- and indomethacin-hydroxypropyl-beta-cyclodextrin (HPBCD) complexes using a single-step, organic-solvent-free supercritical fluid process. Eur J Pharm Sci. 2004;23(2):159-68.
230. Muller RH, Keck CM. Challenges and solutions for the delivery of biotech drugs--a review of drug nanocrystal technology and lipid nanoparticles. J Biotechnol. 2004;113(1-3):151-70.
231. Yang CR, Zhao XL, Hu HY, Li KX, Sun X, Li L, et al. Preparation, optimization and characteristic of huperzine a loaded nanostructured lipid carriers. Chem Pharm Bull (Tokyo). 2010;58(5):656-61.
232. Trotta M, Pattarino F, Ignoni T. Stability of drug-carrier emulsions containing phosphatidylcholine mixtures. Eur J Pharm Biopharm. 2002;53(2):203-8.
233. Goppert TM, Muller RH. Polysorbate-stabilized solid lipid nanoparticles as colloidal carriers for intravenous targeting of drugs to the brain: comparison of plasma protein adsorption patterns. J Drug Target. 2005;13(3):179-87.
234. Li Y, Dong L, Jia A, Chang X, Xue H. Preparation and characterization of solid lipid

nanoparticles loaded traditional Chinese medicine. Int J Biol Macromol. 2006;38(3-5):296-9.
235. Abdelbary G, Fahmy RH. Diazepam-loaded solid lipid nanoparticles: design and characterization. AAPS PharmSciTech. 2009;10(1):211-9.
236. Schwarz C, Mehnert W. Solid lipid nanoparticles (SLN) for controlled drug delivery. II. Drug incorporation and physicochemical characterization. J Microencapsul. 1999;16(2):205-13.
237. Backensfeld T, Müller BW, Kolter K. Interaction of NSA with cyclodextrins and hydroxypropyl cyclodextrin derivatives. Int J Pharm. 1991;74(2-3):85-93.
238. Tommasini S, Calabro ML, Raneri D, Ficarra P, Ficarra R. Combined effect of pH and polysorbates with cyclodextrins on solubilization of naringenin. J Pharm Biomed Anal. 2004;36(2):327-33.
239. Jug M, Kos I, Bećirević-Laćan M. The pH-dependent complexation between risperidone and hydroxypropyl-β-cyclodextrin. J Incl Phenom Macrocycl Chem. 2009;64(1):163-71.
240. Otagiri M, Uekama K, Imai T, Maeda T, Takadate A, Goya S, et al. Comparative study on inclusion complexation of beta-cyclodextrin and tri-O-methyl-beta-cyclodextrin with several drugs in aqueous solution. Acta Pharm Suec. 1984;21(6):357-66.
241. Seyfoddin A, Shaw J, Al-Kassas R. Solid lipid nanoparticles for ocular drug delivery. Drug Deliv. 2010;17(7):467-89.
242. Backensfeld T, Muller BW, Wiese M, Seydel JK. Effect of cyclodextrin derivatives on indomethacin stability in aqueous solution. Pharm Res. 1990;7(5):484-90.
243. Reddy LH, Murthy RS. Etoposide-loaded nanoparticles made from glyceride lipids: formulation, characterization, in vitro drug release, and stability evaluation. AAPS PharmSciTech. 2005;6(2):E158-66.
244. zur Muhlen A, Schwarz C, Mehnert W. Solid lipid nanoparticles (SLN) for controlled drug delivery--drug release and release mechanism. Eur J Pharm Biopharm. 1998;45(2):149-55.
245. Bunjes H, Westesen K, Koch MHJ. Crystallization tendency and polymorphic transitions in triglyceride nanoparticles. Int J Pharm. 1996;129(1-2):159-73.
246. Lim SJ, Kim CK. Formulation parameters determining the physicochemical characteristics of solid lipid nanoparticles loaded with all-trans retinoic acid. Int J Pharm. 2002;243(1-2):135-46.
247. Reddy LH, Vivek K, Bakshi N, Murthy RS. Tamoxifen citrate loaded solid lipid nanoparticles (SLN): preparation, characterization, in vitro drug release, and pharmacokinetic evaluation. Pharm Dev Technol. 2006;11(2):167-77.
248. Majumdar S, Tirucherai GS, Pal D, Mitra AK. Functional differences in nucleoside and nucleobase transporters expressed on the rabbit corneal epithelial cell line (SIRC) and isolated rabbit cornea. AAPS PharmSci. 2003;5(2):E15.
249. Yasukawa T, Ogura Y, Tabata Y, Kimura H, Wiedemann P, Honda Y. Drug delivery systems for vitreoretinal diseases. Prog Retin Eye Res. 2004;23(3):253-81.
250. Kemper EM, Boogerd W, Thuis I, Beijnen JH, van Tellingen O. Modulation of the blood-brain barrier in oncology: therapeutic opportunities for the treatment of brain tumours? Cancer Treat Rev. 2004;30(5):415-23.
251. Golden PL, Pollack GM. Blood-brain barrier efflux transport. J Pharm Sci. 2003;92(9):1739-53.

252. Fromm MF. Importance of P-glycoprotein at blood-tissue barriers. Trends Pharmacol Sci. 2004;25(8):423-9.
253. Kunta JR, Sinko PJ. Intestinal drug transporters: in vivo function and clinical importance. Curr Drug Metab. 2004;5(1):109-24.
254. Fromm MF. Importance of P-glycoprotein for drug disposition in humans. Eur J Clin Invest. 2003;33 Suppl 2:6-9.
255. Karssen AM, Meijer OC, van der Sandt IC, De Boer AG, De Lange EC, De Kloet ER. The role of the efflux transporter P-glycoprotein in brain penetration of prednisolone. J Endocrinol. 2002;175(1):251-60.
256. Augustijns P, Annaert P, Heylen P, Van den Mooter G, Kinget R. Drug absorption studies of prodrug esters using the Caco-2 model: evaluation of ester hydrolysis and transepithelial transport. International Journal of Pharmaceutics. 1998;166(1):45-53.
257. Tsuji A, Tamai I, Sasaki K. Hydrolysis of prednisolone succinate by esterase in rabbit ocular tissue. Ophthalmic Res. 1987;19(6):322-9.
258. Majumdar S, Hingorani T, Srirangam R, Gadepalli RS, Rimoldi JM, Repka MA. Transcorneal Permeation of L: - and D: -Aspartate Ester Prodrugs of Acyclovir: Delineation of Passive Diffusion Versus Transporter Involvement. Pharm Res. 2008.
259. Majumdar S, Kansara V, Mitra AK. Vitreal pharmacokinetics of dipeptide monoester prodrugs of ganciclovir. J Ocul Pharmacol Ther. 2006;22(4):231-41.
260. Macha S, Mitra AK. Ocular pharmacokinetics in rabbits using a novel dual probe microdialysis technique. Exp Eye Res. 2001;72(3):289-99.
261. Macha S, Mitra AK. Ocular pharmacokinetics of cephalosporins using microdialysis. J Ocul Pharmacol Ther. 2001;17(5):485-98.
262. Macha S, Mitra AK. Ocular disposition of ganciclovir and its monoester prodrugs following intravitreal administration using microdialysis. Drug Metab Dispos. 2002;30(6):670-5.
263. Tan AY, LeVatte TL, Archibald ML, Tremblay F, Kelly ME, Chauhan BC. Timolol concentrations in rat ocular tissues and plasma after topical and intraperitoneal dosing. J Glaucoma. 2002;11(2):134-42.
264. Ozturk F, Kortunay S, Kurt E, Inan UU, Ilker SS, Basci N, et al. The effect of long-term use and inflammation on the ocular penetration of topical ofloxacin. Curr Eye Res. 1999;19(6):461-4.
265. Ozturk F, Kurt E, Inan UU, Kortunay MC, Ilker SS, Basci NE, et al. Penetration of topical and oral ofloxacin into the aqueous and vitreous humor of inflamed rabbit eyes. Int J Pharm. 2000;204(1-2):91-5.
266. Salminen L, Urtti A. Disposition of ophthalmic timolol in treated and untreated rabbit eyes. A multiple and single dose study. Exp Eye Res. 1984;38(2):203-6.
267. Acheampong AA, Shackleton M, John B, Burke J, Wheeler L, Tang-Liu D. Distribution of brimonidine into anterior and posterior tissues of monkey, rabbit, and rat eyes. Drug Metab Dispos. 2002;30(4):421-9.
268. Cheruvu NP, Kompella UB. Bovine and porcine transscleral solute transport: influence of lipophilicity and the Choroid-Bruch's layer. Invest Ophthalmol Vis Sci. 2006;47(10):4513-22.
269. Hughes PM, Olejnik O, Chang-Lin JE, Wilson CG. Topical and systemic drug delivery to

the posterior segments. Adv Drug Deliv Rev. 2005;57(14):2010-32.
270. Majumdar S, Hippalgaonkar K, Srirangam R. Vitreal kinetics of quinidine in rabbits in the presence of topically coadministered P-glycoprotein substrates/modulators. Drug Metab Dispos. 2009;37(8):1718-25.
271. Schwab D, Fischer H, Tabatabaei A, Poli S, Huwyler J. Comparison of in vitro P-glycoprotein screening assays: recommendations for their use in drug discovery. J Med Chem. 2003;46(9):1716-25.
272. Bradford MM. A rapid and sensitive method for the quantitation of microgram quantities of protein utilizing the principle of protein-dye binding. Anal Biochem. 1976;72:248-54.
273. Musson DG, Bidgood AM, Olejnik O. Comparative corneal penetration of prednisolone sodium phosphate and prednisolone acetate in NZW rabbits. J Ocul Pharmacol. 1991;7(2):175-82.
274. Ochs HR, Greenblatt DJ, Woo E. Clinical pharmacokinetics of quinidine. Clin Pharmacokinet. 1980;5(2):150-68.
275. Guentert TW, Oie S. Effect of plasma protein binding on quinidine kinetics in the rabbit. J Pharmacol Exp Ther. 1980;215(1):165-71.
276. Attar M, Shen J, Ling KH, Tang-Liu D. Ophthalmic drug delivery considerations at the cellular level: drug-metabolising enzymes and transporters. Expert Opin Drug Deliv. 2005;2(5):891-908.
277. Majumdar S, Hippalgaonkar K, Repka MA. Effect of chitosan, benzalkonium chloride and ethylenediaminetetraacetic acid on permeation of acyclovir across isolated rabbit cornea. Int J Pharm. 2008;348(1-2):175-8.
278. Okabe K, Kimura H, Okabe J, Kato A, Shimizu H, Ueda T, et al. Effect of benzalkonium chloride on transscleral drug delivery. Invest Ophthalmol Vis Sci. 2005;46(2):703-8.
279. Hariharan S, Gunda S, Mishra GP, Pal D, Mitra AK. Enhanced corneal absorption of erythromycin by modulating P-glycoprotein and MRP mediated efflux with corticosteroids. Pharm Res. 2009;26(5):1270-82.
280. Vezmar M, Georges E. Reversal of MRP-mediated doxorubicin resistance with quinoline-based drugs. Biochem Pharmacol. 2000;59(10):1245-52.
281. Makhey VD, Guo A, Norris DA, Hu P, Yan J, Sinko PJ. Characterization of the regional intestinal kinetics of drug efflux in rat and human intestine and in Caco-2 cells. Pharm Res. 1998;15(8):1160-7.
282. Shitara Y, Sugiyama D, Kusuhara H, Kato Y, Abe T, Meier PJ, et al. Comparative inhibitory effects of different compounds on rat oatpl (slc21a1)- and Oatp2 (Slc21a5)-mediated transport. Pharm Res. 2002;19(2):147-53.
283. Kusuhara H, Suzuki H, Terasaki T, Kakee A, Lemaire M, Sugiyama Y. P-Glycoprotein mediates the efflux of quinidine across the blood-brain barrier. J Pharmacol Exp Ther. 1997;283(2):574-80.
284. Suzuki T, Zaima C, Moriki Y, Fukami T, Tomono K. P-glycoprotein mediates brain-to-blood efflux transport of buprenorphine across the blood-brain barrier. J Drug Target. 2007;15(1):67-74.

VITA

July 17th, 1982	Born- Hyderabad, Andhra Pradesh, India
June, 2004	B.S. Pharmacy, Jawaharlal Nehru Technological University, India
January, 2006	Joined Ph.D. Program, Department of Pharmaceutics, The University of Mississippi
Peer-Reviewed Publications	Five
Acheivements/Awards	• Inductee Phi Kappa Phi Honor Society – 2007 • Inductee, Rho Chi Honor Society – 2008 • Best poster presentation award, Sigma Xi Student Research Symposium-2008 • CORE NPN award- 2008. • Graduates School Honor Fellowship, University of Mississippi. 2006- 2011
Professional Activities	• Member of Phi Kappa Phi, Rho Chi, Sigma Xi and AAPS • Chair, AAPS-UM Chapter, 2007-2008 • Chair-Elect, AAPS-UM Chapter ,2006 –2007 • Senator, Graduate Student Council, 2006-2007